'I know that you believe you understand what you think I said, but I am not sure you realise that what you heard is not what I meant.'

Richard M Nixon

ELECTROCHEMICAL REACTIONS AT VERY SMALL ELECTRODES

by

David Nicholas Swan

A thesis submitted to the University of Southampton as part fulfilment of the requirement for the degree of Doctor of Philosophy.

August 1980

UNIVERSITY OF SOUTHAMPTON

ABSTRACT

FACULTY OF SCIENCE

CHEMISTRY

Doctor of Philosophy

ELECTROCHEMICAL REACTIONS AT VERY SMALL ELECTRODES

by David Nicholas Swan

To measure fast electrode processes, high rates of mass transfer of the electroactive species to the electrode surface are essential. This has been achieved in the present study by forming very small electrodes of radius $< 5\mu m$ (appropriately termed microelectrodes); it is shown that mass transfer to these electrodes is enhanced above the rate to a planar electrode of equivalent area by virtue of an additional steady state flux term inversely proportional to the electrode radius, so that under conditions of very slow linear potential sweep, i.e. pseudo steady state, the rate of mass transfer is determined by the steady state term alone.

In the first part of this work, electrodes prepared from lead, tungsten and platinum, all sealed into glass, have been used to measure the rate of the heterogeneous electron transfer reactions of a number of aromatic, nitroaromatic and nitroaliphatic compounds in Dimethylformamide. Both slow linear potential sweep and fast linear potential sweep analyses were performed; the latter with the development of convolution potential sweep voltammetry methods applicable to very small electrodes. It is shown that for the reduction of tert - nitrobutane this technique can be applied over a wide potential range giving results in close agreement with those obtained by other workers using alternative non steady state methods. Deviation from Butler - Volmer behaviour was observed for this reaction and interpreted in terms of the Marcus theory. For faster electron transfer reactions, however, electrode dimensions available at the time were found to be too large to allow measurement of the electron transfer rates due to partial mass transfer control of the electrode reaction, even under fast linear potential sweep conditions.

In the second part of this work, the rates of homogeneous chemical reactions preceding the electron transfer step were studied. The rate of dissociation of acetic acid in sodium acetate solutions was investigated using platinum microelectrodes under conditions of slow linear potential sweep and found to be in reasonable agreement with values obtained by other workers, indicating that enhanced rates of mass transfer at microelectrodes may be employed to measure the rates of both homogeneous and heterogeneous electrode reactions under pseudo steady state conditions.

CONTENTS

CHAPTER 1 INTRODUCTION

1:i Electrode reactions

Electrochemical reactions that involve the transfer of charge across an electrode/electrolyte interface are examples of a general class of reaction referred to as heterogeneous processes. The kinetics of heterogeneous reactions are usually determined by a number of factors involving both mass transport through the solution phase and the reaction at the catalytic surface. In the case of an electrode reaction, for example the reduction of a species O by the addition of an electron to form a product R,

$$O + e = R \qquad 1.1$$

the overall reaction is likely to proceed in the following manner:

(i) transport of O from the bulk solution to the interface;
(ii) adsorption of O onto the surface;
(iii) charge transfer at the electrode to form R;
(iv) desorption of R from the surface;
(v) and finally, transport of R from the interface into the bulk solution.

Steps (i) and (v) represent the mass transport modes of the reaction, while steps (ii), (iii) and (iv) describe the reactions taking place at the electrode surface. Additional steps, for instance homogeneous chemical reactions, may also be included in the reaction sequence, either preceding, following or even interspersed between charge transfer steps. Since these processes all occur in a sequential manner, the overall rate of the reaction, i.e. the observed rate, is equal to the rates of the individual steps although this does not imply equal rate constants.

In this Chapter, a derivation for the rate of

electron transfer processes and their measurement is presented, while in Chapter 2 the influence of diffusion on the observed rate of simple electrode reactions is examined, illustrating the application of very small electrodes to the measurement of the rate of simple charge transfer processes under both pseudo steady state and fast linear potential sweep conditions. Results of measurements obtained for the reduction of some aromatic hydrocarbons and nitro-aliphatic compounds in aprotic media at tungsten and platinum electrodes are presented in Chapter 4.

Finally, in Chapter 5, the theory of electro-chemical reactions at very small electrodes is further developed to include homogeneous chemical reactions preceding the charge transfer reaction. The rate of the dissociation/recombination equilibrium of acetic acid preceding the evolution of hydrogen from aqueous sodium acetate solutions was determined with the aid of several platinum microelectrodes in accordance with the proposed theory after first investigating the general behaviour of platinum microelectrodes in aqueous strong acid media.

1:ii The rate of electron transfer reactions

The simple electrode reaction given earlier (1.1) depicting the one electron reduction of a species O to form a product R, may be expressed more generally by the equation

$$O + ne \underset{k_b}{\overset{k_f}{\rightleftharpoons}} R \qquad 1.2$$

where n is an integer and O and R are stable and soluble in the reaction medium. The heterogeneous rate constants for the forward and reverse reactions are given by k_f and k_b respectively. In deriving the rate of the electron transfer step, all other processes such as mass transport, adsorption and homogeneous chemical reactions will be excluded from consideration, i.e. the electron transfer step will be considered rate determining.

According to the theory of electron transfer reactions at electrodes, developed by Parsons [1] and Delahay [2], based on absolute reaction rate theory, the rates of the forward and reverse reactions in (1.2) can be written as

$$\vec{i} = nFk_fC_o = nF\frac{kT}{h}C_o \exp -\frac{\Delta\vec{G}^o_{\ddagger}}{RT} \qquad 1.3$$

$$\overleftarrow{i} = nFk_bC_r = nF\frac{kT}{h}C_r \exp -\frac{\Delta\overleftarrow{G}^o_{\ddagger}}{RT} \qquad 1.4$$

where

$\vec{i}$, $\overleftarrow{i}$ are the current densities (A cm^{-2}) of the forward and reverse reactions respectively;

$\Delta\vec{G}^o_{\ddagger}$, $\Delta\overleftarrow{G}^o_{\ddagger}$ are the standard free energies of activation;

C_o, C_r are the respective concentrations of O and

R at the electrode surface; and R,F,k,T and h represent the Gas constant, the Faraday constant, the Boltzmann constant, the absolute temperature and Plank's constant respectively.

The standard free energies of activation given in (1.3) and (1.4) will obviously depend on the individual standard free energies of the reactants at the electrode surface. In order to identify these energy states, it is therefore pertinent to first consider the structure of the electrode/electrolyte interface.

A schematic representation of the interfacial region, as proposed by Stern - Graham [3] is illustrated in FIG. 1. It can be seen from this diagram that three distinct regions may be identified close to the electrode surface. The innermost region, adjacent to the metal, contains specifically adsorbed ions (as well as water dipoles) such that the hypothetical inner Helmholtz plane (IHP) passes through their centres. Outside this layer is found an additional layer of non absorbed solvated ions whose centres define the outer Helmholtz plane (OHP). This plane represents the point of closest approach to the electrode surface for all solvated ions. Beyond this plane, extending into the bulk solution, the population of ions of given charge at any point from the surface is determined by the opposing effects of the electrical field and thermal agitation. This region is referred to as the diffuse layer.

In terms of the potential distribution across the interfacial region, the model predicts a linear drop of potential across the metal/(IHP) and (IHP)/(OHP) regions followed by an exponential decay of the potential in the diffuse layer. From FIG. 2, the total potential drop may be written as

$$\Delta\Phi = (\Phi_m - \Phi_1) + (\Phi_1 - \Phi_2) + (\Phi_2 - \Phi_b) \qquad 1.5$$

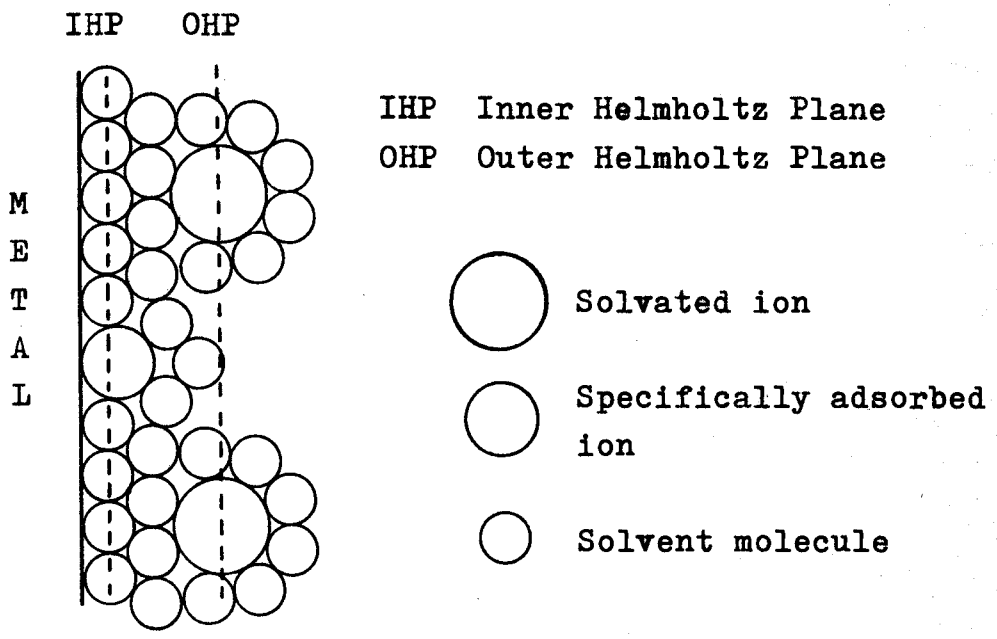

FIG 1 Schematic model of the electrode/ electrolyte interface

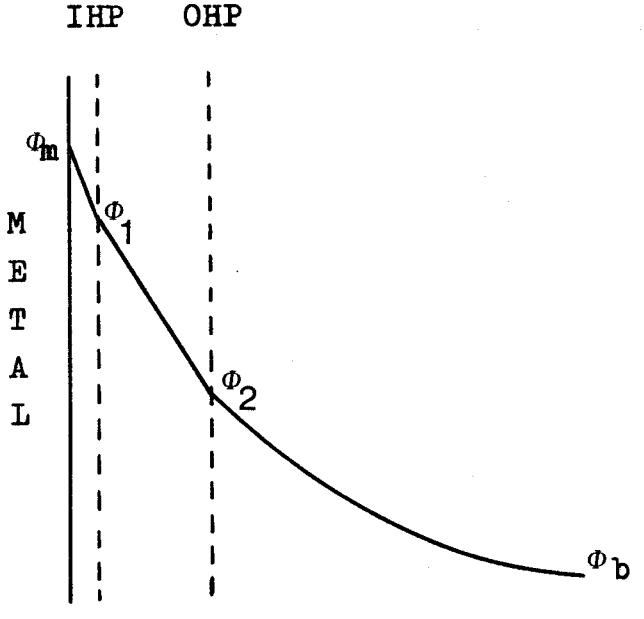

FIG 2 Distribution of charge across the electrode/electrolyte interface

where Φ_m is the inner potential of the metal phase; Φ_1 the potential of the inner Helmholtz plane; Φ_2 the potential of the outer Helmholtz plane and Φ_b the potential of the bulk solution (conventionally taken to be zero).

The theory for the diffuse layer has been derived by Gouy and Chapman [2] showing that the potential Φ_2 may be related to the charge on the solution side of the interface (q_2) up to the outer Helmholtz plane by the equation

$$q_2 = - \frac{\epsilon RTC^{\infty}}{2\pi} \; 2\sinh \frac{zF\Phi_2}{2RT} \qquad 1.6$$

where ϵ is the permittivity of the medium and z the valence of the electrolyte at a bulk concentration C^{∞}.

Since the charge on a metal electrode, q_m, is also governed by the electrode potential and, in the absence of any specific adsorption, may be equated to the charge at the outer Helmholtz plane

$$q_2 = - q_m \qquad 1.7$$

any changes in electrode potential will therefore include changes in Φ_2, i.e.

$$\eta_{effect.} = \eta_{applied} - \Delta\Phi_2 \qquad 1.8$$

where η is the electrode overpotential.

The variation of Φ_2 with electrode potential and concentration is shown in FIG. 3, from which it is evident that the most significant deviations of Φ_2 occur in dilute solutions close to the point of zero charge. At higher concentrations of electrolyte, the changes in Φ_2 are substantially lower over a wide potential range and consequently Φ_2 is usually considered either negligible or at least constant

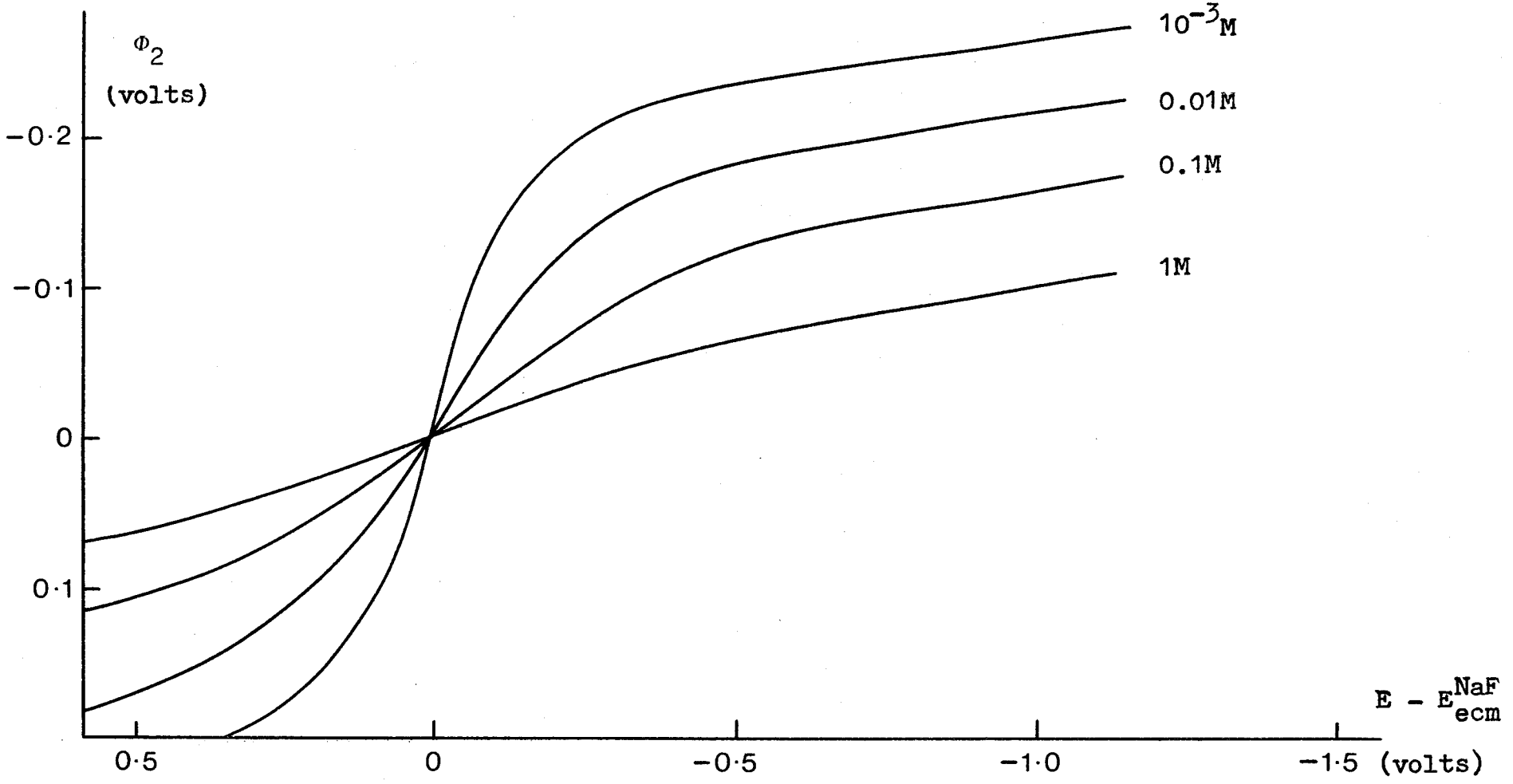

FIG 3 Variation of Φ_2 potential with the applied electrode potential as a function of the electrolyte concentration. The data above relates to aqueous solutions of sodium fluoride on a mercury electrode at 25°C.

in solutions of 1M electrolyte.

Returning now to the free energies of the system, in view of the model of the interfacial region described above, the energy states relating to reaction (1.2) may be summarised as follows:

I the species O in the bulk of the solution and n electrons in the electrode;

II species O in the outer plane of closest approach and n electrons in the electrode;

III the transition state (designated by $\ddagger$)

IV product R in the outer plane of closest approach;

V species R in the bulk of the solution.

Quantitatively, these energy states I - V may be expressed in terms of their electrochemical potentials which in turn may be divided into chemical (μ) and inner potentials (Φ). The standard free energies of states I - V therefore become

$$G_I^o = \mu_o^o + n\mu_e^o - nF\Phi_m \qquad 1.9$$

$$G_{II}^o = \mu_o^o + n\mu_e^o + z_oF\Phi_2 - nF\Phi_m \qquad 1.10$$

$$G_{III}^o = G_{\ddagger}^o \qquad 1.11$$

$$G_{IV}^o = \mu_r^o + z_rF\Phi_2 \qquad 1.12$$

$$G_V^o = \mu_r^o \qquad 1.13$$

where μ_i^o is the standard potential and z_o and z_r are the ionic valences of O and R respectively.

The standard free energies of activation given in (1.3) and (1.4) may now be defined as

$$\Delta\vec{G}_{\ddagger}^o = G_{\ddagger}^o - G_I^o \qquad 1.14$$

and

$$\Delta\overleftarrow{G}_{\ddagger}^o = G_{\ddagger}^o - G_V^o \qquad 1.15$$

A knowledge of $G^o_{\ddagger}$ is necessary therefore, to predict $\vec{i}$, or $\overleftarrow{i}$, from (1.3) or (1.4), but unfortunately the structure and properties of the transition state cannot be explicitly defined except under certain circumstances using quantum statistical methods. Instead, this problem is circumvented by assuming that the potential dependent part of the free energy difference between the states ‡ and II is some fraction α - termed the transfer coefficient - of that between states IV and II. Thus,

$$(G^o_{\ddagger})_e - (G^o_{II})_e = \alpha\left[(G^o_{IV})_e - (G^o_{II})_e\right] \qquad 1.16$$

$$= \alpha nF(\Phi_m - \Phi_2) \qquad 1.17$$

where the subscript denotes the potential dependent part of the standard free energies. Similarly,

$$(G^o_{\ddagger})_e - (G^o_{IV})_e = (\alpha - 1)\left[(G^o_{IV})_e - (G^o_{II})_e\right] \qquad 1.18$$

$$= (\alpha - 1)nF(\Phi_m - \Phi_2) \qquad 1.19$$

For the moment, the transfer coefficient will be assumed to be independent of the potential, but it will be shown in the following section that this assumption is not necessarily valid for all reactions.

As a result of (1.17) and (1.19), the standard free energies of activation for the forward and reverse reactions, given by (1.14) and (1.15) respectively, may be written as a combination of potential dependent and potential independent terms. Thus,

$$\Delta\vec{G}^o_{\ddagger} = G^o_{\ddagger} - G^o_I \qquad 1.14$$

$$= (\Delta\vec{G}^o_{\ddagger})_n + (\Delta\vec{G}^o_{\ddagger})_e$$

$$= (\Delta\vec{G}^o_{\ddagger})_n + \left\{(G^o_{\ddagger})_e - (G^o_{II})_e\right\}$$

$$+ \left\{(G^o_{II})_e - (G^o_I)_e\right\}$$

$$\vec{\Delta G}^{o}_{\ddagger} = (\vec{\Delta G}^{o}_{\ddagger})_n + \alpha nF(\Phi_m - \Phi_2) + z_o F\Phi_2 \qquad 1.20$$

and similarly for the reverse reaction

$$\begin{aligned} \overleftarrow{\Delta G}^{o}_{\ddagger} &= G^{o}_{\ddagger} - G^{o}_{V} \qquad 1.15 \\ &= (\overleftarrow{\Delta G}^{o}_{\ddagger})_n + \left\{(G^{o}_{\ddagger})_e - (G^{o}_{IV})_e\right\} \\ &\quad + \left\{(G^{o}_{IV})_e - (G^{o}_{V})_e\right\} \\ &= (\overleftarrow{\Delta G}^{o}_{\ddagger})_n + (\alpha - 1)nF(\Phi_m - \Phi_2) + (z_o - n)F\Phi_2 \qquad 1.21 \end{aligned}$$

where $(z_o - n)$ is written for z_r. Substitution now for $\vec{\Delta G}^{o}_{\ddagger}$ and $\overleftarrow{\Delta G}^{o}_{\ddagger}$ using (1.20) and (1.21) into (1.3) and (1.4) gives

$$\vec{i} = nF\frac{kT}{h}C_o \exp - \frac{(\vec{\Delta G}^{o}_{\ddagger})_n}{RT} \exp - \frac{(\alpha nF\Phi_m)}{RT} \exp - \frac{(z_o - \alpha n)F\Phi_2}{RT} \qquad 1.22$$

$$\overleftarrow{i} = nF\frac{kT}{h}C_r \exp - \frac{(\overleftarrow{\Delta G}^{o}_{\ddagger})_n}{RT} \exp - \frac{(\alpha - 1)nF\Phi_m}{RT} \exp - \frac{(z_o - \alpha n)F\Phi_2}{RT} \qquad 1.23$$

expressing the rates of the forward and reverse reactions respectively at any potential Φ_m.

At the equilibrium potential Φ^{e}_{m}, the net current density is zero and therefore

$$\vec{i} = \overleftarrow{i} = i'_o \qquad 1.24$$

where i'_o is defined as the apparent exchange current. Thus,

$$i_o' =$$

$$nF \frac{kT}{h} C_o \exp - \frac{(\Delta \vec{G}^o_{\ddagger})_n}{RT} \exp - \frac{(\alpha n F \Phi^e_m)}{RT} \exp - \frac{(z_o - \alpha n) F \Phi^e_2}{RT} \qquad 1.25$$

$$=$$

$$nF \frac{kT}{h} C_r \exp - \frac{(\Delta \overleftarrow{G}^o_{\ddagger})_n}{RT} \exp - \frac{(\alpha - 1) n F \Phi^e_m}{RT} \exp - \frac{(z_o - \alpha n) F \Phi^e_2}{RT} \qquad 1.26$$

where Φ^e_2 is the potential of Φ_2 at the equilibrium potential. Equating (1.25) and (1.26) it is found that

$$\Phi^e_m = \frac{RT}{nF} \left\{ (\Delta \vec{G}^o_{\ddagger})_n - (\Delta \overleftarrow{G}^o_{\ddagger})_n + \ln \frac{C_o}{C_r} \right\} \qquad 1.27$$

$$= \Phi^o_m + \frac{RT}{nF} \ln \frac{C_o}{C_r} \qquad 1.28$$

where Φ^o_m corresponds to the standard electrode potential for the reaction. By substituting (1.28) into (1.25) and (1.26) these expressions may then be written as

$$i_o' = nFk_o'(C_o)^{1-\alpha}(C_r)^{\alpha} \qquad 1.29$$

where k_o' is defined as the apparent standard rate constant and is given by

$$k_o' = \frac{kT}{h} \exp - \frac{(\Delta \vec{G}^o_{\ddagger})_n}{RT} \exp - \frac{(\alpha n F \Phi^o_m)}{RT} \exp - \frac{(z_o - \alpha n) F \Phi^e_2}{RT} \qquad 1.30$$

$$k_o' = \frac{kT}{h} \exp - \frac{(\overleftarrow{\Delta G}^o_{\neq})_n}{RT} \exp - \frac{(\alpha - 1)nF\Phi^o_m}{RT} \exp - \frac{(z_o - \alpha n)F\Phi^e_2}{RT} \qquad 1.31$$

The net cathodic current density at any potential is

$$i = \vec{i} - \overleftarrow{i} \qquad 1.32$$

so that substitution of (1.30) and (1.31) into (1.22) and (1.23) leads to the expression

$$i = nFk_o'C_o \exp - \frac{\alpha nF(\Phi_m - \Phi^o_m)}{RT} \exp - \frac{(z_o - \alpha n)F(\Phi_2 - \Phi^e_2)}{RT}$$

$$- nFk_o'C_r \exp - \frac{(\alpha - 1)nF(\Phi_m - \Phi^o_m)}{RT} \exp - \frac{(z_o - \alpha n)F(\Phi_2 - \Phi^e_2)}{RT} \qquad 1.33$$

In practice Φ_2 and Φ^e_2 are usually not known accurately for solid electrodes, but with reference to FIG. 3 the variation of Φ_2 with potential may be minimised by choosing solutions of high electrolyte concentration. Then, it can be assumed that

$$\Phi_2 - \Phi^e_2 \rightarrow 0 \qquad 1.34$$

and (1.33) approximates to

$$i = nFk_o'C_o \exp - \frac{\alpha nFE}{RT} - nFk_o'C_r \exp - \frac{(\alpha - 1)nFE}{RT} \qquad 1.35$$

writing E for $(\Phi_m - \Phi^o_m)$.

In the special case when

$$\Phi_2 = \Phi^e_2 = 0 \qquad 1.36$$

then (1.35) becomes

$$i = nFk_oC_o \exp - \frac{\alpha nFE}{RT} - nFk_oC_r \exp - \frac{(\alpha - 1)nFE}{RT} \qquad 1.37$$

where k_o is the standard rate constant, defined by (1.30) and (1.31) for $\Phi_2^e = 0$. Thus,

$$k_o' = k_o \exp - \frac{(z_o - \alpha n)F\Phi_2^e}{RT} \qquad 1.38$$

1:iii The transfer coefficient

The transfer coefficient, α , was introduced earlier as the parameter relating the potential to the change in the free energy of activation which it produces. Rigorous mathematical treatments of electron transfer reactions based on quantum mechanical arguments to derive relationships between the transfer coefficient and the standard rate constant have been formulated by several workers; the principal protagonists being Marcus [5 - 7] , Levich [8] , Dogonadze [9] , Hush [10] , Hale [11] , Gerischer [12] and Christov [13] . These theories predict the potential dependent heterogeneous rate constant, k_f for the reduction of neutral molecules to radical anions at metal electrodes to be

$$k_f = \chi Z_{el} \exp - \frac{\lambda}{4RT} \exp-\left[\frac{nF\Phi_r}{2RT} + \frac{n^2F^2\Phi_r^2}{4\lambda RT}\right] \qquad 1.39$$

where χ is the tunnelling coefficient (taken to be unity for adiabatic reactions); Z_{el} is the collision frequency; λ the reorganisation energy and Φ_r the standard overpotential. A dependence of the transfer coefficient on the potential, of the form

$$\alpha = 0{\cdot}5 + \frac{nF(\Phi_r - \Phi_2)}{4\lambda} \qquad 1.40$$

is also predicted, leading to an expected curvature of Tafel plots. The potential dependence of the transfer coefficient can perhaps be better described qualitatively by considering the potential energy profiles for electrode mechanisms [14,15] . In FIGS. 4 and 5 the free energy vs. reaction coordinate profiles for both the reactant and product states are shown for systems with both high and low activation energies respectively in the absence of a potential

difference across the double layer. As the reactant system moves along the reaction coordinate due to the appropriate nuclear motions, the potential energy surface rises and intersects the potential energy surface for the product system. At this point of intersection, the free energies of the electronic states in the electrode and in the reactant are the same and, in accordance with the Frank - Condon principle, electrons can rapidly tunnel from the metal to the reactant.

If a potential $\Delta\Phi$ is applied across the double layer, the free energy of the electrons in the metal, and hence the O + ne state are changed by an amount $- nF\Delta\Phi$. It has been shown [4] that the free energy of activation in the presence of the field $(\Delta G^{o}_{\ddagger})_{\Delta\Phi}$ is related to that without the field $(\Delta G^{o}_{\ddagger})_{n}$ by

$$(\Delta G^{o}_{\ddagger})_{\Delta\Phi} = (\Delta G^{o}_{\ddagger})_{n} - \alpha nF\Delta\Phi \qquad 1.41$$

if α is the ratio of the slope of the reactant curve to the sum of the absolute values of the slopes of the reactant and product curves, i.e.

$$\alpha = \frac{\tan\gamma}{\tan\gamma + |\tan\psi|} \qquad 1.42$$

where γ and ψ are defined in FIGS. 4 and 5.

From this equation, it is seen that for α to assume the often found value of 0·5, the relative slopes of the free energy profiles must be approximately equal at the point of intersection. It is evident from FIGS. 4 and 5, that this is most likely with reactions of high activation energy (i.e. low $k^{!}_{o}$) where the point of intersection occurs far from the free energy minima of the system. As the point of intersection moves along the product free energy curve as potential is applied to the system, the gradients of the curves remain comparatively constant, so that both γ and ψ, and consequently α are unchanged with

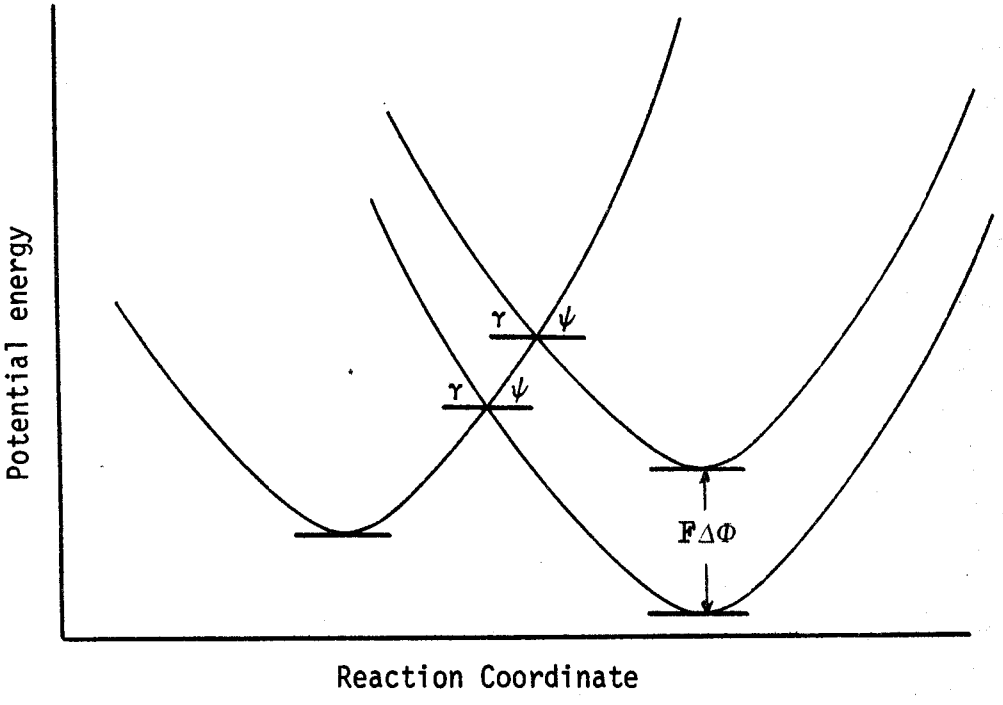

FIG 4 The influence of overpotential on the transfer coefficient for a reaction with low k_o'

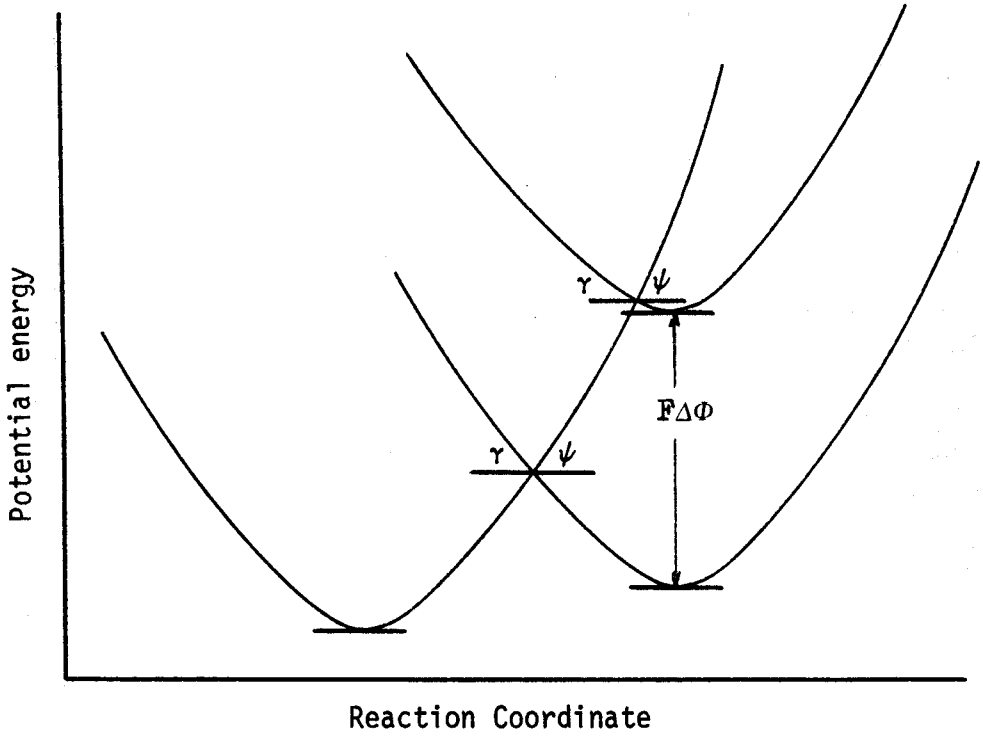

FIG 5 The influence of overpotential on the transfer coefficient for a reaction with high k_o'

potential. In contrast, with low activation energy systems (i.e. high k_o'), the point of intersection occurs close to the free energy minimum for the product system, where the relative slopes of the two free energy profiles experience significant changes as the point of intersection moves along the curve due to applied potential. The value of α, therefore, determined by (1.42) will vary with potential, but only for systems with low activation energies.

1:iv The study of electrode reactions

The study of electrode processes has been influenced in recent years by the development of a wide variety of experimental methods to define, both qualitatively and quantitatively, each of the steps in any given reaction sequence.

A characteristic feature of all heterogeneous reactions and in particular, electrode reactions, is the role of mass transport processes in determining the overall rate of reaction. In many cases, the mass transfer process is of a comparable rate to the rate of the electron transfer reaction and it is therefore not possible to measure directly the rate of electron transfer. Under these circumstances, it is necessary to increase the rate of mass transfer so that it is no longer the rate determining step in the overall reaction sequence. It is the various methods by which this has been achieved that account for a large proportion of the experimental techniques developed in electrochemistry.

Originally, in the early electrochemical experiments conducted by Heyrovsky [16], mass transfer was controlled by diffusion in the presence of an excess of inert electrolyte - termed supporting electrolyte - to reduce migration effects between the electrodes. These experiments were usually performed at a dropping mercury electrode (DME) which produces a clean, uncontaminated electrode surface every few seconds. The main limitation of this technique is the rate of electrode reaction that it may measure: under normal conditions of diffusion controlled mass transfer the upper limit is of the order 10^{-2}cm s^{-1}.

Convective stirring of the solution, coupled with the use of a solid electrode, albeit with possible problems of surface contamination, is able to increase the upper limit by approximately an order of magnitude to around 0·1cm s^{-1}. An excellent example of

convective stirring is provided by the rotating disc electrode [17]. Here the thickness of the diffusion layer adjacent to the electrode surface may be varied as a function of the electrode rotation rate, leading to increased concentration gradients and therefore enhanced mass flux at the electrode surface (see 2:i) at high rotation rates. Unfortunately, very few electrode geometries lend themselves to such a hydrodynamic treatment and, as a result, convective stirring is generally limited to electrodes similar in type to the rotating disc electrode. A technique based on a micro-ring electrode in turbulent pipe flow conditions has recently demonstrated the ability to measure the rates of electron transfer processes with a claimed upper limit of 5cm s^{-1} [18]. The use of a micro-ring electrode takes advantage of the steep concentration gradients at the upstream edge of a ring electrode in turbulent pipe flow conditions: the thinner the electrode ring, the higher is the average mass transfer rate to the reaction surface. In addition, the variation of potential along a tubular electrode due to ohmic losses is considerably reduced with thin electrodes thereby allowing more accurate potential control in kinetic studies. Initial studies with this technique for the determination of the rate of electron transfer of the ferro/ferricyanide system have shown good agreement with the values obtained by other workers using alternative techniques. Faster electrode reactions and the measurement of fast homogeneous reactions preceding the charge transfer are also reported to be under investigation [18].

Both the rotating disc and micro-ring electrode are examples of steady state techniques where the concentration profile and consequently the mass transfer rate remain practically invariant with time allowing measurements to be taken over a relatively long time period ($\sim$1s — 100s).

In an alternative approach to increasing rates of mass transfer, the time dependent response of an

electrode may be monitored following the instantaneous stepped change of the control parameter on the electrode system. This takes advantage of the fact that immediately after the perturbation, large concentration gradients exist at the electrode surface before relaxing, in a timescale up to $\sim$ 10 s, to the steady state situation. Consequently, high rates of mass transfer are obtained at short times only. Despite this limitation, numerous experimental techniques have been developed to exploit this situation, aided by the parallel development of sophisticated fast response potentiostats.

The principal techniques for measuring the rates of electron transfer reactions are listed in TABLE 1 indicating the maximum measurable rate of electron transfer for each technique. Kinetic information is extracted from the time dependent response of the electrode following perturbation by extrapolation of the dependent variable to infinite mass transfer rates. For potentiostatic and galvanostatic experiments this is found at time $t = 0$, while for A.C. techniques extrapolation to infinite frequency is required.

At very short times, however, non faradaic processes such as double layer charging/discharging and coupled or parallel surface processes are particularly prominent, in addition to the faradaic reaction and this can often lead to difficulty in accurate extrapolation procedures giving rise to misleading results. These non faradaic processes, therefore, effectively impose the upper limit of rate constants able to be measured by these techniques. Recently, doubt has been expressed concerning the measurement of very fast electrode reactions amid conflicting results obtained for the same system using different experimental techniques. In particular, Aoyagui and coworkers [55] have measured apparent standard rate constants with the galvanostatic double pulse method for several nitroaromatic compounds in N,N Dimethylformamide solutions and found them all to

TABLE 1

EXPERIMENTAL TECHNIQUE	MAXIMUM k_o (cm s^{-1})	REFERENCE
Non steady state		
Potential step	1	(19) - (21)
Cyclic voltammetry	0•5	(22) - (26)
Current step	0•2	(27) - (31)
Galvanostatic double pulse	1	(32) - (36)
Coulostatic reverse pulse	5	(37)
A C Impedance	10	(38) - (46)
Steady state		
Polarography	0•01	(47) - (48)
Rotating disc	0•1	(49) - (52)
Micro ring	5	(18)
Micro electrode	1	(53),(54),(56),(57)

be approximately an order of magnitude lower than those measured by faradaic rectification [46]. This prompted Aoyagui to doubt the existence of fast electrode reactions beyond the reach of existing techniques, pointing out that the higher rates observed with the other techniques are probably due to inadequate compensation for ohmic drop, especially with regard to the faradaic rectification method.

In this work, a third method of increasing mass transfer rates is advocated; a method which does not require forced convective stirring nor does it require measurements to be made at short times. The technique is simply to produce electrodes of sufficiently small radius such that they can be assumed to be operating in a spherical diffusion field. Under these conditions, the mass transfer rate is enhanced above the rate in a linear diffusion field by an additional steady state component inversely proportional to the radius of the electrode, so that under pseudo steady state conditions (i.e. very slow linear potential sweep) the mass transfer rate is determined by the steady state term only. The basic principle of this technique has already been effectively demonstrated by Fleischmann et al. [53,54] for the Hg/Hg^{2+} reaction by the nucleation of mercury droplets onto a vitreous carbon electrode plunged into a mercury pool counter electrode, thereby forming an ultra thin layer cell. The mercury droplets thus formed then served as very small electrodes to which spherical diffusion was assumed to occur. With these small radii hemispheres however, ($\sim$10nm) inconveniently small currents are obtained and consequently these experiments were conducted with an ensemble of approximately 10^6 spheres.

Distinct advantages would therefore accrue from a single 'microelectrode' of known radius able to operate under a wide range of experimental conditions without the necessity of pre-nucleation as an in situ experimental variable.

Although recent investigations have been

reported, examining the voltammetric behaviour of 8μm carbon fibres, under potential sweep and potential step conditions [56], electrodes of even smaller dimensions are characterised in this work for both electron transfer reactions and homogeneous reactions preceding an electron transfer step.

CHAPTER 2 DIFFUSION TO MICROELECTRODES

2:i Fick's Laws of Diffusion

Although essentially a random process, the diffusion of any species through a particular medium is subject to two very important empirical laws first postulated by Fick in 1855 [58]. His first law relates the flux of species i, J_i, to the concentration gradient of species i in the medium

$$J_i = - D_i \frac{\partial C_i}{\partial x} \qquad 2.1$$

where D_i is the diffusion coefficient of species i and has the units $cm^2\ s^{-1}$. The units of J_i are mol $cm^{-2}\ s^{-1}$. Since Fick's first law contains no time dependence, it is only applicable to cases of steady state diffusion. Of more fundamental importance to electrochemists is the knowledge of how the concentration of species i varies with time and distance away from the electrode surface. By considering the fluxes passing through two planes placed at a distance x and $(x + \delta x)$ from the electrode surface ($x = 0$), the rate of change of concentration of species i with time is given by

$$\frac{\partial C_i}{\partial t} = \frac{J(x) - J(x + \delta x)}{\delta x} \qquad 2.2$$

$$= \frac{\delta J}{\delta x} \qquad 2.3$$

whereupon substitution of (2.1) into (2.2) gives

$$\frac{\partial C_i}{\partial t} = \frac{\partial}{\partial x}\left(D_i \frac{\partial C_i}{\partial x}\right) \qquad 2.4$$

$$= D_i \frac{\partial^2 C_i}{\partial x^2} \qquad 2.5$$

which is known as Fick's second law. This law, or the equivalent form for cylindrical or spherical diffusion, provides the basis for solution of all time dependent diffusion problems in electrochemistry.

The solution of equation (2.5) and associated equations, requires both the initial and boundary conditions to be defined prior to any integration procedure. These conditions are normally determined by the experimental conditions. In most cases where the electrode reaction is a simple electron transfer reaction, equation (2.5) may be evaluated by means of the Laplace transform method [59], to give the concentrations of species as a function of distance from the electrode surface and of time from the start of electrolysis.

Randles [60] and Sevcik [61], both working independently, were first to solve the time dependent diffusion problem for a reversible reaction at a planar electrode where the potential of the working electrode is varied linearly with time. Their results are presented in the form of a current - potential curve, the potential axis embodying the time dependence. This theory was soon extended by Delahay [62] to cover totally irreversible charge transfer reactions before Matsuda and Ayabe [63] in re-deriving the Randles-Sevcik and Delahay theories were able to extend the treatment further to include quasi - reversible reactions. In addition, the theory of linear sweep voltammetry was soon applied to electrodes of other geometries: reversible reactions on cylindrical [64 - 66] and spherical electrodes [67,68] were investigated and even totally irreversible reactions on spherical electrodes were considered [69]. In many cases the mathematical complexity of the diffusion equations prevented extensive study of the reactions in all but the simplest of systems. The mathematical approaches employed in these studies included: Laplace transform techniques; direct numerical solution using finite difference techniques

and conversion of the boundary value problem to an integral equation. Of these, the Laplace transform is by far the simplest method but unfortunately may only be applied to relatively simple electrode reactions. The remaining two approaches are, however, more generally applicable at the expense of being more tedious to evaluate.

More recently, Oldham [70] and Saveant [71] have developed, independently, new and similar approaches to examine the role of diffusion in electrochemical reactions. Each defines a quantity, a 'semi - integral' according to Oldham and a 'convolution integral' according to Saveant, which is related to both the surface and bulk concentrations of the electroactive species. This quantity is shown to be independent of the path between the initial and final potentials applied to the working electrode for reversible reactions and furthermore, rapidly approaches a constant value at the diffusion controlled limiting current. Both authors, in a series of papers [72 - 81] have developed their respective techniques to cover a wide range of reaction schemes including both reversible and irreversible charge transfer reactions at a planar electrode. In addition, each author has considered corrections to their respective planar models to account for spherical effects at mercury drop electrodes [82 - 84]. These corrections are applicable, however, only to cases where the magnitude of the spherical effect is small and cannot therefore be applied to very small spherical electrodes.

In these cases, it is necessary to consider the diffusion of species in a totally spherical diffusion field. In the following pages the process of diffusion in a semi - infinite spherical diffusion field is examined showing that the total current on a spherical electrode comprises two components - a time dependent term equal to the current on a planar electrode of equivalent area and a steady state

term dependent on the electrode radius. It is shown that at high sweep rates the total current is dominated by the time dependent term while at sufficiently slow sweep rates it approaches the steady state term. Under both fast and slow linear potential sweep conditions, the theory is then further developed to include irreversible electrode reactions on very small electrodes, showing that for suitably small electrodes kinetic parameters should be readily obtained from the analysis of experimental current - potential curves.

2:ii Reversible Reactions at a Planar Electrode

Consider the simple electrochemical reaction

$$O + ne = R \qquad 2.6$$

involving either the gain or loss of n electrons from a species O to form a product R where both O and R are soluble in the reaction medium. For a reversible process where the rate of electron transfer is high compared to the rate of diffusion of electroactive species to the electrode surface, the concentrations of species O and R may be related to the applied potential by the Nernst equation

$$E = E_o + \frac{RT}{nF} \ln \frac{C_o}{C_r} \qquad 2.7$$

where E_o is the standard electrode potential, E is the applied potential and R, T and F have their usual significance. The concentrations of O and R at the electrode surface are represented by C_o and C_r respectively. For the case where the potential of the electrode (E_t) is varied in the form

$$E_t = E_1 - at \qquad 2.8$$

where E_1 is the initial potential set at a value where no net reaction occurs and a is the ramp speed, the surface concentrations of O and R at the initial potential will assume the bulk concentrations of their respective species, denoted by C_o^∞ and C_r^∞ . Thus

$$E_1 = E_o + \frac{RT}{nF} \ln \frac{C_o^\infty}{C_r^\infty} \qquad 2.9$$

As the potential of the electrode changes, according to (2.8) then the surface concentrations of O and R must also change to maintain Nernstian equilibrium at the electrode surface. Therefore at time t,

$$E_t = E_o + \frac{RT}{nF} \ln \frac{C_o}{C_r} \qquad 2.10$$

Equations (2.8),(2.9) and (2.10) may be combined to eliminate E_1, E_t and E_o leaving

$$\frac{RT}{nF} \ln \frac{C_o^\infty}{C_r^\infty} = \frac{RT}{nF} \ln \frac{C_o}{C_r} - at \qquad 2.11$$

or, alternatively

$$\frac{C_o}{C_r} = \frac{C_o^\infty}{C_r^\infty} \exp - \frac{anFt}{RT} \qquad 2.12$$

This may be abbreviated for convenience to

$$\frac{C_o}{C_r} = w \exp(-bt) \qquad 2.13$$

where

$$w = \frac{C_o^\infty}{C_r^\infty} \qquad 2.14$$

which is normally chosen to be large, and

$$b = \frac{anF}{RT} \qquad 2.15$$

Combining now (2.13) with the diffusion of species O and R towards the electrode surface, the diffusion equations representing semi - infinite diffusion to a planar surface may be written as

$$\frac{\partial C_o}{\partial t} = D_o \frac{\partial^2 C_o}{\partial x^2} \qquad 2.16$$

$$\frac{\partial C_r}{\partial t} = D_r \frac{\partial^2 C_r}{\partial x^2} \qquad 2.17$$

The initial conditions are

$$t = 0 \qquad 0 < x < \infty \qquad C_o = C_o^{\infty} \tag{2.18}$$

$$C_r = C_r^{\infty} \tag{2.19}$$

and the boundary conditions

$$t > 0 \qquad x = \infty \qquad C_o = C_o^{\infty} \tag{2.20}$$

$$C_r = C_r^{\infty} \tag{2.21}$$

$$x = 0 \qquad i_{pl} = nFD_o \frac{\partial C_o}{\partial x} = -nFD_r \frac{\partial C_r}{\partial x} \tag{2.22}$$

$$\frac{C_o}{C_r} = w \exp(-bt) \tag{2.23}$$

For reactions where O and R are similar, it may be assumed that

$$D_o \simeq D_r = D \tag{2.24}$$

Furthermore, the boundary condition (2.22) gives rise to the additional equality

$$C_o + C_r = C_o^{\infty} + C_r^{\infty} \tag{2.25}$$

from which C_r may be substituted into (2.23) to give after rearrangement

$$C_o = \frac{(C_o^{\infty} + C_r^{\infty})\, w \exp(-bt)}{1 + w \exp(-bt)} \tag{2.26}$$

A more appropriate form of (2.26) is obtained by expanding the equation binomially, thus

$$C_o = (C_o^\infty + C_r^\infty)\, w \exp(-bt)\left[1 + w \exp(-bt)\right]^{-1}$$

$$= (C_o^\infty + C_r^\infty)\, w \exp(-bt)\left[1 - w \exp(-bt) + w^2 \exp(-2bt) - w^3 \exp(-3bt) + \ldots.\right]$$

$$= (C_o^\infty + C_r^\infty) \sum_{m=1}^{\infty} (-1)^{m+1} w^m \exp(-mbt) \qquad 2.27$$

The corresponding expression for C_r is given by

$$C_r = (C_o^\infty + C_r^\infty) \sum_{m=1}^{\infty} (-1)^m w^m \exp(-mbt) + (C_o^\infty + C_r^\infty) \qquad 2.28$$

The diffusion equations (2.16) and (2.17) may now be solved, subject to the initial and boundary conditions given above with the aid of the Laplace transform technique. It can be shown that the Laplace transform of (2.16) is given by [59]

$$\frac{d^2\overline{C}_o}{dx^2} - q^2\overline{C}_o + \frac{C_o^\infty}{D} = 0 \qquad 2.29$$

and similarly for (2.17)

$$\frac{d^2\overline{C}_r}{dx^2} - q^2\overline{C}_r + \frac{C_r^\infty}{D} = 0 \qquad 2.30$$

where

$$q^2 = \frac{s}{D} \qquad 2.31$$

and s is the transform variable with $\overline{C}_o$ and $\overline{C}_r$ denoting the transforms of the concentrations of species O and R respectively.

Equations (2.29) and (2.30) are now in the form of ordinary second order differential equations for

which the general solutions are

$$\overline{C}_o = \frac{C_o^\infty}{s} + K \exp(qx) + L \exp(-qx) \qquad 2.32$$

and

$$\overline{C}_r = \frac{C_r^\infty}{s} + M \exp(qx) + N \exp(-qx) \qquad 2.33$$

where K,L,M and N are arbitrary constants to be determined from the boundary conditions. At $x = \infty$, the Laplace transforms of (2.20) and (2.21) become

$$\overline{C}_o = \frac{C_o^\infty}{s} \qquad 2.34$$

$$\overline{C}_r = \frac{C_r^\infty}{s} \qquad 2.35$$

so that applying (2.34) and (2.35) to (2.32) and (2.33) respectively, at $x = \infty$, it is found that

$$M = K = 0 \qquad 2.36$$

Similarly, the boundary conditions (2.27) and (2.28) at x = 0 transform to

$$\overline{C}_o = (C_o^\infty + C_r^\infty) \sum_{m=1}^{\infty} \frac{(-1)^{m+1} w^m}{s + mb} \qquad 2.37$$

and

$$\overline{C}_r = (C_o^\infty + C_r^\infty) \sum_{m=1}^{\infty} \frac{(-1)^m w^m}{s + mb} + (C_o^\infty + C_r^\infty) \qquad 2.38$$

Therefore, combining (2.32) and (2.37) a value for L is obtained

$$L = (C_o^\infty + C_r^\infty) \sum_{m=1}^{\infty} \frac{(-1)^{m+1} w^m}{s + mb} - \frac{C_o^\infty}{s} \qquad 2.39$$

which may then be substituted back into (2.32) to give

$$\bar{C}_o = (C_o^\infty + C_r^\infty) \exp(-qx) \sum_{m=1}^{\infty} \frac{(-1)^{m+1} w^m}{s + mb} - \frac{C_o^\infty}{s} \exp(-qx) + \frac{C_o^\infty}{s} \qquad 2.40$$

In a similar manner, N may be eliminated from (2.33) and (2.38) resulting in

$$\bar{C}_r = (C_o^\infty + C_r^\infty) \exp(-qx) \sum_{m=1}^{\infty} \frac{(-1)^m w^m}{s + mb} + \frac{C_o^\infty}{s} \exp(-qx) + \frac{C_r^\infty}{s} \qquad 2.41$$

The current density may now be determined with the aid of the boundary condition (2.22). First, taking the Laplace transform of (2.22)

$$\bar{i}_{pl} = nFD \frac{d\bar{C}_o}{dx} = -nFD \frac{d\bar{C}_r}{dx} \qquad 2.42$$

and then differentiating either (2.40) or (2.41) with respect to x, at x = 0

$$\bar{i}_{pl} = \frac{D^{\frac{1}{2}} F C_o^\infty}{s^{\frac{1}{2}}} + D^{\frac{1}{2}} s^{\frac{1}{2}} F (C_o^\infty + C_r^\infty) \sum_{m=1}^{\infty} \frac{(-1)^m w^m}{s + mb} \qquad 2.43$$

using (2.31).

The inverse transformation of (2.43) from Laplace transform tables [59], now leads to the

current density at a planar electrode. Thus,

$$i_{pl} = \frac{nFD^{\frac{1}{2}}C_o^{\infty}}{(\pi t)^{\frac{1}{2}}} + \frac{nFD^{\frac{1}{2}}(C_o^{\infty} + C_r^{\infty})}{(\pi t)^{\frac{1}{2}}} \sum_{m=1}^{\infty} (-1)^m w^m$$

$$- \frac{2nFD^{\frac{1}{2}}(C_o^{\infty} + C_r^{\infty})}{\pi^{\frac{1}{2}}} \sum_{m=1}^{\infty} (-1)^m w^m (mb)^{\frac{1}{2}} \exp(-mbt) \int_0^{\sqrt{mbt}} \exp \xi^2 \, d\xi \qquad 2.44$$

where ξ is a dummy variable.

Equation (2.44) may be simplified by noting that

$$\frac{nFD^{\frac{1}{2}}(C_o^{\infty} + C_r^{\infty})}{(\pi t)^{\frac{1}{2}}} \sum_{m=1}^{\infty} (-1)^m w^m = - \frac{nFD^{\frac{1}{2}}(C_o^{\infty} + C_r^{\infty})w}{(\pi t)^{\frac{1}{2}}(1 + w)} \qquad 2.45$$

$$= - \frac{nFD^{\frac{1}{2}}C_o^{\infty}}{(\pi t)^{\frac{1}{2}}} \qquad 2.46$$

from the definition of w in (2.14). Hence, (2.44) may finally be written as

$$i_{pl} =$$

$$- \frac{2nFD^{\frac{1}{2}}(C_o^{\infty} + C_r^{\infty})}{\pi^{\frac{1}{2}}} \sum_{m=1}^{\infty} (-1)^m w^m (mb)^{\frac{1}{2}} \exp(-mbt) \int_0^{\sqrt{mbt}} \exp \xi^2 \, d\xi \qquad 2.47$$

This expression has been derived by Sevcik [61].

Clearly, the maximum value of (2.47) will occur when

$$\frac{di_{pl}}{dt} = 0 \qquad 2.48$$

i.e.

$$\sum_{m=1}^{\infty} (-1)^m w^m (mb)^{3/2} \exp(-mbt) \int_0^{\sqrt{mbt}} \exp \xi^2 \, d\xi$$

$$= \sum_{m=1}^{\infty} \frac{(-1)^m w^m (mb)}{2t^{\frac{1}{2}}} \qquad 2.49$$

from which the maximum current density is observed to be some function of $b^{\frac{1}{2}}$, occurring at a fixed potential (bt). The evaluation of (2.47) and (2.49) is complex and is not presented here.

However, the function

$$F(x) = \exp(-x^2) \int_0^x \exp \xi^2 \, d\xi \qquad 2.50$$

has been evaluated numerically by Miller and Gordon [85] and shown to have a maximum value of 0·541 when x = 0·924. Substitution of these values into (2.47) with the appropriate change of variable therefore gives the maximum instantaneous current density at a planar electrode,

$$i_{pl} = \frac{2nFD^{\frac{1}{2}}(C_o^{\infty} + C_r^{\infty})}{(\pi t)^{\frac{1}{2}}} \sum_{m=1}^{\infty} (-1)^{m+1} w^m (0{\cdot}924)(0{\cdot}541)$$

$$= \frac{nFD^{\frac{1}{2}}(C_o^{\infty} + C_r^{\infty})}{(\pi t)^{\frac{1}{2}}} \sum_{m=1}^{\infty} (-1)^{m+1} w^m$$

$$= \frac{nFD^{\frac{1}{2}}C_o^{\infty}}{(\pi t)^{\frac{1}{2}}} \qquad 2.51$$

2:iii Reversible Reactions at a Spherical Electrode

An analogous argument to that used for planar electrodes may also be applied to spherical electrodes. In this case, however, the form of the diffusion equations must be amended to account for spherical diffusion.

In spherical coordinates, equations (2.16) and (2.17) become

$$\frac{\partial C_o}{\partial t} = D_o \frac{\partial^2 C_o}{\partial r^2} + \frac{2D_o}{r} \frac{\partial C_o}{\partial r} \qquad 2.52$$

$$\frac{\partial C_r}{\partial t} = D_r \frac{\partial^2 C_r}{\partial r^2} + \frac{2D_r}{r} \frac{\partial C_r}{\partial r} \qquad 2.53$$

where r is the distance measured from the centre of the electrode (of radius r_o). Once again, the approximation

$$D_o \simeq D_r = D \qquad 2.24$$

is made.

The initial conditions are now,

$$t = 0 \qquad r_o < r < \infty \qquad C_o = C_o^\infty \qquad 2.54$$

$$C_r = C_r^\infty \qquad 2.55$$

and the boundary conditions,

$$t > 0 \qquad r = \infty \qquad C_o = C_o^\infty \qquad 2.56$$

$$C_r = C_r^\infty \qquad 2.57$$

$$r = r_o \qquad i_s = nFD \frac{\partial C_o}{\partial r} = - nFD \frac{\partial C_r}{\partial r} \qquad 2.58$$

together with the potential dependent boundary condition at $r = r_o$,

$$C_o = (C_o^\infty + C_r^\infty) \sum_{m=1}^{\infty} (-1)^{m+1} w^m \exp(-mbt) \qquad 2.27$$

and

$$C_r = (C_o^\infty + C_r^\infty) \sum_{m=1}^{\infty} (-1)^m w^m \exp(-mbt) + (C_o^\infty + C_r^\infty) \qquad 2.28$$

As before, taking the Laplace transforms of (2.52) and (2.53) subject to the initial conditions (2.54) and (2.55)

$$\frac{d^2\overline{C}_o}{dr^2} + \frac{2}{r}\frac{d\overline{C}_o}{dr} - q^2\overline{C}_o + \frac{C_o^\infty}{D} = 0 \qquad 2.59$$

$$\frac{d^2\overline{C}_r}{dr^2} + \frac{2}{r}\frac{d\overline{C}_r}{dr} - q^2\overline{C}_r + \frac{C_r^\infty}{D} = 0 \qquad 2.60$$

The substitution,

$$\overline{V} = r\overline{C} \qquad 2.61$$

allows (2.59) and (2.60) to be simplified to

$$\frac{d^2\overline{V}_o}{dr^2} - q^2\overline{V}_o + \frac{rC_o^\infty}{D} = 0 \qquad 2.62$$

$$\frac{d^2\overline{V}_r}{dr^2} - q^2\overline{V}_r + \frac{rC_r^\infty}{D} = 0 \qquad 2.63$$

for which the general solutions are

$$\overline{V}_o = G \exp(qr) + H \exp(-qr) + \frac{rC_o^\infty}{s} \qquad 2.64$$

$$\overline{V}_r = P \exp(qr) + Q \exp(-qr) + \frac{rC_r^\infty}{s} \qquad 2.65$$

or, in view of (2.61)

$$\overline{C}_o = \frac{G}{r} \exp(qr) + \frac{H}{r} \exp(-qr) + \frac{C_o^\infty}{s} \qquad 2.66$$

$$\overline{C}_r = \frac{P}{r} \exp(qr) + \frac{Q}{r} \exp(-qr) + \frac{C_r^\infty}{s} \qquad 2.67$$

where G,H,P and Q are arbitrary constants to be determined from the boundary conditions.

Laplace transforming the boundary conditions (2.56) and (2.57) at $r = \infty$, then applying them to (2.66) and (2.67) it is found that

$$G = P = 0 \qquad 2.68$$

The Laplace transforms of the boundary conditions (2.27) and (2.28) have been given earlier by (2.37) and (2.38) for the case of linear diffusion. Applying these to (2.66) and (2.67) respectively, expressions for the constants H and Q are obtained; thus

$$H = (C_o^\infty + C_r^\infty)\, r_o \sum_{m=1}^{\infty} \frac{(-1)^{m+1}\, w^m}{s + mb} \exp(qr_o) - \frac{r_o C_o^\infty}{s} \exp(qr_o) \qquad 2.69$$

$$Q = (C_o^\infty + C_r^\infty)\, r_o \sum_{m=1}^{\infty} \frac{(-1)^{m}\, w^m}{s + mb} \exp(qr_o) + \frac{r_o C_o^\infty}{s} \exp(qr_o) \qquad 2.70$$

Substituting these expressions for H and Q

back into (2.66) and (2.67) respectively, the concentration profiles for O and R in Laplace space are defined by

$$\bar{C}_o = \frac{(C_o^\infty + C_r^\infty)}{r} r_o \sum_{m=1}^{\infty} \frac{(-1)^{m+1} w^m}{s + mb} \exp(-q(r - r_o))$$

$$+ \frac{C_o^\infty}{s} - \frac{r_o C_o^\infty}{rs} \exp(-q(r - r_o)) \qquad 2.71$$

and

$$\bar{C}_r = \frac{(C_o^\infty + C_r^\infty)}{r} r_o \sum_{m=1}^{\infty} \frac{(-1)^{m} w^m}{s + mb} \exp(-q(r - r_o))$$

$$+ \frac{C_r^\infty}{s} + \frac{r_o C_o^\infty}{rs} \exp(-q(r - r_o)) \qquad 2.72$$

As before, in the linear case, the current density at a spherical electrode may be determined by first taking the Laplace transform of the boundary condition (2.58), thus

$$\bar{i}_s = nFD \frac{d\bar{C}_o}{dr} = - nFD \frac{d\bar{C}_r}{dr} \qquad 2.73$$

and then differentiating either (2.71) or (2.72) with respect to r, at $r = r_o$, to obtain

$$\bar{i}_s = - nFD \frac{(C_o^\infty + C_r^\infty)}{r_o} \sum_{m=1}^{\infty} \frac{(-1)^{m+1} w^m}{s + mb} + \frac{nFDC_o^\infty}{r_o s}$$

$$- nFDq(C_o^\infty + C_r^\infty) \sum_{m=1}^{\infty} \frac{(-1)^{m+1} w^m}{s + mb} + \frac{nFDqC_o^\infty}{s} \qquad 2.74$$

If (2.74) is now compared to the equivalent expression describing the transform of the current on a planar electrode (2.43), it can be seen that (2.74) may be written as

$$\bar{i}_s = \bar{i}_{pl} + \frac{nFDC_o^\infty}{r_o} + \frac{nFD(C_o^\infty + C_r^\infty)}{r_o} \sum_{m=1}^{\infty} \frac{(-1)^m w^m}{s + mb} \qquad 2.75$$

This expression may be inverted, with the aid of tables of Laplace transforms, to

$$i_s = i_{pl} + \frac{nFDC_o^\infty}{r_o} + \frac{nFD(C_o^\infty + C_r^\infty)}{r_o} \sum_{m=1}^{\infty} (-1)^m w^m \exp(-mbt) \qquad 2.76$$

and further simplified by noting that

$$C_o = (C_o^\infty + C_r^\infty) \sum_{m=1}^{\infty} (-1)^{m+1} w^m \exp(-mbt) \qquad 2.27$$

leading finally to the expression

$$i_s = i_{pl} + \frac{nFD(C_o^\infty - C_o)}{r_o} \qquad 2.77$$

This shows that the total current density at a spherical electrode is composed of two terms: the current to a planar electrode of equivalent area and a steady state term dependent upon the radius of the electrode. Now it was shown earlier that the maximum instantaneous current density at a planar electrode was given by

$$i_{pl} = \frac{nFD^{\frac{1}{2}}C_o^\infty}{(\pi t)^{\frac{1}{2}}} \qquad 2.51$$

so that incorporating this into (2.77), the maximum instantaneous current density at a spherical electrode becomes

$$i_s = \frac{nFD^{\frac{1}{2}}C_o^{\infty}}{(\pi t)^{\frac{1}{2}}} + \frac{nFD(C_o^{\infty} - C_o)}{r_o} \qquad 2.78$$

This equation clearly has two limiting forms. At short times, corresponding to fast potential sweep rate voltammetry,

$$\frac{nFD^{\frac{1}{2}}C_o^{\infty}}{(\pi t)^{\frac{1}{2}}} \gg \frac{nFD(C_o^{\infty} - C_o)}{r_o} \qquad 2.79$$

and the current, i_s, will be governed by the transient term, i_{pl}. i.e. at high sweep rates

$$i_s \sim i_{pl} \qquad 2.80$$

Conversely, at long times, corresponding to slow potential sweep rate voltammetry,

$$\frac{nFD^{\frac{1}{2}}C_o^{\infty}}{(\pi t)^{\frac{1}{2}}} \ll \frac{nFD(C_o^{\infty} - C_o)}{r_o} \qquad 2.81$$

and the current is now determined by the steady state current

$$i_s \sim \frac{nFD(C_o^{\infty} - C_o)}{r_o} \qquad 2.82$$

A measure of the time required for the steady state to become established can be gained by inserting typical values of $D = 10^{-5}cm^2\ s^{-1}$, $r_o = 10^{-4}cm$ and $C_o^{\infty} = 2 \times 10^{-6}mol\ cm^{-3}$ into (2.78) at the diffusion controlled limiting current (i.e. when $C_o = 0$). With these values, it is calculated that the transient term

will contribute less than 1% of the total current in approximately three seconds.

It may be justifiably claimed therefore, that with sufficiently slow potential sweep rates, the diffusion controlled current density at a spherical microelectrode is given by the steady state current defined by (2.82).

2:iv Irreversible Reactions at a Spherical Electrode

The analysis given in the previous section for reversible reactions at a spherical electrode may easily be extended to include irreversible reactions, taking advantage of the steady state at very slow potential sweep rates. Under these conditions, the diffusion equations describing the flux of O and R are given by

$$D_o \frac{d^2C_o}{dr^2} + \frac{2D_o}{r} \frac{dC_o}{dr} = 0 \qquad 2.83$$

$$D_r \frac{d^2C_r}{dr^2} + \frac{2D_r}{r} \frac{dC_r}{dr} = 0 \qquad 2.84$$

As in the previous analyses, it will be assumed that

$$D_o \simeq D_r = D \qquad 2.24$$

The initial conditions remain

$$t = 0 \qquad r_o < r < \infty \qquad C_o = C_o^\infty \qquad 2.85$$

$$C_r = C_r^\infty \qquad 2.86$$

but for an irreversible reaction, the boundary conditions are now

$$t > 0 \qquad r = \infty \qquad C_o = C_o^\infty \qquad 2.87$$

$$C_r = C_r^\infty \qquad 2.88$$

$$r = r_o \qquad nFD \frac{dC_o}{dr} = - nFD \frac{dC_r}{dr} \qquad 2.89$$

$$i_s = nFD \frac{dC_o}{dr}$$

$$= nFk'_o C_o \exp - \frac{\alpha nFE}{RT} - nFk'_o C_r \exp \frac{(1-\alpha)nFE}{RT} \qquad 2.90$$

where the boundary condition (2.90) is derived from the rate of an electrode reaction given by (1.35) in Chapter 1.

The general solutions to equations (2.83) and (2.84) may be expressed as

$$C_o = \frac{A}{r} + B \qquad 2.91$$

and

$$C_r = \frac{X}{r} + Y \qquad 2.92$$

respectively, where the values of the arbitrary constants A,B,X and Y are, once again, determined from the boundary conditions. Thus, (2.87) in (2.91) at $r = \infty$ gives

$$B = C_o^{\infty} \qquad 2.93$$

and similarly, (2.88) in (2.92) yields

$$Y = C_r^{\infty} \qquad 2.94$$

In addition, the boundary condition (2.89) shows that

$$A = - X \qquad 2.95$$

so that combining (2.93) - (2.95) into (2.91) and (2.92)

$$C_o = \frac{A}{r} + C_o^{\infty} \qquad 2.96$$

$$C_r = -\frac{A}{r} + C_r^{\infty} \qquad 2.97$$

On substituting for C_o and C_r into the boundary condition (2.90) the expression

$$-\frac{DA}{r_o^2} = k_o'\left(\frac{A}{r} + C_o^{\infty}\right)\exp -\frac{\alpha nFE}{RT} - k_o'\left(-\frac{A}{r} + C_r^{\infty}\right)\exp \frac{(1-\alpha)nFE}{RT} \qquad 2.98$$

is obtained, which may be solved for A.

By choosing the experimental conditions such that

$$C_r^{\infty} \longrightarrow 0 \qquad 2.99$$

equation (2.98) may be rearranged to

$$A = \frac{-k_o' r_o^2 C_o^{\infty} \exp -\frac{\alpha nFE}{RT}}{D + k_o' r_o \exp -\frac{\alpha nFE}{RT}\left[1 + \exp \frac{nFE}{RT}\right]} \qquad 2.100$$

This expression for A may then be substituted back into (2.96) giving

$$C_o = C_o^{\infty} - \frac{k_o' r_o^2 C_o^{\infty} \exp -\frac{\alpha nFE}{RT}}{r\left\{D + k_o' r_o \exp -\frac{\alpha nFE}{RT}\left[1 + \exp \frac{nFE}{RT}\right]\right\}} \qquad 2.101$$

and the current density is now readily determined using the boundary condition at $r = r_o$,

$$i_s = nFD\frac{dC_o}{dr} \qquad 2.90$$

Hence,

$$i_s = \frac{nFDk'_oC^{\infty}_o \exp - \frac{\alpha nFE}{RT}}{D + k'_or_o \exp - \frac{\alpha nFE}{RT}\left[1 + \exp \frac{nFE}{RT}\right]} \qquad 2.102$$

At the standard electrode potential, i.e. when $E = 0$, (2.102) reduces to

$$i_s = \frac{nFDk'_oC^{\infty}_o}{D + 2k'_or_o} \qquad 2.103$$

Clearly, two limiting forms exist for this equation. If

$$D \gg 2k'_or_o \qquad 2.104$$

then

$$i_s \longrightarrow nFk'_oC^{\infty}_o \qquad 2.105$$

and the current density at the standard electrode potential is kinetically controlled. In contrast, when

$$D \ll 2k'_or_o \qquad 2.106$$

then

$$i_s \longrightarrow \frac{nFDC^{\infty}_o}{2r_o} \qquad 2.107$$

and the current density is governed by diffusion.

A value for the apparent standard rate constant, k'_o, may therefore be easily evaluated, according to (2.105), from the observed current density at the standard electrode potential, provided that the condition (2.104) is fulfilled. Alternatively, k'_o may be determined by noting that in (2.102) at large and negative potentials

$$\exp \frac{nFE}{RT} \longrightarrow 0 \qquad 2.108$$

leading to

$$i_s = \frac{nFDC_o^{\infty}}{r_o} = i_d \qquad 2.109$$

where i_d is the diffusion controlled limiting current density.

Incorporating (2.109) into (2.102) and rearranging, an expression of the form

$$\frac{i_s}{i_d - i_s\left[1 + \exp\frac{nFE}{RT}\right]} = \frac{nFk_o'C_o^{\infty}}{i_d} \exp - \frac{\alpha nFE}{RT} \qquad 2.110$$

is obtained, which may then be applied to experimental current voltage curves to determine values of k_o' and α.

FIGS. 6,7,8 and 9 show simulated voltammograms calculated using equation (2.110) for a system in which the diffusion coefficient, D, is taken to be 1×10^{-5}cm^2 s^{-1} and the concentration, C_o^{∞} as 2·0mM. FIGS. 6 and 7 show the effect of decreasing apparent standard rate constant on the shape of the current voltage curves using microelectrodes of radius 10^{-5}cm and 10^{-4}cm respectively. In both diagrams, the transfer coefficient, α, is assumed to be unity. FIGS. 8 and 9 depict the same system except that the transfer coefficient in this case is taken to be 0·5.

From these diagrams, and with reference to (2.105) it can be seen that with a 1μm electrode, the upper limit of rate constant measurable is of the order 0·1cm s^{-1} while the corresponding limit for a microelectrode of radius 0·1μm increases to about 1cm s^{-1}. Above these values, the current voltage curves become indistinguishable from the reversible wave and (2.110) cannot be applied.

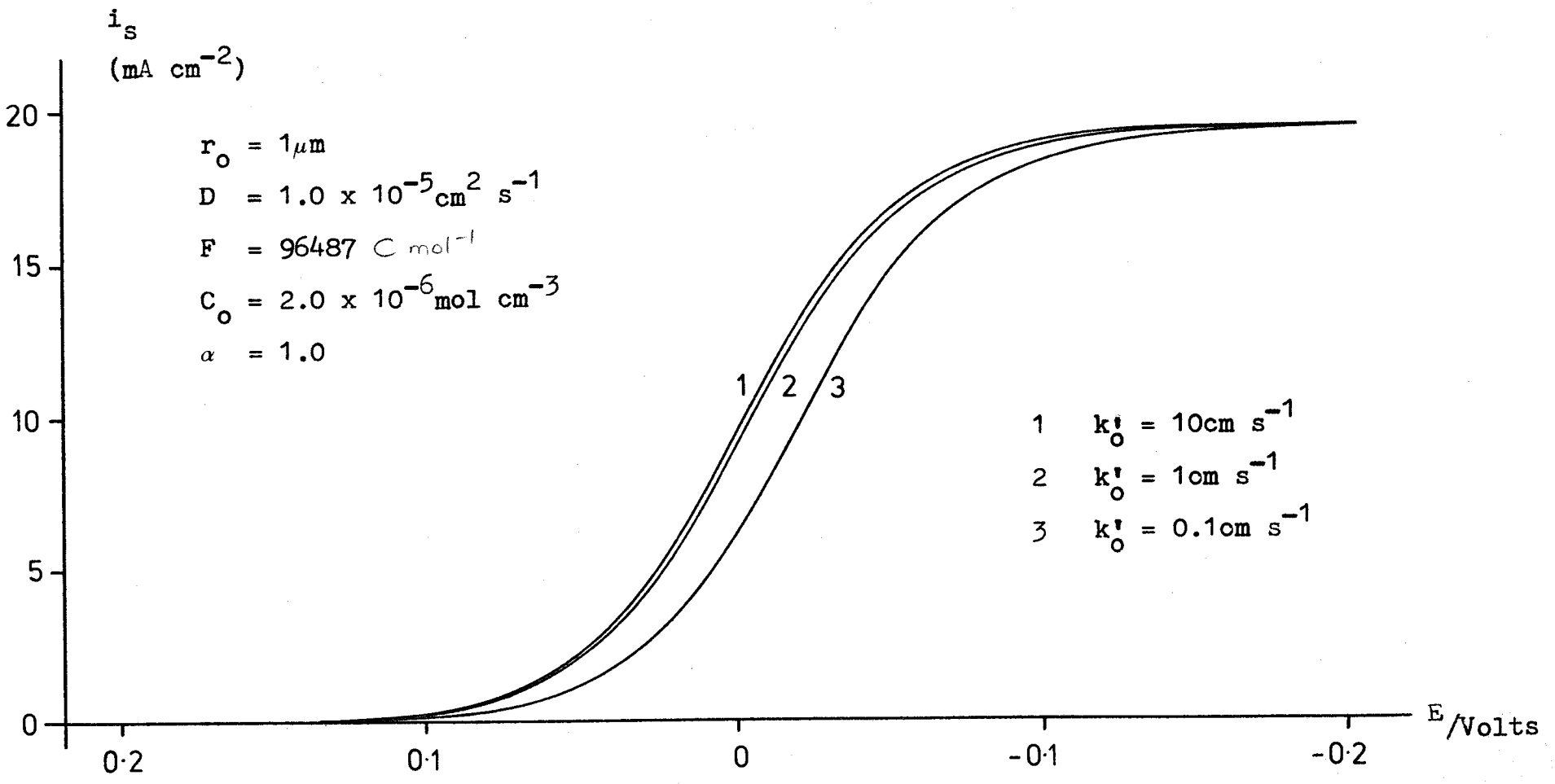

FIG 6 Theoretical voltammogram for a microelectrode of radius 1μm.

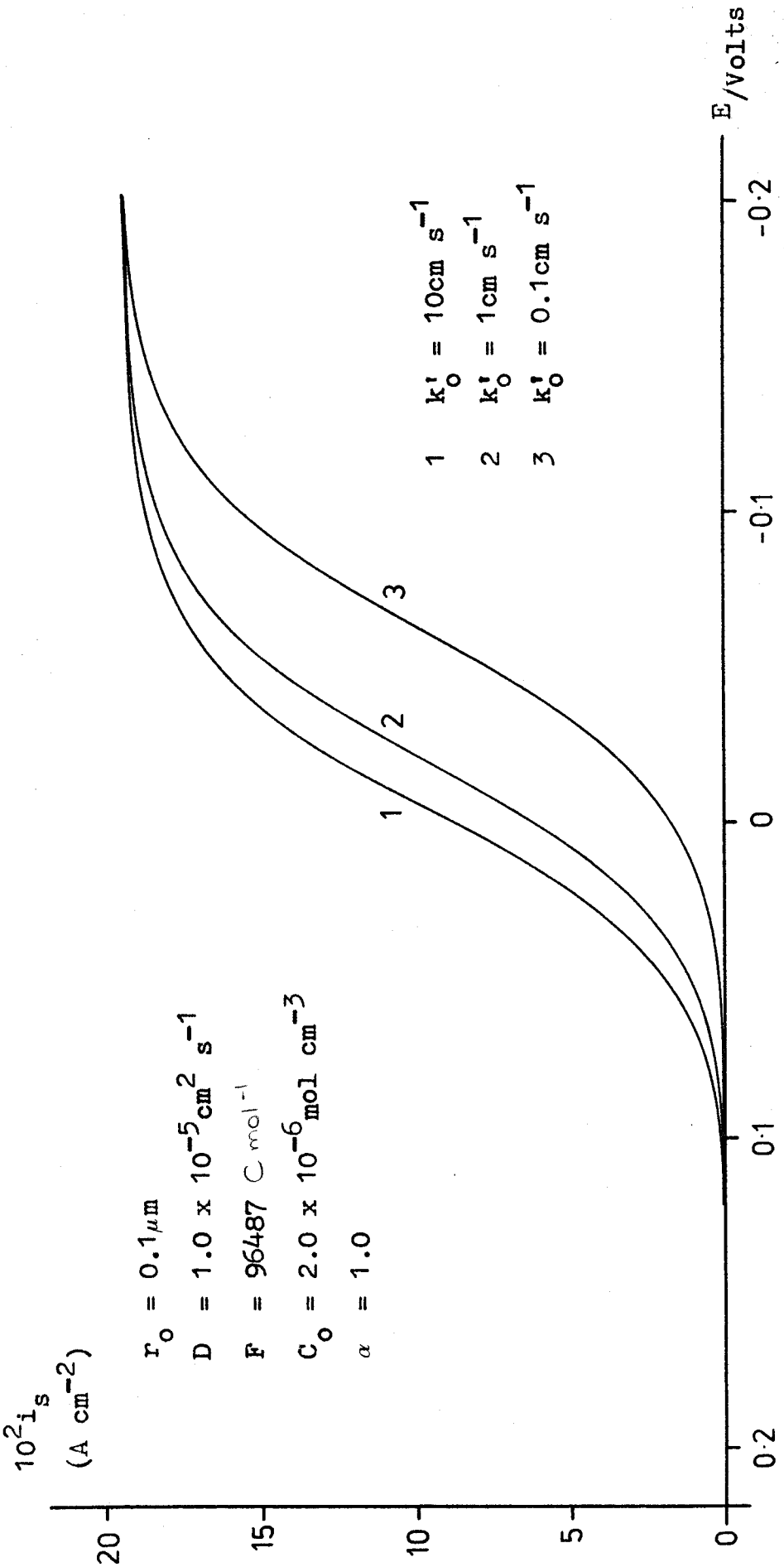

FIG 7 Theoretical voltammogram for a microelectrode of radius 0.1μm.

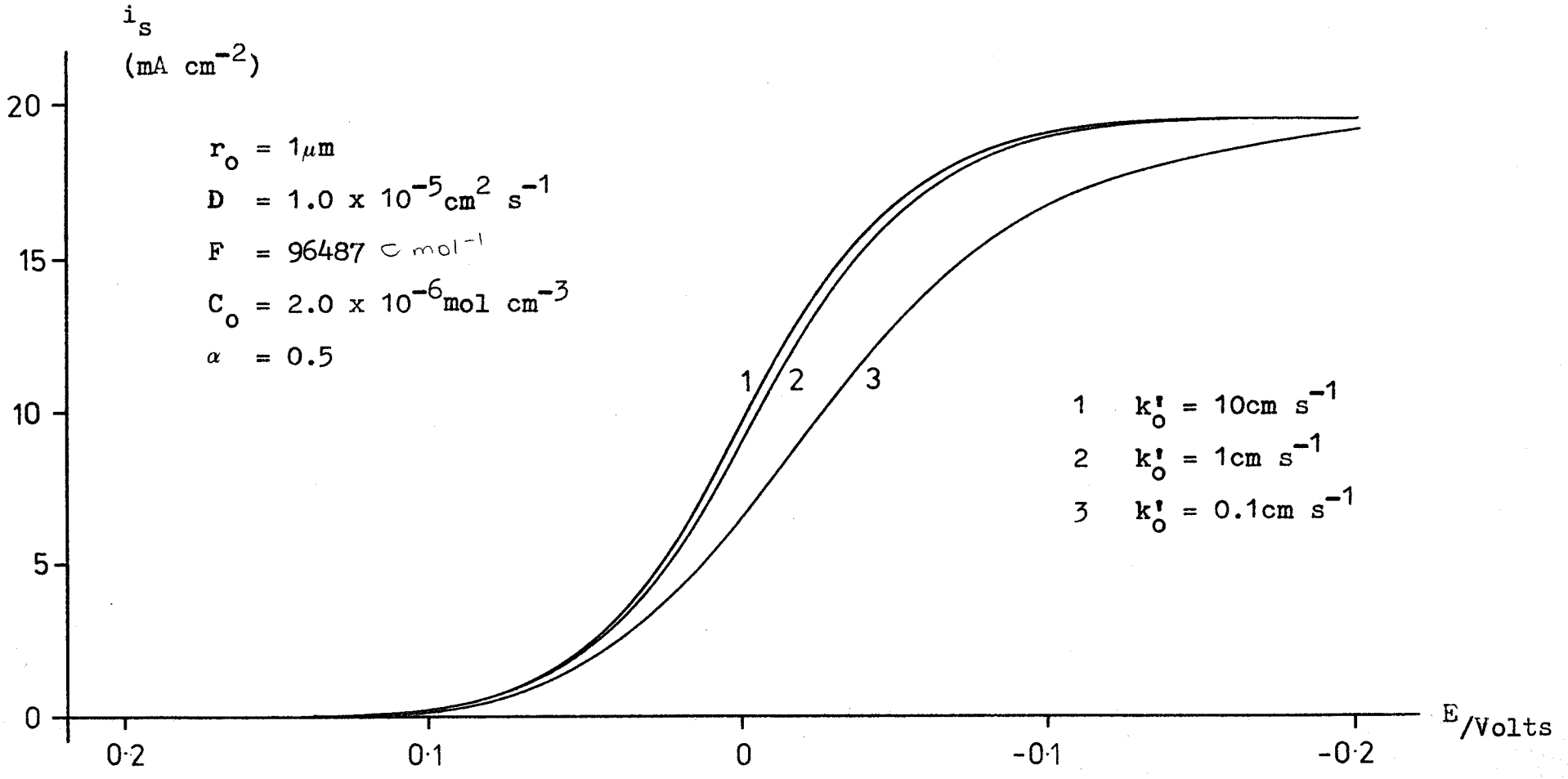

FIG 8 Theoretical voltammogram for a microelectrode of radius 1μm.

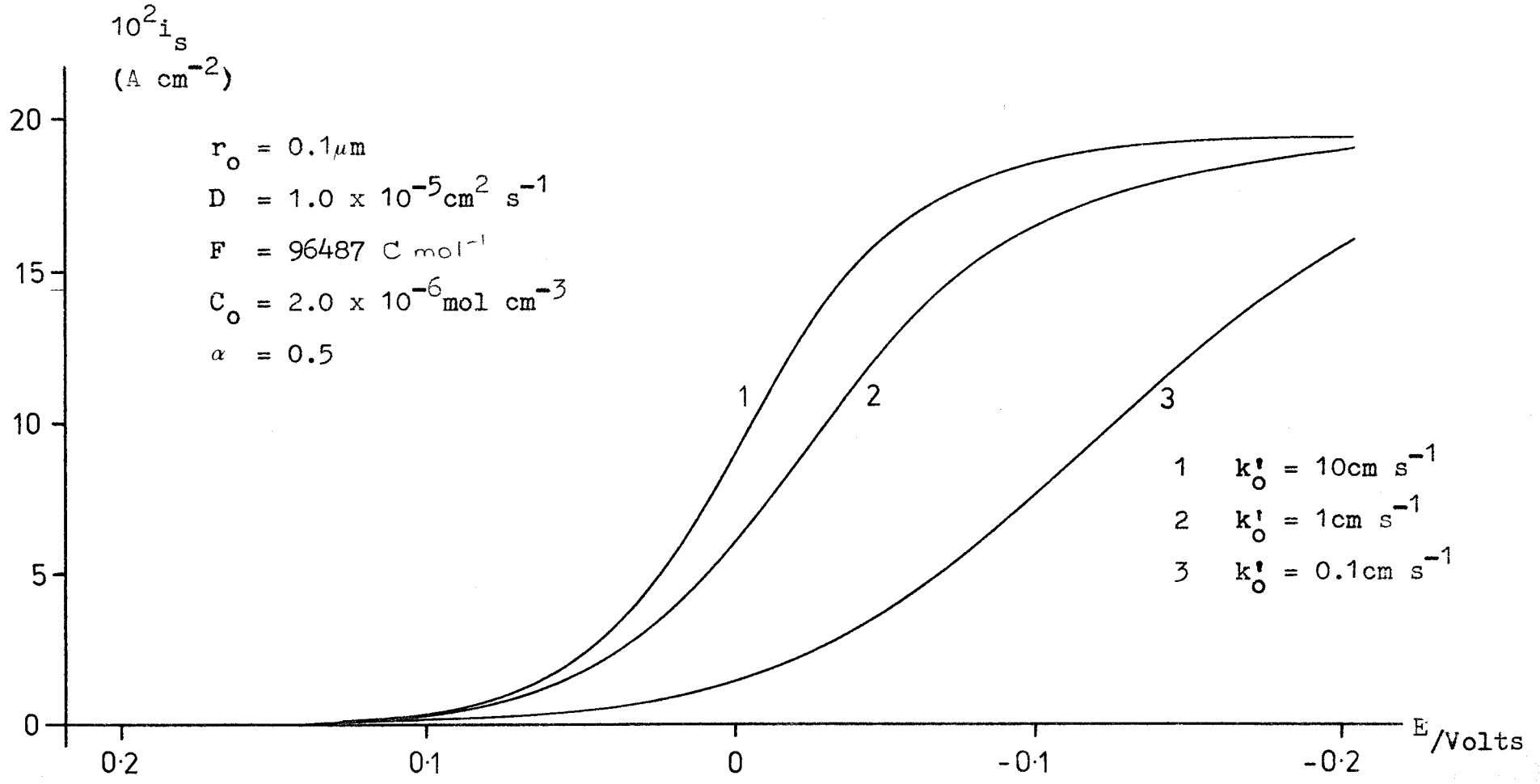

FIG 9 Theoretical voltammogram for a microelectrode of radius 0.1μm.

2:v Convolution Linear Potential Sweep Voltammetry

At very slow potential sweep rates, the flux of electroactive species towards a spherical electrode has been shown, in terms of the current density from (2.82) to be inversely proportional to the radius of the electrode, i.e.

$$i_s = \frac{nFDC_o^\infty}{r_o} \qquad 2.111$$

At higher sweep rates however, account must also be taken of the time dependent term, equivalent to the current density at a planar electrode of comparable area so that

$$i_s = i_{pl} + \frac{nFDC_o^\infty}{r_o} \qquad 2.112$$

Consequently, the enhanced flux at higher potential sweep rates should enable faster rates of reaction to be measured than were possible under very slow sweep conditions.

A means of extracting kinetic information from fast sweep voltammograms is provided by the convolution voltammetry technique. The basis of this method is to compute convolution integrals directly from the current time data obtained from linear sweep voltammograms. Since it is likely that at high potential sweep rates the current density at a spherical electrode may be approximated to the current density at a planar electrode of equivalent area, the essential features of this method for simple charge transfer reactions will first be described for semi - infinite linear diffusion conditions.

The basic diffusion equations and initial and boundary conditions for this case have already been described:

$$\frac{\partial C_o}{\partial t} = D_o \frac{\partial^2 C_o}{\partial x^2} \qquad 2.16$$

$$\frac{\partial C_r}{\partial t} = D_r \frac{\partial^2 C_r}{\partial x^2} \qquad 2.17$$

with the conditions

$$t = 0 \qquad 0 < x < \infty \qquad C_o = C_o^\infty \qquad 2.18$$

$$C_r = C_r^\infty \qquad 2.19$$

$$t > 0 \qquad x = \infty \qquad C_o = C_o^\infty \qquad 2.20$$

$$C_r = C_r^\infty \qquad 2.21$$

$$x = 0 \qquad i_{pl} = nFD_o \frac{\partial C_o}{\partial x} = - nFD_r \frac{\partial C_r}{\partial x} \qquad 2.22$$

and

$$D_o \simeq D_r = D \qquad 2.24$$

(Note that a second boundary condition at x = 0, defining the potential dependent concentrations of O and R is not necessary for this method).

From (2.32) and (2.33) the general solutions to the diffusion equations (2.16) and (2.17) in terms of the Laplace concentrations of O and R are given by

$$\overline{C}_o = \frac{C_o^\infty}{s} + K \exp(qx) + L \exp(-qx) \qquad 2.32$$

and

$$\overline{C}_r = \frac{C_r^\infty}{s} + M \exp(qx) + N \exp(-qx) \qquad 2.33$$

The boundary conditions (2.20) and (2.21) at $x = \infty$, after Laplace transformation, show that

$$K = M = 0 \qquad 2.36$$

hence (2.32) and (2.33) can be written as

$$\overline{C}_o = \frac{C_o^\infty}{s} + L \exp(-qx) \qquad 2.113$$

$$\overline{C}_r = \frac{C_r^\infty}{s} + N \exp(-qx) \qquad 2.114$$

At $x = 0$, the boundary condition (2.22) may be transformed to

$$\overline{i}_{pl} = nFD \frac{d\overline{C}_o}{dx} = - nFD \frac{d\overline{C}_r}{dx} \qquad 2.115$$

and then applied to (2.113) and (2.114) to give

$$\overline{i}_{pl} = nFD(-qL) = - nFD(-qN) \qquad 2.116$$

The values of the arbitrary constants L and N are therefore

$$L = - \frac{\overline{i}_{pl}}{nFDq} \qquad 2.117$$

and

$$N = \frac{\overline{i}_{pl}}{nFDq} \qquad 2.118$$

Substitution for L and N back into (2.113) and (2.114) therefore yield the expressions

$$\bar{C}_o = \frac{C_o^\infty}{s} - \frac{\bar{i}_{pl}}{nFDq} \exp(-qx) \qquad 2.119$$

$$\bar{C}_r = \frac{C_r^\infty}{s} + \frac{\bar{i}_{pl}}{nFDq} \exp(-qx) \qquad 2.120$$

If the bulk concentration of R is very low, such that

$$C_r^\infty \longrightarrow 0 \qquad 2.121$$

then equation (2.120) reduces to

$$\bar{C}_r = \frac{\bar{i}_{pl}}{nFDq} \exp(-qx) \qquad 2.122$$

The inverse transformation of (2.119) and (2.122) at the electrode surface (i.e. x = 0) can now be effected, with the aid of (2.31) using the Convolution theorem [59] to yield

$$C_o = C_o^\infty - \frac{1}{nFD^{\frac{1}{2}}\pi^{\frac{1}{2}}} \int_o^t \frac{i_{pl}(\tau)}{(t-\tau)^{\frac{1}{2}}} \, d\tau \qquad 2.123$$

and

$$C_r = \frac{1}{nFD^{\frac{1}{2}}\pi^{\frac{1}{2}}} \int_o^t \frac{i_{pl}(\tau)}{(t-\tau)^{\frac{1}{2}}} \, d\tau \qquad 2.124$$

where τ is a dummy variable for integration. Similar expressions defining the concentrations of O and R at the electrode surface have been derived by Saveant [71] and Oldham [70] .

By introducing the term

$$I_p = \frac{1}{nFD^{\frac{1}{2}}\pi^{\frac{1}{2}}} \int_o^t \frac{i_{pl}(\tau)}{(t-\tau)^{\frac{1}{2}}} \, d\tau \qquad 2.125$$

equations (2.123) and (2.124) may be simplified for

convenience to

$$C_o = C_o^{\infty} - I_p \qquad 2.126$$

$$C_r = I_p \qquad 2.127$$

Thus, for irreversible reactions where the current density is defined by

$$i_{pl} = nFk_o'C_o \exp - \frac{\alpha nFE}{RT} \qquad 2.128$$

substitution for C_o from (2.126) and rearranging produces an expression of the form

$$E = \frac{RT}{\alpha nF} \ln k_o' + \frac{RT}{\alpha nF} \ln \frac{(C_o^{\infty} - I_p)}{i_{pl}} \qquad 2.129$$

After evaluation of the convolution integral I_p, values for the apparent standard rate constant k_o', and transfer coefficient α can therefore be obtained by plotting the second term on the right hand side of (2.129) against the potential and measuring the intercept and slope of the resulting straight line.

At slower potential sweep rates, spherical effects become increasingly important and the convolution integral I_p must be suitably amended to account for spherical diffusion. An analogous derivation to that described above for linear diffusion with, in this case a spherical diffusion field, may be performed to derive the corresponding expressions describing the concentrations of O and R at a spherical electrode. In a spherical diffusion field, the diffusion equations are represented by

$$\frac{\partial C_o}{\partial t} = D_o \frac{\partial^2 C_o}{\partial r^2} + \frac{2D_o}{r} \frac{\partial C_o}{\partial r} \qquad 2.52$$

$$\frac{\partial C_r}{\partial t} = D_r \frac{\partial^2 C_r}{\partial r^2} + \frac{2D_r}{r} \frac{\partial C_r}{\partial r} \qquad 2.53$$

together with the initial and boundary conditions

$$t = 0 \qquad r_o < r < \infty \qquad C_o = C_o^\infty \qquad 2.54$$

$$C_r = C_r^\infty \qquad 2.55$$

$$t > 0 \qquad r = \infty \qquad C_o = C_o^\infty \qquad 2.56$$

$$C_r = C_r^\infty \qquad 2.57$$

$$r = r_o \quad i_s = nFD_o \frac{\partial C_o}{\partial r} = - nFD_r \frac{\partial C_r}{\partial r} \qquad 2.58$$

As before, it will be assumed that

$$D_o \simeq D_r = D \qquad 2.24$$

The general solutions of (2.52) and (2.53) have previously been described by (2.66) and (2.67) as

$$\overline{C}_o = \frac{G}{r} \exp(qr) + \frac{H}{r} \exp(-qr) + \frac{C_o^\infty}{s} \qquad 2.66$$

$$\overline{C}_r = \frac{P}{r} \exp(qr) + \frac{Q}{r} \exp(-qr) + \frac{C_r^\infty}{s} \qquad 2.67$$

where G,H,P and Q are arbitrary constants and

$$q^2 = \frac{s}{D} \qquad 2.31$$

Substitution of the boundary conditions (2.56) and (2.57) into (2.66) and (2.67) show, as before that

$$G = P = 0 \qquad 2.68$$

Hence, (2.66) and (2.67) may be written as

$$\bar{C}_o = \frac{H}{r} \exp(-qr) + \frac{C_o^\infty}{s} \qquad 2.130$$

$$\bar{C}_r = \frac{Q}{r} \exp(-qr) + \frac{C_r^\infty}{s} \qquad 2.131$$

From the boundary condition at $r = r_o$, (2.58), the transform of the current density, defined by (2.73)

$$\bar{i}_s = nFD \frac{d\bar{C}_o}{dr} = -nFD \frac{d\bar{C}_r}{dr} \qquad 2.73$$

when applied to (2.130) and (2.131) respectively, give expressions for H and Q as

$$H = -\frac{\bar{i}_s r_o^2 \exp(qr_o)}{nFD(1 + qr_o)} \qquad 2.132$$

$$Q = \frac{\bar{i}_s r_o^2 \exp(qr_o)}{nFD(1 + qr_o)} \qquad 2.133$$

whereupon substitution for H and Q back into (2.130) and (2.131) respectively gives

$$\bar{C}_o = \frac{C_o^\infty}{s} - \frac{\bar{I}_s r_o^2 \exp[-q(r - r_o)]}{nFDr(1 + qr_o)} \qquad 2.134$$

$$\bar{C}_r = \frac{C_r^\infty}{s} + \frac{\bar{I}_s r_o^2 \exp[-q(r - r_o)]}{nFDr(1 + qr_o)} \qquad 2.135$$

At $r = r_o$, and also assuming that

$$C_r^{\infty} \longrightarrow 0$$

equations (2.134) and (2.135) reduce to

$$\bar{C}_o = \frac{C_o^{\infty}}{s} - \frac{\bar{i}_s}{nFD\left\{\frac{1}{r_o} + \left(\frac{s}{D}\right)^{\frac{1}{2}}\right\}} \qquad 2.136$$

$$\bar{C}_r = \frac{\bar{i}_s}{nFD\left\{\frac{1}{r_o} + \left(\frac{s}{D}\right)^{\frac{1}{2}}\right\}} \qquad 2.137$$

The inverse Laplace transformation of (2.136) and (2.137) at the electrode surface, ($r = r_o$) can now be accomplished with the aid of the Convolution theorem and tables of Laplace transforms [59] , noting that the inverse of

$$\mathcal{L}\left\{\frac{1}{r_o} + \left(\frac{s}{D}\right)^{\frac{1}{2}}\right\}^{-1} = \left(\frac{D}{\pi t}\right)^{\frac{1}{2}} - \frac{D}{r_o} \exp\frac{Dt}{r_o^2}\,\operatorname{erfc}\left(\frac{Dt}{r_o^2}\right)^{\frac{1}{2}}$$

2.138

The expressions for C_o and C_r are now given by

$$C_o = C_o^{\infty} - \frac{1}{nFD^{\frac{1}{2}}\pi^{\frac{1}{2}}}\int_o^t i_s(\tau)\left[\frac{1}{(t-\tau)^{\frac{1}{2}}} - \left(\frac{\pi D}{r_o^2}\right)^{\frac{1}{2}} \exp\frac{D(t-\tau)}{r_o^2}\,\operatorname{erfc}\left(\frac{D(t-\tau)}{r_o^2}\right)^{\frac{1}{2}}\right] d\tau$$

2.139

$$C_r = \frac{1}{nFD^{\frac{1}{2}}\pi^{\frac{1}{2}}}\int_o^t i_s(\tau)\left[\frac{1}{(t-\tau)^{\frac{1}{2}}} - \left(\frac{\pi D}{r_o^2}\right)^{\frac{1}{2}} \exp\frac{D(t-\tau)}{r_o^2}\,\operatorname{erfc}\left(\frac{D(t-\tau)}{r_o^2}\right)^{\frac{1}{2}}\right] d\tau$$

2.140

Denoting the convolution integral for a spherical

electrode by I_s, where

$$I_s = \frac{1}{nFD^{\frac{1}{2}}\pi^{\frac{1}{2}}} \int_0^t i_s(\tau) \left[\frac{1}{(t-\tau)^{\frac{1}{2}}} - \left(\frac{\pi D}{r_o^2}\right)^{\frac{1}{2}} \exp \frac{D(t-\tau)}{r_o^2} \operatorname{erfc}\left(\frac{D(t-\tau)}{r_o^2}\right)^{\frac{1}{2}} \right] d\tau$$

2.141

it is obvious that this expression is far more difficult to evaluate than the corresponding expression for a planar electrode. For small values of the radius, r_o however, it is possible to expand the error function term in the form of a power series, thus

$$\left(\frac{\pi D}{r_o^2}\right)^{\frac{1}{2}} \exp \frac{D(t-\tau)}{r_o^2} \operatorname{erfc} \left(\frac{D(t-\tau)}{r_o^2}\right)^{\frac{1}{2}}$$

$$\simeq \frac{D^{\frac{1}{2}}}{r_o} \left\{ \frac{r_o}{D(t-\tau)^{\frac{1}{2}}} - \frac{r_o^3}{2\{D(t-\tau)\}^{3/2}} + \frac{r_o^5}{2^2\{D(t-\tau)\}^{5/2}} - \ldots \right\}$$

2.142

Provided that

$$\left(\frac{D(t-\tau)}{r_o^2}\right)^{\frac{1}{2}} \gg 5 \qquad 2.143$$

convergence of the series is reasonably rapid and may be limited to three or four terms.

Therefore, incorporating (2.142) into (2.141), the convolution integral I_s becomes

$$I_s = \frac{1}{nF\pi^{\frac{1}{2}}r_o} \int_0^t i_s(\tau) \left[\frac{r_o^3}{2\{D(t-\tau)\}^{3/2}} - \frac{3r_o^5}{4\{D(t-\tau)\}^{5/2}} + \frac{15r_o^7}{8\{D(t-\tau)\}^{7/2}} \right] d\tau$$

2.144

which may be computed for given values of D and r_o as before.

For irreversible reactions at a spherical electrode, the spherical convolution integral I_s, may then be substituted into (2.129), replacing the planar integral I_p and plotting against the electrode potential as described earlier to obtain values for the apparent standard rate constant, k_o' from the intercept.

CHAPTER 3 MICROELECTRODES

3:i Introduction

The design and development of very small electrodes - termed microelectrodes - has centred mainly on the electrochemical study of biological systems, where the need to measure potentials within single cells has necessitated the development of electrodes with extremely small dimensions.

Essentially two types of microelectrode have emerged from these studies: solid metal wire electrodes sheathed in an insulating material such as glass leaving the end circular portion exposed and all glass electrodes, commonly containing an ionic solution into which is immersed a suitable reference electrode.

The radii of microelectrodes are normally found in the range 0·25μm - 25μm depending on their method of fabrication and application. Unfortunately, those electrodes with the smallest dimensions are often of low mechanical strength: this is especially true for glass electrodes which are particularly prone to fracture. In this work, only metal microelectrodes were considered for use. In all, three different designs were attempted: lead capillary, etched tungsten and platinum fibre microelectrodes. The progression of one electrode design to another reflected, amongst other factors, the change in emphasis from physically very small, fragile microelectrodes like the lead capillary to physically larger, but more robust and reproducible microelectrodes of the platinum fibre type.

In the following pages the detailed methods of construction of the various microelectrode types are described as well as some of the many problems encountered. A brief description of the electrical properties of microelectrodes is also presented.

3:ii Capillary microelectrodes

Capillary microelectrodes, as their name suggests, are formed from very fine glass capillaries into which low melting point metals may be melted.

The choice of metal is in fact very important and is dependent on a number of factors:

(i) its melting point must be lower than the softening temperature of the glass capillary,

(ii) it should have a high work of adhesion to glass,

(iii) its linear coefficient of thermal expansion must be comparable to that of the glass capillary to ensure a good glass to metal seal at all temperatures and

(iv) it must have a sufficiently low surface tension and high cohesive strength to form fine metallic threads. (It is for this reason that mercury microelectrodes are not available; in very small capillaries surface tension effects cause the mercury thread to break up into very small globules on the capillary wall.)

In view of these limitations and the availability of capillaries fashioned from 'Pyrex' glass, lead and an indium/Wood's metal alloy were chosen as the most suitable low melting point metals. (The use of Wood's metal in conjunction with indium for the fabrication of microelectrodes has been suggested by Dowben and Rose [87] to aid wetting of the glass capillary.)

Lead and indium capillary microelectrodes were prepared by first heating, then drawing a coarse glass 'Pyrex' tube to produce a capillary of approximately 50μm internal diameter. The capillary was then thoroughly cleaned in chromic acid followed by washing in triply distilled water before oven drying and storing in a dust free dry box. The metal meanwhile, was melted and any oxide slag removed as it formed from the surface of the melt. When completely molten and free from oxide, the liquid was introduced

into a pre-warmed capillary under suction. The resultant capillary was then drawn down again taking care to maintain the metal meniscus as close to the glass tip as possible. This particular procedure could be repeated until the desired radius was obtained. With lead microelectrodes, the molten metal often had to be forced to the tip under pressure of nitrogen gas, whilst being drawn down. This obviously presented major problems in controlling the glass capillary whilst still in a molten state. Nevertheless, despite these difficulties, several microelectrodes were formed from indium and lead in this way.

The next stage was to produce a reasonably flat electrode surface at the extreme tip of the capillary. After first allowing the electrode to cool and checking that the metal had not contracted away from the capillary wall, the tip of the electrode was placed very gently on a hot plate until metal was observed flowing from the tip. The electrode was then removed from the hot plate and a small bead of metal allowed to form. After cooling, this bead was very carefully tapped away from the electrode tip, exposing hopefully, a flat, clean electrode surface.

The radii of electrodes formed in this manner were found to be typically 1μm - 10μm when compared to an 8μm carbon fibre viewed under a powerful optical microscope.

Electrical connections to the microelectrode were made by inserting the centre cable of a low noise coaxial cable into the metal, aided by gentle warming. Then finally, to complete the assembly, a glass syringe barrel was attached to the main shaft of the capillary for use in a two electrode cell. FIG. 10 illustrates a completed microelectrode, giving some indication of the size and fragility of the electrode tip in comparison to the rest of the electrode assembly.

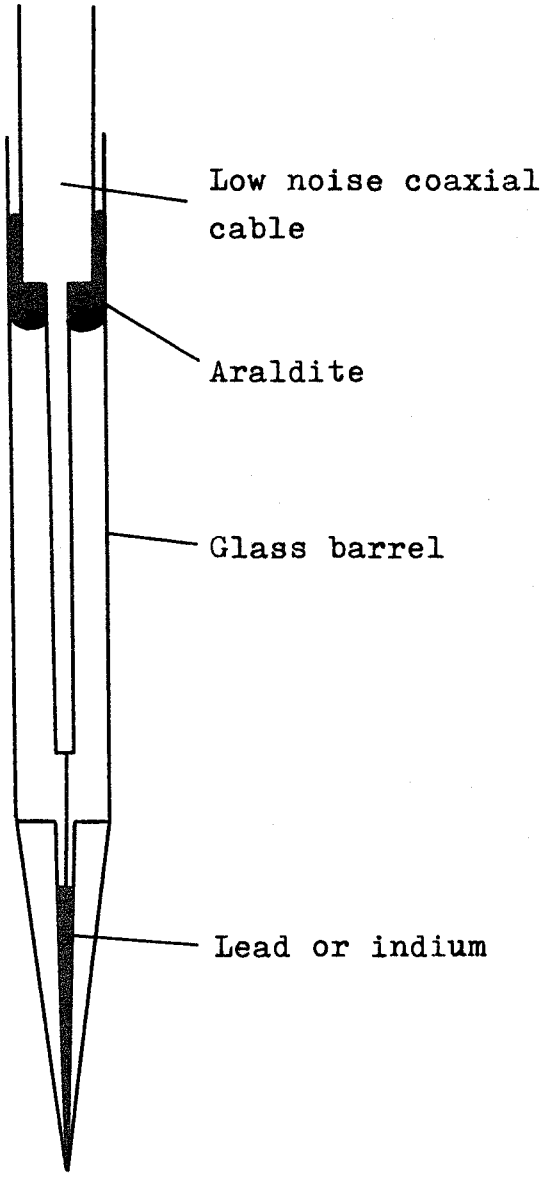

FIG 10 Complete microelectrode assembly for lead/indium microelectrode

3:iii Tungsten microelectrodes

In terms of the mechanics of assembly, tungsten microelectrodes are much simpler to produce than their capillary counterparts. The choice of metal is not limited to tungsten but to any metal which may be etched, preferably electrochemically and does not melt below the softening temperature of glass. Again, as with capillary microelectrodes described previously, the linear coefficient of thermal expansion of the metal must be comparable to that of the glass in order to ensure a good glass to metal seal.

The choice of tungsten for these experiments was influenced mainly by the ease of etching of this particular metal, its inherent strength and its resistance to atmospheric corrosion. The method of fabrication described below has been adapted from the original technique developed by Hubel [89] . Modifications to the etching process were made to produce extremely short tapered tips to enhance even further the overall strength of the electrode.

A tungsten rod, of diameter 1mm was electrochemically etched in an aqueous solution of sodium hydroxide (10%). The simple cell is shown in FIG. 11a, indicating the tungsten anode and a silver wire cathode. Current to the cell was provided by a standard 9V battery source connected in series with the cell. The formation of the tip proceeded essentially in three stages.

The tungsten rod was first partially immersed in the alkali solution to a depth of approximately 20mm - 25mm and the voltage applied. As dissolution of the oxide layer occurred, the surface of the tungsten rod was observed to become very bright and smooth. After approximately five minutes about 5mm of the rod was withdrawn from the solution and the etching continued. This was repeated until only 5mm of the rod remained in solution. On inspection, the rod was observed to have formed small 'ridges' on

the surface of the polished metal (FIG. 11b) where the meniscus had obviously been in contact with the metal rod. About 15mm of the rod were then etched further until the tungsten rod appeared as shown in FIG. 11c, with a small ball of tungsten suspended from the main shaft. (During this latter etching process, dissolution was observed to occur preferentially at the 'ridges' i.e. the areas of highest curvature of the electrode).

The voltage was then reduced to approximately 2V, resulting in a decrease in the rate of dissolution of the tungsten thereby obtaining greater control over the final stages of the etching process. As soon as the ball of tungsten fell away from the main electrode, the cell was disconnected and the electrode washed with triply distilled water. The resultant tungsten electrode when viewed under an optical microscope consisted of a thick metal shaft tapering very quickly to a very fine point (FIG. 11d) and was now ready for insulation.

Various materials have been used to insulate metal electrodes for use in either aqueous or non aqueous solutions. For aqueous use, polymer resins such as 'Collodion' or 'Formvar' are usually adequate and simple to apply but in non aqueous solvents these organic based resins are liable to dissolve and therefore cannot be used. An obvious alternative is glass which is impervious to non aqueous media and is also a good electrical insulator. Although generally more difficult to seal, it does however offer greater protection to the metal tip, giving electrodes a substantially longer life than the capillary type microelectrode.

The most effective glass to metal seal was achieved under vacuum. This also reduced the risk of oxidation of the tip as well as minimising the formation of air bubbles at the glass/metal interface. Although special glasses are available for effecting tungsten to glass seals, 'Pyrex' glass was found

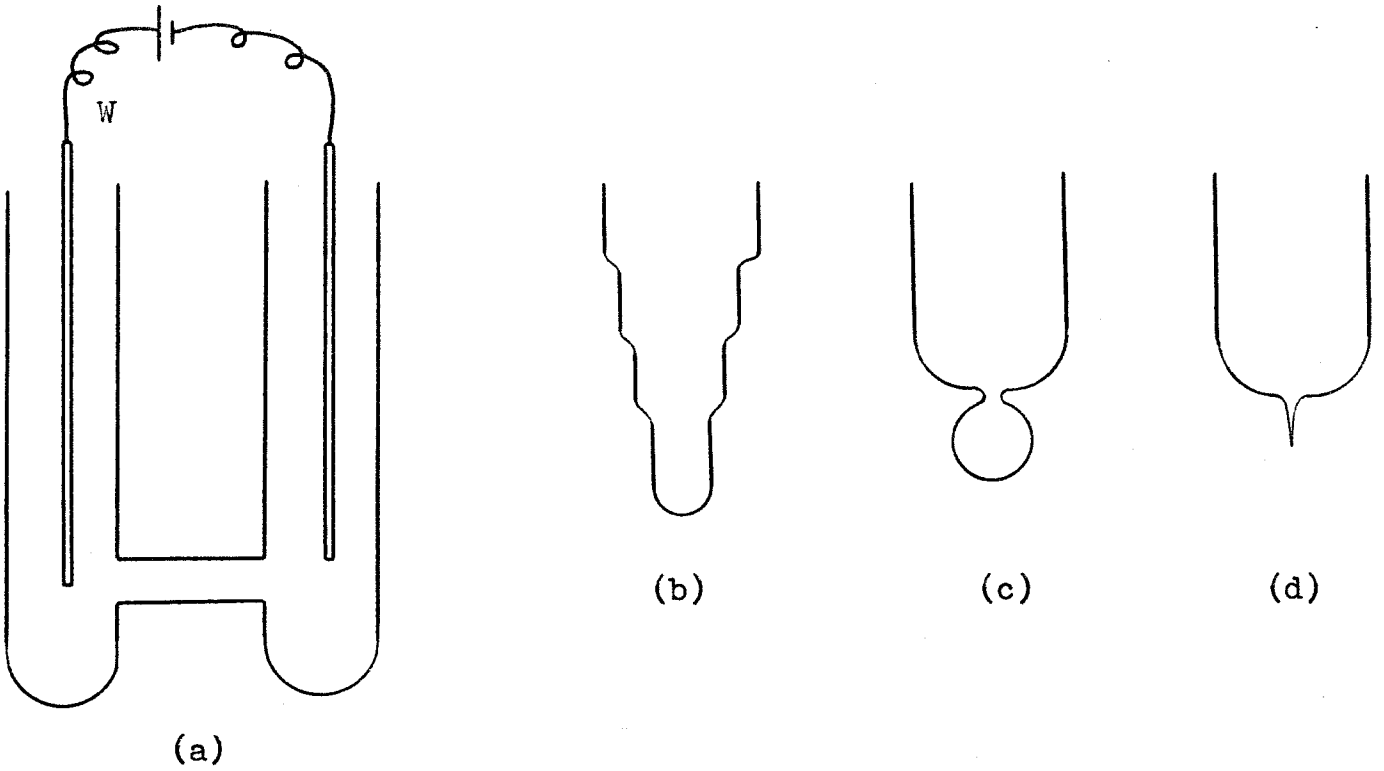

FIG 11 (a) H cell for tungsten etching

(b) ridge formation on tungsten rod

(c) formation of droplet at tip of tungsten electrode

(d) final electrode

to be entirely adequate under the prevailing experimental conditions.

Having sealed the metal tip into glass under vacuum, the final task was to expose the extreme tip of the metal through careful polishing of the glass tip. This was achieved using in succession very fine emery paper followed by 6μm and 1μm diamond paste as a suspension in an oil based lubricating fluid (Hyprez 5 star diamond compounds) on a special polishing cloth (1m Metron: Banner Scientific Ltd.). The response of the electrode in a test solution of perylene in tetrabutyl ammonium tetraflouroborate/ dimethylformamide to a cathodic voltage of -1·3 V (vs Hg pool) was repeatedly checked (see Chapter 4), so as not to polish beyond the extreme tip of the electrode giving rise to larger electrode radii than desired due to the very sharp taper of the metal.

After many hours of patient polishing (by hand) several tungsten microelectrodes with radii of 1μm or less were prepared. (The radii of these very small electrodes were determined electrochemically from the limiting diffusion currents: this is explained in more detail in Chapter 4:ii). In common with capillary microelectrodes, electrical connections were made using low noise coaxial cable soldered, in this case, to the tungsten rod and a glass syringe completed the assembly (FIG. 12a). These electrodes were generally found to be less 'noisy' than the capillary electrodes and far more robust but tungsten is limited as an electrode material, particularly in aqueous media where it enjoys only a limited potential range and therefore methods of constructing platinum microelectrodes were investigated.

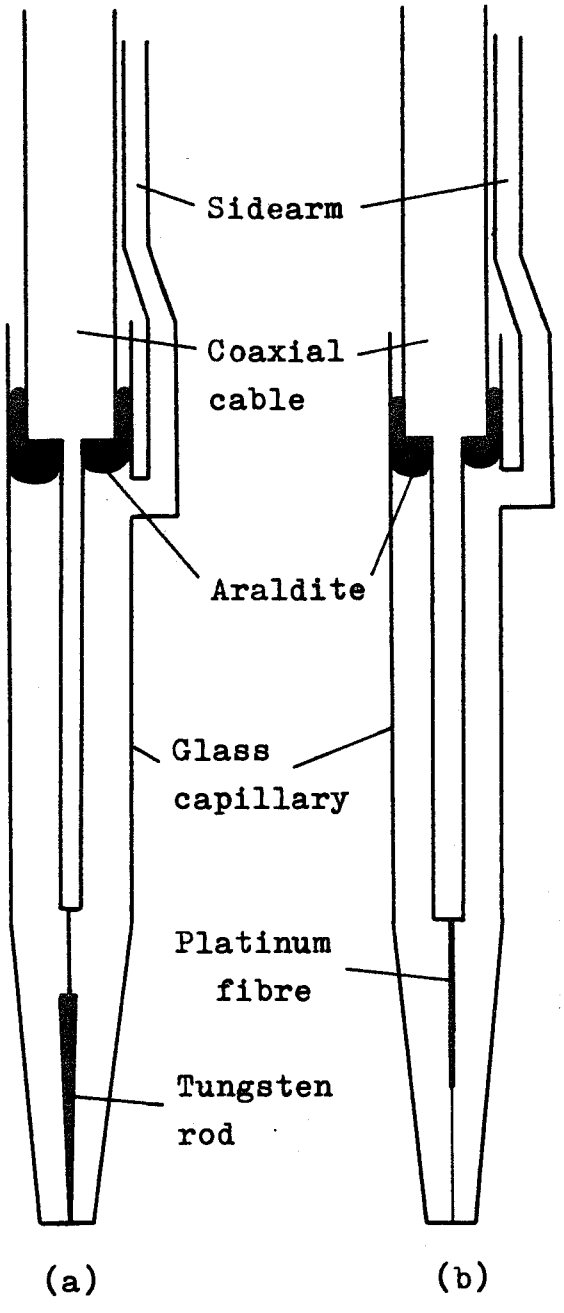

FIG 12 Microelectrode assemblies for
(a) tungsten microelectrode
(b) platinum microelectrode

3:iv Platinum fibre microelectrodes

Until recently, the most popular method of making extremely small platinum electrodes was by electroetching hard platinum (30% iridium, 70% platinum) in a 30% solution of sodium hydroxide saturated with sodium cyanide [90]. Apart from the obvious disadvantages of working with cyanide solutions, this technique results in alloy electrode surfaces of varying composition. These difficulties have been overcome, however, by the availability of very thin platinum fibres in the form of Wollaston wires (platinum fibres coated with a layer of silver). These allow platinum electrodes with radii down to 1μm to be made with comparative ease and, moreover, since the electrode is a long fibre it may be polished without fear of the electrode radius increasing dramatically. To construct these microelectrodes, first a 1cm length of Wollaston wire is silver soldered to one end of a fine helical spring while the other end of the spring is soldered to the central core of a low noise coaxial cable. The assembly is then placed inside a pre-drawn 'Pyrex' glass capillary complete with sidearm (as shown in FIG. 12b) until the Wollaston wire protrudes through the end of the capillary. About 0·5cm of the Wollaston wire is then immersed in 50% nitric acid for approximately 4 - 8 hours to dissolve the protective coating of silver and reveal the fine platinum fibre. This is then drawn very carefully back into the capillary and the whole assembly washed thoroughly with triply distilled water. (Washing the fibre outside the capillary often resulted in the fibre breaking away from the Wollaston wire.) The glass capillary and contents are then carefully dried before sealing the coaxial cable, with screening exposed, into position using thermo-setting silver conducting 'Araldite' (Johnson Matthey Co. Ltd.). This provided an earth connection to the inside of the capillary, reducing

as far as possible any extraneous noise originating from the electrode construction. (Care should be taken during this step to ensure that the platinum fibre does not become entangled in the hair spring due to excessive movement of the cable).

Once the 'Araldite' has dried, the glass tip can be sealed under vacuum as before. The function of the hair spring is to absorb any tension between the fixed coaxial cable and the Wollaston wire. In its absence a frequent cause for microelectrode failure is the breaking of the very fine fibre during the sealing process.

The electrode tip can now be exposed by simply breaking the glass filament anywhere along the encapsulated platinum fibre followed by careful polishing with 6μm and 1μm diamond polishing compounds as before. Alumina powder (0·5μm and 0·05μm: Banner Scientific Ltd.) in an aqueous suspension was also used to polish the electrode surface: the finer grade being used before each experiment. A complete electrode assembly is shown in FIG. 12b.

The final radii of these microelectrodes are obviously governed by the radius of the platinum fibre. In this work, electrodes were prepared from the smallest platinum fibres available. These were, in terms of their diameters 2μm, 5μm, 10μm, 25μm and 50μm; the last three being available as platinum fibres without the silver coating.

Attempts to procure even smaller platinum microelectrodes by electroetching the fine platinum fibres in cyanide solutions before sealing into glass were generally unsuccessful, resulting only in electrodes of the original diameter.

3:v Electrical properties of microelectrodes

The internal resistance of microelectrodes may, in the first instance, be approximated to the resistance of a conductor of uniform right cylindrical geometry by the equation

$$R_m = \frac{l}{\sigma A} \Omega \qquad 3.1$$

where l is the length of the conductor (cm); A is the cross sectional area (cm^2); and σ is the conductivity (mhos cm^{-1}). Thus, for a platinum fibre microelectrode of length 2cm and conductivity $9{\cdot}43 \times 10^4$ mhos cm^{-1} the following internal resistances are obtained:

Radius	Resistance (Ω)
1μm	675
5μm	30
10μm	7
25μm	1
50μm	0·3

For tapered microelectrodes, Amatniek [91] has derived a more rigorous relationship involving the angle of taper and other parameters. When the tip taper angle ϕ is small and the tip diameter $d \ll l\phi$, the internal resistance of the electrode simplifies to

$$R_m \simeq \frac{4}{\pi \phi d \sigma} \Omega \qquad 3.2$$

In addition to the internal resistances of microelectrodes, the resistance between the electrode tip and an external electrode must also be considered. For a spherical electrode, this resistance is given by [92,93]

$$R_u = \left(\frac{\rho}{4\pi}\right)\left(\frac{1}{r_1} - \frac{1}{r_2}\right) \qquad 3.3$$

where ρ is the specific resistance of the solution; r_1 the radius of the microelectrode; and r_2 the distance of the external electrode from the microelectrode. In aqueous 1M KCl solutions, with $r_1 = 10^{-4}$cm and $r_2 = 1$cm and $\rho = 8{\cdot}98\,\Omega$ cm [94], the value of R_u is $7{\cdot}15 \times 10^3\,\Omega$. Similarly, in N,N Dimethylformamide solutions containing tetrabutyl ammonium iodide (0·2M) with the same values of r_1 and r_2 and with $\rho \simeq 100\,\Omega$ cm [95], R_u is now $\sim 8 \times 10^4\,\Omega$. Clearly, this resistance exceeds that for the internal resistance of small microelectrodes. Nevertheless, the total voltage drop - termed 'iR' drop - attributable to a microelectrode in view of equations (3.1), (3.2) and (3.3) will remain less than a millivolt for measured currents $< 10^{-8}$amps, corresponding to current densities $< 0{\cdot}5$A cm^{-2}. Since this condition is fulfilled for the majority of electrode reactions at these microelectrodes, the low 'iR' drop associated with microelectrodes allows two electrode cell systems to be conveniently utilised for microelectrode experiments.

CHAPTER 4 MEASUREMENT OF THE RATE OF ELECTRON TRANSFER REACTIONS

4:i Introduction: preliminary experiments

In Chapter 2, it was shown that apparent standard rate constants of simple electron transfer reactions having values up to 10cm s^{-1} could, in principle, be measured with microelectrodes of radius 0·1μm under conditions of both pseudo steady state (i.e. very slow linear potential sweep) and fast linear potential sweep.

According to equations (2.110) and (2.129) the calculation of k_o' from experimental voltammograms requires an a priori knowledge of the standard electrode potential and diffusion coefficients of the system under investigation. Preliminary experiments, using relatively large wire electrodes were therefore conducted on a number of systems to determine these values and to establish the stability of the reaction product of each redox couple over a range of experimental conditions.

Due to the narrow potential range of tungsten in aqueous solution, the envisaged use of tungsten as a microelectrode material unfortunately restricted the scope of suitable redox reactions available for study to those occurring in non aqueous media. Inorganic redox couples in aqueous media have been shown, in a large number of cases, to be either electrochemically very slow or complicated by homogenous chemical reactions [96,97] .

In contrast, many examples of simple, relatively fast one electron transfer reactions in non aqueous media are reported in the literature [98] . In particular, the reduction of several aromatic hydrocarbons in solvents such as N,N Dimethylformamide (DMF) and Acetonitrile (ACN) have been studied in attempts to characterise the reduction processes kinetically [99].

A selection of aromatic hydrocarbons of apparent standard rate constant of the order 1cm s^{-1} in Dimethylformamide, (i.e. reversible reactions under normal conditions) were consequently chosen for study.

Values of the standard electrode potential and diffusion coefficients of the selected systems were determined using cyclic voltammetry methods. For simple reversible processes, the peak current density, i_p, for a cathodic potential sweep is given by the expression

$$i_p = 2{\cdot}72 \times 10^5 n^{3/2} D_o^{\frac{1}{2}} C_o^{\infty} a^{\frac{1}{2}} \qquad 4.1$$

at 25°C, while the peak potential, E_p, which is independent of the potential sweep rate, a, is related to the polarographic half wave potential, $E_{\frac{1}{2}}$, by the equation

$$E_p = E_{\frac{1}{2}} - \frac{0{\cdot}029}{n} \text{ volts} \qquad 4.2$$

The half wave potential in turn, is related to the standard electrode potential by [27]

$$E_{\frac{1}{2}} = E_o + \frac{RT}{nF} \ln \left(\frac{D_o}{D_r}\right)^{\frac{1}{2}} \frac{f_r}{f_o} \qquad 4.3$$

where f_o and f_r represent the activity coefficients of the oxidised and reduced species respectively, in solution. In most systems, the activity and diffusion coefficients of O and R are approximately equal, so that the half wave potential approximates to the standard electrode potential, viz.

$$E_{\frac{1}{2}} \simeq E_o \qquad 4.4$$

and (4.2) can consequently be written as

$$E_p \simeq E_o - \frac{0{\cdot}029}{n} \text{ volts} \qquad 4.5$$

For a redox couple, the peak potentials corresponding to the anodic and cathodic peak currents will therefore be separated by

$$\Delta E_p \simeq \frac{0{\cdot}059}{n} \text{ volts} \qquad 4.6$$

One further property may be derived from the shape of the peak, and that is

$$E_p - E_{p/2} = \frac{0{\cdot}057}{n} \text{ volts} \qquad 4.7$$

where $E_{p/2}$ is the potential at half peak height. Thus, from (4.1), (4.5) and (4.7) values of n, D_o and E_o may be determined from the size, shape and position of the experimental curve.

The stability of the reaction products is readily ascertained by comparing the relative heights of the peak currents for both cathodic and anodic potential sweeps. For a stable reaction product, the ratio

$$i_p^c/i_p^a \simeq 1$$

with this ratio becoming larger and dependent on the potential sweep rate as the reaction product becomes less stable.

TABLE 2 shows data for the voltammetric reduction in a three electrode, two compartment cell, of the aromatic hydrocarbons indicating the supporting electrolyte, reference electrode, working electrode and observed half wave potential. All reductions were conducted in Dimethylformamide solutions thoroughly degassed with dry nitrogen before each experiment. (Full experimental details are given in Chapter 6).

A typical cyclic voltammogram is shown in FIG. 13 for the reduction of perylene in DMF/Bu_4NBF_4 (0·2M) at a platinum wire electrode. The essential features of a reversible, stable system are clearly illustrated; the peak current potentials are invariant

TABLE 2

COMPOUND	SUPPORTING ELECTROLYTE	ELECTRODE	$-E_p$ Volts	$-E_{\frac{1}{2}}$ Volts	REFERENCE
Perylene	Bu_4NBF_4 (0·2M)	Pt	1·66	1·63	SCE
	"	W	1·65	1·62	SCE
	"	Pt	1·68	1·65	Ag/AgCl
	"	W	1·67	1·64	Ag/AgCl
	Me_4NBF_4 (0·1M)	Pt	1·68	1·65	SCE
	"	W	1·71	1·68	SCE
	"	Pt	1·59	1·56	Ag/AgCl
	"	W	1·62	1·59	Ag/AgCl
9,10 Dimethyl anthracene	Bu_4NBF_4 (0·2M)	Pt	1·98	1·95	SCE
	"	W	1·97	1·94	SCE
	"	Pt	2·00	1·97	Ag/AgCl
	"	W	1·99	1·96	Ag/AgCl
	Me_4NBF_4 (0·1M)	Pt	1·86	1·83	SCE
	"	W	1·86	1·83	SCE
	"	Pt	1·78	1·75	Ag/AgCl
	"	W	1·80	1·77	Ag/AgCl
9,10 Diphenyl anthracene	Bu_4NBF_4 (0·2M)	Pt	1·85	1·82	SCE
	"	W	1·85	1·82	SCE
	"	Pt	1·87	1·84	Ag/AgCl
	"	W	1·86	1·83	Ag/AgCl
	Me_4NBF_4 (0·1M)	Pt	1·87	1·84	SCE
	"	W	1·86	1·83	SCE
	"	Pt	1·75	1·72	Ag/AgCl
	"	W	1·76	1·73	Ag/AgCl

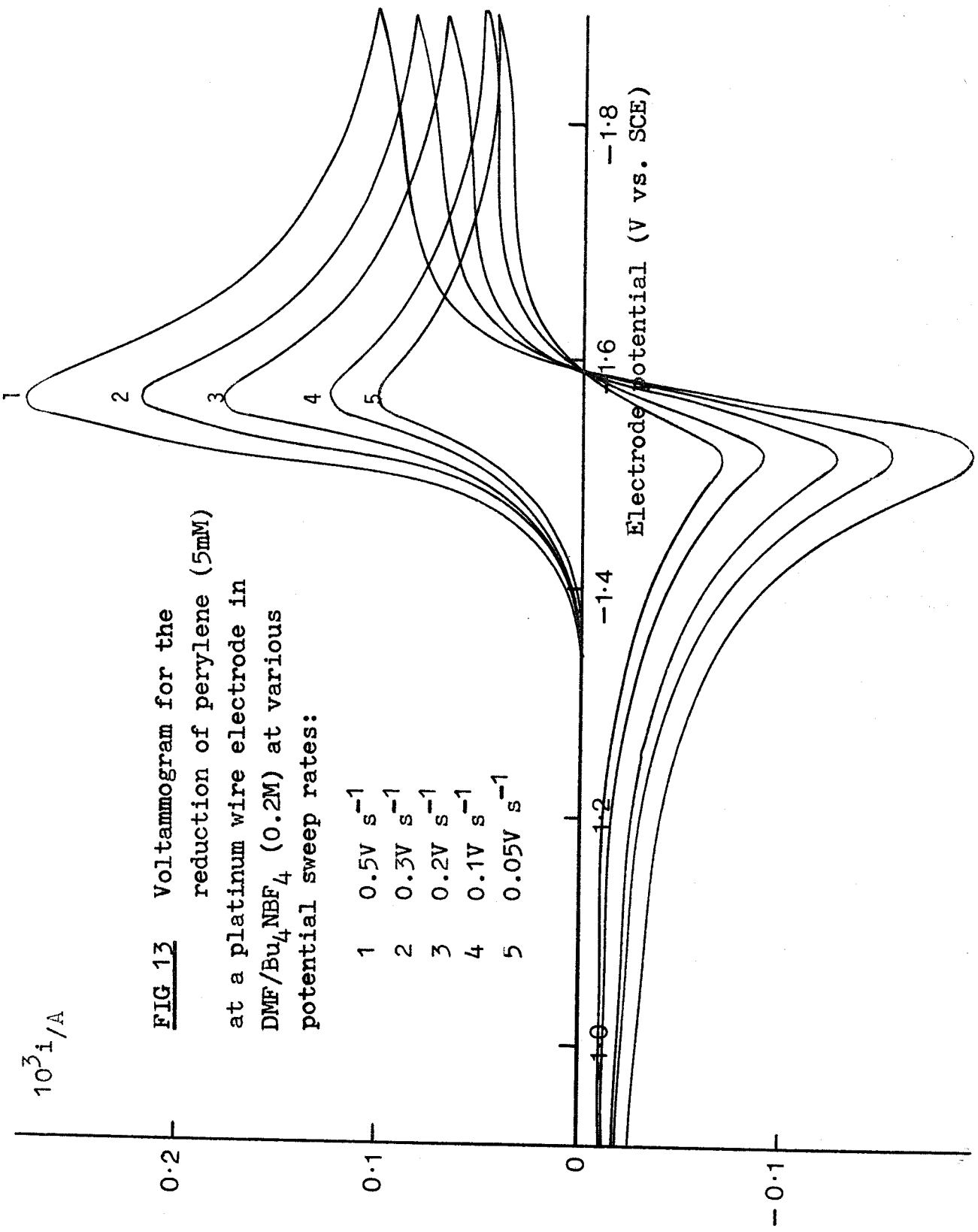

FIG 13 Voltammogram for the reduction of perylene (5mM) at a platinum wire electrode in DMF/Bu_4NBF_4 (0.2M) at various potential sweep rates:

1 0.5V s^{-1}
2 0.3V s^{-1}
3 0.2V s^{-1}
4 0.1V s^{-1}
5 0.05V s^{-1}

with sweep rate and $\Delta E_p \simeq 60mV$; a plot of peak current against the square root of the potential sweep rate is linear and the ratio of anodic to cathodic peak currents is approximately unity.

Different supporting electrolytes were chosen to investigate any variation in the half wave potential with cation, but, as can be seen from TABLE 2 the observed half wave potential, corresponding to the reduction of the neutral compound to the anion radical

$$R + e \longrightarrow R^{\bullet -} \qquad 4.7$$

is independent of the cation used. This is consistent with the work performed by Parker [100] in his studies of aromatic hydrocarbons, although he does report a cation dependence for the second reduction process corresponding to the formation of the dianion from the anion radical

$$R^{\bullet -} + e \longrightarrow R^{--} \qquad 4.8$$

This, he attributes to ion pairing effects between the dianions and the cations, with the strongest effect being observed in the presence of the smallest cations.

The comparison between platinum and tungsten for future use as microelectrode materials in non aqueous media indicated no discernable difference between the two metals as reflected in their observed half wave potentials.

One of the more important features of TABLE 2 is the choice of reference electrode. Suitable reference electrodes for use in non aqueous media are limited; many of the more common reference couples in aqueous systems are known to be unstable in certain non aqueous media [101]. For instance, the silver/silver (I) reference electrode with soluble silver (I) present in large excess when used in DMF solutions rapidly becomes unstable due to the reduction of

silver (I) to the metal by the solvent. Similarly, the Hg_2Cl_2/Hg couple is also unsatisfactory due to disproportionation of Hg_2Cl_2 in DMF. Commercial aqueous calomel electrodes are, nevertheless, widely employed as a reference electrode in aprotic media since their simplicity of use overrides many of the doubts concerning accuracy, particularly as regards the variable liquid junction potential between the electrode assembly and the solvent. Certainly, the half wave potentials measured with this reference electrode and listed in TABLE 2 show good agreement with those determined by other workers [98]. However, following the use of this reference electrode in some initial microelectrode experiments (see 4:ii) the apparent contamination of the catholyte solution with trace quantities of aqueous solution showed that alternative reference systems had to be used. A silver/silver chloride reference electrode was subsequently chosen and compared against the calomel electrode, both for stability and behaviour. Naturally the potentials recorded differed from those of the calomel electrode, but in addition, a dependence of the potential on the supporting electrolyte was found: in the presence of tetrabutyl ammonium salts a potential slightly more cathodic ($\sim 0{\cdot}02V$) of the calomel was recorded, whilst for the tetramethyl ammonium salts the silver/silver chloride reference recorded potentials more anodic ($\sim 0{\cdot}10V$) of the calomel electrode. This discrepancy may be attributed to the changes in the activity coefficient of the chloride ion with change of cation, with the silver/silver chloride electrode responding directly to the changes in chloride activity. In addition, problems also arose with the 'aging' of the electrode after prolonged immersion in DMF, producing variations in the reference potential from experiment to experiment; this could only be cured by re-anodisation of the silver electrode in solutions of hydrochloric acid (5M).

4:ii Determination of k_o' from steady state measurements

Initial experiments with lead and indium capillary microelectrodes to determine the apparent standard rate constant for the reduction of the aromatic hydrocarbons listed in TABLE 2, were conducted in a two compartment cell using a saturated calomel electrode as a counter/reference electrode. The electronic instrumentation, circuit diagrams and cells for these experiments are fully described in Chapter 6.

A series of voltammograms at very slow potential sweep rates ($\sim 10mV\ s^{-1}$) were recorded for solutions of known concentration of the aromatic hydrocarbons ($\sim 5mM$) and supporting electrolyte in Dimethylformamide. FIG. 14 illustrates the first reduction of 9,10 Diphenylanthracene in DMF/Bu_4NBF_4 (0·2M) at a lead capillary microelectrode at a linear potential sweep rate of $8{\cdot}33mV\ s^{-1}$. A well defined, although electronically 'noisy' polarographic wave corresponding to the reduction of Diphenylanthracene to the anion radical is observed reaching a diffusion controlled limiting current at high cathodic potentials. It is noticed, however, that the forward and reverse potential scans are not superimposed; the current voltage profile for the reverse scan being lower than that for the forward sweep. Furthermore, a slight increase in the value of the limiting current with increasing cathodic potential may also be detected. With slower sweep rates, the degree of hysteresis is accentuated although the current voltage profile for the forward sweep remains unchanged; the latter indicating that the steady state has been attained. This behaviour is consistent with protonation of the anion radical product through contamination of the electrolyte solution by leakage of aqueous solution from the calomel reference electrode. The reaction mechanism would then proceed as

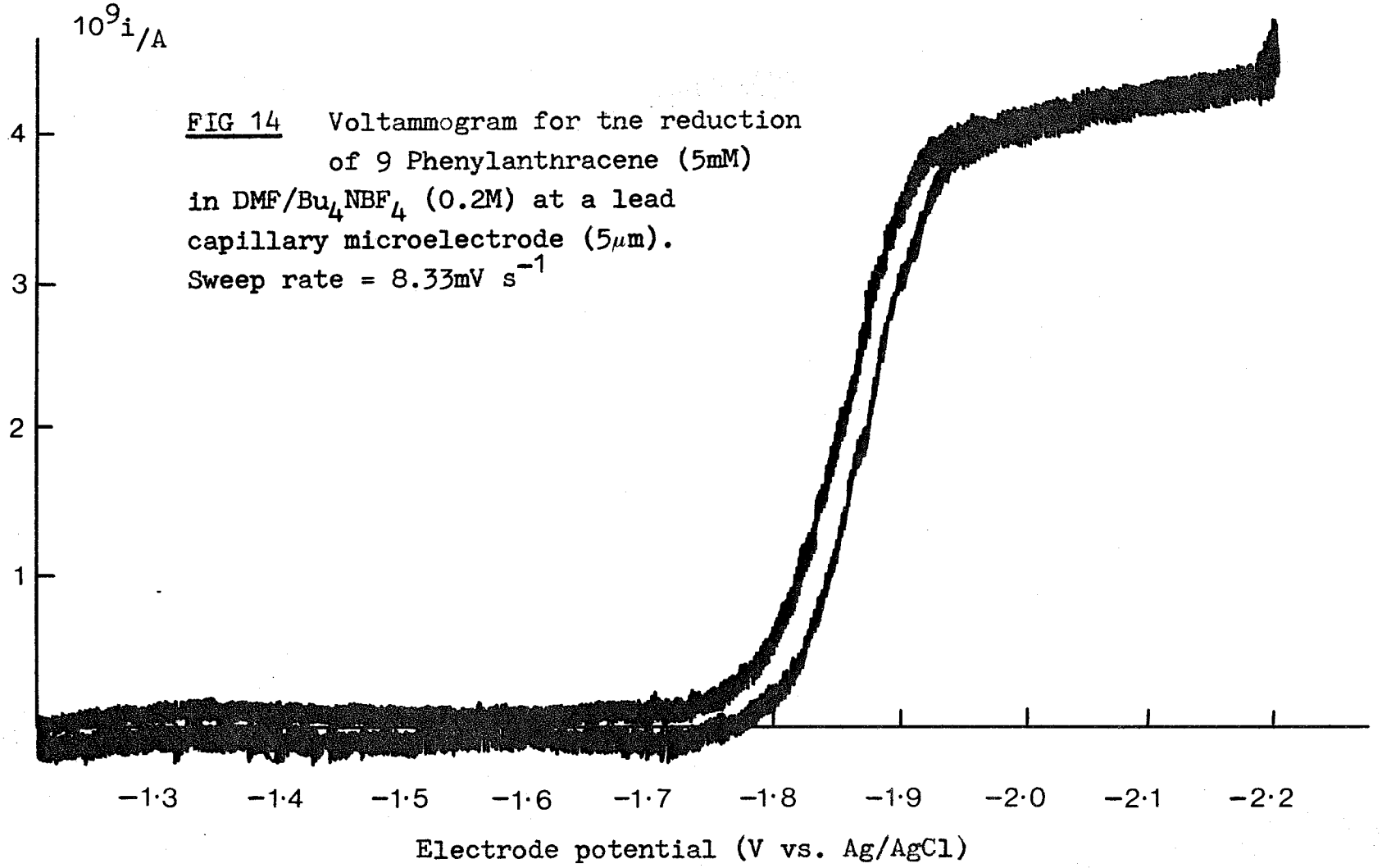

FIG 14 Voltammogram for tne reduction of 9 Phenylantnracene (5mM) in DMF/Bu_4NBF_4 (0.2M) at a lead capillary microelectrode (5μm). Sweep rate = 8.33mV s^{-1}

$$R + e = R^{\bullet -} \qquad 4.9$$

$$R^{\bullet -} + H^{+} = RH^{\bullet} \qquad 4.10$$

$$RH^{\bullet} + e = RH^{-} \qquad 4.11$$

$$RH^{-} + H^{+} = RH_2 \qquad 4.12$$

leading to higher observed currents since two electrons are consumed in the process as opposed to one in the normal reaction. The depleted concentration of $R^{\bullet -}$ by reaction with protons in solution will also shift the half wave potential to more cathodic potentials and therefore give rise to the observed hysteresis.

Silver/silver nitrate, silver/silver chloride and mercury pool reference electrodes were each in turn substituted for the calomel electrode in the appropriate cell, producing in each case a reduction in the degree of hysteresis and a more constant value of the limiting current.

The operation of a mercury pool reference electrode in DMF is conditional on the presence of iodide ions, provided by the supporting electrolyte, to form an insoluble complex HgI_4^{--} of constant activity, with the mercuric ions formed by the anodic oxidation of mercury during its function as a counter electrode. This reference system can only be used as a consequence in two electrode cells where it acts simultaneously as both reference electrode and anode. The potential of the mercury pool electrode relative to the saturated calomel electrode in DMF solutions has been established [102] and this value was confirmed from measurements of the half wave potential of the perylene system in DMF/Bu_4NI in both three electrode cyclic voltammetry (with calomel electrode) and slow potential sweep microelectrode voltammetry, with a mercury pool electrode, (viz. Hg pool is -0·55V with respect to calomel).

The addition of alumina, specially activated

for solvent drying (Hopkin & Williams Ltd.), to the electrolyte following experiments by Parker in Acetonitrile and Dimethylformamide [103] removed the hysteresis effect completely and also produced extremely flat limiting currents. This suggests that even after extensive precautions to dry the solvent through distillation procedures and storage under dry nitrogen conditions, residual water is still present in the electrolyte which may only be removed in situ by a suitable dessicating agent.

The reproducibility of the current voltage profiles was improved by the replacement of lead and indium capillary microelectrodes with those prepared from tungsten and later, platinum. These electrodes were inherently less 'noisy' than their capillary counterparts [104] , but the improved reproduciblity was due almost entirely to the ability to repolish the electrodes with alumina powder between experiments. A variable rise time facility featured on the Keithley picoammeter was able to even further improve the profile by the virtual elimination of all extraneous 'noise' so frequently encountered at these low currents.

With these improvements, a number of slow linear potential sweep voltammograms of the first reduction process of perylene in Dimethylformamide were recorded for several microelectrodes prepared from both tungsten and platinum encompassing a wide range of electrode radii. Two examples of the steady state current voltage curves obtained on tungsten and platinum microelectrodes are shown in FIGS. 15 & 16 respectively, illustrating the lack of hysteresis between the forward and reverse potential sweeps and the flat limiting currents obtained at high cathodic potentials in the presence of alumina.

The analysis of the current voltage profiles was aided by a computer program based on equation (2.110). The logarithmic form of which may be written

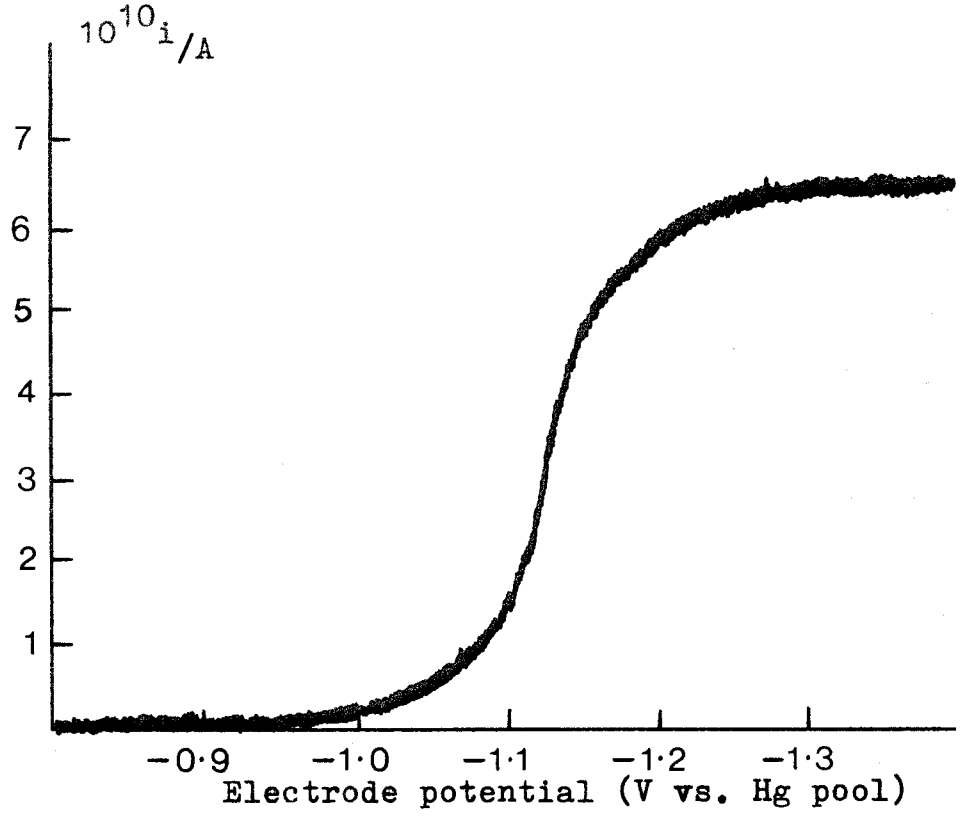

FIG 15 Voltammogram for the reduction of perylene (1·7mM) at a tungsten microelectrode (1·2μm) in DMF/Et_4NI. Sweep rate = 8·33mV/s.

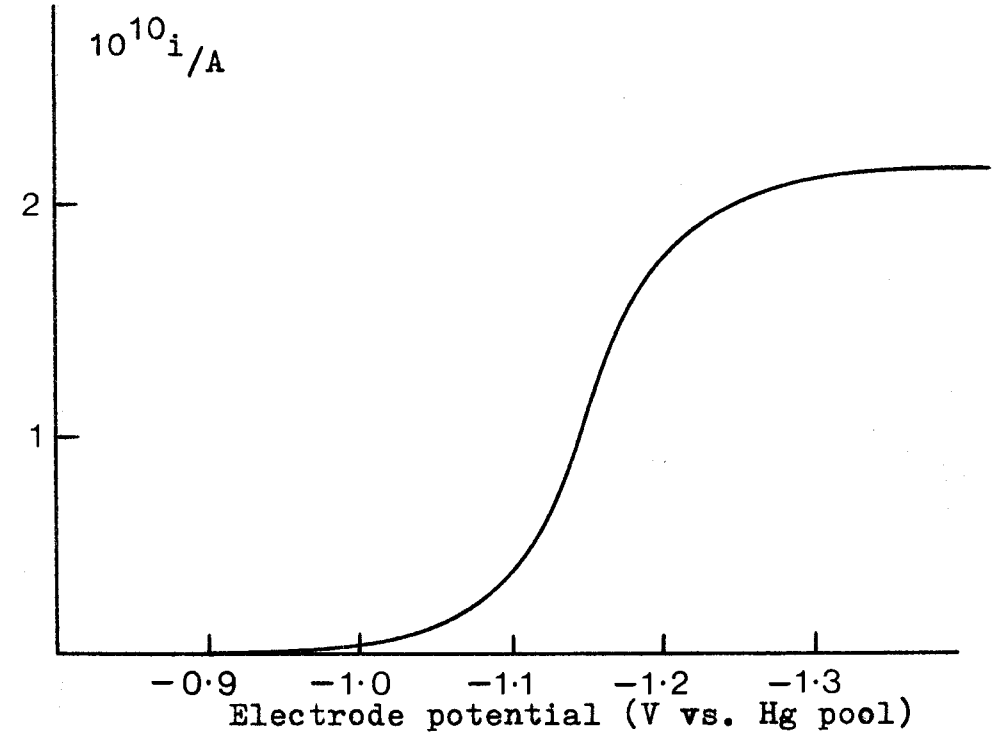

FIG 16 Voltammogram for the reduction of perylene (3·6mM) at a platinum microelectrode (3μm) in DMF/Bu_4NBF_4. Sweep rate = 8·33mV/s.

$$\ln \frac{i_s}{i_d - i_s(1 + \exp \frac{nFE}{RT})} = \ln \frac{nFk'_o C_o^\infty}{i_d} - \frac{\alpha nFE}{RT} \qquad 4.13$$

so that a plot of the left hand side of (4.13) against potential, E, should produce a straight line with

$$\text{slope} = \frac{\alpha nF}{RT} \qquad 4.14$$

$$\text{intercept} = \ln \frac{nFk'_o C_o^\infty}{i_d} \qquad 4.15$$

from which values for the apparent standard rate constant, k'_o, and the transfer coefficient, α, may be calculated for known values of the limiting current density, i_d. The limiting current density could be calculated from the observed limiting current, i_{obs} by assuming an electrode of circular disc cross section of area πr^2. This enables (2.82) for the limiting current density at a spherical electrode under pseudo steady state conditions to be expressed as

$$i_{obs} = i_s \times \pi r^2 \qquad 4.16$$

$$= \frac{nFDC_o^\infty}{r} \pi r^2 \qquad 4.17$$

$$= nFDC_o^\infty \pi r \qquad 4.18$$

Hence, with known values of i_{obs}, n, F, D and C_o^∞ a value for the radius, r, could be calculated which could then be substituted back into (2.82) to obtain the limiting current density.

A computer program was compiled in BASIC (Appendix A) to evaluate k'_o and α for a given set of current voltage data points together with values for the limiting current and half wave potential. A

facility was also incorporated into the program to vary the half wave potential both positive and negative of its true value as determined from cyclic voltammetry measurements, so as to observe the effect on the calculated values of the apparent standard rate constant and transfer coefficient due to any small error in the half wave potential. For each value of the half wave potential the computer program then produced a Tafel plot of the logarithmic term on the left hand side of (4.13) against potential. From the intercept and slope at the prescribed half wave potential, values for the apparent standard rate constant and transfer coefficient were then calculated using (4.15) and (4.14) respectively.

The results of the analysis described above for the reduction of perylene are shown in FIGS. 17 and 18 for a number of different electrodes. It is noticeable from FIG. 17 that values for k_o' are not presented at potentials close to the experimentally determined value for the half wave potential of $E_{\frac{1}{2}} = -1{\cdot}10V$ (vs. Hg pool). Values for the apparent standard rate constant could not be calculated from the Tafel plots due to the logarithmic term on the left hand side of (4.13)

$$\ln \frac{i_s}{i_d - i_s(1 + \exp \frac{nFE}{RT})} = \ln \frac{nFk_o'C_o^{\infty}}{i_d} - \frac{\alpha nFE}{RT} \qquad 4.13$$

registering a negative argument at increasingly less anodic potentials to the half wave potential as the value for the half wave potential was varied cathodically towards its true value. This infers that

$$i_s(1 + \exp \frac{nFE}{RT}) > i_d \qquad 4.19$$

for large anodic potentials relative to the chosen

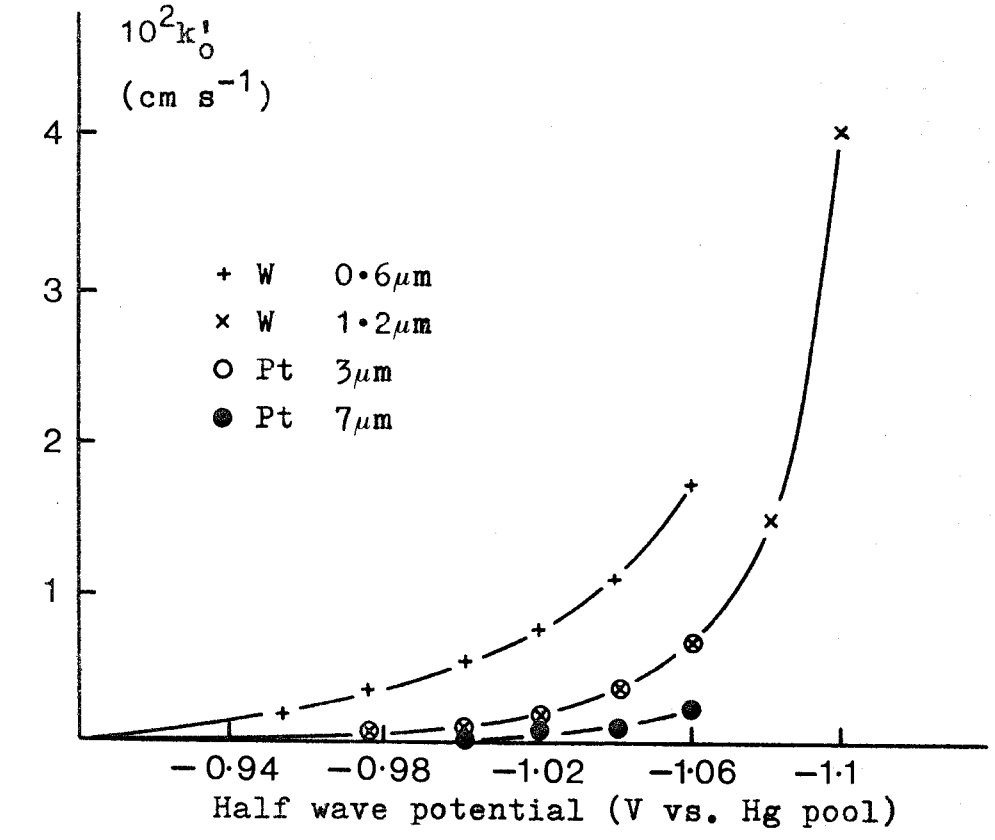

FIG 17 Variation of k_o' with half wave potential for the reduction of perylene in DMF/Bu_4NI

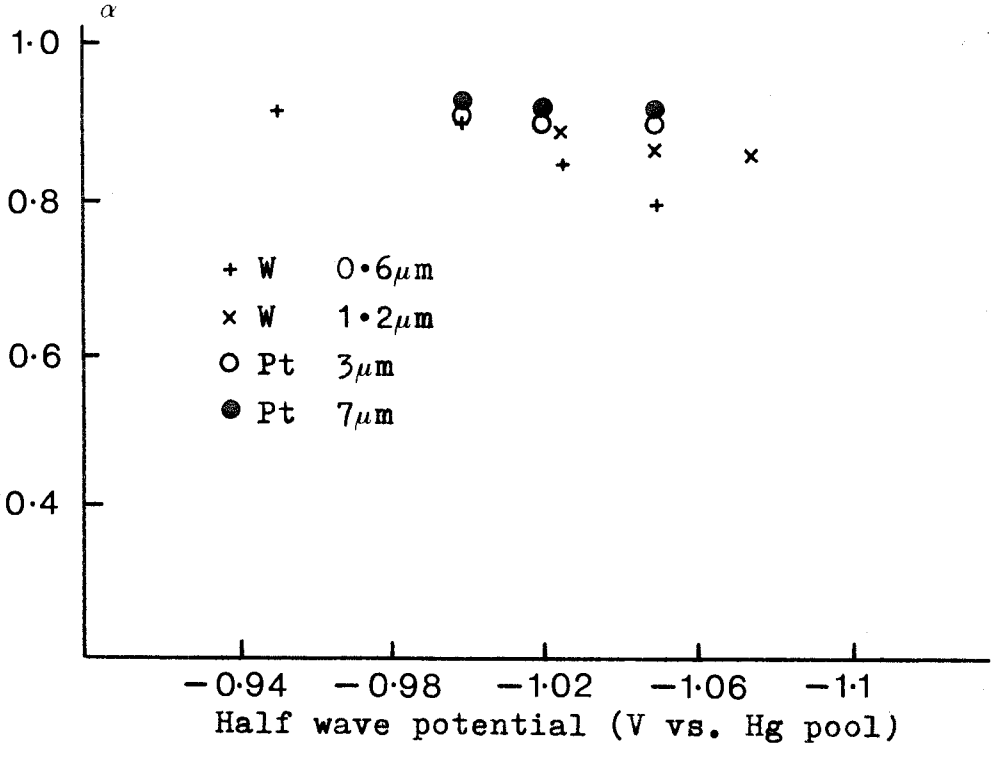

FIG 18 Variation of α with half wave potential for the reduction of perylene in DMF/Bu_4NI

half wave potential. The problem here is the accurate measurement of the current at these high anodic potentials, i.e. at the foot of the reduction wave. Graphical determination of the current invariably overestimates the real values, resulting in the inequality of (4.19) and the subsequent negative logarithmic arguments. This situation, furthermore, worsens as the half wave potential is varied cathodically and a larger proportion of the reduction wave, anodic to the half wave potential, is included for analysis.

However, for values of k_o' that were obtained, it can be seen from FIG. 17 that for each value of the half wave potential, the calculated value of k_o' increases as the electrode radius becomes smaller. This is consistent, with reference to equations (2.105) and (2.107) with mass transfer control at the standard electrode potential.

The values of k_o' obtained by this analysis are therefore representative of the rate of mass transfer to the electrode rather than the rate of electron transfer at the electrode surface. The true rate of electron transfer can consequently be concluded to exceed the calculated values of k_o' indicated by FIG. 17. The validity in applying (4.13) for an irreversible electrode reaction to these current voltage curves is therefore also questionable and this is further reflected in the values of the transfer coefficient, α, determined from the same Tafel plots. As can be seen from FIG. 18, the values of the transfer coefficient obtained do not vary significantly from unity and while this may represent a barrierless transition [105], it is far more probable that the true values are obscured by mass transfer effects.

Diffusion control at the standard electrode potential was also established, in a similar manner, for the other aromatic hydrocarbons listed in TABLE 2 with the tungsten and platinum microelectrodes available. As a result, alternative systems with

reported slower electron transfer rates were studied. The reduction of some nitroaromatic and nitroaliphatic compounds, in similar aprotic media were selected based on earlier studies by Peover and Powell [106].

Voltammograms for the reduction of para nitroaniline (FIGS. 19 and 20), tert nitrobutane (FIGS. 23 and 24) and nitromesitylene (FIGS. 29 and 30) using both tungsten and platinum microelectrodes under conditions of pseudo steady state slow linear potential sweep were recorded in solutions of DMF/Bu_4NI (0·2M). These current voltage curves were then analysed, as before with the aid of the computer program, to obtain values for the apparent standard rate constant and transfer coefficient.

The results of the analysis of the current voltage curves for the reduction of para nitroaniline are shown in FIGS. 21 and 22. Values for the diffusion coefficient and standard electrode potential were taken from [106]. From FIG. 21, a dependence of the calculated value of k_o' on the electrode radius, at each selected value of the half wave potential is clearly visible, indicating once again diffusion control at the electrode surface. The values of the transfer coefficient, α, obtained from the same Tafel plots (FIG. 22) are similarly assumed to be unrepresentative of the electron transfer reaction.

At the true standard electrode potential, the calculated value for the apparent standard rate constant at a tungsten microelectrode (0·8μm) is $\sim 7 \times 10^{-2}$cm s^{-1}, well below the value of 1·21cm s^{-1} measured by Peover and Powell [106]. The value of $\sim 7 \times 10^{-2}$cm s^{-1} represents therefore the upper limit of electron transfer reactions measurable with these electrodes before mass transfer effects dominate the observed rate of reaction.

An electron transfer reaction which does fall within this upper limit, however, is the reduction of tert nitrobutane in DMF/Bu_4NI (0·2M) with a reported value of $k_o' = 0{\cdot}009$cm s^{-1} [106].

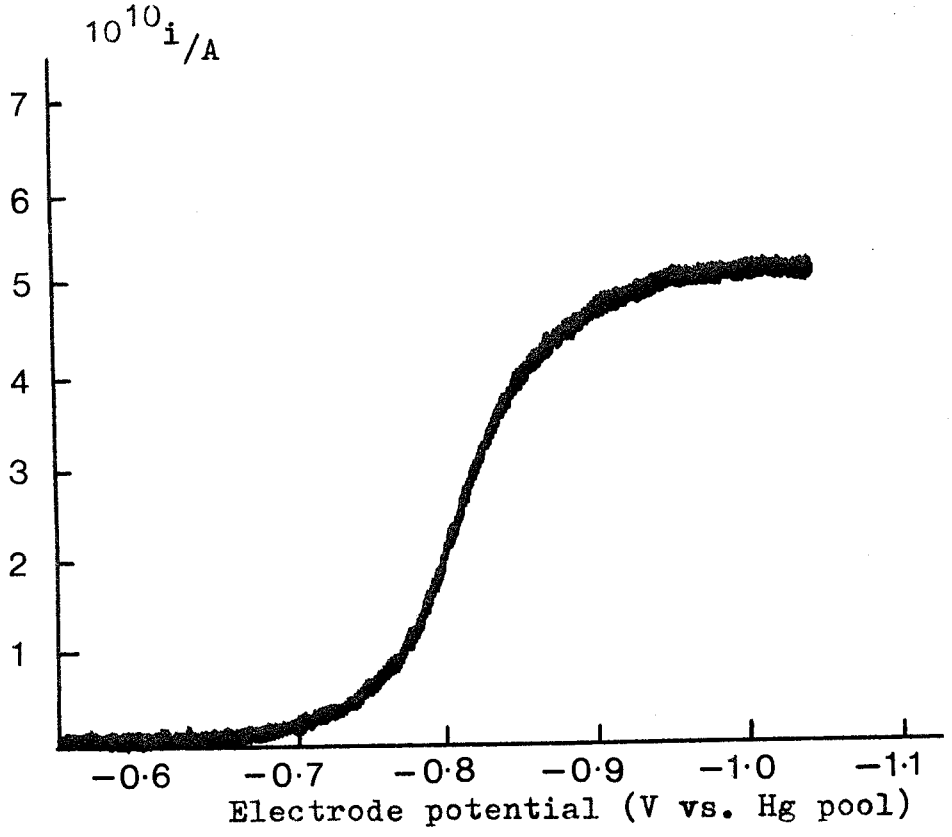

FIG 19 Voltammogram for the reduction of p nitroaniline (1·9mM) at a tungsten microelectrode (0·8μm) in DMF/Bu_4NI. Sweep rate = 8·33mV/s.

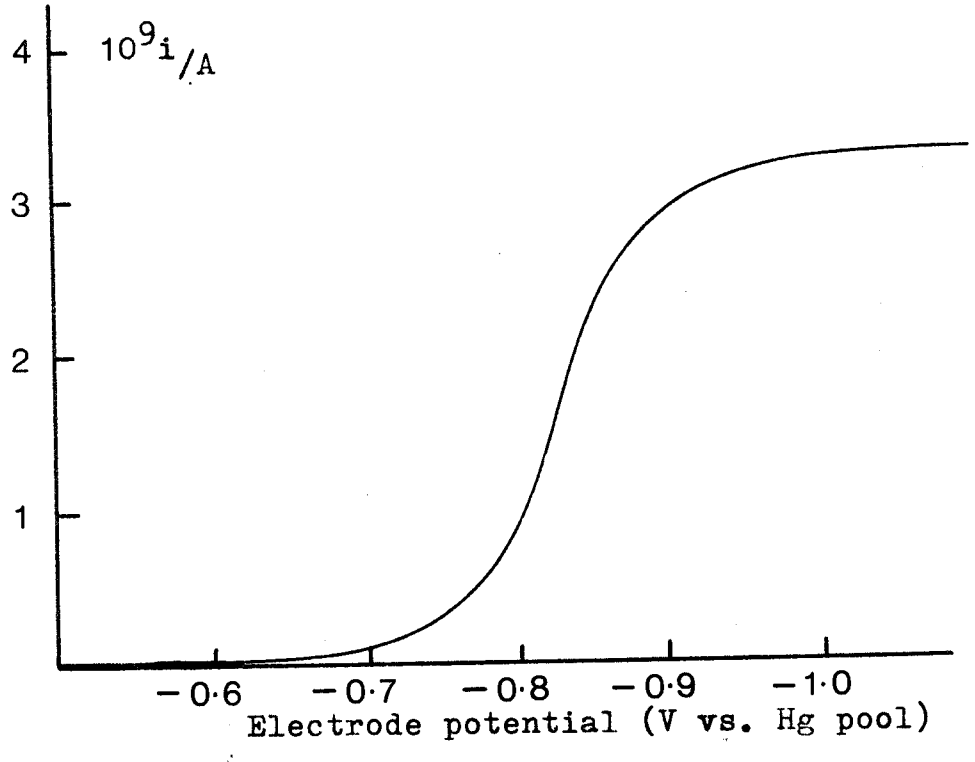

FIG 20 Voltammogram for the reduction of p nitroaniline (7mM) at a platinum microelectrode (1·6μm) in DMF/Bu_4NI. Sweep rate = 8·33mV/s.

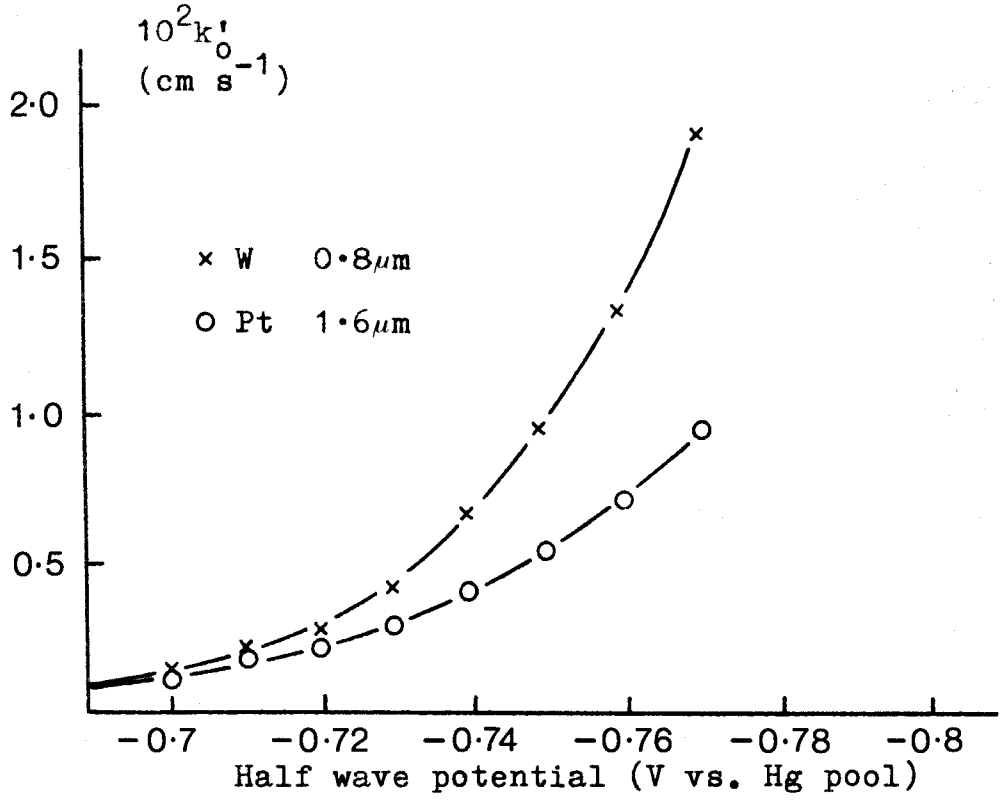

FIG 21 Variation of k'_o with half wave potential for the reduction of p nitroaniline in DMF/Bu_4NI

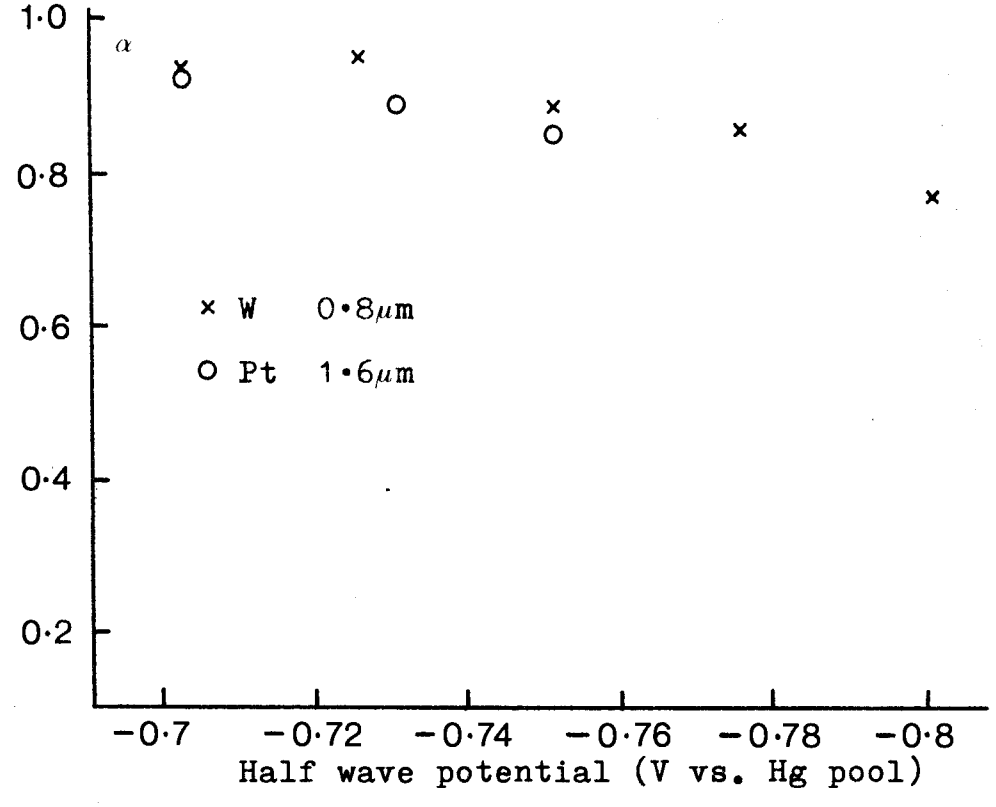

FIG 22 Variation of α with half wave potential for the reduction of p nitroaniline in DMF/Bu_4NI

Voltammograms for the reduction of tert nitrobutane at tungsten and platinum microelectrodes are shown in FIGS. 23 and 24 respectively. It can be seen that for both microelectrodes, the current voltage profile extends over a wide potential range and also that at high cathodic potentials a flat, well defined limiting current is not obtained, due to the proximity of the reduction wave to the cathodic limit of the electrolyte. Nevertheless, these voltammograms were analysed, in the usual manner, using extrapolated values for the limiting current and values for the standard electrode potential and diffusion coefficient taken from [106] .

The results from this analysis are presented in FIGS. 25 and 26. In marked contrast to the previous analyses, calculated values for the apparent standard rate constant are much less dependent on the electrode radius at each chosen half wave potential than was found, for example, with perylene (FIG. 25). The values for the transfer coefficient, too, appear independent of the electrode radius, varying between $\sim 0{\cdot}7 - 0{\cdot}4$ depending on the value of the half wave potential; both factors typical of a kinetically controlled electron transfer reaction.

At the true standard electrode potential (-1·10V vs. Hg pool) the apparent standard rate constant, determined at a tungsten microelectrode ($0{\cdot}2\mu m$) is calculated to be $3{\cdot}6 \times 10^{-3}$cm s^{-1} with a transfer coefficient of 0·6. These values compare with $k_o' = 4{\cdot}5 \times 10^{-3}$cm s^{-1} and $\alpha = 0{\cdot}5$ measured by Saveant and Tessier [74,75] on mercury electrodes in DMF/Bu_4NI using convolution potential sweep methods and $k_o' = 4{\cdot}1 \times 10^{-3}$cm s^{-1} with $\alpha = 0{\cdot}43$ obtained by Corrigan and Evans [107] in ACN/Bu_4NClO_4 on mercury electrodes using cyclic voltammetry and potential step methods; the latter figure being one of several determined in a range of electrolytes of various concentrations on both platinum and mercury electrodes. In their investigations, Corrigan and Evans found

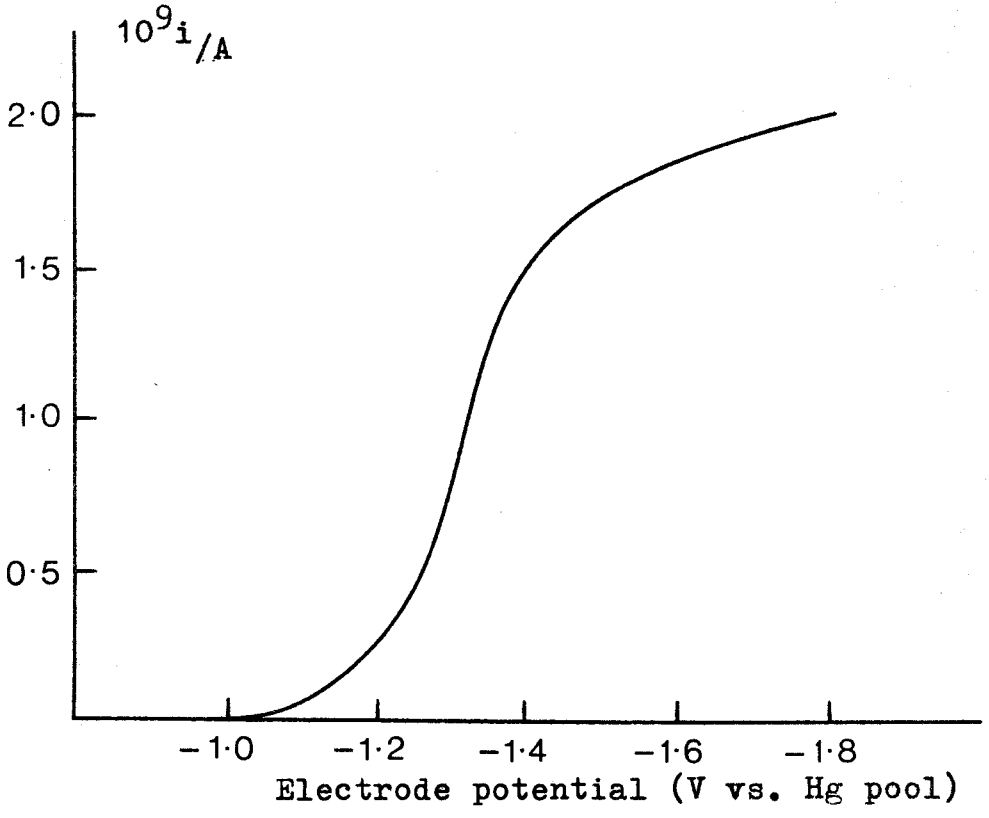

FIG 23 Voltammogram for the reduction of t-nitrobutane (12mM) at a tungsten microelectrode (0·38μm) in DMF/Bu_4NI. Sweep rate = 8·33mV/s.

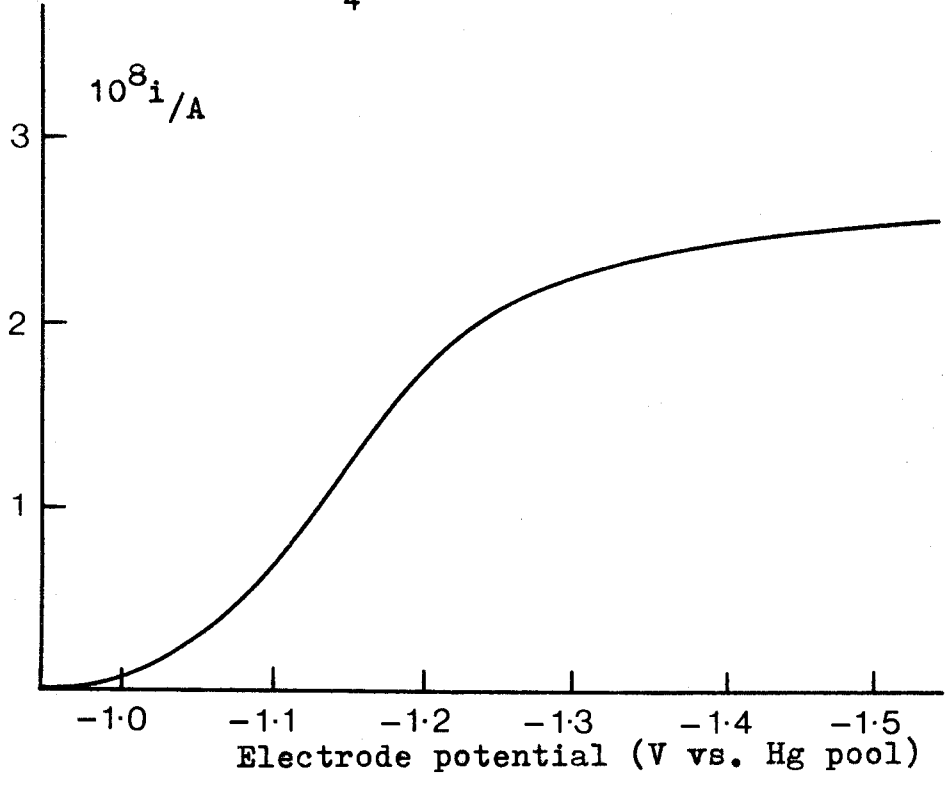

FIG 24 Voltammogram for the reduction of t-nitrobutane (12mM) at a platinum microelectrode (5·8μm) in DMF/Bu_4NI. Sweep rate = 8·33mV/s.

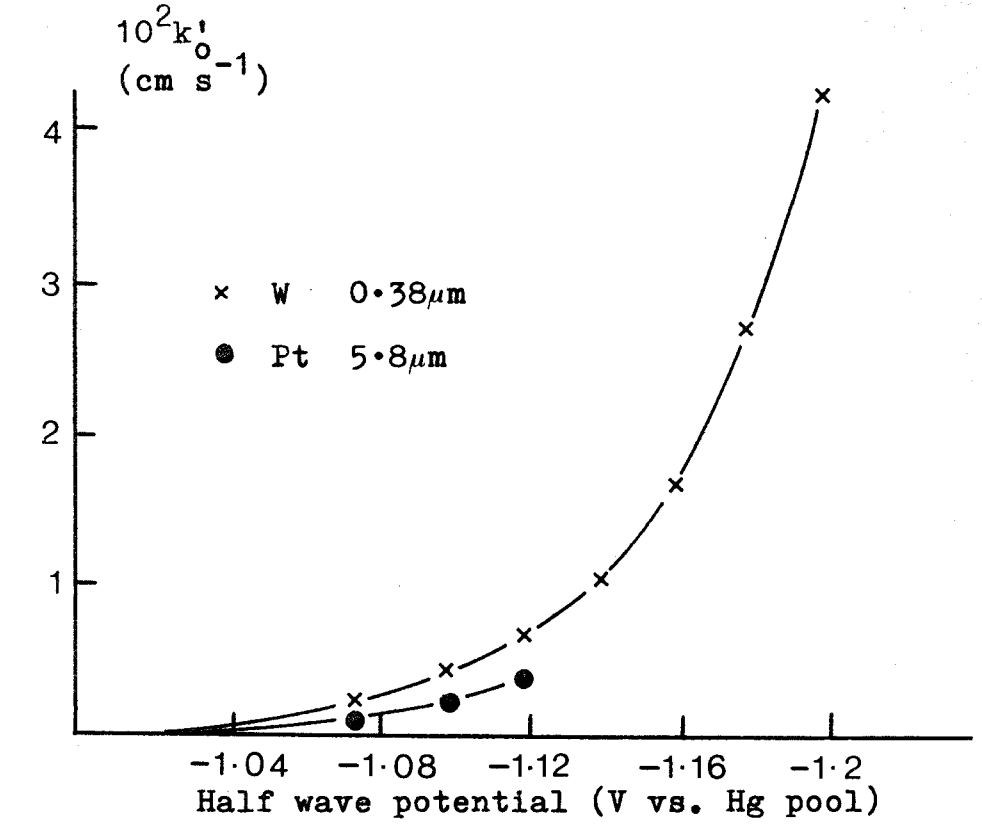

FIG 25 Variation of k'_o with half wave potential for the reduction of t-nitrobutane in DMF/Bu_4NI

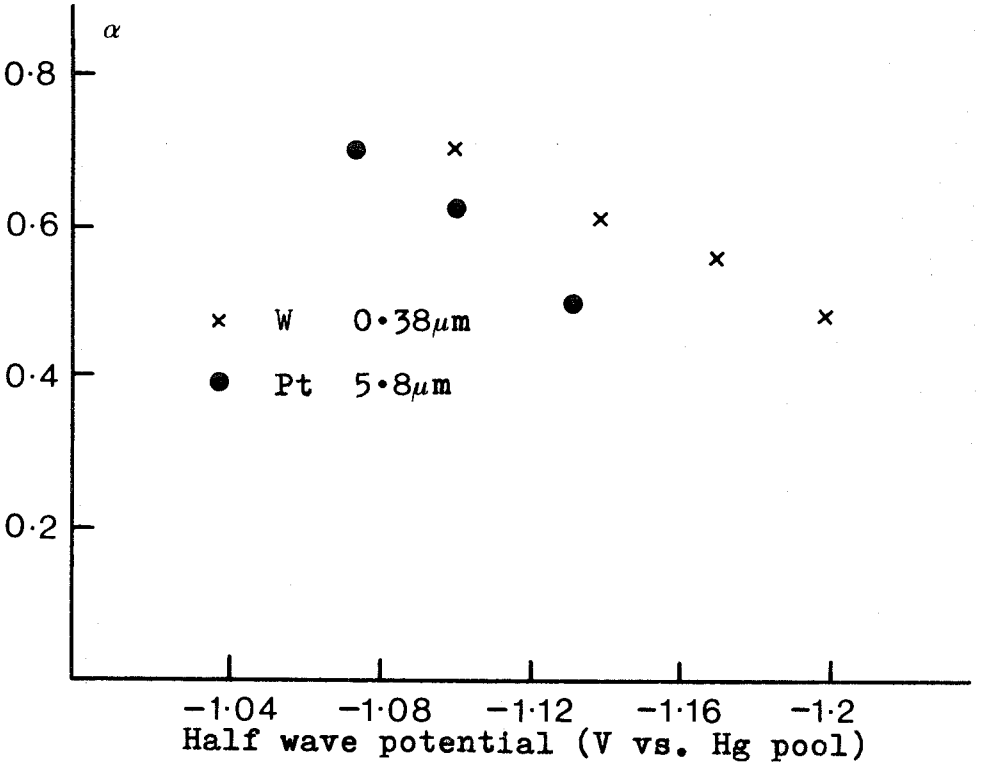

FIG 26 Variation of α with half wave potential for the reduction of t-nitrobutane in DMF/Bu_4NI.

the results obtained on platinum and mercury to differ in several respects. The rate constant at platinum was lower than the rate constant measured in the same solution at a mercury electrode. Also, the platinum data were generally very irreproducible due to extreme sensitivity of the reaction rate parameters to the surface condition of the electrode. Reproducibility was improved, it was found, by polishing the electrode surface before use and the addition of activated alumina to the solution - both these measures being standard practice in the present study. The slow rates and irreproducibility of rate measurements at platinum electrodes was tentatively ascribed to the blockage of the electrode surface by a film or some absorbed species following evidence found by Lane and Hubbard in studies of slow electrode reactions in aprotic media that chemisorbed solvent molecules were actually blocking the electrode surface [108] .

More significant perhaps than the actual measurement of the rate parameters themselves, is the variation of the transfer coefficient with applied potential. In FIG. 27 the Tafel plots at the true standard electrode potential on both platinum and tungsten microelectrodes are illustrated, showing curvature of the Tafel plot as a function of the applied potential. The corresponding value of the transfer coefficient, determined from the slope of the Tafel plot is shown in FIG. 28 as a function of the applied potential for both electrodes. It is seen from FIG. 28 that the rate of change of the transfer coefficient with applied potential,

$$\frac{d\alpha}{dE} = 1{\cdot}04\ V^{-1} \qquad \text{(Pt electrode)}$$

$$\frac{d\alpha}{dE} = 0{\cdot}66\ V^{-1} \qquad \text{(W electrode)}$$

In terms of the Marcus theory of outer sphere

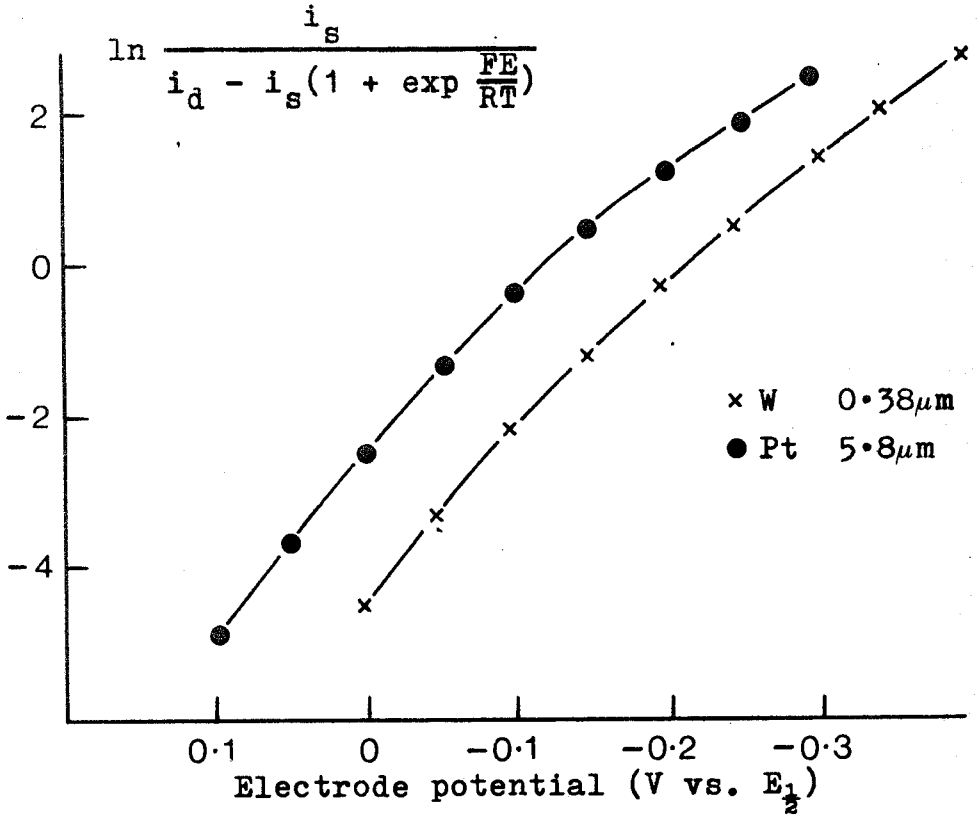

FIG 27 Tafel plot according to (2.110) for the reduction of t-nitrobutane in DMF/Bu_4NI.

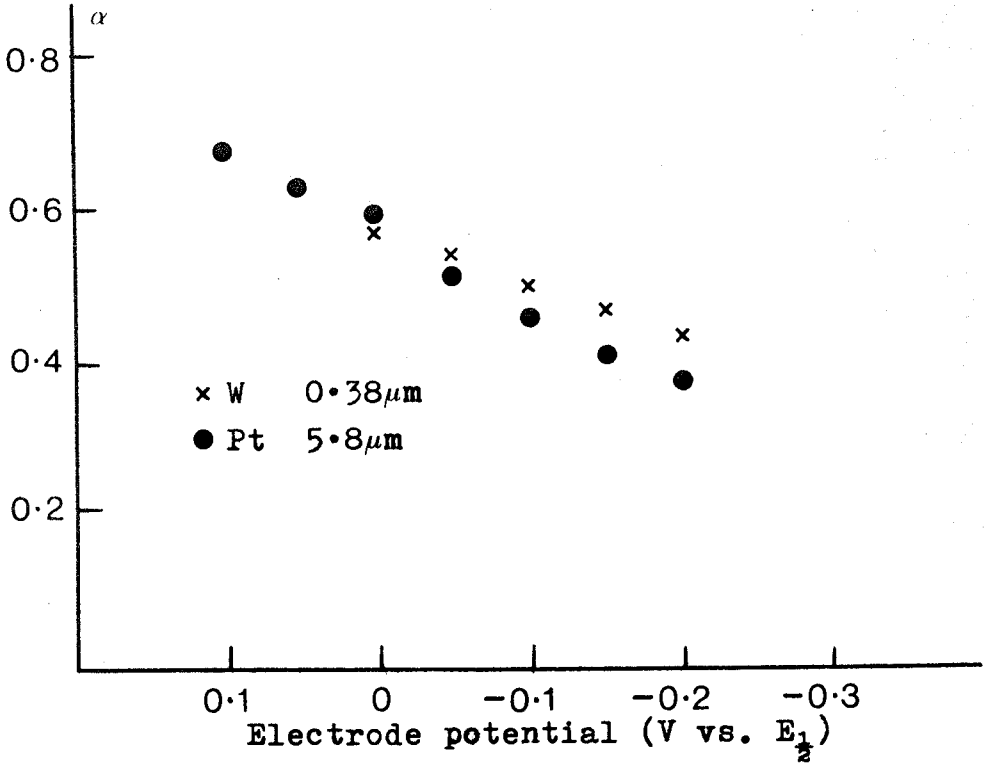

FIG 28 Variation of α with applied potential for the reduction of t-nitrobutane in DMF/Bu_4NI.

electron transfer [5 - 7] where a dependence of the transfer coefficient, α, upon potential is predicted

$$\alpha = 0{\cdot}5 + \frac{nF}{4\lambda}(E - E_{\frac{1}{2}} - \Phi_2) \qquad 4.20$$

and the apparent standard rate constant is given by

$$k'_o = xZ_{el} \exp -\frac{\lambda}{4RT} \exp \frac{\alpha nF\Phi_2}{RT} \qquad 4.21$$

theoretical estimates of the dependence of α on the electrode potential may be calculated, from (4.20) and (4.21) with the experimentally determined value of $k'_o = 3{\cdot}6 \times 10^{-3}$cm s^{-1} to give

$$\frac{d\alpha}{dE} = 0{\cdot}21\ V^{-1}$$

The value of Z_{el} was calculated from

$$Z_{el} = \left(\frac{RT}{2\pi M}\right)^{\frac{1}{2}} \qquad 4.22$$

where M is the molar mass; in the present case $Z_{el} = 6 \times 10^3$cm s^{-1}. The value of Φ_2 was estimated as -145mV based on the double layer data of Saveant and Tessier [109] and assuming the difference in potentials of zero charge between mercury and platinum to be the same as the difference in work functions between the two metals. It was further assumed that the value of Φ_2 was not influenced by compression of the double layer due to sphericity effects [110].

The experimentally determined slope $d\alpha/dE$ for both platinum and tungsten microelectrodes are seen to be significantly larger than the value predicted from the Marcus theory. The figure of $1{\cdot}04V^{-1}$ for the platinum 6μm microelectrode is particularly high but in view of the lower rate constant recorded at this electrode, mass transfer effects are suspected. For the tungsten microelectrode, the value of $0{\cdot}66V^{-1}$ compares favourably with a value of $0{\cdot}7V^{-1}$ obtained by Corrigan and Evans at a polished, clean, platinum

surface, although they also obtained lower values depending on the electrode pretreatment. In general, a number of workers, working with solid electrodes, have found higher values for $d\alpha/dE$ than theoretically predicted [111 - 113]. Samec and Weber [112] suggested that better agreement between theory and experiment would result if the tunnelling coefficient could be assumed to be less than unity i.e. the reaction assumed to be non adiabatic. A small tunnelling coefficient could result, they suggest, from a surface film or absorbed species blocking the close approach to the electrode surface.

Although the results given above do not represent an accurate verification of the Marcus theory, significant deviation from the Butler - Volmer behaviour is nevertheless detected. It is with this measured degree of success in determining the rate parameters of tert nitrobutane in DMF/Bu_4NI that attempts were subsequently made to measure the corresponding rate parameters for the slightly faster reduction of nitromesitylene ($k_o' \sim 0{\cdot}1cm\ s^{-1}$ [106]) in the same electrolyte.

Voltammograms for the reduction of nitromesitylene at both platinum and tungsten microelectrodes are presented in FIGS. 29 and 30. Analysis of the current voltage curves was conducted in the usual manner with the aid of the computer program, to produce the results shown in FIGS. 31 and 32 for the variation of k_o' and α with the chosen half wave potential. Once again however, the electrode radius is seen to influence the measured value of k_o' quite markedly, to give a maximum value at the true standard electrode potential (-0·82V vs. Hg pool) of $k_o' = 0{\cdot}08cm\ s^{-1}$ with $\alpha = 0{\cdot}82$. The value of k_o' measured here is lower than that obtained by Peover [106], while the value of the transfer coefficient is substantially higher. These values can only be explained in terms of partial mass transfer at the standard electrode potential, requiring even higher rates of mass transfer to establish full kinetic control.

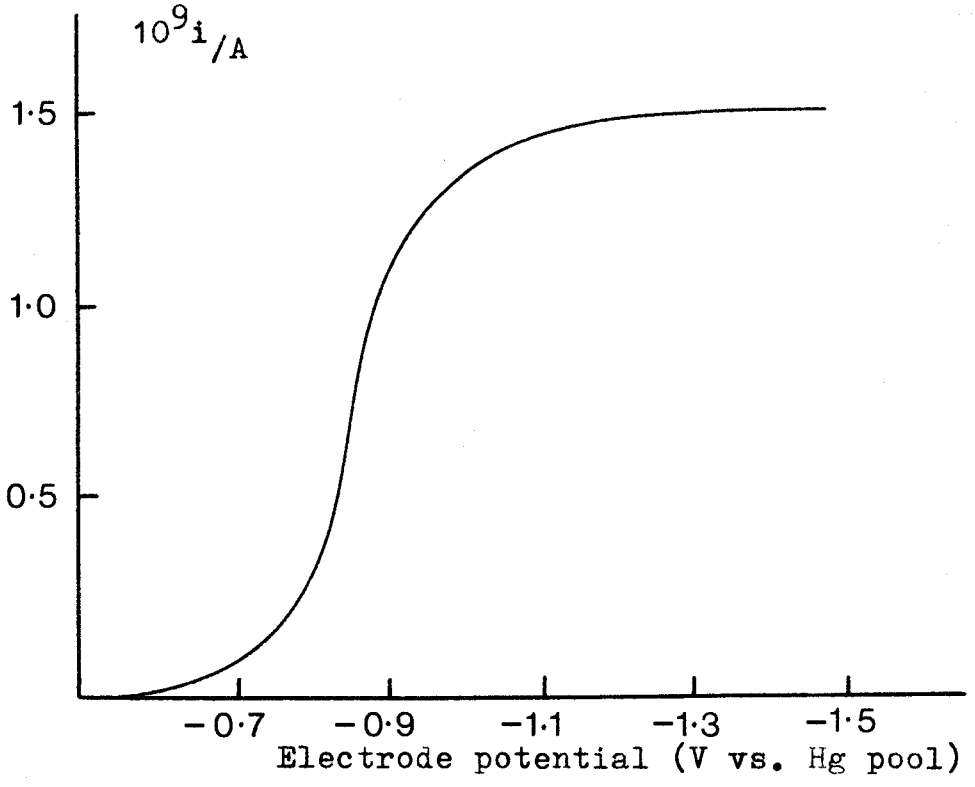

FIG 29 Voltammogram for the reduction of nitromesitylene (21mM) at a tungsten microelectrode (0·28μm) in DMF/Bu_4NI. Sweep rate = 8·33mV/s.

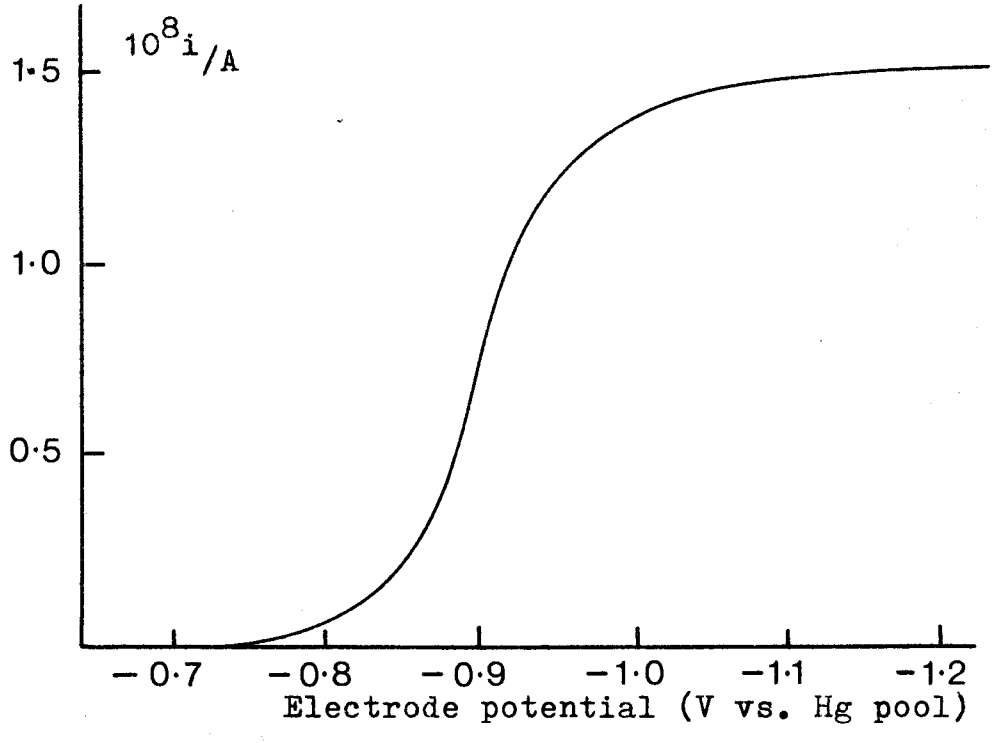

FIG 30 Voltammogram for the reduction of nitromesitylene (26mM) at a platinum microelectrode (2·2μm) in DMF/Bu_4NI. Sweep rate = 8·33mV/s.

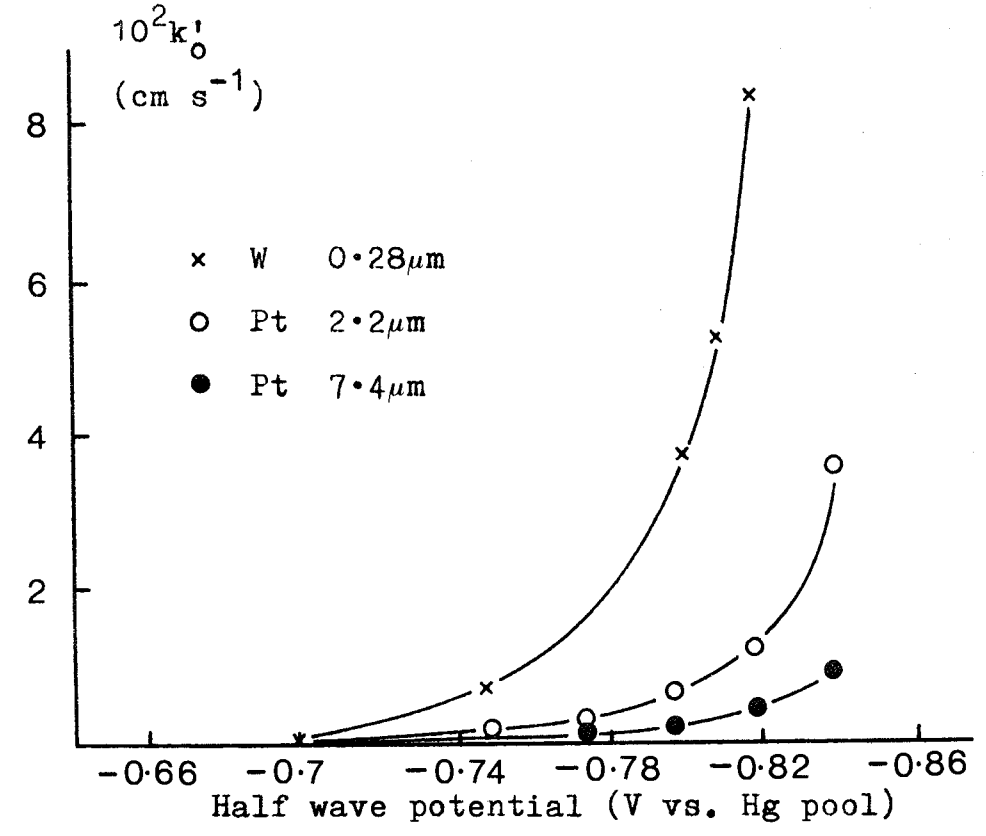

FIG 31 Variation of k_o' with half wave potential for the reduction of nitromesitylene in DMF/Bu_4NI

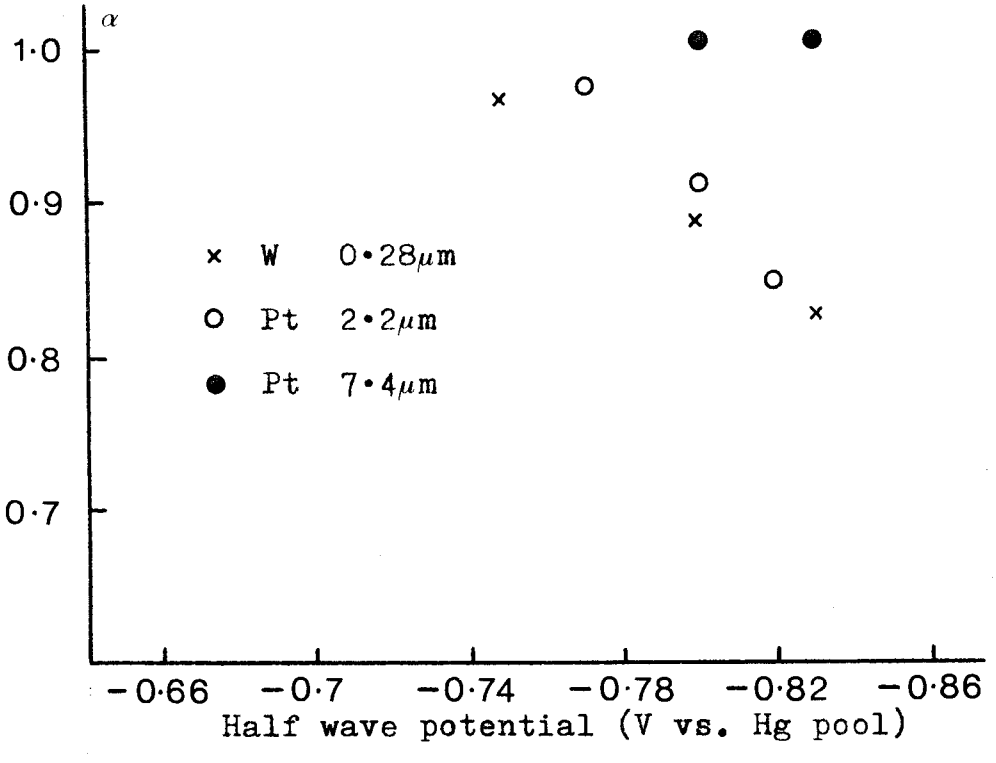

FIG 32 Variation of α with half wave potential for the reduction of nitromesitylene in DMF/Bu_4NI

4:iii Fast linear potential sweep analysis

To enhance the rate of mass transfer even further, cyclic voltammograms were recorded at higher potential sweep rates in order to take advantage of the time dependent term of equation (2.77)

$$i_s = i_{pl} + \frac{nFD(C_o^{\infty} - C_o)}{r_o} \qquad 2.77$$

in addition to the steady state term utilised in the previous analysis for very slow, pseudo steady state linear potential sweep experiments.

Cyclic voltammograms of compounds analysed previously in (4:ii) under slow linear sweep conditions were recorded for a number of sweep rates at both tungsten and platinum microelectrodes in the same two electrode cell used previously. A selection of these voltammograms for the reduction of perylene, para nitroaniline and nitromesitylene are presented in FIGS. 33 - 37. Cyclic voltammograms at high potential sweep rates for the reduction of tert - nitrobutane were unfortunately found to be unsuitable for analysis due to the proximity of the reduction peak to the background reduction wave; the peak being almost totally obscured by the background reaction.

The current voltage profile of these cyclic voltammograms are similar to those obtained on larger platinum and tungsten wire electrodes. Although the differences in peak potentials are larger ($\Delta E_p \simeq$ 60mV - 120mV) than those observed on the larger electrodes and are also sweep rate dependent, a plot of the peak current against the square root of the sweep rate gave a linear relationship for each of the cyclic voltammograms. The increase in the difference in peak potentials may be ascribed to either the ohmic drop across the cell or the irreversible nature of the electrode reaction [114] ; both suppositions would

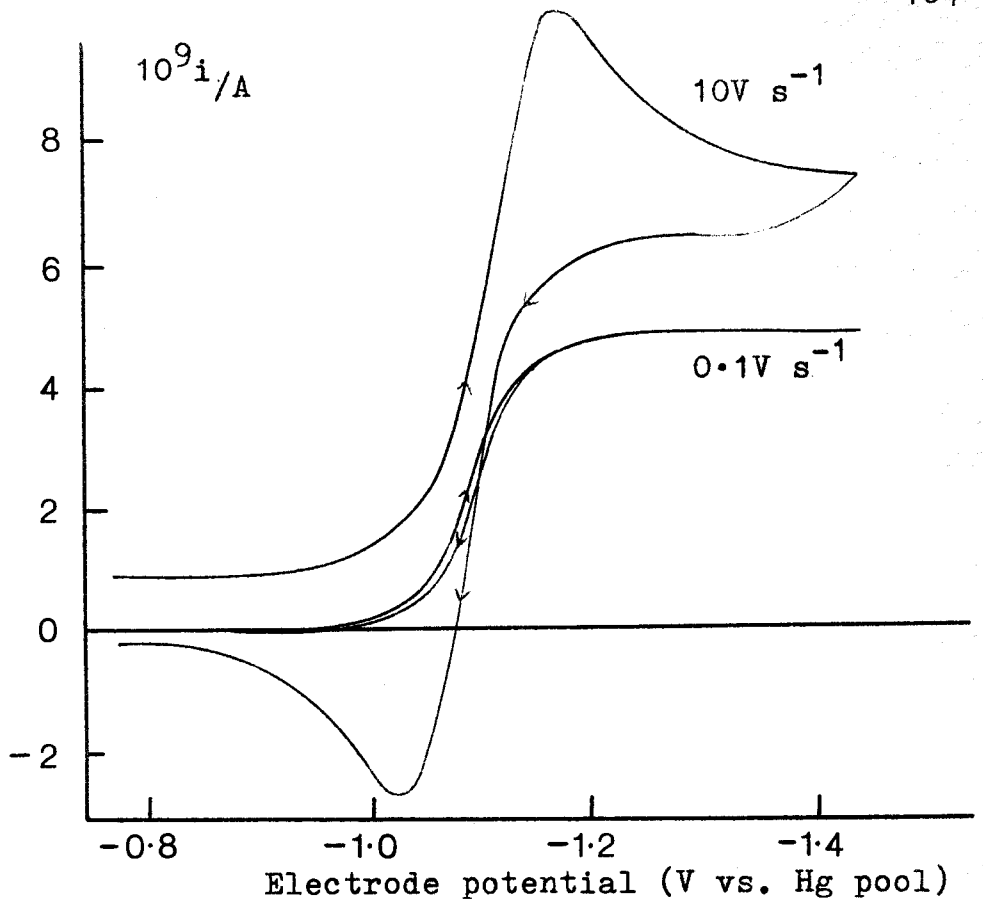

FIG 33 Cyclic voltammogram for the reduction of perylene (4mM) at a platinum microelectrode (6μm) in DMF/Bu_4NI.

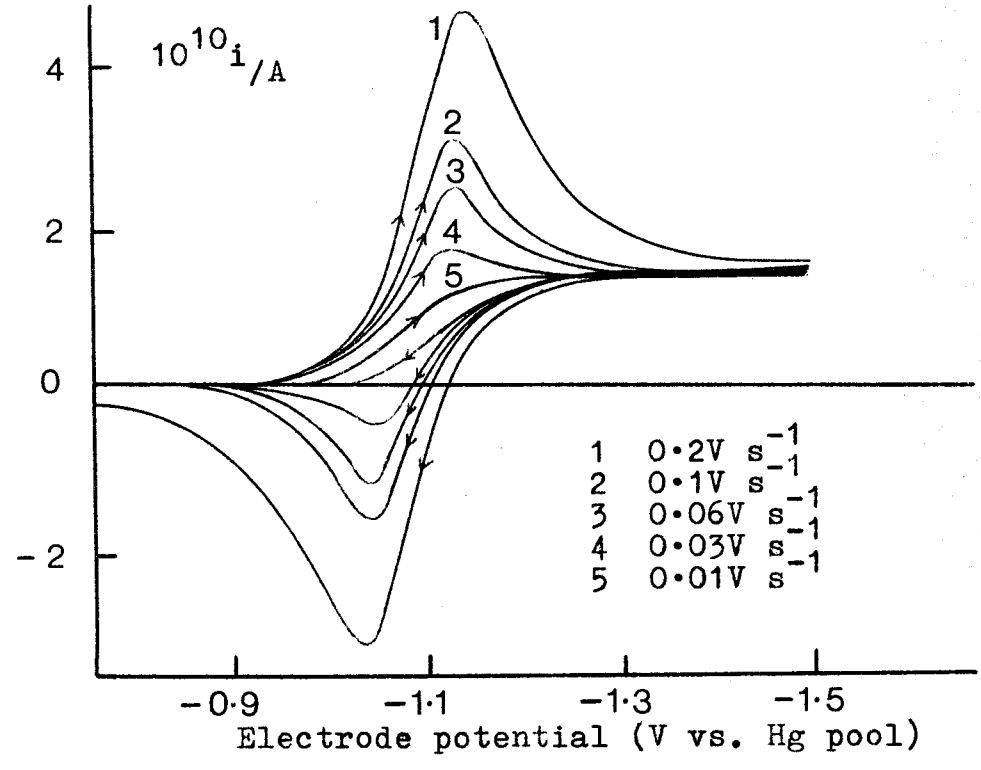

FIG 34 Cyclic voltammogram for the reduction of perylene (2·6mM) at a tungsten microelectrode (0·3μm) in DMF/Bu_4NI.

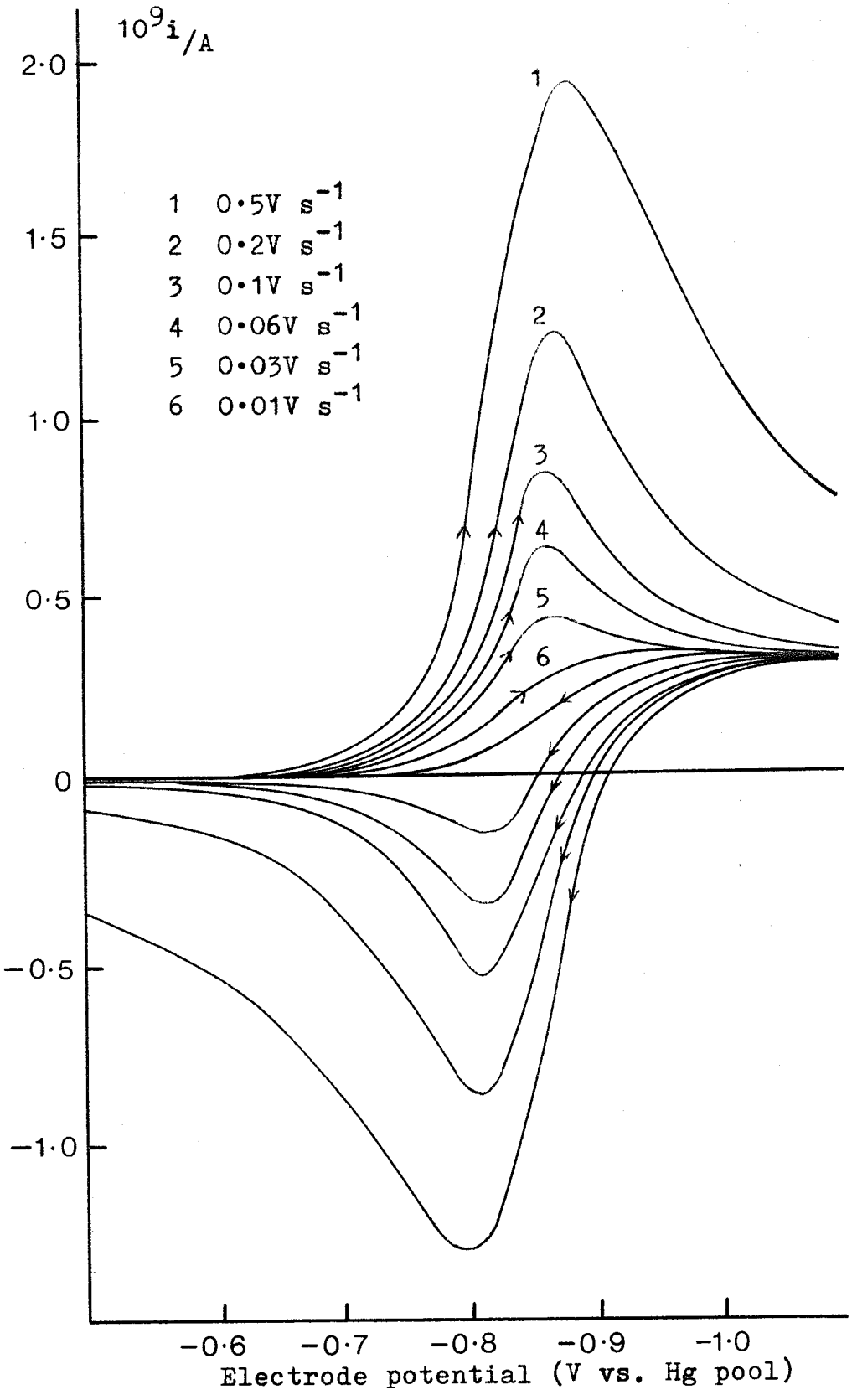

FIG 35 Cyclic voltammogram for the reduction of p nitroaniline (6mM) at a tungsten micro-electrode (0·2μm) in DMF/Bu_4NI.

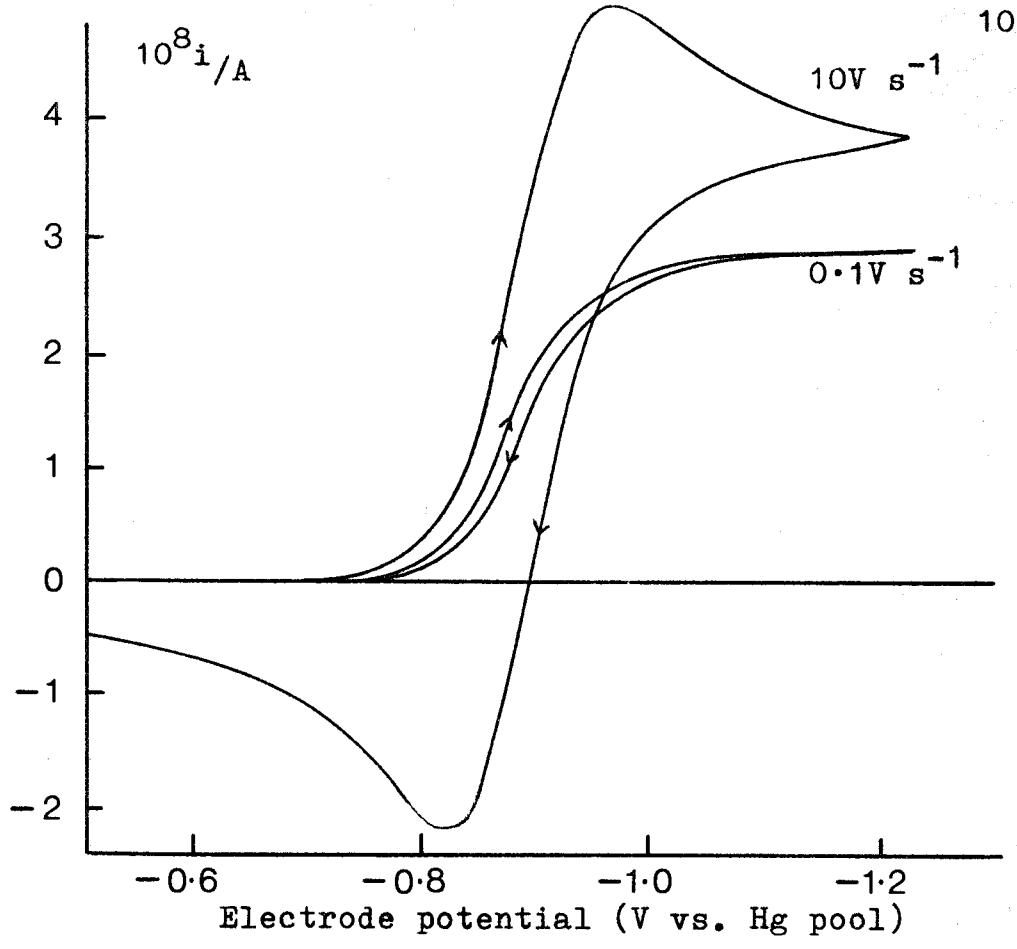

FIG 36 Cyclic voltammogram for the reduction of nitromesitylene (13mM) at a platinum microelectrode (8μm) in DMF/Bu_4NI.

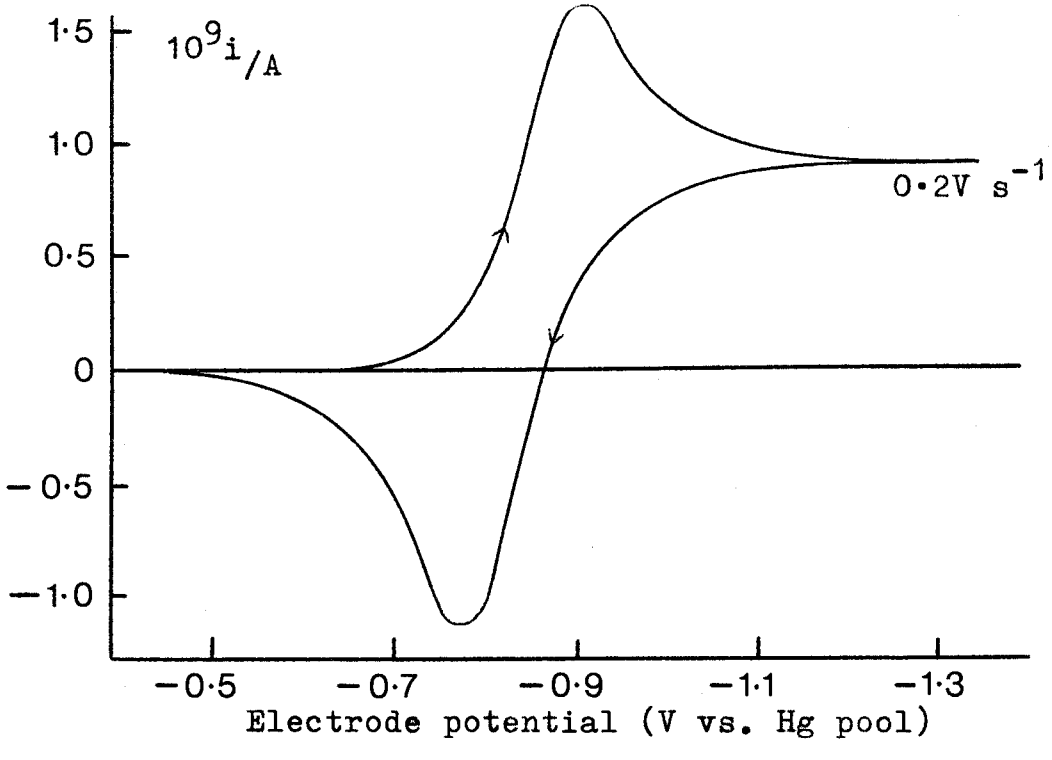

FIG 37 Cyclic voltammogram for the reduction of nitromesitylene (15mM) at a tungsten microelectrode (0·24μm) in DMF/Bu_4NI.

account for the dependence on sweep rate. With the small currents measured in these experiments, however, the former is unlikely.

These voltammograms were analysed according to equations (2.125) and (2.144)

$$I_p = \frac{1}{nFD^{\frac{1}{2}}\pi^{\frac{1}{2}}} \int_o^t \frac{i_{pl}(\tau)}{(t-\tau)^{\frac{1}{2}}}\, d\tau \qquad 2.125$$

$$I_s = \frac{1}{nF\pi^{\frac{1}{2}}r_o} \int_o^t i_s(\tau) \left[\frac{r_o^3}{2(D(t-\tau))^{3/2}} - \frac{3r_o^5}{4(D(t-\tau))^{5/2}} + \frac{15r_o^7}{8(D(t-\tau))^{7/2}} \right] d\tau \qquad 2.144$$

for both planar and spherical diffusion at the electrode surface. A computer program was compiled (Appendix B) to evaluate the complex convolution integrals above.

Input to the computer program was made in the form of current/time data points together with values for the diffusion coefficient and electrode radius, the latter being determined from the limiting current at slower sweep rates. The computer program then calculated values for the convolution integrals at each time point for both planar or spherical analysis as selected. The resulting convoluted voltammograms or 'neopolarograms' in the terminology of Oldham are illustrated in FIGS. 38 - 47.

Several observations may be made from these neopolarograms. The first and most obvious observation, is the difference between the planar and spherical analysis. Here the effect of sweep rate can be seen to be of major importance. Generally, planar analysis of cyclic voltammograms recorded on platinum micro-electrodes at 10V s^{-1} leads to a sinusoidal type wave with steadily increasing value (eg. FIG. 38), but

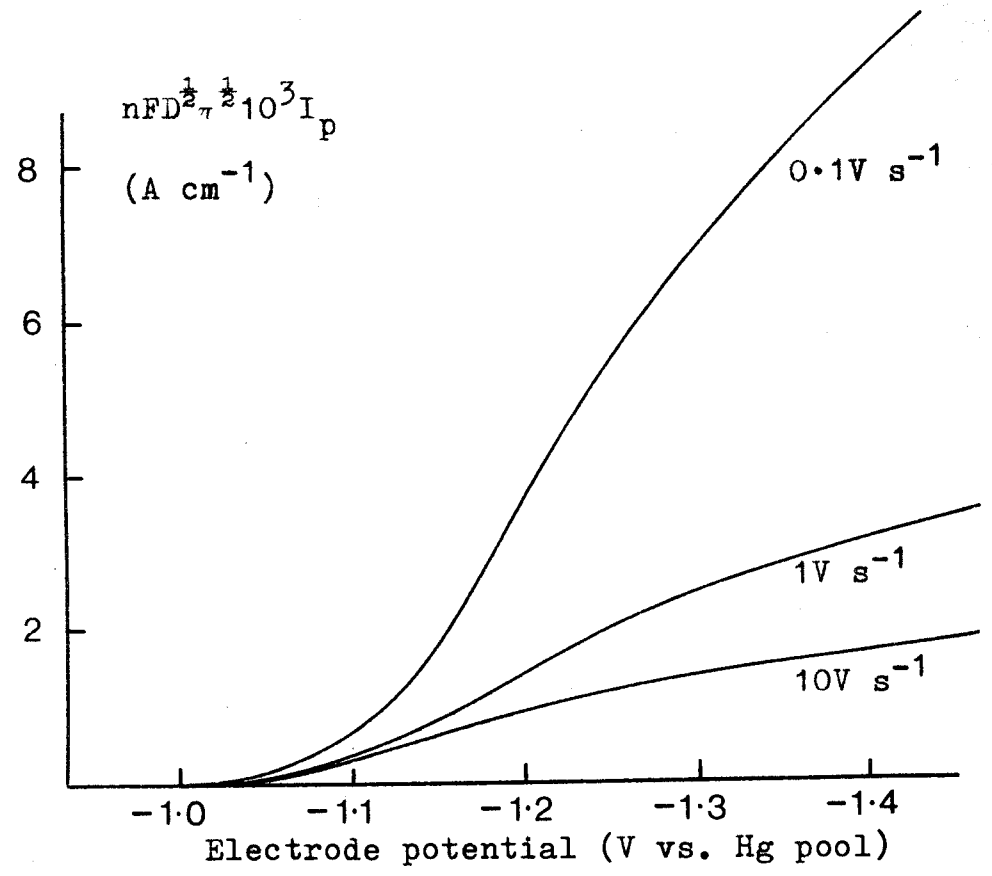

FIG 38 Convolution neopolarogram (planar analysis) for the reduction of perylene (4mM) at a platinum microelectrode (6μm).

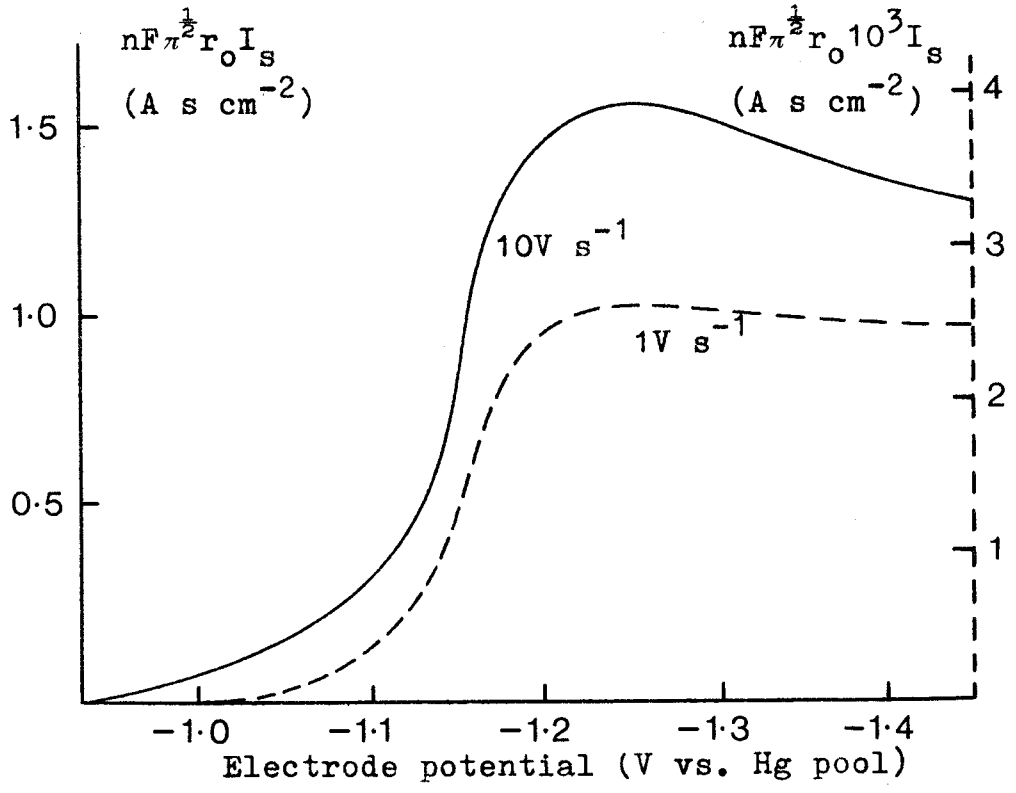

FIG 39 Convolution neopolarogram (spherical analysis) for the reduction of perylene (4mM) at a platinum microelectrode (6μm)

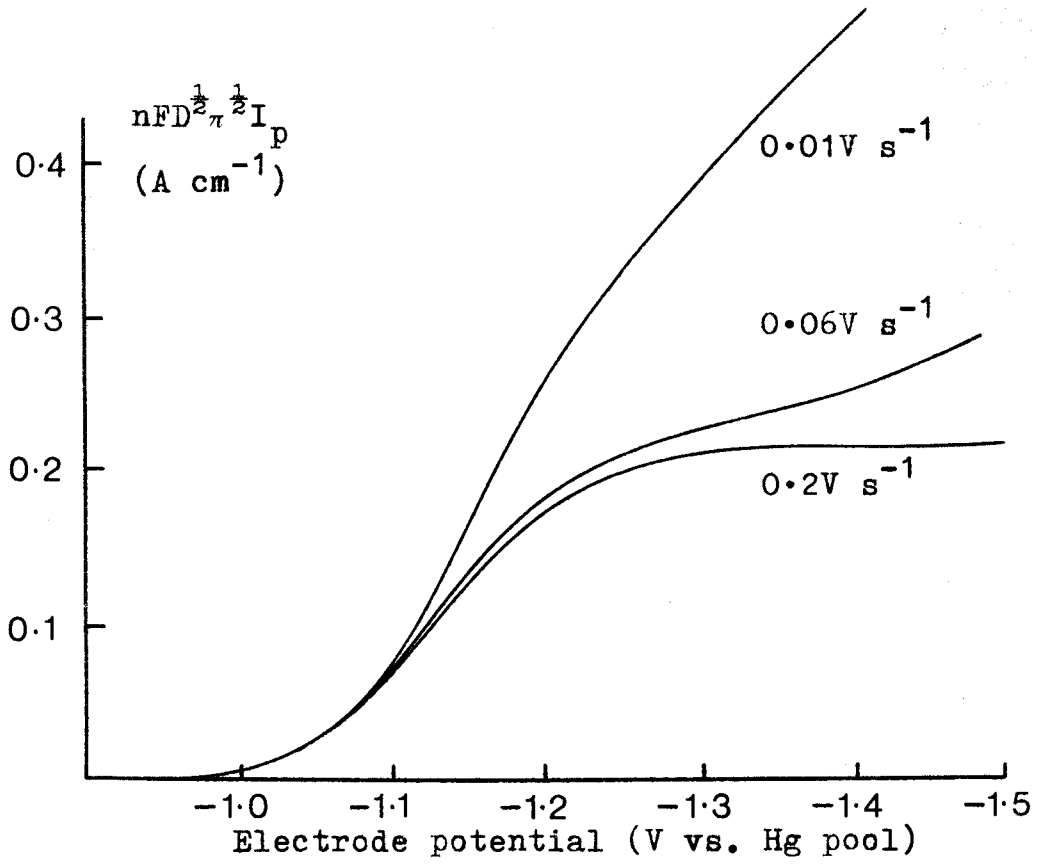

FIG 40 Convolution neopolarogram (planar analysis) for the reduction of perylene (2.6mM) at a tungsten microelectrode (0·3μm).

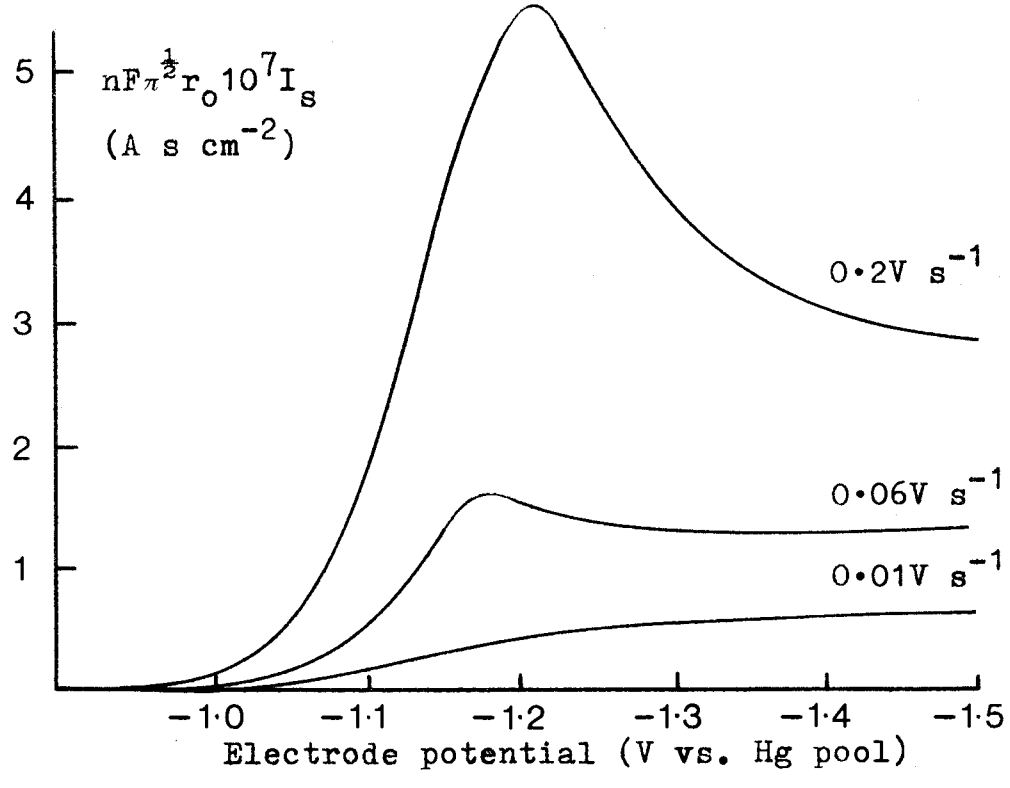

FIG 41 Convolution neopolarogram (spherical analysis) for the reduction of perylene (2·6mM) at a tungsten microelectrode (0·3μm).

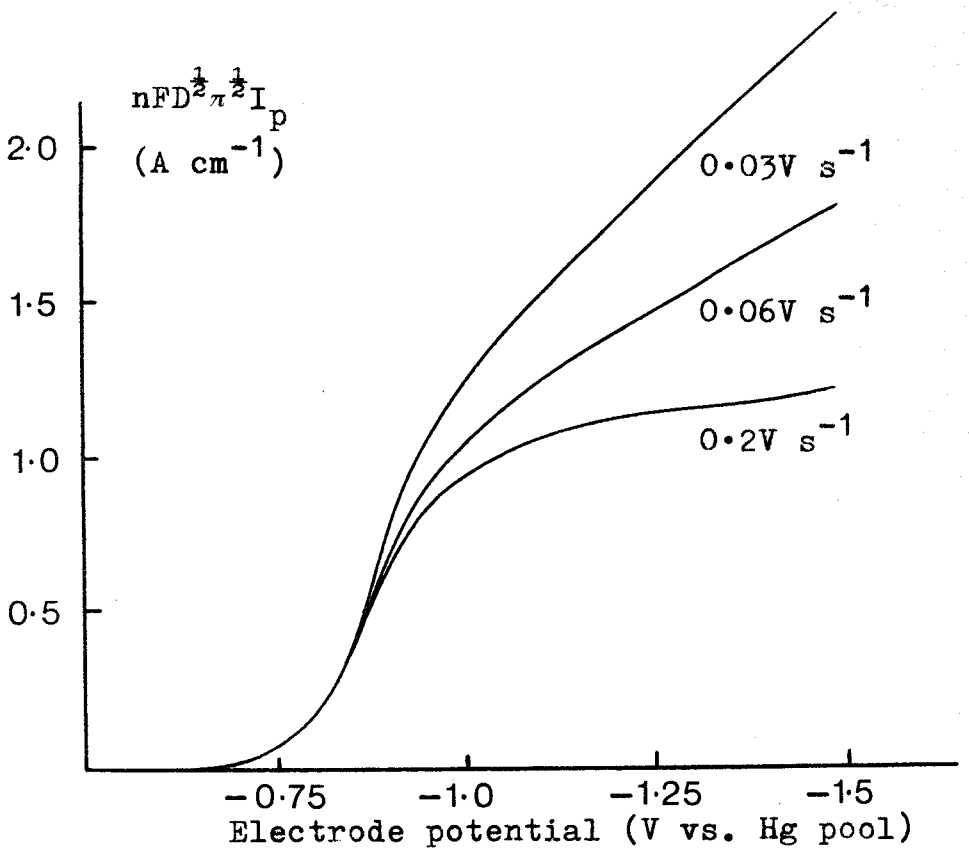

FIG 42 Convolution neopolarogram (planar analysis) for the reduction of p nitroaniline (6mM) at a tungsten microelectrode (0·2μm)

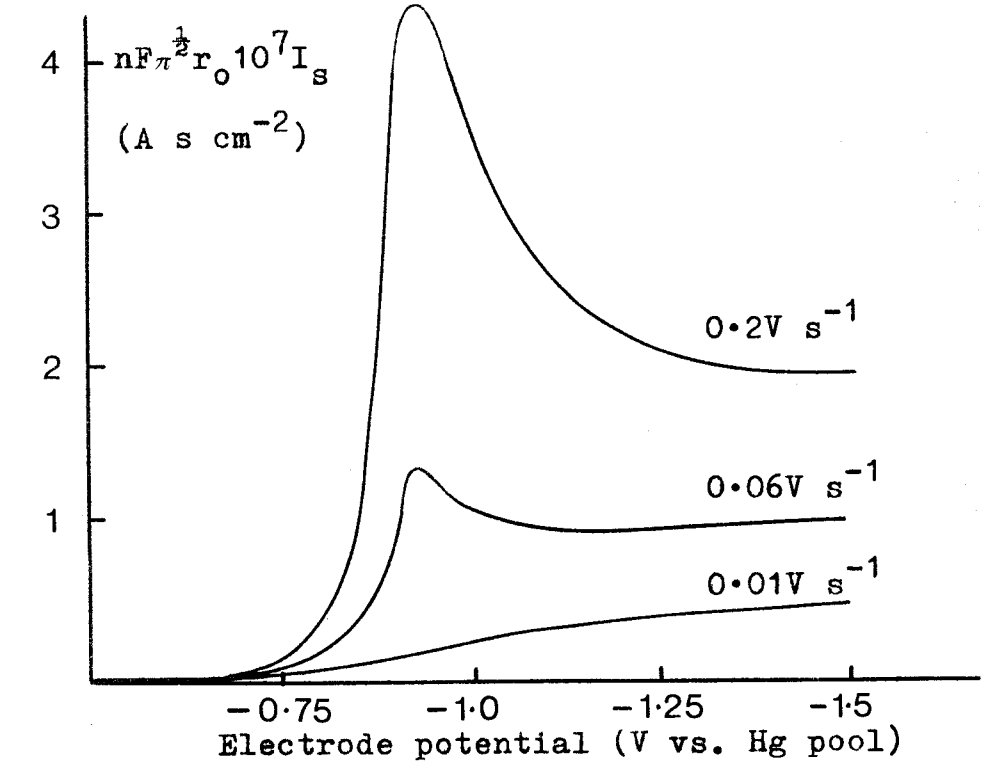

FIG 43 Convolution neopolarogram (spherical analysis) for the reduction of p nitroaniline (6mM) at a tungsten microelectrode (0·2μm)

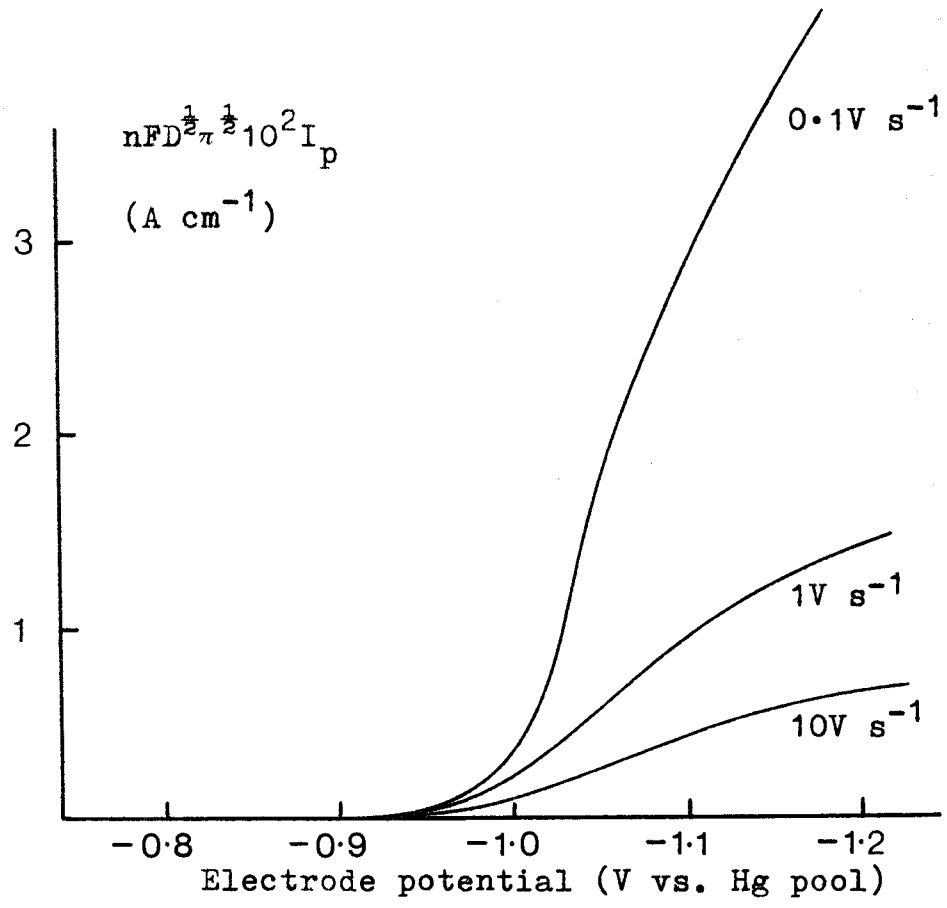

FIG 44 Convolution neopolarogram (planar analysis) for the reduction of nitromesitylene (13mM) at a platinum microelectrode (8μm)

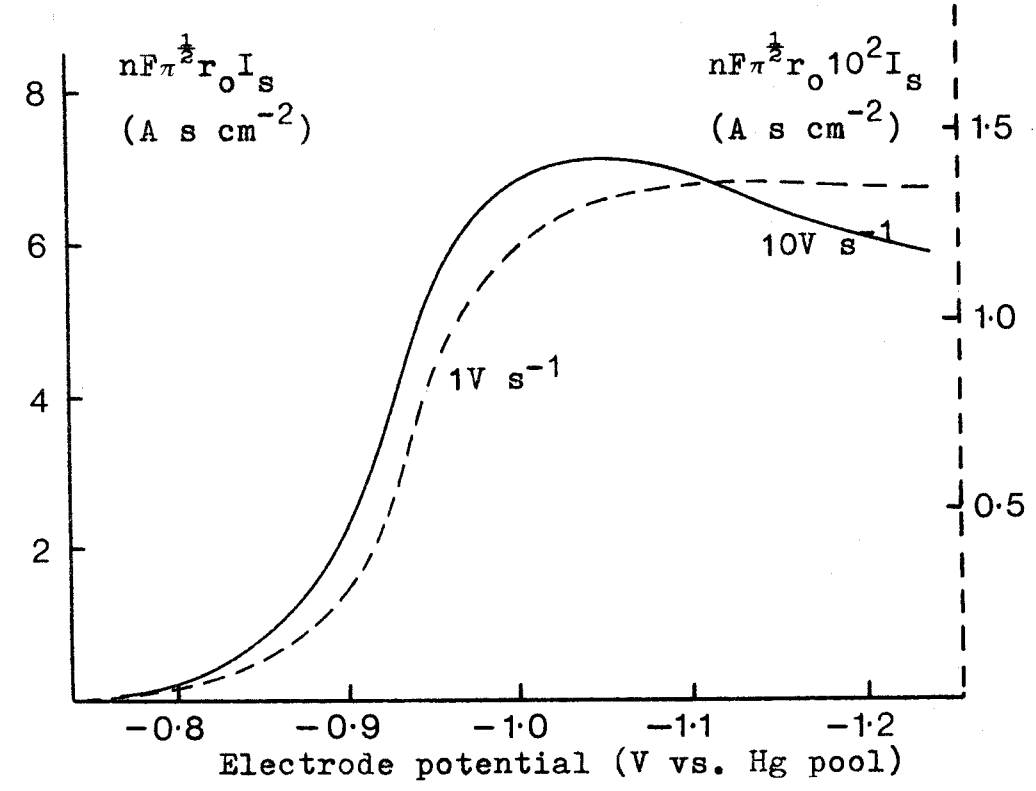

FIG 45 Convolution neopolarogram (spherical analysis) for the reduction of nitromesitylene (13mM) at a platinum microelectrode (8μm)

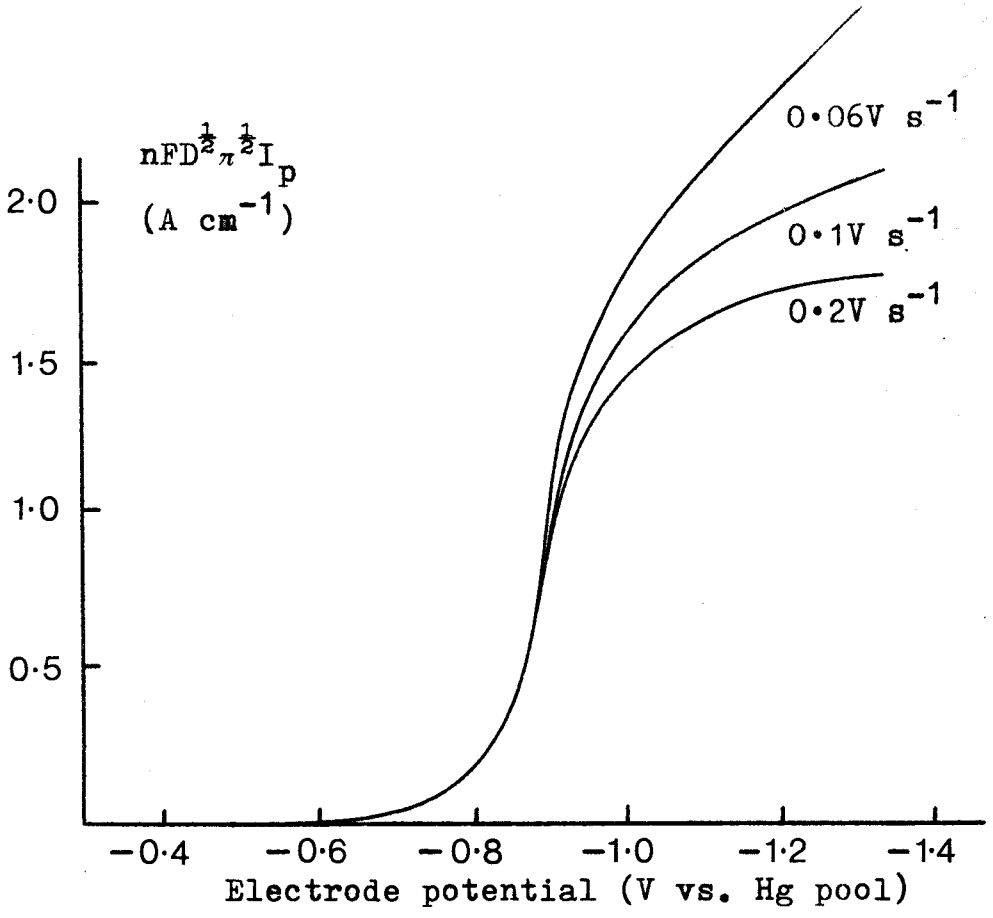

FIG 46 Convolution neopolarogram (planar analysis) for the reduction of nitromesitylene (15mM) at a tungsten microelectrode (0·24μm)

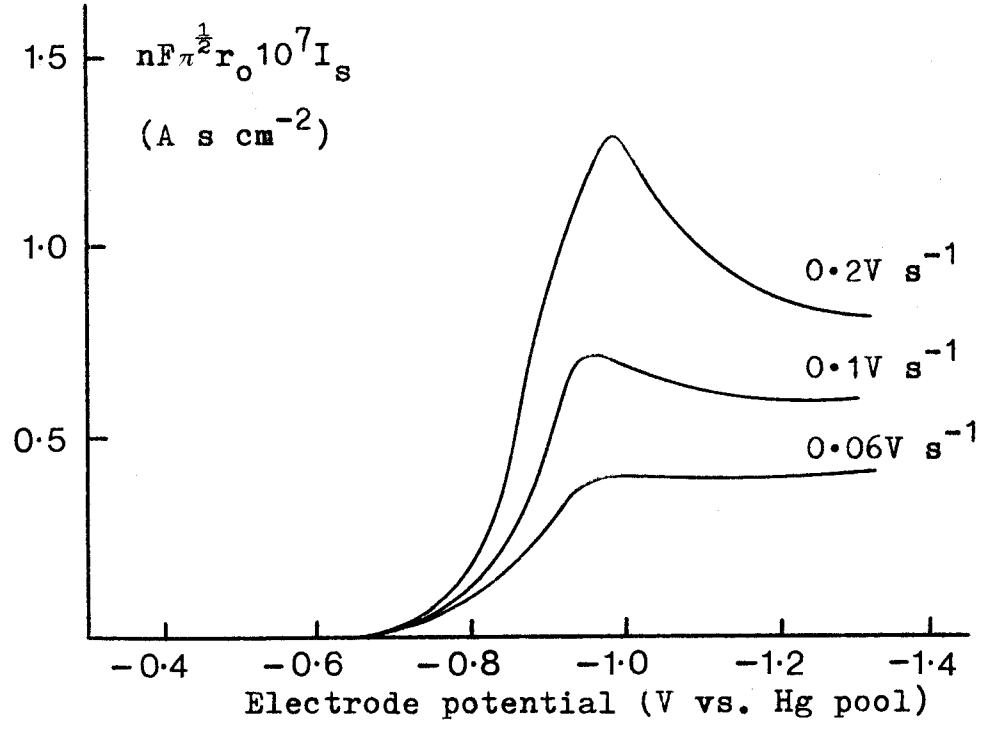

FIG 47 Convolution neopolarogram (spherical analysis) for the reduction of nitromesitylene (15mM) at a tungsten microelectrode (0·24μm).

with the same data points spherical analysis produces a peaked neopolarogram, not dissimilar in shape to the original voltammetric peak, (FIG. 39). As the potential sweep rate is decreased, the neopolarogram for planar analysis is observed to increase steadily, with the limiting value rising even more rapidly with potential; while for spherical analysis the opposite is seen to occur, with the neopolarogram gradually diminishing in value. This is because at high potential sweep rates, the total current density at a microelectrode is dominated by the time dependent term of (2.77), (which is also equal to the current density at a planar electrode of equivalent area) so that the application of convolution techniques, essentially a time dependent analysis, is in effect acting on the total electrode current. As the potential sweep rate is decreased, the contribution to the total current density of the time dependent term also decreases, leaving ultimately only the steady state term. Since this term is time independent, its value after convolution tends to zero, so that convolution analysis can only be meaningfully applied to current voltage profiles in which the current density is wholly time dependent (i.e. at fast potential sweep rates).

Similar behaviour is observed on tungsten microelectrodes (eg. FIGS. 40 and 41), even though for reasons to be explained shortly, the tungsten microelectrodes exhibit certain anomalous characteristics in comparison to the platinum microelectrodes.

The effect of potential sweep rate on the observed convoluted current at a spherical electrode has been considered previously by Saveant [71], only as a corrective parameter to the planar analysis. A sphericity parameter, σ, was introduced as a function of the electrode radius, r_o, and potential sweep rate, a, where

$$\sigma = \frac{D^{\frac{1}{2}}}{r_o}\left(\frac{RT}{nFa}\right)^{\frac{1}{2}} \qquad 4.20$$

showing that as the sweep rate is increased, the value of the spherical correction term σ diminishes. The value of the convolution integral at a spherical electrode, I'_s, was then defined as

$$I'_s = I_p + f(\sigma) \qquad 4.21$$

so that at very fast sweep rates, i.e. as $\sigma \rightarrow 0$, the convolution integral I'_s approximates to the convolution integral at a planar electrode of equivalent area.

The second observation to be made from these neopolarograms is rather more subtle and concerns only the neopolarograms calculated from tungsten microelectrodes. At the limiting current, the convoluted current under planar analysis, according to (2.125) and (2.126) is equal to

$$\int_0^t \frac{i_{pl}(\tau)}{(t-\tau)^{\frac{1}{2}}}\, d\tau = nFD^{\frac{1}{2}}\pi^{\frac{1}{2}}C_o^{\infty} \qquad 4.22$$

When applied to platinum microelectrodes at the highest potential sweep rates ($10V\ s^{-1}$), this equality is observed, when the appropriate values for the diffusion coefficient and bulk concentration are substituted into (4.22). However, with tungsten microelectrodes, the limiting value of the convolution integral at the highest sweep rates are much larger than predicted from (4.22), often by a factor of one hundred or more. Since the observed current is input to the computer program as current density, this implies that the current density values used in the calculation of the convolution integral are too large and by inference the values of the electrode area to calculate the current densities, too small. The effective electrode area may be calculated using the expression

Effective electrode area =

$$\frac{\left(\int_0^t \frac{i_{pl}(\tau)}{(t-\tau)^{\frac{1}{2}}}\, d\tau\right)_{lim,obs}}{\left(\int_0^t \frac{i_{pl}(\tau)}{(t-\tau)^{\frac{1}{2}}}\, d\tau\right)_{lim,calc}} \times (\text{electrode area})_{calc} \qquad 4.23$$

An apparent increased electrode area at high potential sweep rates may result from a poorly sealed tungsten electrode. Here, in this instance, two distinct regions surrounding the electrode must be considered: the electrolyte in the immediate vicinity of the imperfect seal (eg. in a small crevasse adjacent to the electrode surface) and the bulk electrolyte of the main solution. At short times, i.e. fast potential sweep rates, the diffusion layer thickness, rather simply represented by the term $(Dt)^{\frac{1}{2}}$ will extend equally over all the exposed electrode surface, including the region of the imperfect seal. At longer times however, the diffusion layer will extend far beyond the region of the imperfect seal, into the bulk solution so that once the reactants in the imperfect seal have been consumed, electroactive species diffusing from the bulk solution to the electrode will react preferentially at the tip of the electrode. Thus, the electrode area will appear larger at high potential sweep rates than at the slow sweep rates. One other way in which this apparent change in electrode area should manifest itself is the ease with which voltammetric current peaks are formed when comparing electrodes of different areas at the same potential sweep rate.

Peak formation occurs as a result of initial high, sweep rate dependent, mass transfer rates in the non steady state, relaxing to a steady state value as the reactant concentration in the diffusion layer is depleted. For spherical electrodes at constant

potential sweep rate, as the electrode area decreases generating an increase in the steady state mass transfer rate, the difference between the peak current mass transfer rate and the steady state mass transfer rate also decreases. This is reflected in a decrease in peak height, until eventually at sufficiently small spherical electrodes, the peak disappears completely when the steady state mass transfer rate is comparable to the peak current mass transfer rate. In comparing two microelectrodes of different areas therefore, at the same potential sweep rate and concentration etc., the appearance of voltammetric current peaks on one should, in principle, correspond to the electrode of significantly larger area. Inspection of FIGS. 36 and 37 for the reduction of nitromesitylene shows an apparent contradiction to this argument, at least when taken on face value. Using values of the electrode area calculated from the observed limiting current using (4.18) the tungsten microelectrode ($r_o \simeq 0{\cdot}2\mu m$) is seemingly much smaller than the platinum microelectrode ($r_o \simeq 8\mu m$). However, at a potential sweep rate of $0{\cdot}1V\ s^{-1}$ voltammetric oxidation/reduction current peaks are observed on the tungsten microelectrode but not on the platinum microelectrode of supposed larger area. This suggests a much larger area of the tungsten microelectrode at the beginning of the potential sweep than was calculated from the limiting current of the same voltammogram. This then, further supports the likelihood of a poor seal between the glass and tungsten as described earlier.

Fortunately, an accurate evaluation of the electrode area at all times is not required for the determination of kinetic parameters as defined by equation (2.129)

$$E = \frac{RT}{\alpha nF} \ln k_o' + \frac{RT}{\alpha nF} \ln \frac{(C_o^\infty - I_p)}{i_{pl}} \qquad 2.129$$

The variable electrode area incorporated in the evaluation of I_p through current density calculations is compensated by the same variable area of the observed current density in the second term of (2.129). Similarly, for analysis of a reversible process [71], where

$$E = \frac{RT}{nF} \ln \frac{(C_o^{\infty} - I_p)}{I_p} \qquad 4.24$$

the electrode area will again be a common factor between the numerator and denominator in the logarithmic term and will therefore not influence the final result.

The neopolarograms for the reduction of each compound recorded at both platinum and tungsten microelectrodes were analysed according to (2.129) and (4.24) for both irreversible and reversible reaction mechanisms respectively, noting that the convolution integral for planar analysis has been used in both expressions. Only the neopolarograms recorded at the highest potential sweep rates were therefore analysed, assuming that at these high sweep rates the current density at a spherical electrode approximates to the current density at a planar electrode of equivalent area.

The results of the analyses are shown in FIGS. 48 - 57. These figures show that under reversible analysis (using (4.24)), a linear relationship between the potential and the logarithmic term is not evident; while under irreversible analysis linearity of the plot is markedly improved. The apparent standard rate constant and transfer coefficient for each reaction calculated from the intercept and slope respectively of the plots for the irreversible analysis according to (2.129) are tabulated in TABLE 3 together with the corresponding values obtained using slow linear potential sweep conditions.

From TABLE 3 it is seen that values of the transfer coefficient obtained at tungsten microelectrodes

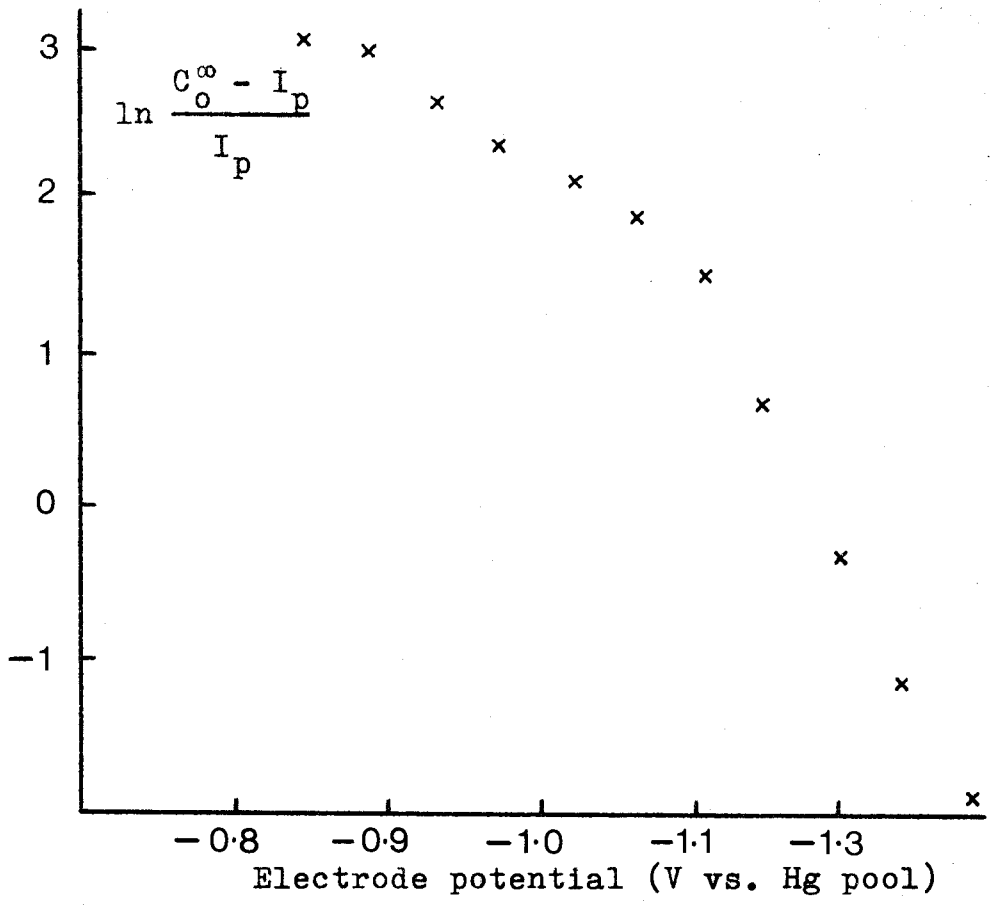

FIG 48 Reversible analysis, according to (4.24) for the reduction of perylene (4mM) at 10V/s on a platinum microelectrode (6μm)

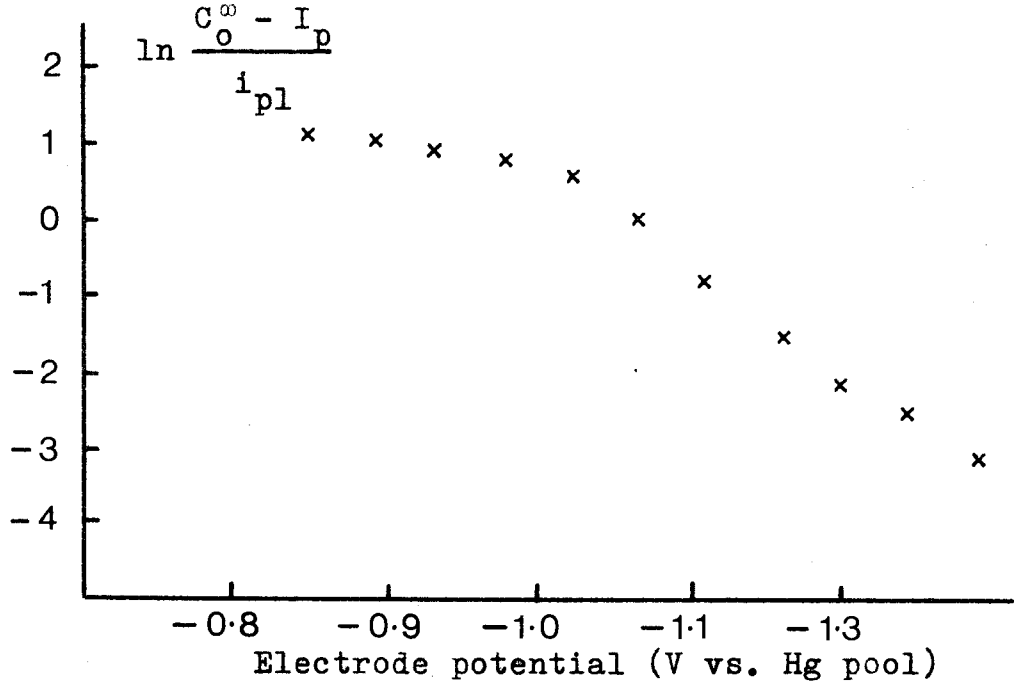

FIG 49 Irreversible analysis, according to (2.129) for the reduction of perylene (4mM) at 10V/s on a platinum microelectrode (6μm)

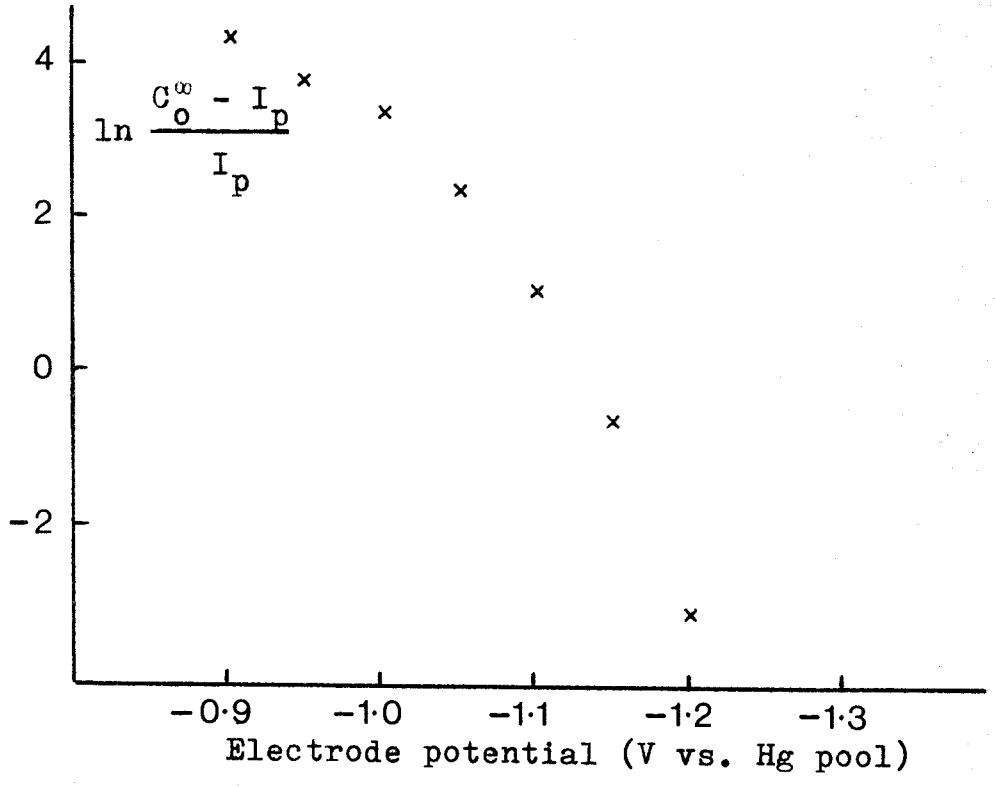

FIG 50 Reversible analysis, according to (4.24) for the reduction of perylene (2·7mM) at 0·2V/s on a tungsten microelectrode (0·3μm).

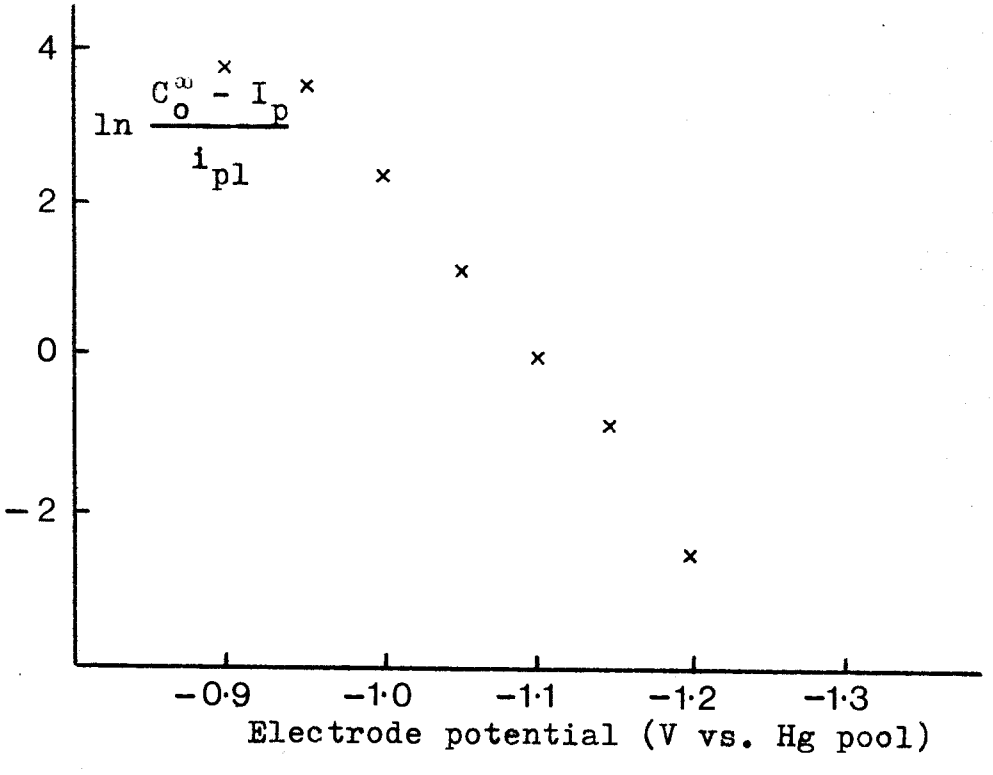

FIG 51 Irreversible analysis, according to (2.129) for the reduction of perylene (2·7mM) at 0·2V/s on a tungsten microelectrode (0·3μm)

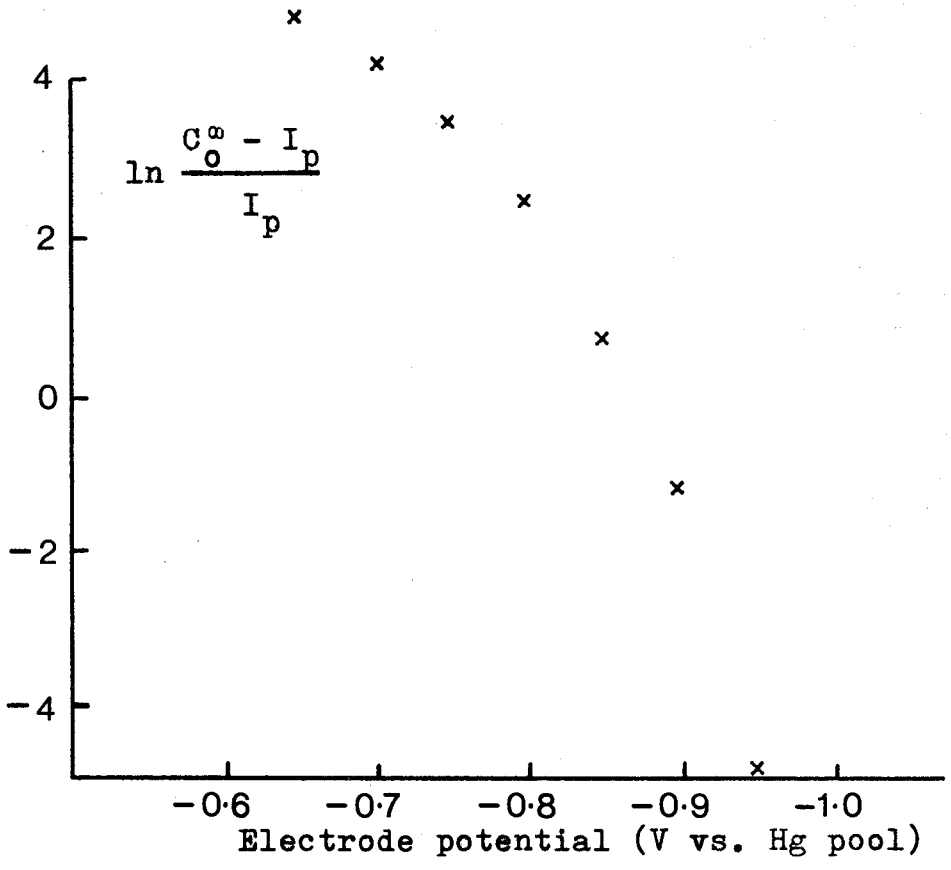

FIG 52 Reversible analysis, according to (4.24) for the reduction of p nitroaniline (6mM) at 0·2V/s on a tungsten microelectrode (0·2μm)

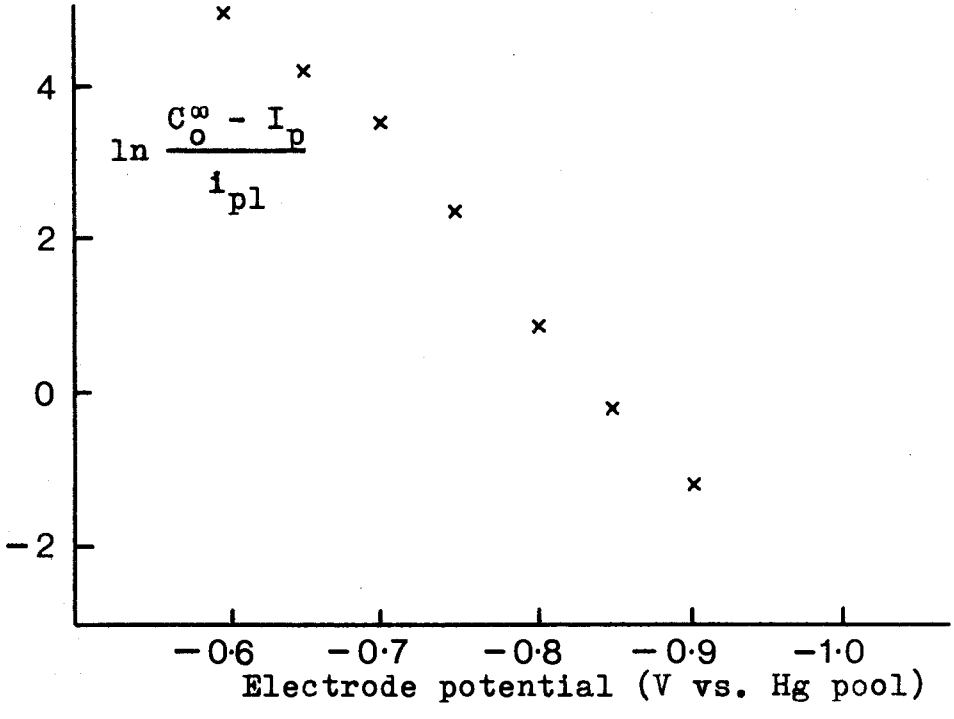

FIG 53 Irreversible analysis, according to (2.129) for the reduction of p nitroaniline (6mM) at 0·2V/s on a tungsten microelectrode (0·2μm)

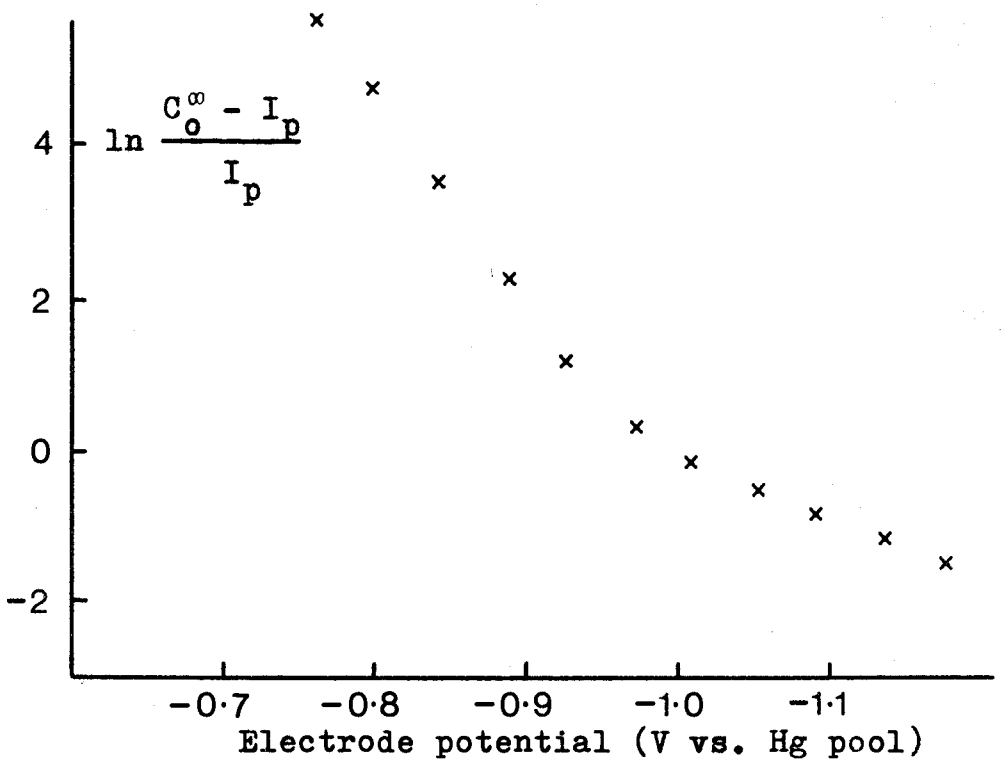

FIG 54 Reversible analysis, according to (4.24) for the reduction of nitromesitylene (13mM) at 10V/s on a platinum microelectrode (8μm)

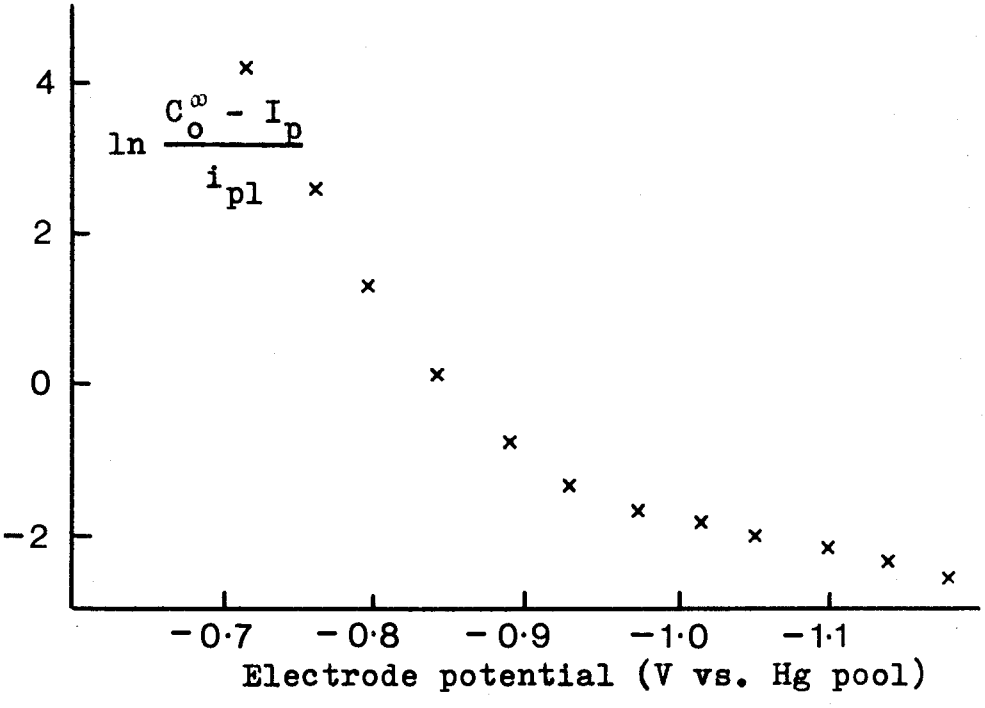

FIG 55 Irreversible analysis, according to (2.129) for the reduction of nitromesitylene (13mM) at 10V/s on a platinum microelectrode (8μm)

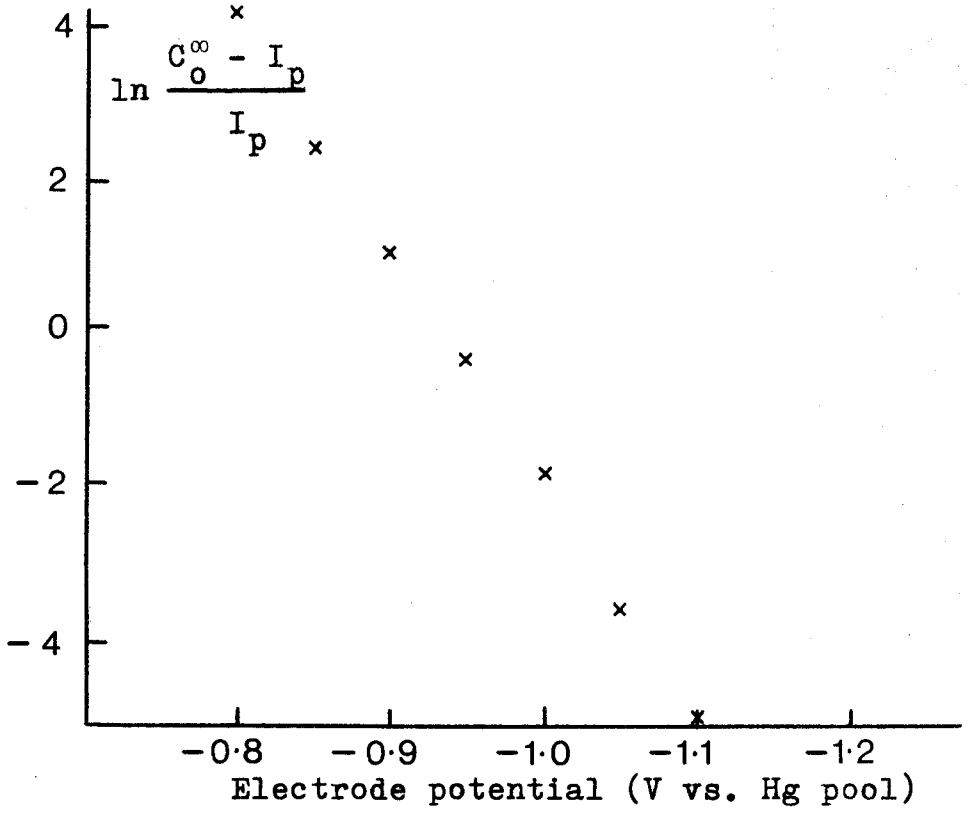

FIG 56 Reversible analysis, according to (4.24) for the reduction of nitromesitylene (15mM) at 0·2V/s on a tungsten microelectrode (0·24μm)

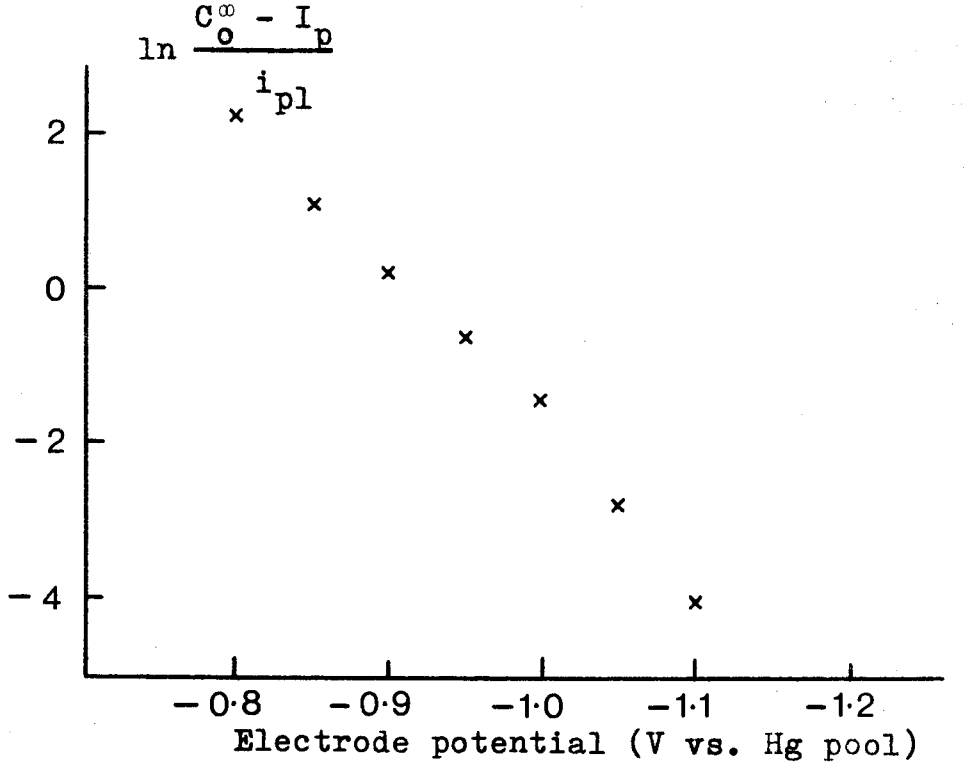

FIG 57 Irreversible analysis, according to (2.129) for the reduction of nitromesitylene (15mM) at 0·2V/s on a tungsten microelectrode (0·24μm)

TABLE 3a Slow linear potential sweep

Compound	Perylene				p Nitroaniline		t-Nitrobutane		Nitromesitylene		
$E_{\frac{1}{2}}$ (vs. Hg pool)	-1.06				-0.8		-1.10		-0.82		
Electrode radius (μm)	3	7	0.6	1.2	0.8	1.6	0.38	5.8	0.2	1	5
Electrode	Pt	Pt	W	W	W	Pt	W	Pt	W	Pt	Pt
$10^3 k_o'$ (cm s^{-1})	5.8	2.6	1.7	6.4	76.7	30.2	3.64	2.01	82.8	11.2	2.92
α	0.9	0.9	0.9	0.9	0.8	0.82	0.63	0.65	0.83	0.8	0.84
$d\alpha/dE$							0.66	1.04			

TABLE 3b Fast linear potential sweep

Compound	Perylene		p Nitroaniline	Nitromesitylene	
$E_{\frac{1}{2}}$ (vs. Hg pool)	-1.06		-0.8	-0.82	
Electrode radius (μm)	0.3	6.6	0.2	0.24	8.0
Electrode	W	Pt	W	W	Pt
$10^3 k_o'$ (cm s^{-1})	1.52	4.8	2.10	0.79	2.5
α	0.57	0.88	0.56	0.58	0.85

under fast linear potential sweep conditions, are all surprisingly low, i.e. 0·5 - 0·6. These values should, however, be viewed against a corresponding decrease in the measured rate of reaction, at electrodes of similar radius, when compared to the rates of reaction determined under slow sweep conditions. This discrepancy arising, it is suggested, from the increased area of the electrode at short times.

A better comparison between the two analyses may be obtained by comparing platinum microelectrodes of equivalent area. An increase in the observed rate of reaction at high potential sweep rates is noted for a Pt ($\sim 7\mu$m) electrode for the reduction of perylene, than was measured under pseudo steady state conditions. More generally, the measured rate of reaction at platinum microelectrodes is observed to vary inversely with the electrode radius, in gratifying agreement with the proposed theory, for both slow and fast linear potential sweep methods.

4:iv Conclusions

With the exception of tert nitrobutane, all the electrode reactions studied using microelectrodes were found to be mass transfer controlled at the standard electrode potential. The electrode radii, by implication, were too large to sufficiently enhance the rate of mass transfer to the electrode surface above the rate of the electron transfer process even under fast potential sweep conditions. Much smaller microelectrodes, therefore, are required to measure the kinetic parameters of these fast electrode reactions. Although many difficulties were experienced in producing the microelectrodes used in this investigation particularly with the lead and tungsten microelectrodes the introduction of platinum microelectrodes in the latter stages of this work, constructed from very fine platinum fibre in the form of Wollaston wire, offers considerable hope of achieving smaller microelectrodes if and when the diameter of the commercial platinum fibre can be reduced even further.

One of the many problems of the lead and tungsten microelectrodes was the uncertainty of the electrode radius prior to each experiment; the electrode radius in each case being determined from the experimentally observed limiting current, even then assuming an electrode of circular cross section. Many electrodes were constructed, particularly of tungsten, only to discover, after careful polishing that the electrode radius was too large for meaningful studies. With platinum microelectrodes at least, the electrode radius could be estimated from the diameter of the platinum fibre used in the construction of the microelectrode.

Although not overwhelmingly successful in obtaining kinetic data, the general technique has nevertheless, proved successful for the reduction of tert nitrobutane in DMF/Bu_4NI. Reasonable agreement was obtained with previously reported results,

although in the light of the preceding section concerning the poor sealing qualities of the tungsten microelectrodes, some doubt must exist as to the accuracy of the measurements obtained under slow potential sweep conditions. In addition, the imperfect tungsten seal, highlighted so effectively by the fast potential sweep analysis may have contributed to the increased currents at the foot of the reduction wave leading to negative logarithmic arguments encountered during slow sweep analysis.

A dependence of the transfer coefficient on the electrode potential was also detected. The analysis of tert nitrobutane in terms of the Marcus theory agreed reasonably well with previously reported results [107], although the results obtained were not in particularly good agreement with predicted values from the Marcus theory.

CHAPTER 5 PRECEDING CHEMICAL REACTIONS

5:i Introduction

So far in this study, attention has been restricted to the measurement of the apparent standard rate constant of fast, simple electron transfer reactions. This was achieved by enhancing the rate of diffusion of the electroactive species, with the aid of microelectrodes, until the diffusion process was no longer the rate determining step in the overall reaction sequence. With more complex reaction schemes, the measurement of the individual rates of reaction becomes more difficult. For instance, consider the dissociation of a weak acid, HA,

$$HA \underset{k_2}{\overset{k_1}{\rightleftharpoons}} H^+ + A^- \qquad 5.1$$

$$H^+ + e = \tfrac{1}{2}H_2 \qquad 5.2$$

where H^+ is the only electroactive species in the potential range under investigation and k_1 and k_2 are the formal rate constants governing the forward and reverse reactions, respectively, of the equilibrium (5.1).

The overall rate of the reaction may be governed by either the rate of the equilibrium reaction, the rate of diffusion of H^+, the rate of the electron transfer reaction at the electrode surface or a combination of all three. Clearly, the measurement of the rate of a fast homogeneous chemical reaction is only possible when both the rate of diffusion and the rate of electron transfer are fast compared to the rate of the chemical reaction. For reactions where the electrode reaction is reversible, this may be accomplished using very small electrodes under steady state conditions, as in the case of simple electron

transfer reactions.

Under these conditions, the flux of each species given in (5.1) and (5.2) in a spherical diffusion field is described by

$$D_{HA}\frac{d^2C_{HA}}{dr^2} + \frac{2D_{HA}}{r}\frac{dC_{HA}}{dr} - k_1C_{HA} + k_2C_HC_A = 0 \qquad 5.3$$

$$D_H\frac{d^2C_H}{dr^2} + \frac{2D_H}{r}\frac{dC_H}{dr} + k_1C_H - k_2C_HC_A = 0 \qquad 5.4$$

$$D_A\frac{d^2C_A}{dr^2} + \frac{2D_A}{r}\frac{dC_A}{dr} + k_1C_A - k_2C_AC_H = 0 \qquad 5.5$$

where the subscripts, HA, H, and A are applied to the respective reactants.

In the presence of a large excess of A, such that

$$C_A \gg C_{HA} > C_H \qquad 5.6$$

the initial and boundary conditions may be written

$t = 0 \quad r_o < r < \infty \quad C_H = C_H^\infty$ 5.7

$C_{HA} = C_{HA}^\infty$ 5.8

$C_A = C_A^\infty$ 5.9

$t > 0 \quad r = \infty \quad C_H = C_H^\infty$ 5.10

$C_{HA} = C_{HA}^\infty$ 5.11

$C_A = C_A^\infty$ 5.12

$t > 0 \quad r = r_o \quad C_H = 0$ 5.13

$$t > 0 \qquad r = r_o \qquad \frac{dC_{HA}}{dr} = 0 \qquad 5.14$$

$$i_s = nFD_H \frac{dC_H}{dr} \qquad 5.15$$

Since the concentration of H^+ is controlled by the equilibrium reaction (5.1), the diffusion equations (5.3) - (5.5) should be solved simultaneously. However, in view of (5.6), the concentration of A may be assumed to remain constant. Thus adding (5.3) and (5.4)

$$D_{HA} \frac{d^2C_{HA}}{dr^2} + D_H \frac{d^2C_H}{dr^2} + \frac{2D_{HA}}{r} \frac{dC_{HA}}{dr} + \frac{2D_H}{r} \frac{dC_H}{dr} = 0 \qquad 5.16$$

The substitution

$$D_{HA}C_{HA} + D_HC_H = \frac{V}{r} \qquad 5.17$$

converts (5.16) into

$$\frac{d^2V}{dr^2} = 0 \qquad 5.18$$

for which the general solution is

$$V = M + Nr \qquad 5.19$$

or, from (5.17)

$$D_{HA}C_{HA} + D_HC_H = \frac{M}{r} + N \qquad 5.20$$

The arbitrary constants M and N are, as usual, determined from the boundary conditions.

At $r = \infty$, the boundary conditions (5.10) and (5.11) show that

$$N = D_{HA}C^{\infty}_{HA} + D_H C^{\infty}_H \qquad 5.21$$

but at $r = r_o$, the boundary condition (5.15) together with (5.14) and (5.20) give

$$i_s = -\frac{nFM}{r_o^2} \qquad 5.22$$

so that, for the moment, the arbitrary constant M will be retained in (5.20) for determination at a later stage. Hence, (5.20) becomes

$$D_{HA}C_{HA} + D_H C_H = \frac{M}{r} + D_{HA}C^{\infty}_{HA} + D_H C^{\infty}_H \qquad 5.23$$

Substituting now for C_{HA} from (5.23) into the main diffusion equation (5.4), the expression

$$D_H \frac{d^2C_H}{dr^2} + \frac{2D_H}{r}\frac{dC_H}{dr} + k_1\left\{\frac{M}{D_{HA}r} + C^{\infty}_{HA} + \frac{D_H C^{\infty}_H}{D_{HA}}\right\}$$

$$- C_H\left\{\frac{k_1 D_H}{D_{HA}} + k_2 C^{\infty}_A\right\} = 0 \qquad 5.24$$

is obtained. Putting

$$C_H = \frac{V}{r} \qquad 5.25$$

(5.24) simplifies to

$$\frac{d^2V}{dr^2} + k_1 r\left\{\frac{D_{HA}C^{\infty}_{HA} + D_H C^{\infty}_H}{D_{HA}D_H}\right\} - V\left\{\frac{k_1 D_H + k_2 D_{HA}C^{\infty}_A}{D_{HA}D_H}\right\} + \frac{k_1 M}{D_{HA}D_H} = 0$$

5.26

and the general solution is given by

$$V = A \exp \left[\frac{k_1 D_H + k_2 D_{HA} C_A^\infty}{D_{HA} D_H} \right]^{\frac{1}{2}} r + k_1 r \left\{ \frac{D_{HA} C_{HA}^\infty + D_H C_H^\infty}{k_1 D_H + k_2 D_{HA} C_A^\infty} \right\}$$

$$+ B \exp - \left[\frac{k_1 D_H + k_2 D_{HA} C_A^\infty}{D_{HA} D_H} \right]^{\frac{1}{2}} r + \frac{k_1 M}{k_1 D_H + k_2 D_{HA} C_A^\infty} \qquad 5.27$$

where A and B are additional constants to be determined from the boundary conditions. In terms of the concentration, in view of (5.25), (5.27) can be written

$$C_H = \frac{A}{r} \exp \left[\frac{k_1 D_H + k_2 D_{HA} C_A^\infty}{D_{HA} D_H} \right]^{\frac{1}{2}} r + k_1 \left\{ \frac{D_{HA} C_{HA}^\infty + D_H C_H^\infty}{k_1 D_H + k_2 D_{HA} C_A^\infty} \right\}$$

$$+ \frac{B}{r} \exp - \left[\frac{k_1 D_H + k_2 D_{HA} C_A^\infty}{D_{HA} D_H} \right]^{\frac{1}{2}} r + \frac{k_1 M}{r(k_1 D_H + k_2 D_{HA} C_A^\infty)} \qquad 5.28$$

From the boundary conditions at $r = \infty$

$$A = 0 \qquad 5.29$$

as before, and at $r = r_o$, when

$$C_H = 0$$

according to (5.13), an expression for B is obtained after rearranging,

$$B = -\frac{k_1 M}{k_1 D_H + k_2 D_{HA} C_A^\infty} \exp\left[\frac{k_1 D_H + k_2 D_{HA} C_A^\infty}{D_{HA} D_H}\right]^{\frac{1}{2}} r_o$$

$$- k_1 r_o \frac{D_{HA} C_{HA}^\infty + D_H C_H^\infty}{k_1 D_H + k_2 D_{HA} C_A^\infty} \exp\left[\frac{k_1 D_H + k_2 D_{HA} C_A^\infty}{D_{HA} D_H}\right]^{\frac{1}{2}} r_o$$

5.30

Backsubstituting for B therefore into (5.28) gives

$$C_H = \frac{k_1 M}{r(k_1 D_H + k_2 D_{HA} C_A^\infty)} + k_1 \left\{\frac{D_{HA} C_{HA}^\infty + D_H C_H^\infty}{k_1 D_H + k_2 D_{HA} C_A^\infty}\right\}$$

$$- \frac{k_1 M}{r(k_1 D_H + k_2 D_{HA} C_A^\infty)} \exp -\left[\frac{k_1 D_H + k_2 D_{HA} C_A^\infty}{D_{HA} D_H}\right]^{\frac{1}{2}} (r - r_o)$$

$$- \frac{r_o k_1 (D_{HA} C_{HA}^\infty + D_H C_H^\infty)}{r(k_1 D_H + k_2 D_{HA} C_A^\infty)} \exp -\left[\frac{k_1 D_H + k_2 D_{HA} C_A^\infty}{D_{HA} D_H}\right]^{\frac{1}{2}} (r - r_o)$$

5.31

The current density at the electrode surface can therefore now be obtained, according to the boundary condition

$$i_s = nFD_H \frac{dC_H}{dr} \qquad 5.15$$

$$= nFD_H \frac{k_1 M}{r_o(k_1 D_H + k_2 D_{HA} C_A^\infty)} \left\{\frac{k_1 D_H + k_2 D_{HA} C_A^\infty}{D_{HA} D_H}\right\}^{\frac{1}{2}}$$

$$+ nFD_H \frac{k_1 (D_{HA} C_{HA}^\infty + D_H C_H^\infty)}{k_1 D_H + k_2 D_{HA} C_A^\infty} \left\{\frac{1}{r_o} + \left(\frac{k_1 D_H + k_2 D_{HA} C_A^\infty}{D_{HA} D_H}\right)^{\frac{1}{2}}\right\}$$

5.32

with the arbitrary constant M still undetermined. However, from (5.22)

$$i_s = -\frac{nFM}{r_o^2} \qquad 5.22$$

so that (5.22) may be combined with (5.32) to produce a value for M,

$$M = -\frac{\dfrac{k_1(D_{HA}C_{HA}^{\infty} + D_H C_H^{\infty})}{k_1 D_H + k_2 D_{HA} C_A^{\infty}} \left\{ \frac{1}{r_o} + \left(\frac{k_1 D_H + k_2 D_{HA} C_A^{\infty}}{D_{HA} D_H} \right)^{\frac{1}{2}} \right\}}{\dfrac{1}{r_o^2 D_H} \left\{ 1 + \dfrac{D_H k_1 r_o}{(D_{HA} D_H)^{\frac{1}{2}} (k_1 D_H + k_2 D_{HA} C_A^{\infty})^{\frac{1}{2}}} \right\}} \qquad 5.33$$

so that the current density at $r = r_o$ becomes

$$i_s = nFD_H \frac{\dfrac{k_1(D_{HA}C_{HA}^{\infty} + D_H C_H^{\infty})}{k_1 D_H + k_2 D_{HA} C_A^{\infty}} \left\{ \frac{1}{r_o} + \left(\frac{k_1 D_H + k_2 D_{HA} C_A^{\infty}}{D_{HA} D_H} \right)^{\frac{1}{2}} \right\}}{1 + \dfrac{k_1 r_o (D_H)^{\frac{1}{2}}}{(D_{HA})^{\frac{1}{2}} (k_1 D_H + k_2 D_{HA} C_A^{\infty})^{\frac{1}{2}}}} \qquad 5.34$$

This expression for the current density at a spherical electrode is clearly difficult to apply in the form shown above. The equation may, however, be simplified by making the approximations

$$D_{HA}C_{HA}^{\infty} \gg D_H C_H^{\infty} \qquad 5.35$$

and

$$k_2 C_A^{\infty} D_{HA} \gg k_1 D_H \qquad 5.36$$

so that (5.34) reduces to

$$i_s = nFD_H \frac{\frac{k_1 C_{HA}^{\infty}}{k_2 C_A^{\infty}} \left\{ \frac{1}{r_o} + \left(\frac{k_2 C_A^{\infty}}{D_H} \right)^{\frac{1}{2}} \right\}}{1 + \frac{k_1 r_o (D_H)^{\frac{1}{2}}}{D_{HA} (k_2 C_A^{\infty})^{\frac{1}{2}}}} \qquad 5.37$$

Further simplifications may be made for reactions of high k_2 by noting that

$$\frac{k_2 C_A^{\infty}}{D_H} \gg \frac{1}{r_o} \qquad 5.38$$

leading to a final form of

$$i_s = \frac{\frac{nF(D_H)^{\frac{1}{2}} k_1 C_{HA}^{\infty}}{(k_2 C_A^{\infty})^{\frac{1}{2}}}}{1 + \frac{k_1 r_o (D_H)^{\frac{1}{2}}}{D_{HA} (k_2 C_A^{\infty})^{\frac{1}{2}}}} \qquad 5.39$$

or, alternatively,

$$\frac{1}{i_s} = \frac{(k_2 C_A^{\infty})^{\frac{1}{2}}}{nF(D_H)^{\frac{1}{2}} k_1 C_{HA}^{\infty}} + \frac{r_o}{nFD_{HA} C_{HA}^{\infty}} \qquad 5.40$$

so that a plot of

$$\frac{1}{i_s} \quad \text{vs.} \quad r_o \qquad 5.41$$

should produce a straight line of intercept

$$\text{intercept} = \frac{(k_2 C_A^{\infty})^{\frac{1}{2}}}{nF(D_H)^{\frac{1}{2}} k_1 C_{HA}^{\infty}} \qquad 5.42$$

and

$$\text{slope} = \frac{1}{nFD_{HA}C^{\infty}_{HA}} \qquad 5.43$$

enabling values of k_1 and k_2 to be evaluated assuming a knowledge of the pK_a of the acid solution.

The reduction of acetic acid in aqueous sodium acetate solutions was chosen as a suitable system for study and the results of the investigation, using platinum microelectrodes of various radii are presented in 5:ii.

5:ii Hydrogen Evolution from Aqueous Strong Acid Media

Before attempting to measure the rates of the equilibrium reaction preceding the evolution of hydrogen from a weak acid solution at a platinum microelectrode, the response of the microelectrode in strong acid solutions under conditions of high rates of mass transfer was first investigated.

There is ample evidence in the literature to suggest that the rate of electron transfer at a metal electrode is sensitive to both the surface state and previous history of the electrode. Various methods of pretreatment have been proposed to clean, or 'activate' the surface of metal electrodes [22] , particularly in aqueous media, with the dual aim of enhancing the reversibility of the electrode reaction while also producing a clean, reproducible electrode surface. Electrode activation is normally achieved in two ways - by the removal of adsorbed species, which may inhibit electron transfer, from the electrode surface and by changing the microstructure of the electrode surface.

Although simple polishing techniques are usually adequate for work in dipolar aprotic solvents, where adsorption may be less significant, more stringent pretreatment methods are necessary for aqueous systems. Chemical oxidation of the electrode surface to a reproducible state using for example hot nitric acid, is recommended [22] . Alternatively, the same result may be obtained by anodising the electrode surface to remove adsorbed material. The oxide layer then is reduced at a potential sufficient to remove the oxide layer but not reduce hydrogen ion, or solvent, thereby producing a clean, 'active' electrode surface.

For these experiments, a combination of polishing with an aqueous suspension of alumina powder (0·05μm) and electrochemical anodisation was employed to activate the platinum microelectrodes. A comparison of the behaviour of activated and deactivated platinum microelectrodes is shown in FIG. 58 for the reduction

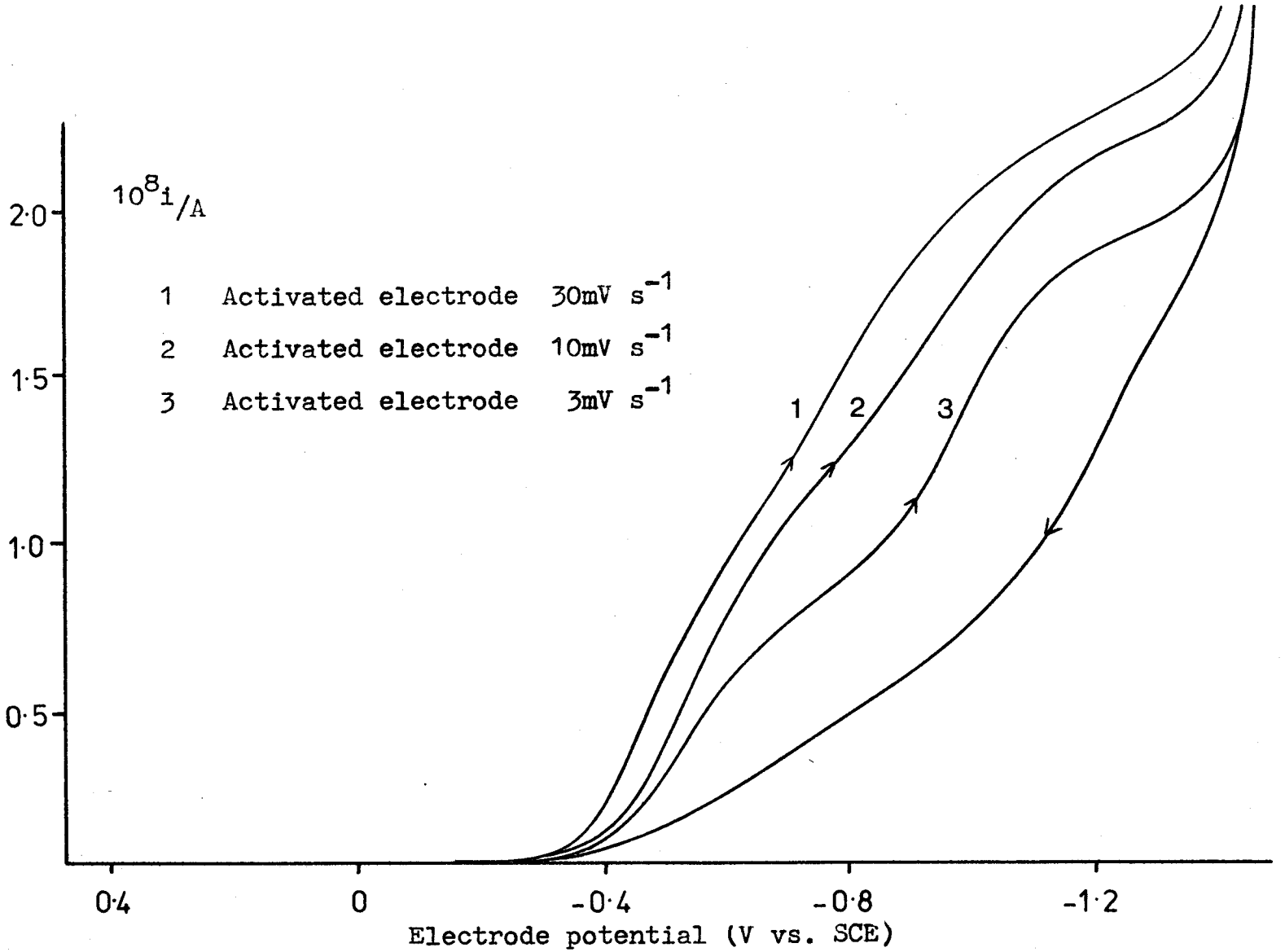

FIG 58 Voltammogram for the reduction of perchloric acid (10mM) in sodium perchlorate (1M) at a platinum microelectrode (1.5μm).

of perchloric acid ($HClO_4$: 10mM) in aqueous sodium perchlorate ($NaClO_4$: 1M) solution at a platinum 1μm electrode. Here the polished electrode was subjected to a linear potential sweep cycle (30mV s^{-1}) of the form 0·0V (vs. SCE) → -1·3V → +1·0V → -1·3V → 0·0V beginning with an initially deactivated electrode and activating during the second potential cycle. A substantial increase in electron transfer rate for the bulk acid reduction is observed for the activated electrode in comparison to the response of the deactivated electrode.

In FIGS. 59 - 62 examples of voltammograms obtained for the reduction of perchloric acid, in sodium perchlorate solutions, at activated 1μm, 3μm and 5μm platinum microelectrodes recorded as a function of potential sweep rate and acid concentration are shown. Well defined polarographic waves at ~ 0·35V (vs. SCE), corresponding to the reduction of bulk acid protons on the activated platinum microelectrodes at potential sweep rates of 30mV s^{-1} are observed, while at more cathodic potentials, the reduction of water is visible on activated electrodes only, indicating enhanced general acid catalysis of the hydrogen ion discharge reaction.

The half wave potentials for the reduction of bulk acid protons are found to be in close agreement with those values predicted by the Nernst equation for a one electron transfer reaction

$$E = E_o + \frac{RT}{F} \ln [H^+] \qquad 5.44$$

i.e. for a 10mM acid solution,

$$E = E_o + \frac{RT}{F} \ln 10^{-2}$$

$$= -0{\cdot}12 \text{ vs. NHE}$$

$$-0{\cdot}36 \text{ vs. SCE} \qquad 5.45$$

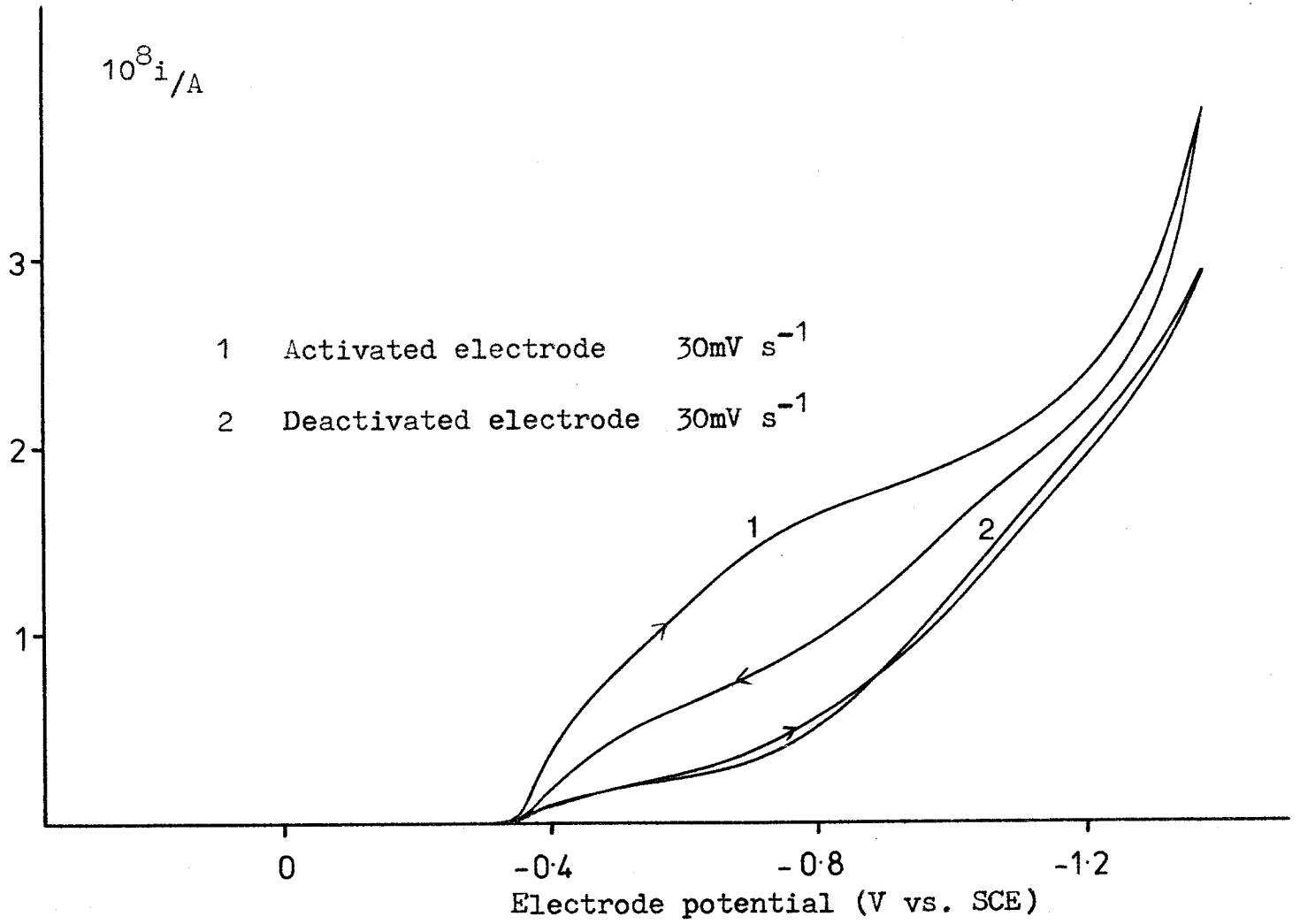

FIG 59 Voltammogram for tne reduction of perchloric acid (10mM) in sodium perchlorate (1M) at a platinum microelectrode (1.5μm).

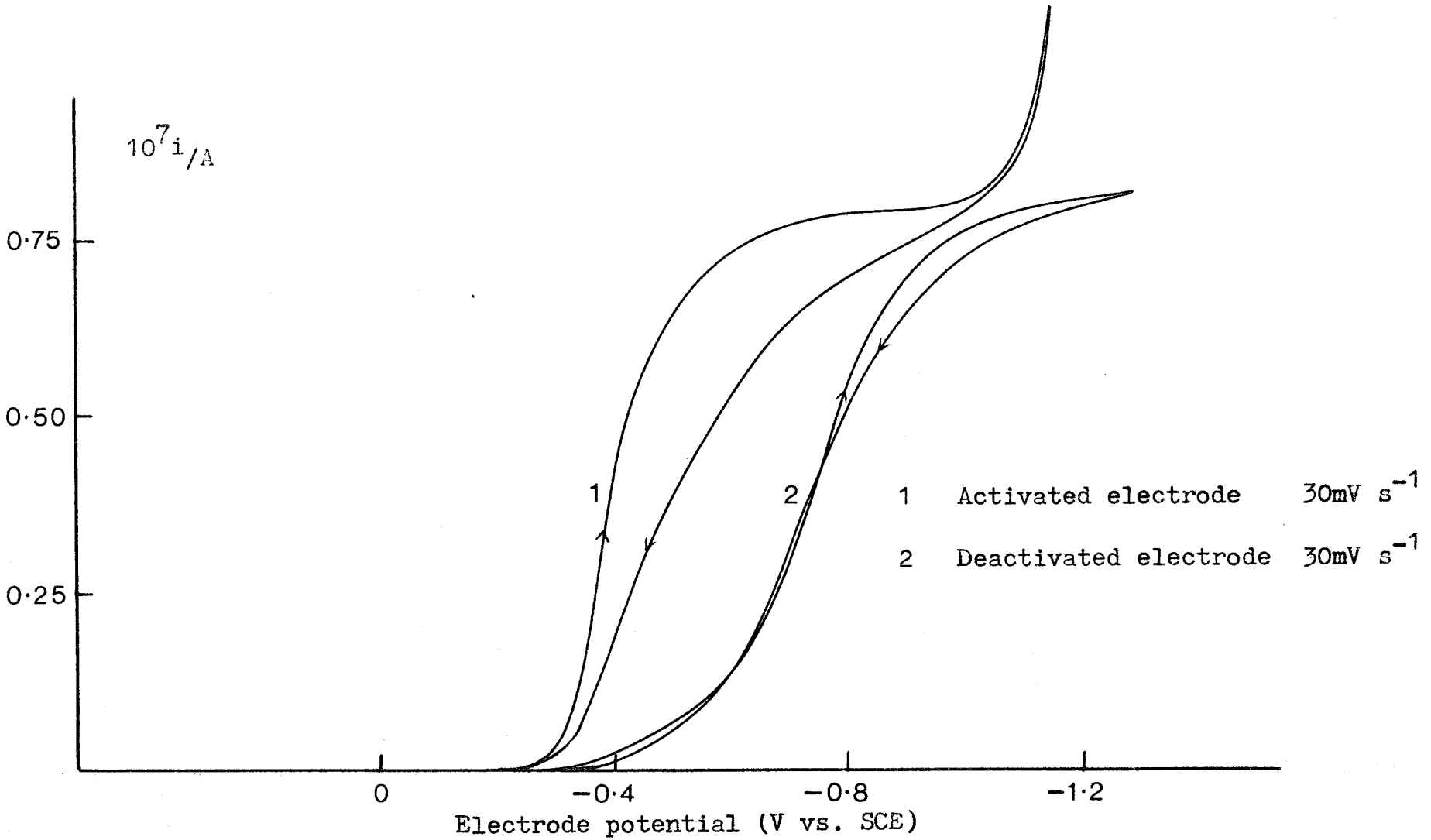

FIG 60 Voltammogram for the reduction of perchloric acid (10mM) in sodium perchlorate (1M) at a platinum microelectrode (3.5μm).

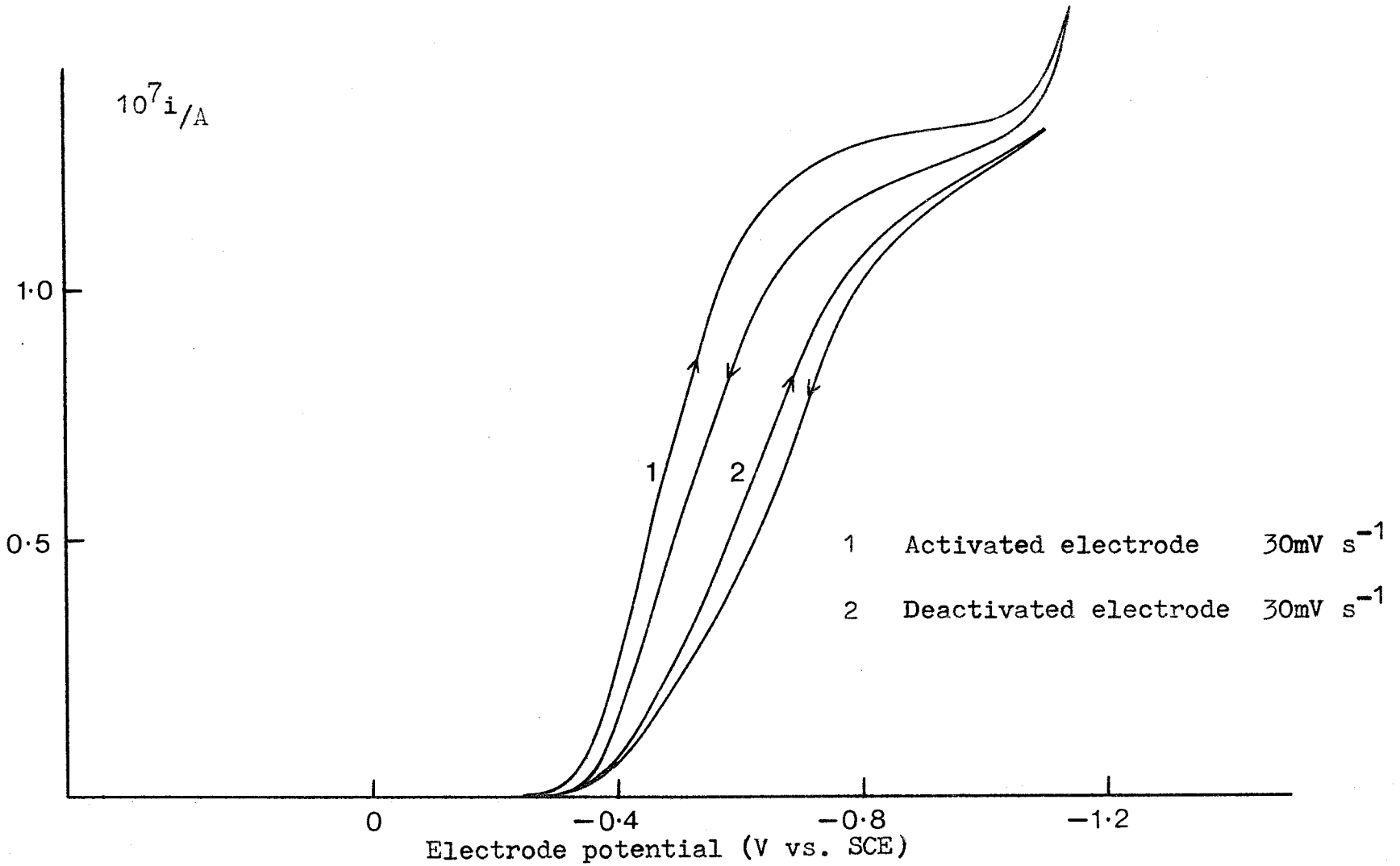

FIG 61 Voltammogram for the reduction of perchloric acid (10mM) in sodium perchlorate (1M) at a platinum microelectrode (6μm).

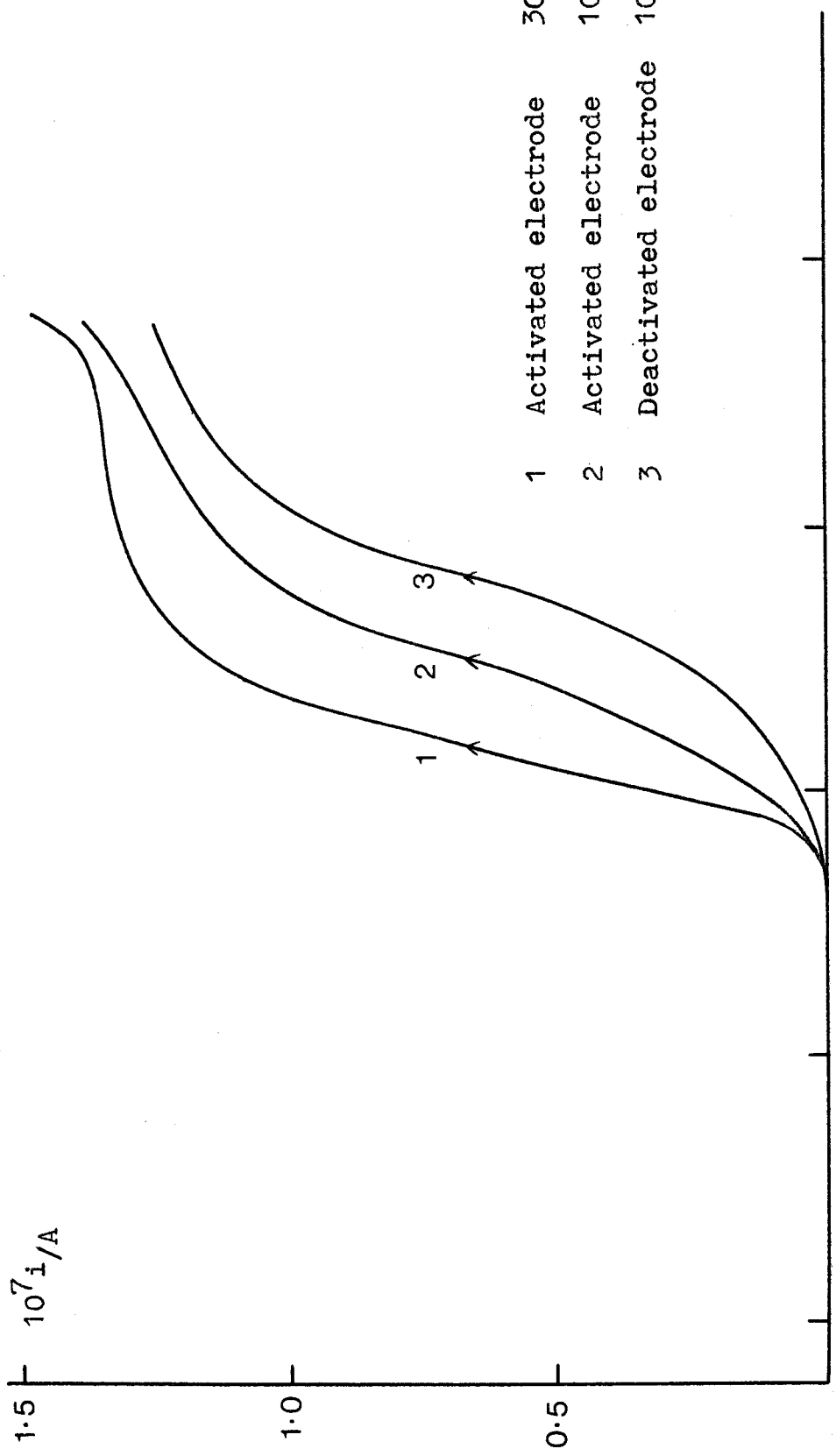

FIG 62 Voltammogram for the reduction of perchloric acid (10mM) in sodium perchlorate (1M) at a platinum microelectrode (6μm).

The assumption of a one electron transfer reaction is justified from the analysis of the observed diffusion controlled limiting current, using

$$i_d = nFD_H C_o^{\infty} \pi r \qquad 5.46$$

with the known bulk acid concentration (assuming complete dissociation), assumed approximate electrode radius and a diffusion coefficient $D_H = 7{\cdot}2 \times 10^{-5} cm^2\ s^{-1}$, obtained from the literature [115] and confirmed in FIG. 63 for a plot of i_d/C_o^{∞} vs. r_o for a range of acid concentrations and microelectrode radii. Subsequent calculations of the limiting current density shows that high rates of mass transfer have been achieved in comparatively dilute solutions with these microelectrodes.

Analysis of the current voltage curves was not feasible, however, due to the rapid deactivation of the microelectrodes. In FIGS. 58 - 62 it can be seen that as the potential sweep rate is decreased from 30mV s^{-1} to 3mV s^{-1} the single reduction wave becomes more irreversible and forms two overlapping waves; the height of the first wave diminishing as the potential sweep rate is decreased, so that at the slowest sweep rates the current voltage profile is virtually indistinguishable from the profile for a deactivated electrode. Furthermore, in comparing current voltage curves at microelectrodes of different radii at comparable potential sweep rates (FIGS. 59 - 61) this effect is seemingly more pronounced at the smallest microelectrodes. The two dependent variables of time (i.e. potential sweep rate) and electrode radius suggest some kind of deactivation mechanism related to either the charge passed through the electrode, the increased current density at the smaller microelectrodes or the increased ratio of electrode edge sites to total surface area found with the smaller microelectrodes, or even a combination of all three.

To understand how these factors may influence the electron transfer process it is first necessary

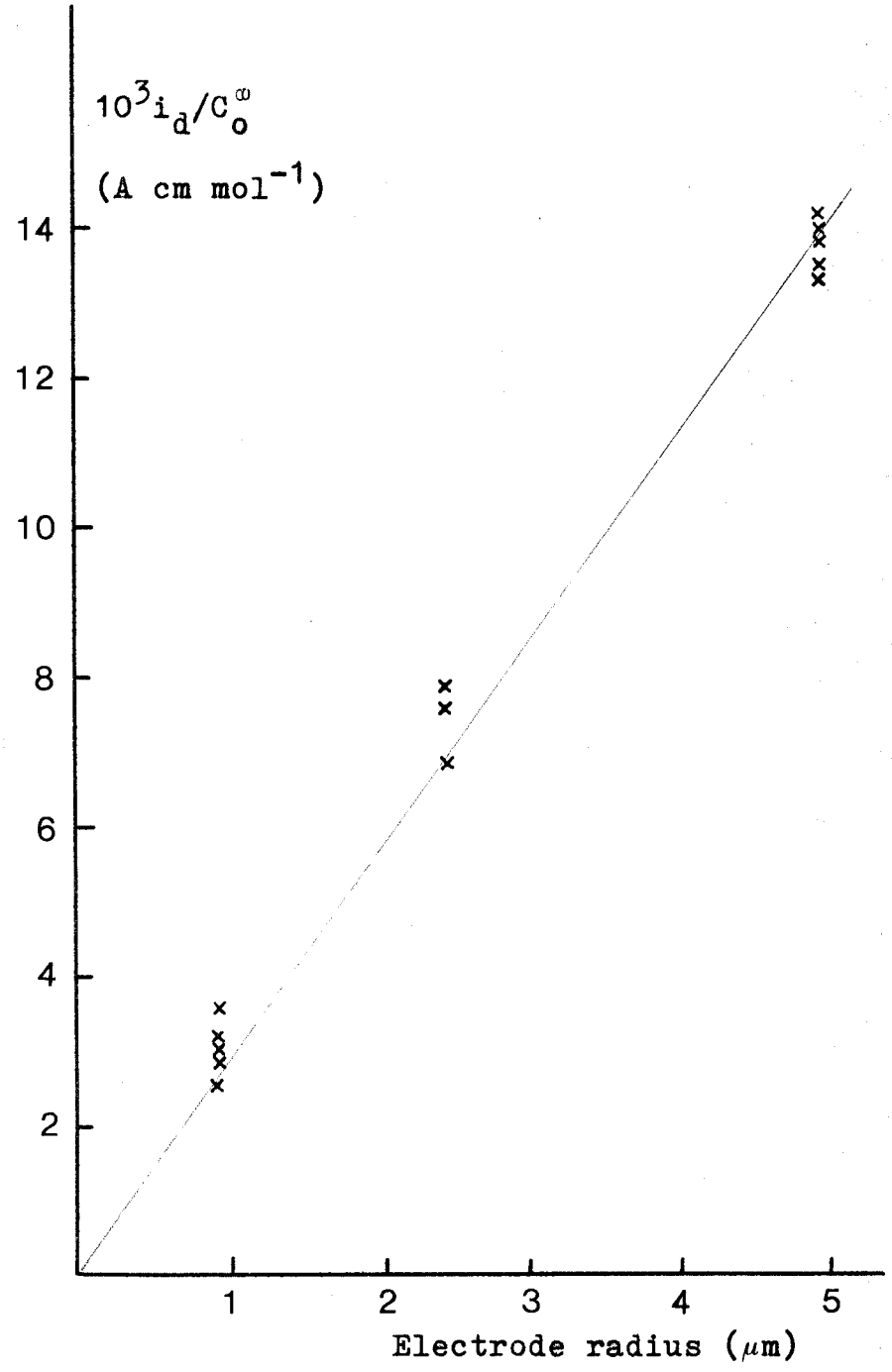

FIG 63 Plot of i_d/C_o^∞ vs. electrode radius for the reduction of perchloric acid in sodium perchlorate at platinum microelectrodes

to examine the mechanism of the hydrogen evolution reaction at a platinum surface. It is generally accepted to proceed via a two step 'atom - atom' recombination mechanism [4] , i.e.

$$Pt + H^+ + e \longrightarrow Pt - H_{ads} \qquad 5.47$$

$$Pt - H_{ads} + Pt - H_{ads} \longrightarrow 2Pt + H_2 \qquad 5.48$$

At low overpotentials, however, an alternative 'ion - atom' recombination reaction according to

$$Pt + H^+ + e \longrightarrow Pt - H_{ads} \qquad 5.47$$

$$Pt - H_{ads} + H^+ + e \longrightarrow Pt + H_2 \qquad 5.49$$

has also been proposed [116] . In both these reaction mechanisms the second recombination step is considered rate determining, although on particularly activated platinum electrodes the diffusion of molecular hydrogen away from the electrode surface has also been suggested as a rate determining step [4] . This may contribute, in part, to the apparent deactivation of the smaller microelectrodes due to the higher current densities experienced with these electrodes.

From equations (5.47) - (5.49), the role of the platinum surface in the hydrogen evolution reaction is seen to be particularly important. The surface structure of polycrystalline platinum electrodes in acidic and alkaline media has been examined by many workers, including Breiter [117] , Will [118] , Bagotskii [119] and Schuldiner [120] to name but a few. The most widely used experimental technique has been fast linear potential sweep where surface reactions such as adsorption/desorption processes are clearly discernable although not always easily evaluated in a quantitative manner.

More recent investigations by Ross [121,122]

and Hubbard [123] and others [124] have sought to establish the contribution of individual crystallographic faces to the overall activity of the metal. Elsewhere, other workers have investigated the effect of platinum morphology on the observed electrocatalytic activity [125 - 128]. The structural rearrangement and disordering of the surfaces of single crystals is commonplace in the literature of surface science, including numerous examples involving platinum [129 - 131], but the role of edge sites, kinks, dislocations and other surface defects on the activity of heterogeneous catalysts remains the subject of current research [132].

The presence of defects (usually of the order 10^7 - $10^8 cm^{-2}$) will undoubtedly lead to different active sites on the electrode surface, so that in the particular case of microelectrodes where edge sites contribute an increasing proportion of the total number of available sites as the electrode radius decreases, it is feasible to consider that some variation in specific activity with electrode radius should occur. Structural rearrangement of the surface atoms during anodic activation leading to the formation of sites of variable activity might well account for the current voltage behaviour observed at slow potential sweep rates seen in FIGS. 58 - 62. In attempts to investigate the surface reaction further, a series of cyclic voltammograms at fast potential sweep rates were recorded on platinum microelectrodes of various radii for the reduction of perchloric acid ($HClO_4$: 10mM) in aqueous sodium perchlorate ($NaClO_4$: 1M). A selection of the voltammograms are shown in FIGS. 64 - 71.

In comparison to the voltammograms recorded at slower potential sweep rates shown in FIGS. 58 - 62, using the same platinum microelectrodes, additional, sweep rate dependent electrode processes may be identified. At potentials more anodic than 0·5V (vs. SCE) an anodic current due to the surface oxidation of platinum is observed, with an accompanying broad reduction peak, centred at ~ 0·4V (vs. SCE) on the

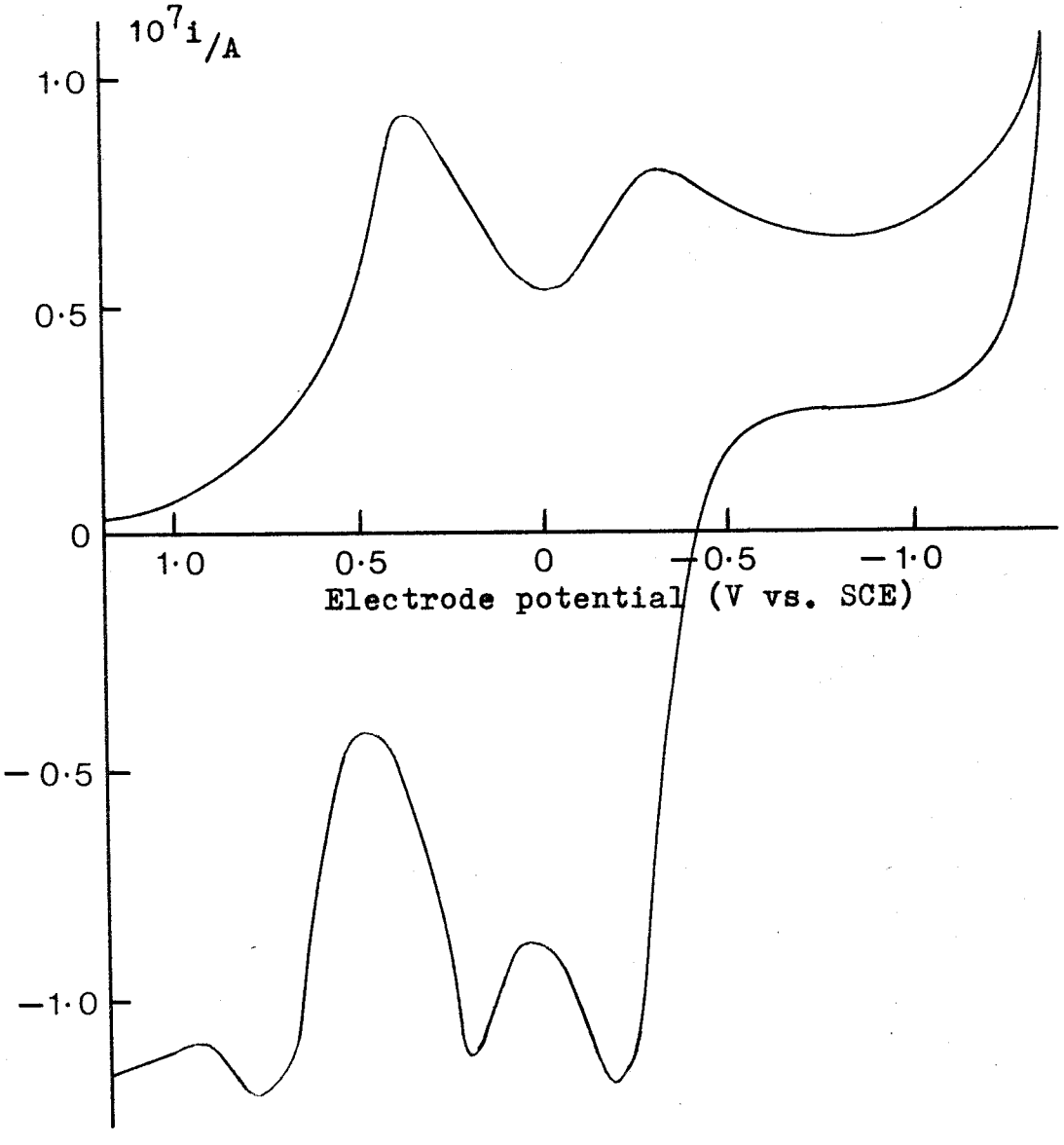

FIG 64 Voltammogram for the reduction of perchloric acid (10mM) in sodium perchlorate (1M) at a platinum microelectrode (12μm). Sweep rate = 100V s^{-1}: continuous sweep

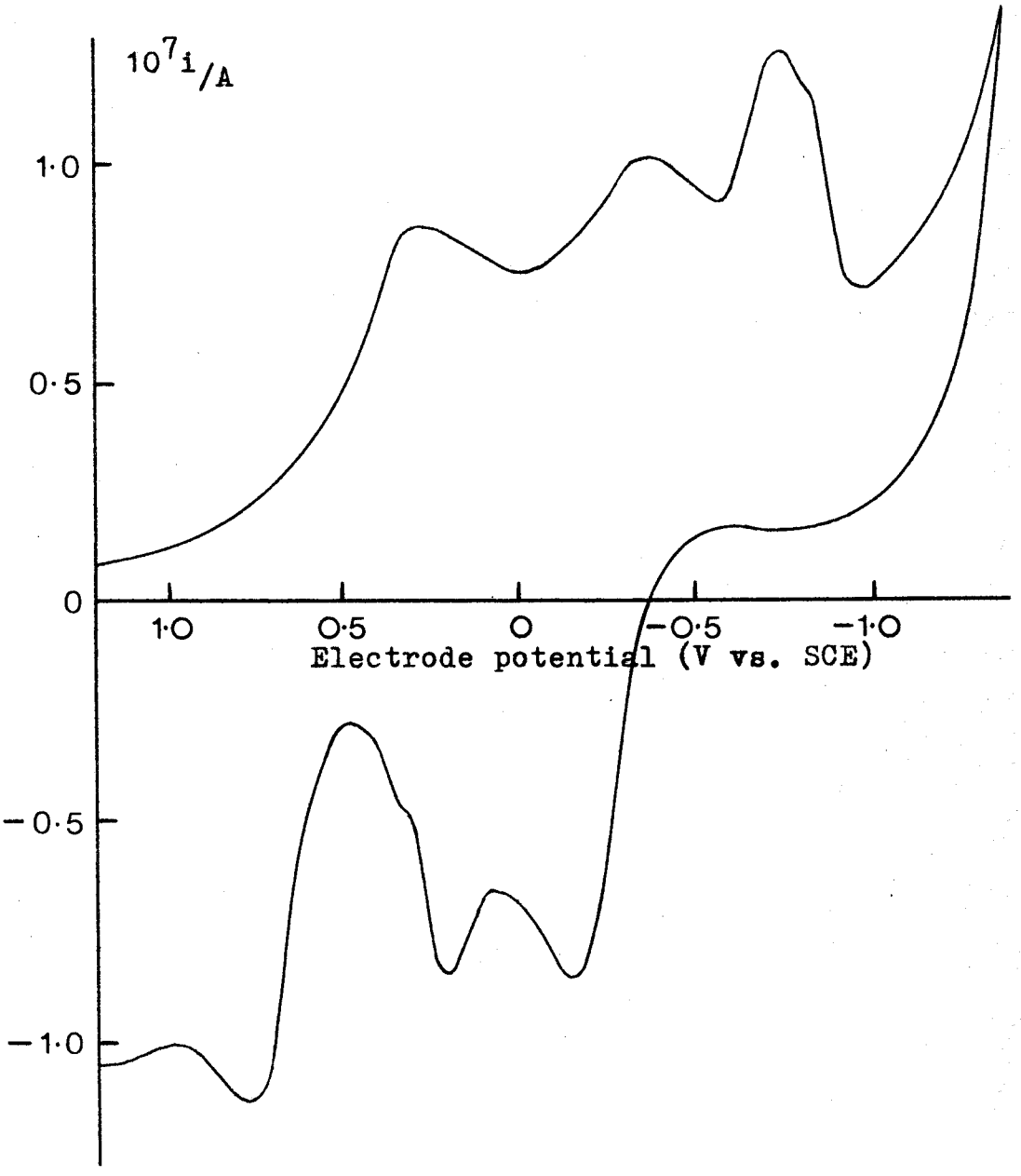

FIG 65 Voltammogram for the reduction of perchloric acid (10mM) in sodium perchlorate (1M) at a platinum microelectrode (12μm). Sweep rate = 100V s^{-1}: 1 second delay at 1·0V (vs. SCE).

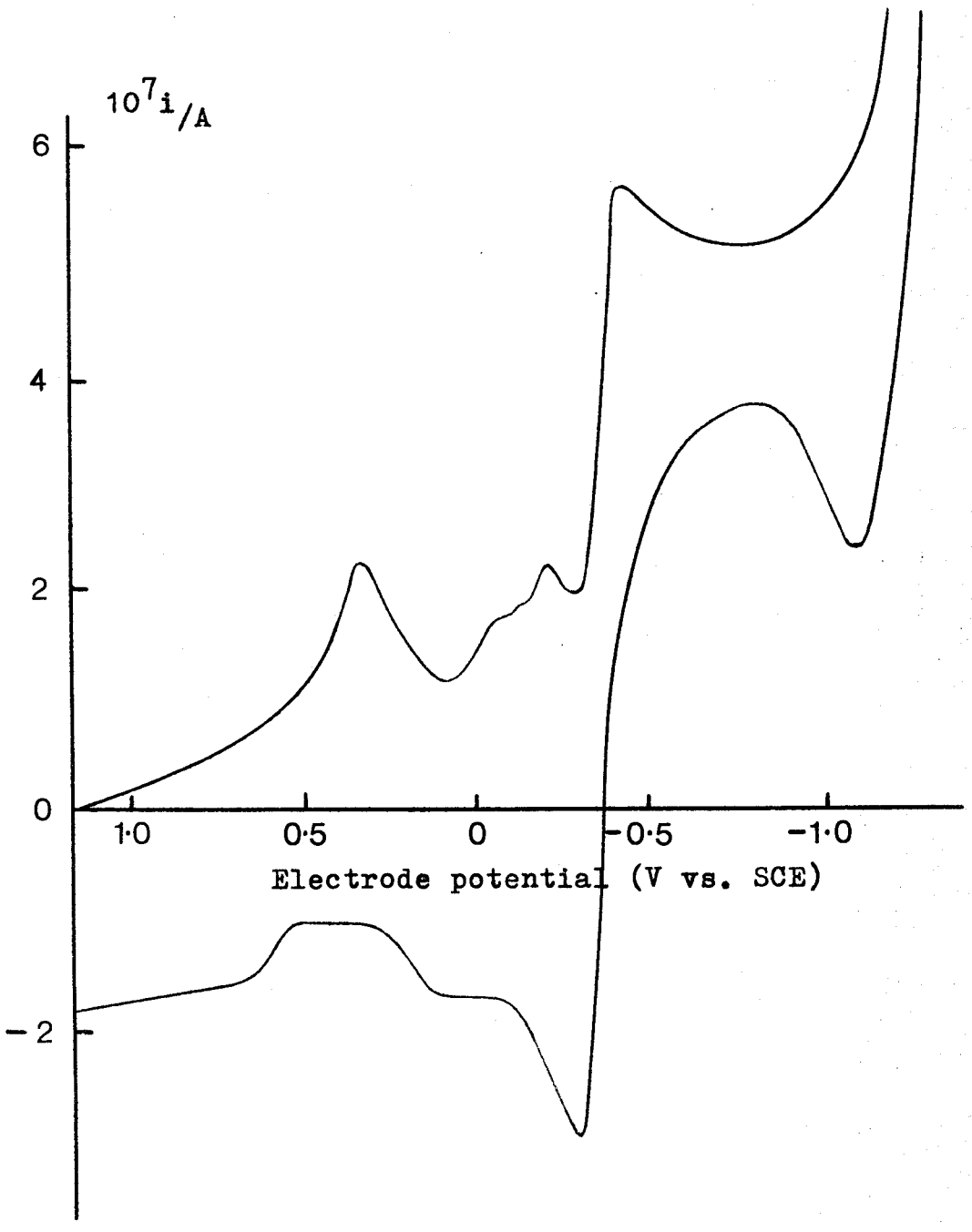

FIG 66 Voltammogram for the reduction of perchloric acid (10mM) in sodium perchlorate (1M) at a platinum microelectrode (12μm). Sweep rate = 10V s^{-1}: 1 second delay at 1·0V (vs. SCE)

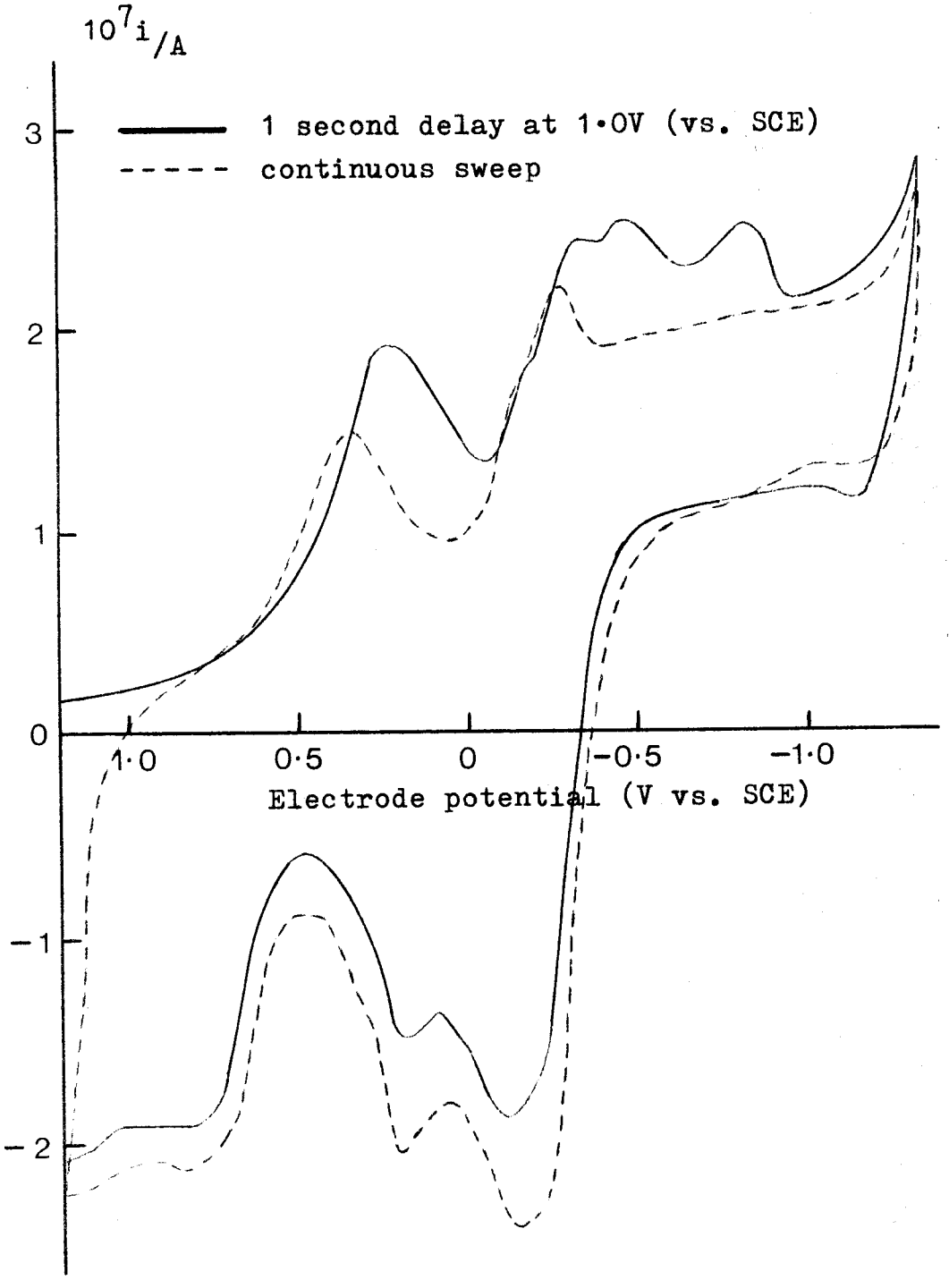

FIG 67 Voltammogram for the reduction of perchloric acid (10mM) in sodium perchlorate (1M) at a platinum microelectrode (6μm). Sweep rate = 100V s^{-1}

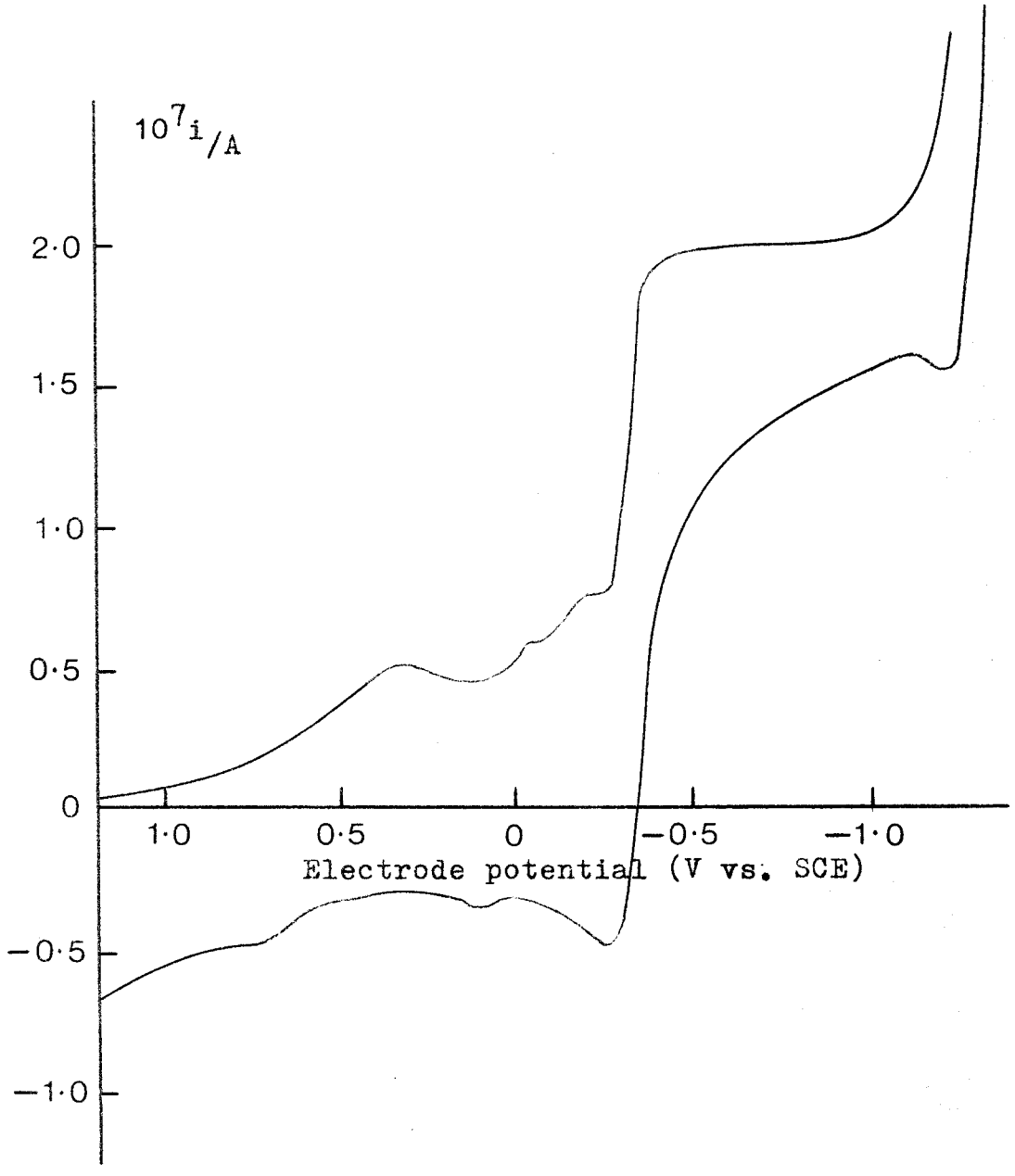

FIG 68 Voltammogram for the reduction of perchloric acid (10mM) in sodium perchlorate (1M) at a platinum microelectrode (6μm). Sweep rate = 10V s^{-1}: 1 second delay at 1·0V (vs. SCE).

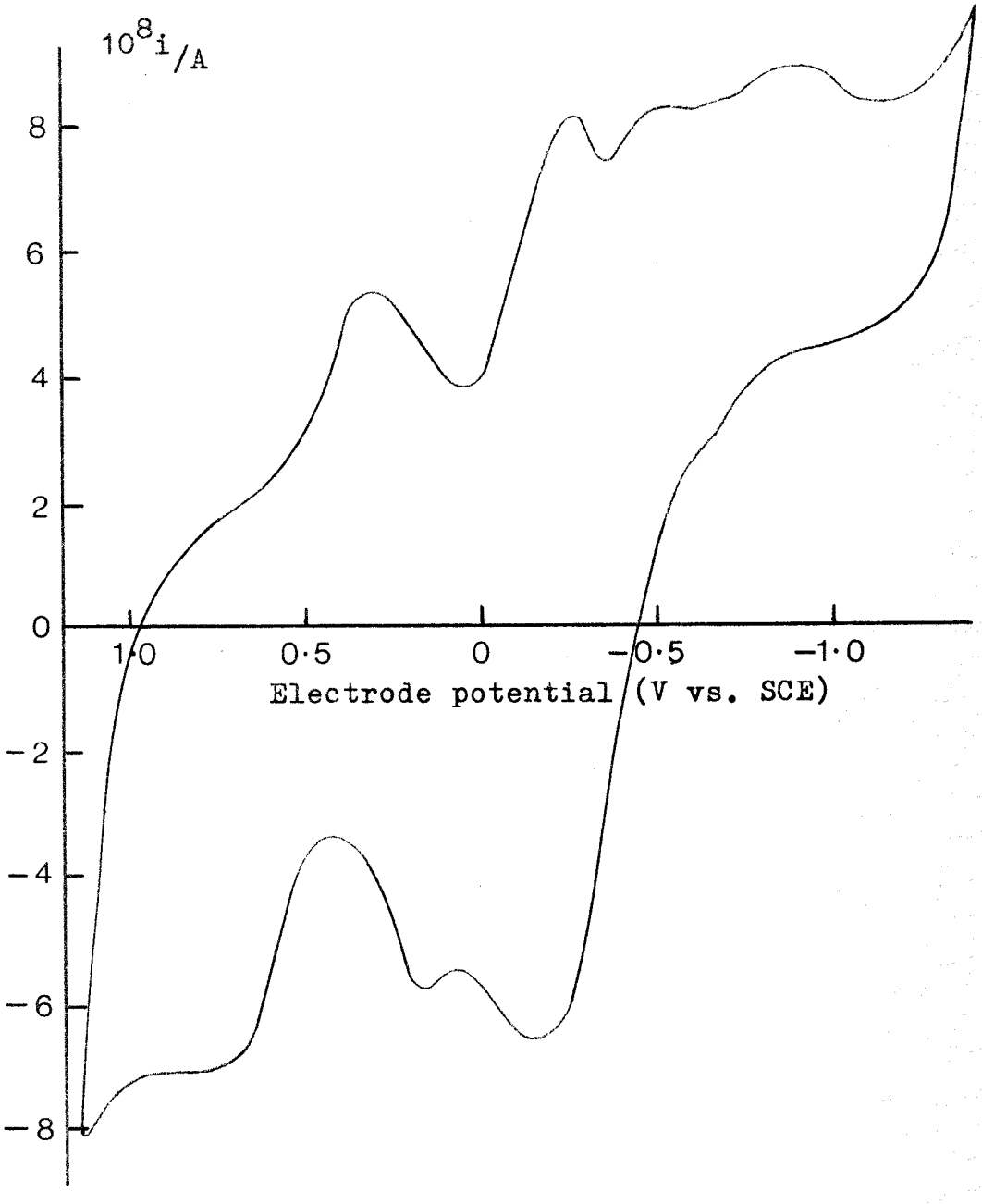

FIG 69 Voltammogram for the reduction of perchloric acid (10mM) in sodium perchlorate (1M) at a platinum microelectrode (1·6μm). Sweep rate = 100V s^{-1}: continuous sweep

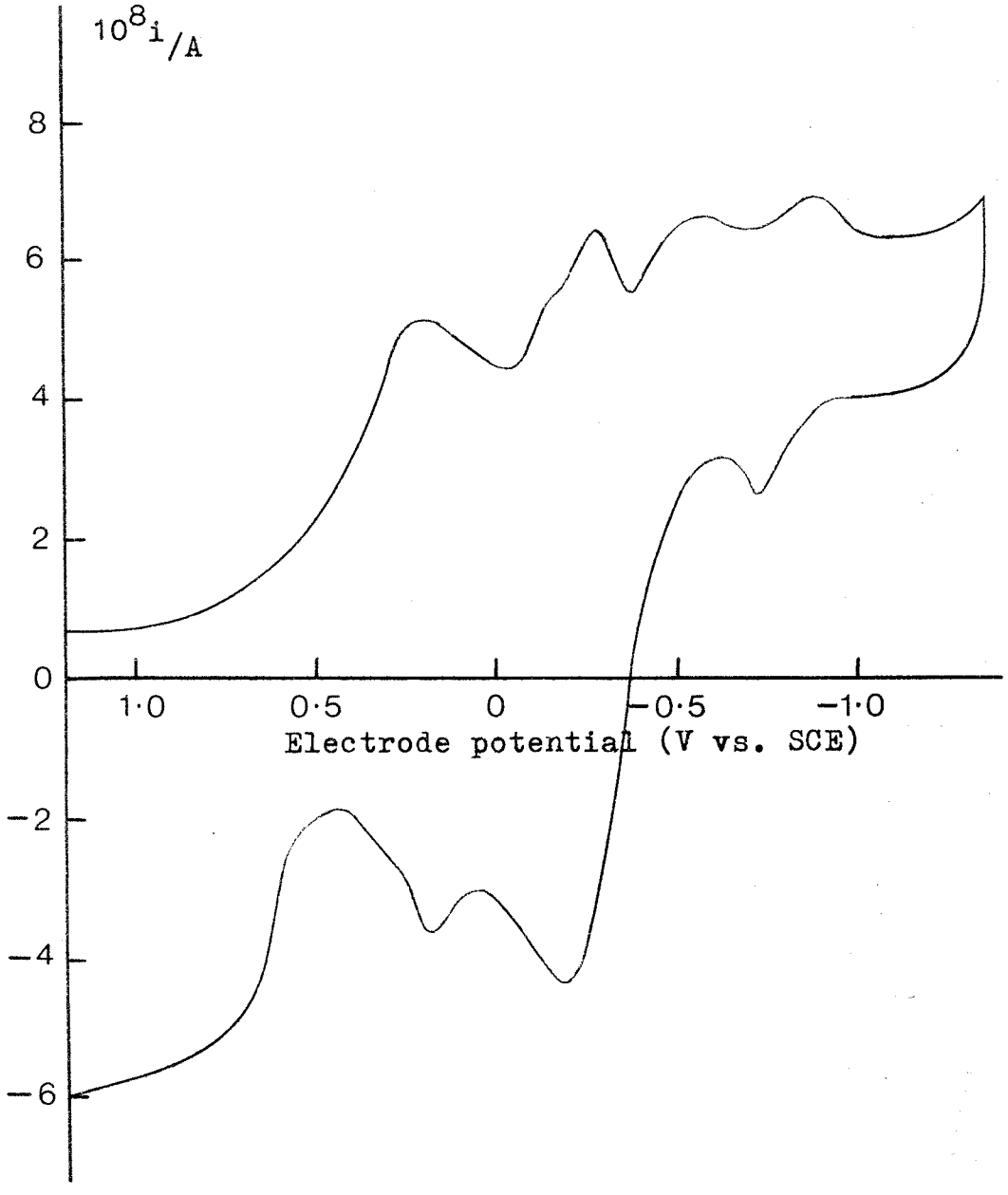

FIG 70 Voltammogram for the reduction of perchloric acid (10mM) in sodium perchlorate (1M) at a platinum microelectrode (1·6μm). Sweep rate = 100V s^{-1}: 1 second delay at 1·0V (vs. SCE).

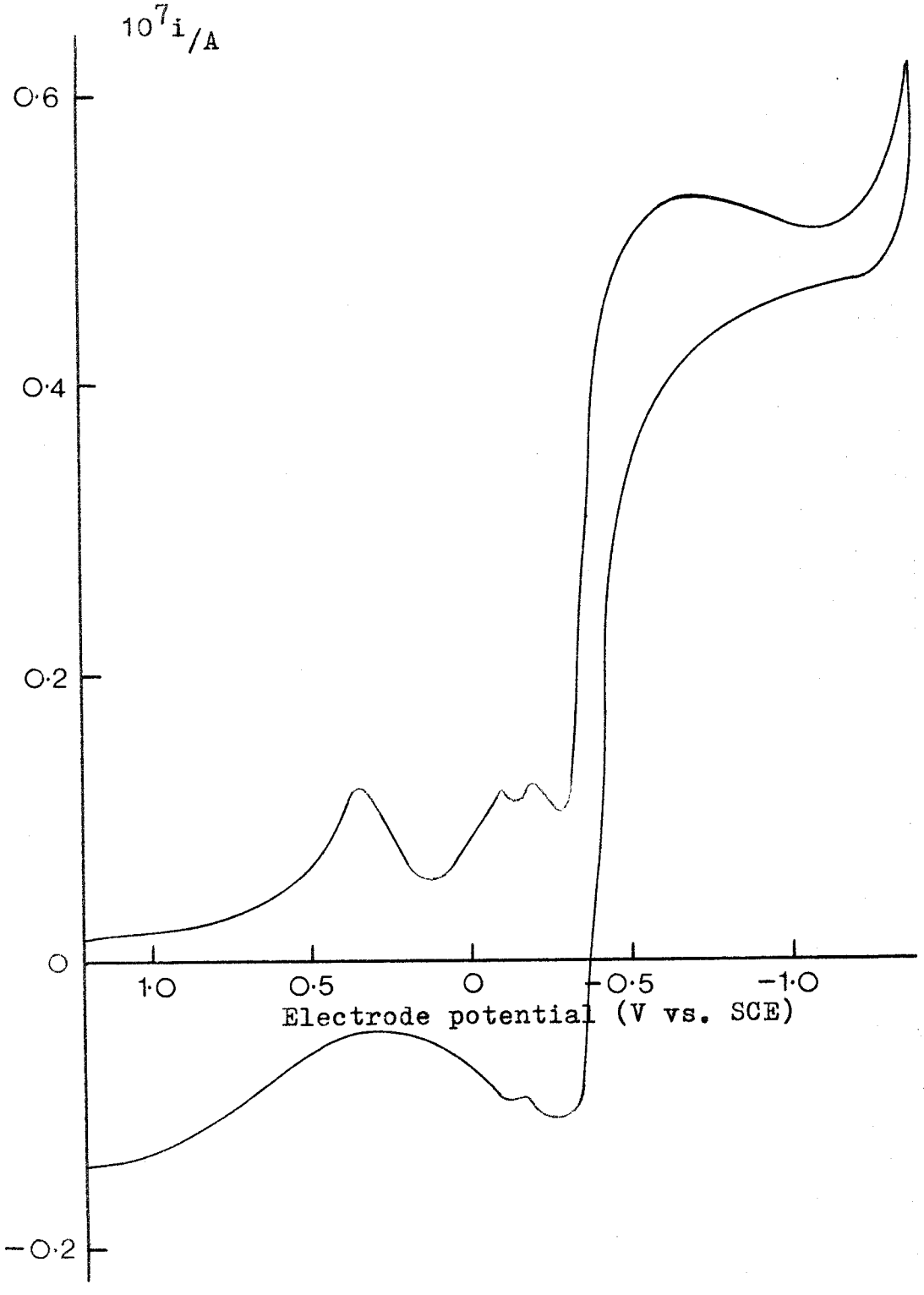

FIG 71 Voltammogram for the reduction of perchloric acid (10mM) in sodium perchlorate (1M) at a platinum microelectrode (1·6μm). Sweep rate = 10V s^{-1}: 1 second delay at 1·0V (vs. SCE).

reverse potential scan, for the surface oxide reduction. The characteristic hydrogen ion adsorption/desorption peaks depicting strong and weakly bound hydrogen to the platinum surface are also visible at potentials immediately anodic to the bulk acid proton reduction wave although at high potential sweep rates and/or low acid concentrations, the two adsorption peaks tend to coalesce with each other and merge into the reduction wave. It is noticed also that the current voltage profile obtained from each platinum microelectrode is strongly influenced by the method of potential cycling. For example, in FIG. 67 for the reduction of $HClO_4$ at a platinum 5μm microelectrode at 100V s^{-1}, an additional reduction peak at ~ -0·8V (vs. SCE) is observed when the electrode potential is allowed to remain for one second at the anodic limit of +1·0V (vs. SCE) during the course of the potential sweep. At slower potential sweep rates (i.e. 10V s^{-1}), this additional reduction peak is not observed for any of the platinum microelectrodes. One possible explanation to account for this additional peak is the existence of an even more weakly bound hydrogen atom on the platinum surface which manifests itself only on particularly activated electrodes.

Under similar fast potential sweep conditions at platinum microelectrodes, the reduction of acetic acid (40mM) in aqueous sodium acetate solutions (1M) also shows several distinct adsorption/desorption peaks anodic to the bulk acid proton reduction wave. It can be seen from FIGS. 72 - 76 that an increase in potential sweep rate increases the area of the strongly bound hydrogen adsorption/desorption peaks relative to the weakly bound hydrogen (found at slightly more cathodic potentials). In addition other peaks are also observed. At this stage it is not possible to interpret fully these peaks in terms of the hydrogen evolution reaction in dilute acid solutions on platinum microelectrodes; further experiments are necessary to establish the reaction mechanisms by which these reactions

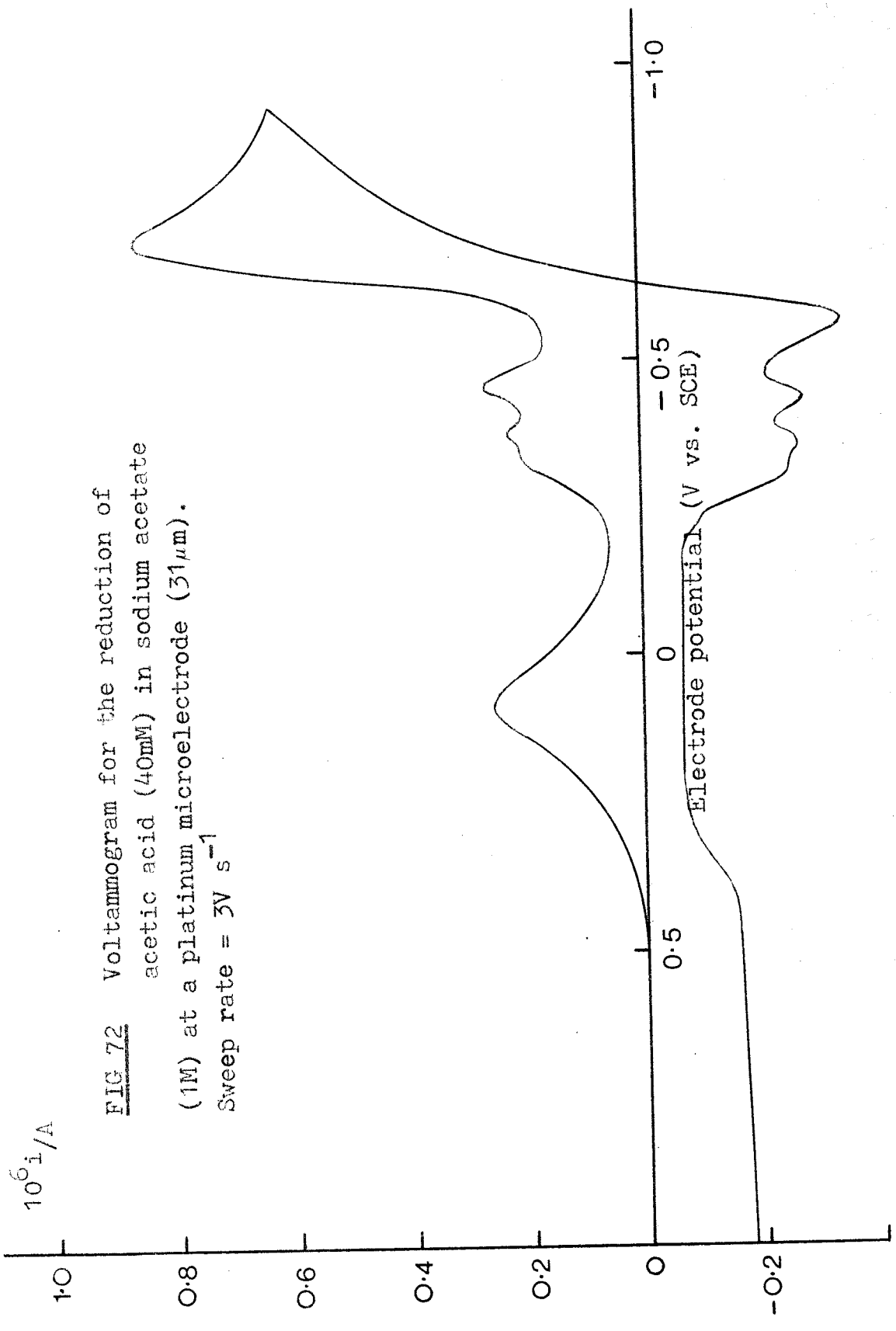

FIG 72 Voltammogram for the reduction of acetic acid (40mM) in sodium acetate (1M) at a platinum microelectrode (31μm). Sweep rate = 3V s^{-1}

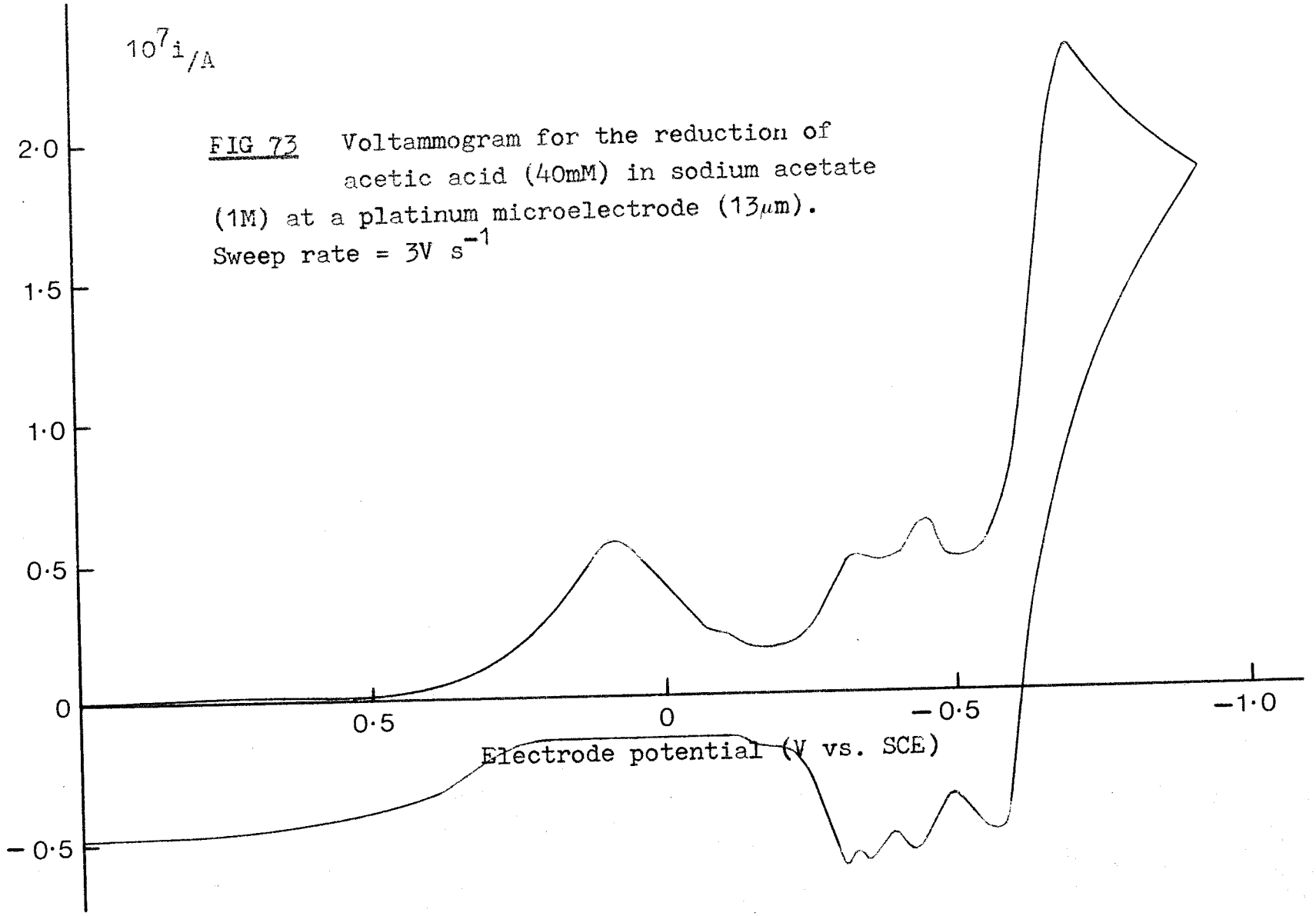

FIG 73 Voltammogram for the reduction of acetic acid (40mM) in sodium acetate (1M) at a platinum microelectrode (13μm). Sweep rate = 3V s^{-1}

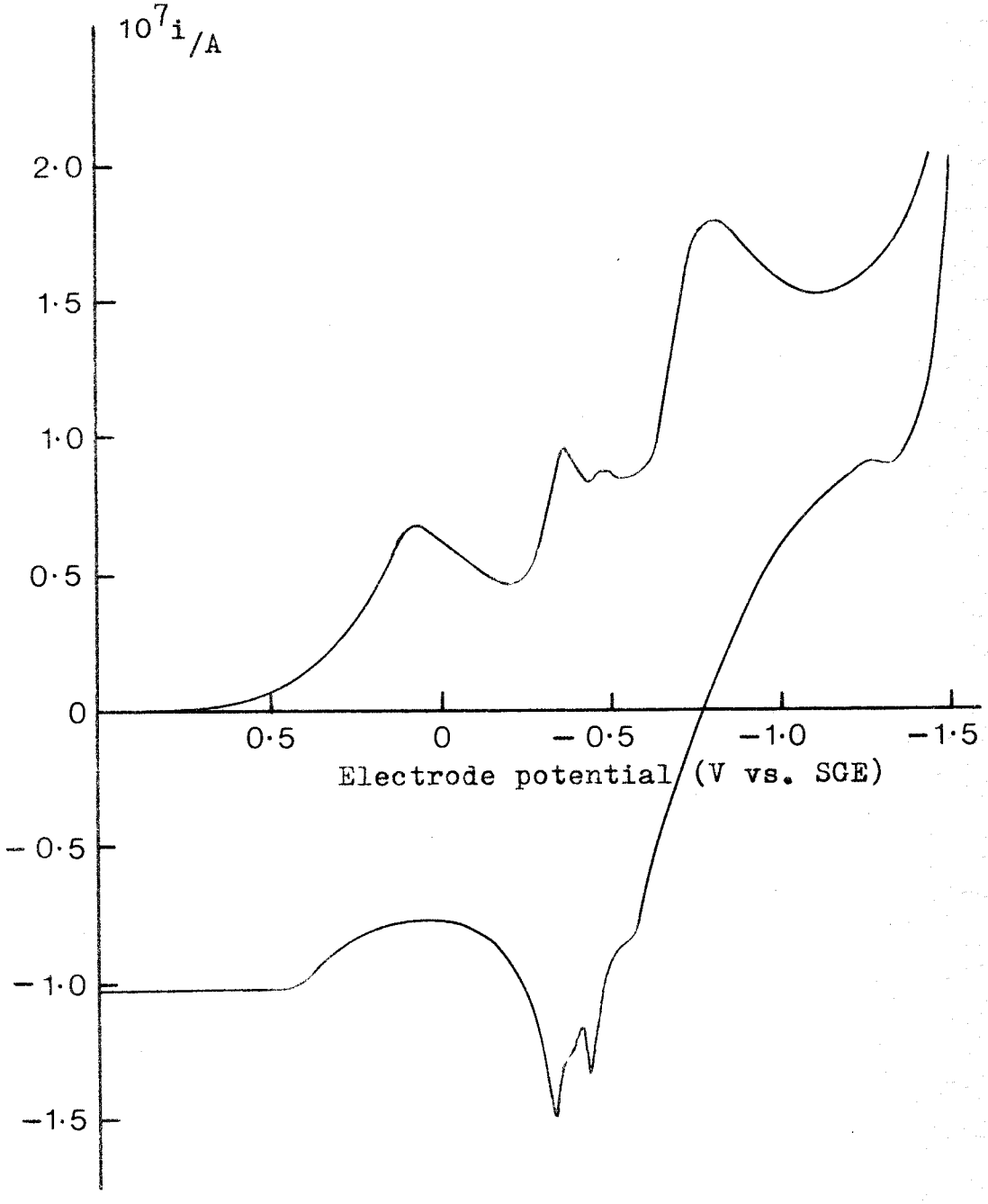

FIG 74 Voltammogram for the reduction of acetic acid (40mM) in sodium acetate (1M) at a platinum microelectrode (7μm). Sweep rate = 10V s^{-1}: continuous sweep

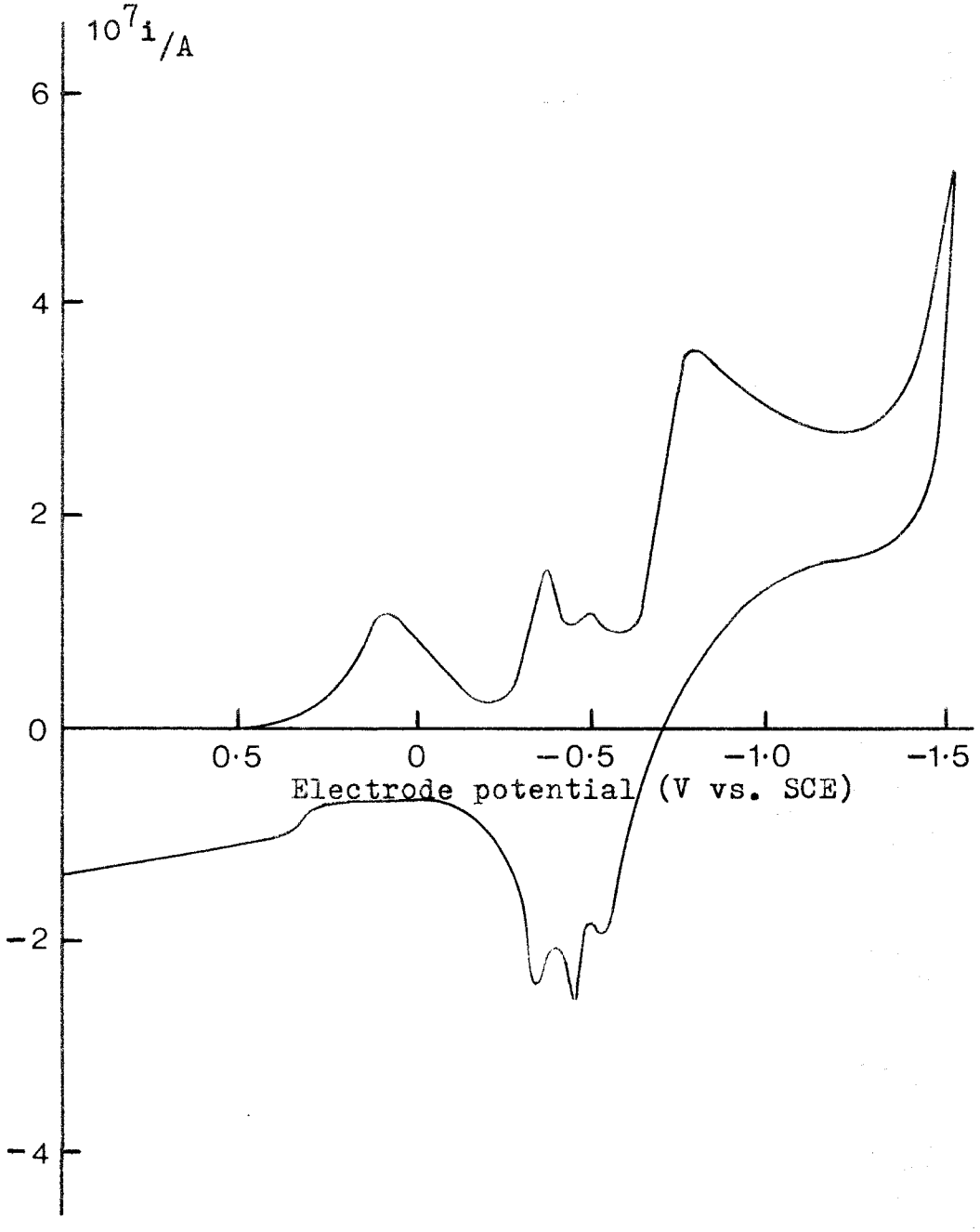

FIG 75 Voltammogram for the reduction of acetic acid (40mM) in sodium acetate (1M) at a platinum microelectrode (13μm). Sweep rate = 10V s^{-1}: continuous sweep

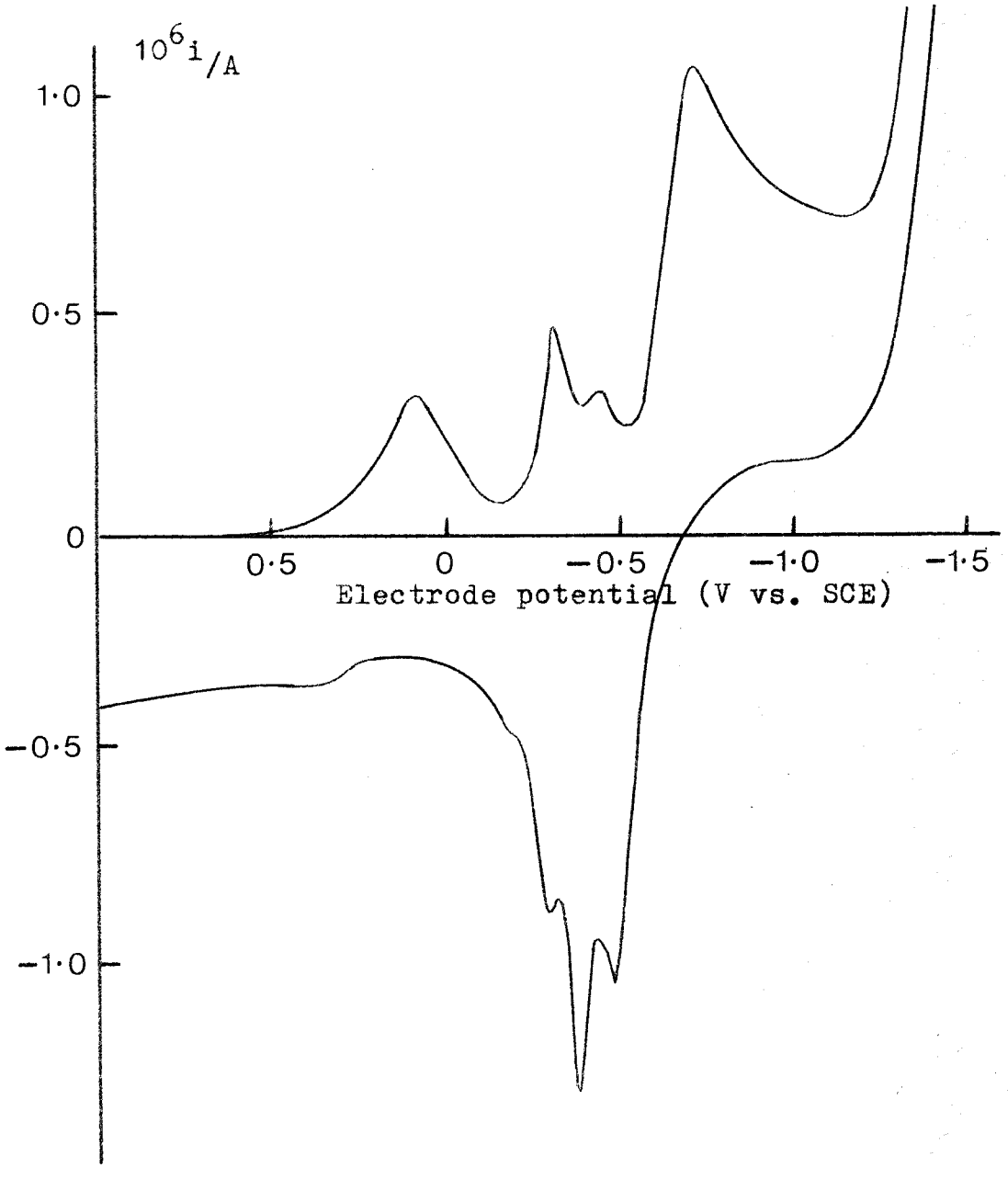

FIG 76 Voltammogram for the reduction of acetic acid (40mM) in sodium acetate (1M) at a platinum microelectrode (31μm). Sweep rate = 10V s^{-1}: continous sweep

occur. It is, however, interesting to compare the rather indistinct adsorption/desorption peaks obtained in dilute acid solutions to those obtained in more concentrated solutions. In FIGS. 77 and 78 for the reduction of sulphuric acid (H_2SO_4: 4M) two well defined adsorption/desorption peaks are observed. The areas of the platinum microelectrodes following anodic activation calculated from the charge under the adsorption peaks, assuming a value of $\sim 250\mu C/cm^2$ for a monolayer deposit after correcting for double layer charging, indicates a true surface area in excess of four times the geometric area. This may be explained simply by the surface roughness of the electrode caused by polishing, increasing the real electrode surface area on a microscopic scale. The fact that the electrode area calculated from the diffusion controlled limiting currents correspond to the geometric area, indicates that the surface roughness lies within the diffusion layer thickness.

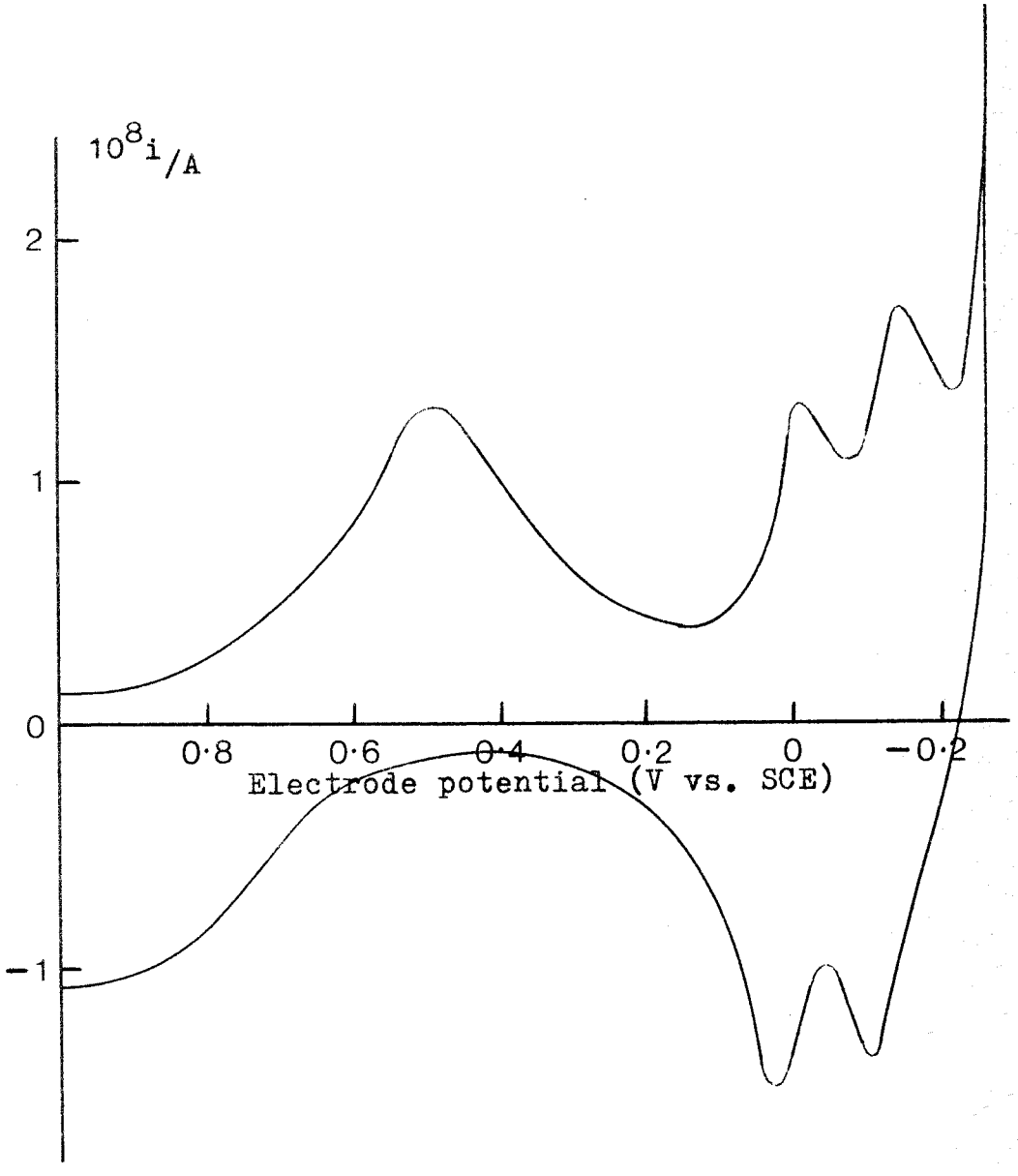

FIG 77 Voltammogram for the reduction of sulphuric acid (4M) at a platinum microelectrode (1·6μm).
Sweep rate = 10V s^{-1}: continuous sweep

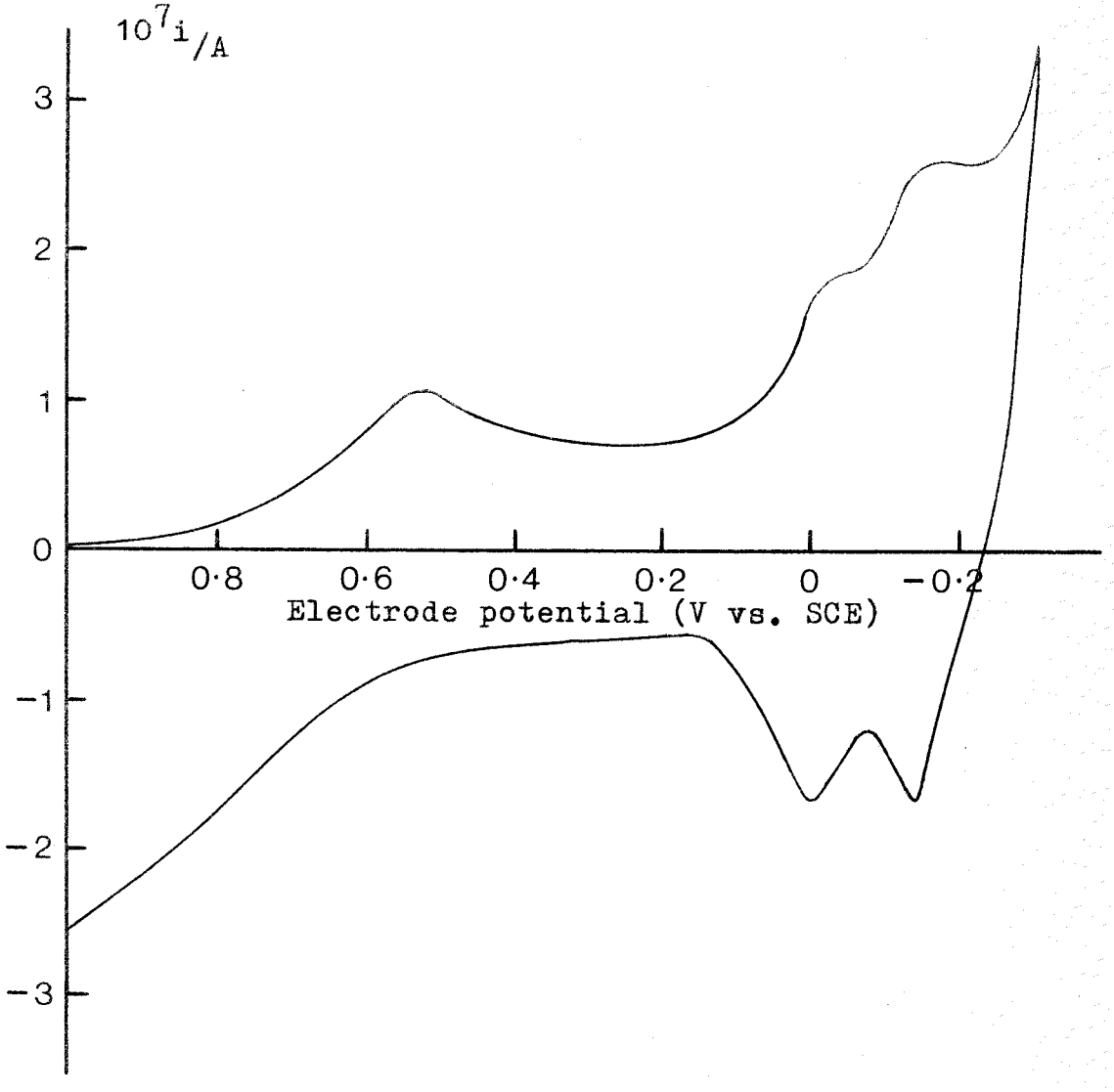

FIG 78 Voltammogram for the reduction of sulphuric acid (4M) at a platinum microelectrode (6μm).
Sweep rate = 10V s^{-1}: continuous sweep

5:iii Hydrogen Evolution from Aqueous Acetic Acid Solution

The reduction of acetic acid (CH_3COOH: 40mM) in aqueous sodium acetate (CH_3COONa: 1M) was conducted in a two electrode cell over an extended range of linear potential sweep rates on platinum microelectrodes of dissimilar radii.

At low potential sweep rates ($\leq 30mV\ s^{-1}$) kinetic currents corresponding to the reduction of the acid proton at activated platinum microelectrodes were observed. Measurements of the limiting values of these kinetic currents confirmed that free acid proton concentration was much lower than would be expected for a fully dissociated acid. In addition, a dependence of the limiting current on the potential sweep rate was also detected, particularly for the smaller microelectrodes. It was noticeable that with the larger platinum microelectrodes ($r_o \sim 25\mu m$) flat, well defined limiting currents, independent of the sweep rate were obtained at sweep rates $\simeq 30mV\ s^{-1}$, whereas with the smaller microelectrodes ($r_o \leq 10\mu m$) considerably higher potential sweep rates (up to $300mV\ s^{-1}$) were necessary to achieve the same degree of linearity of limiting current, definition and independence of sweep rate. This was attributed to deactivation of the electrode surface, in a manner similar to that discussed in the previous section. Effects due to the influence of mass transfer may be discounted since as the electrode radius is decreased, the rate of mass transfer of the undissociated acid is enhanced as compared to the rate of reduction of protons produced by dissociation, i.e. the kinetic waves should become progressively better defined with decreasing electrode radii. In practice, however, the reverse is observed, (FIGS. 79 and 80).

The voltammograms recorded for acetic acid (40mM) solution in sodium acetate (1M) were analysed according to equation (5.40). Values for the limiting current density were calculated from the observed limiting

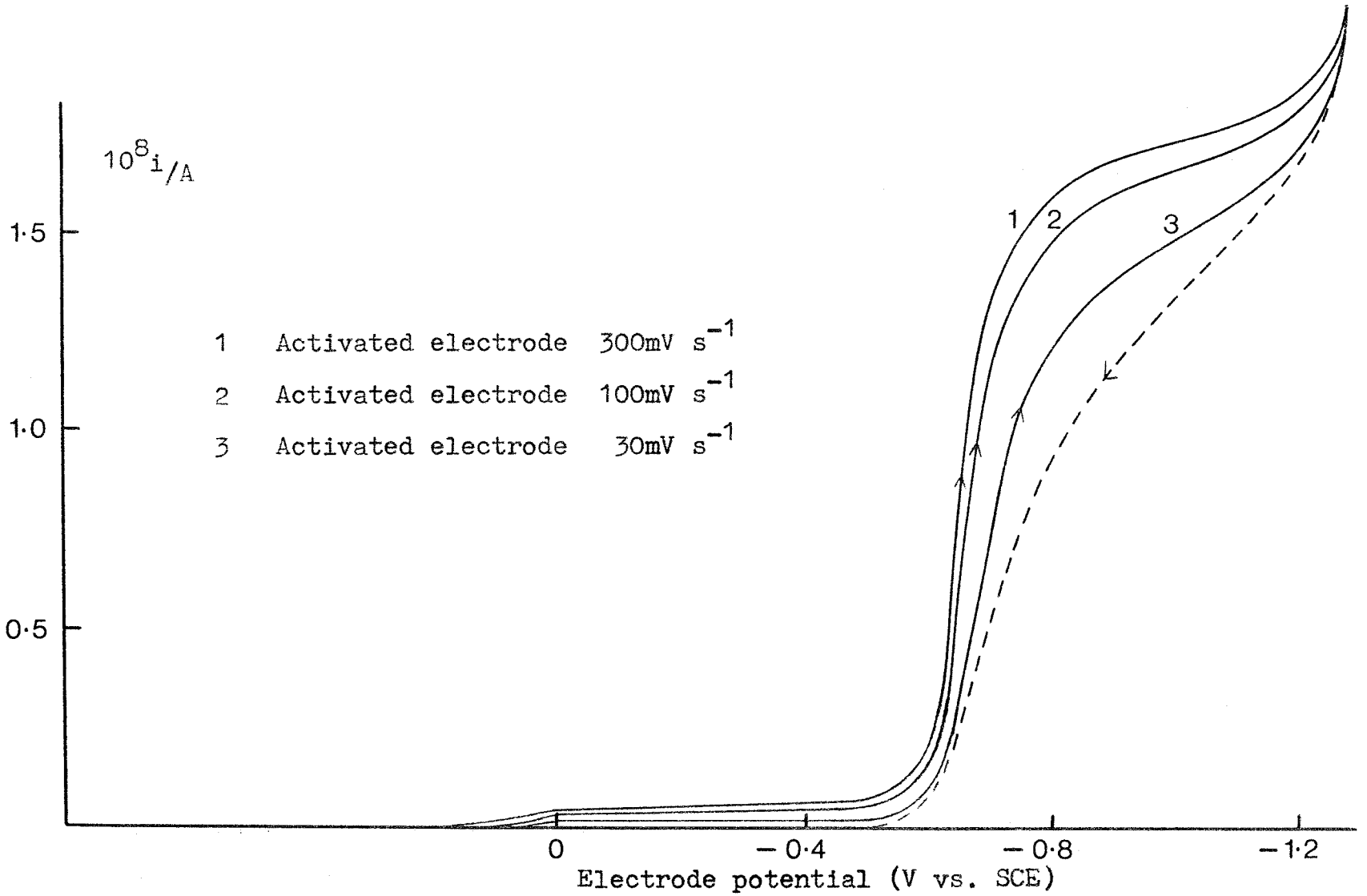

FIG 79 Voltammogram for the reduction of acetic acid (40mM) in sodium acetate (1M) at a platinum microelectrode (1.6μm) as a function of potential sweep rate.

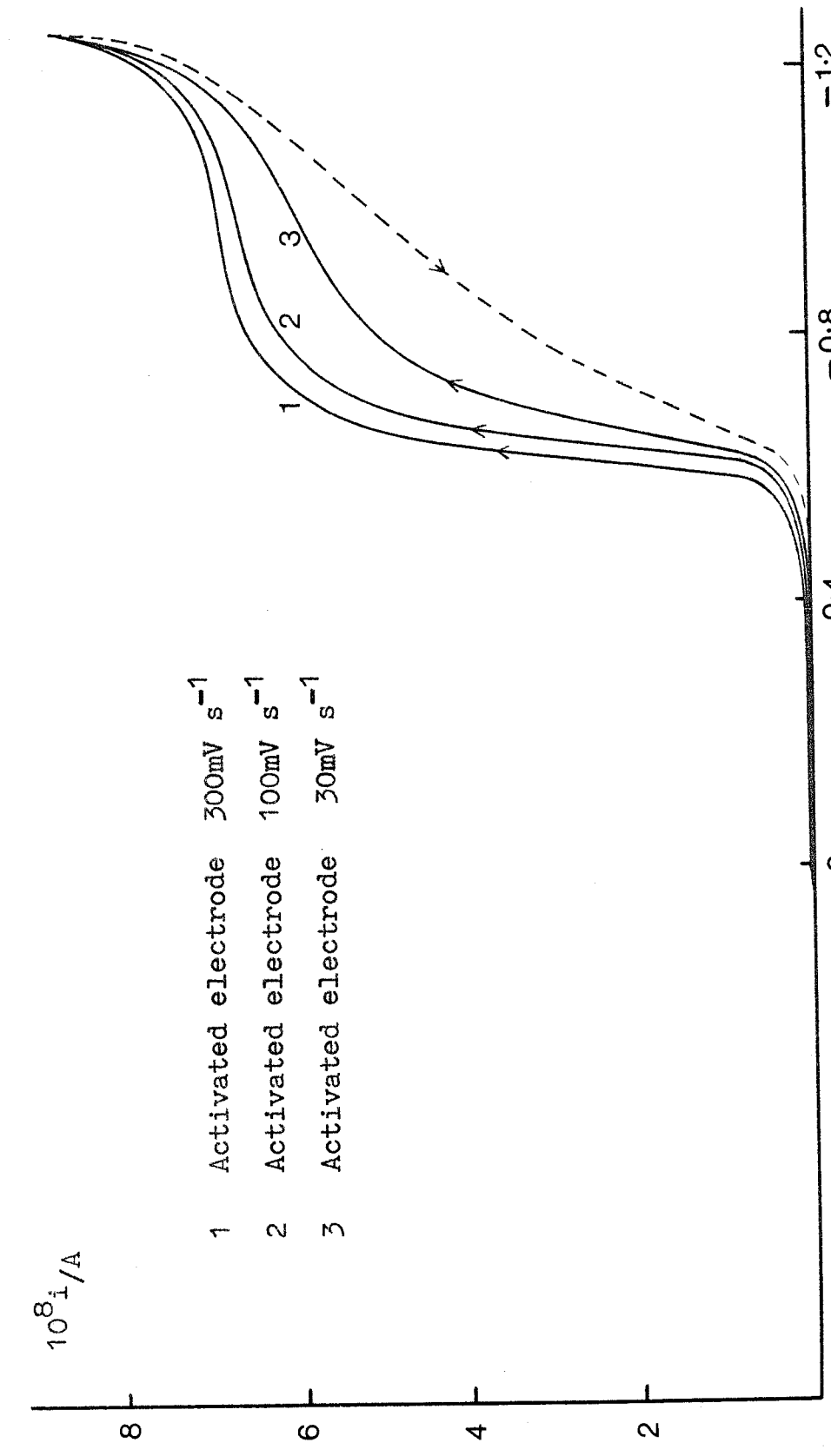

FIG 80 Voltammogram for the reduction of acetic acid (40mM) in sodium acetate (1M) at a platinum microelectrode (6μm) as a function of potential sweep rate.

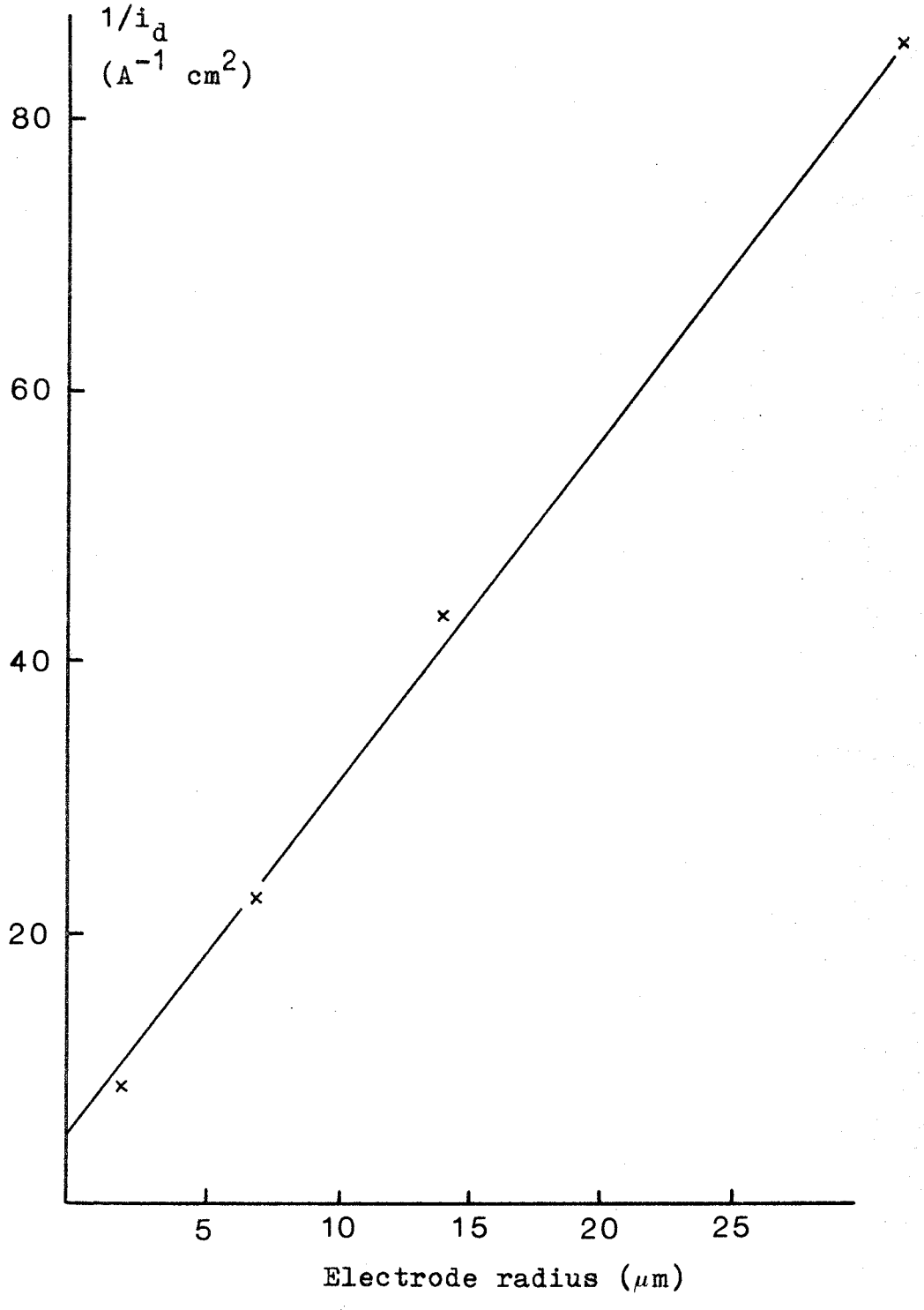

FIG 81 Plot of the reciprocal limiting current density vs. electrode radius for the reduction of acetic acid (40mM) in sodium acetate (1M) at platinum microelectrodes

current, using a value of the electrode radius determined previously from diffusion controlled limiting currents in strong acid media. The reciprocal of the limiting current density was then plotted against the electrode radius for each electrode dimension. The resulting plot for acetic acid (40mM) is shown in FIG. 81. The slope and intercept of a straight line drawn through these points was determined, using linear regression analysis and found to be

$$\text{slope} = 2{\cdot}69 \times 10^{4}$$

$$\text{intercept} = 4{\cdot}18$$

so that from (5.42) and (5.43)

$$\frac{1}{nFD_{HA}C^{\infty}_{HA}} = 2{\cdot}69 \times 10^{4} \qquad 5.50$$

and

$$\frac{(k_2 C^{\infty}_{A})^{\frac{1}{2}}}{nF(D_H)^{\frac{1}{2}}k_1 C^{\infty}_{HA}} = 4{\cdot}18 \qquad 5.51$$

With a value for $D_{HA} \simeq 1 \times 10^{-5}\text{cm}^2\ \text{s}^{-1}$, assuming that $D_H \simeq 8D_{HA}$ [135] and $D_H \simeq 7{\cdot}5 \times 10^{-5}\text{cm}^2\ \text{s}^{-1}$, substitution for D_{HA} into (5.50) together with the appropriate constants, gives

$$C^{\infty}_{HA} \simeq 3{\cdot}9 \times 10^{-6}\text{mol cm}^{-3} \qquad 5.52$$

indicating that the acid is only sparingly dissociated as indeed would be expected from a solution containing a high acid anion concentration.

From (5.51),

$$\frac{(k_2 C_A^{\infty})^{\frac{1}{2}}}{(D_H)^{\frac{1}{2}} k_1 C_{HA}^{\infty}} = 4{\cdot}03 \times 10^5 \qquad 5.53$$

or, since

$$k_1 C_{HA}^{\infty} = k_2 C_H^{\infty} C_A^{\infty} \qquad 5.54$$

from the equilibrium condition,

$$D_H C_H^{\infty 2} k_2 C_A^{\infty} = 6{\cdot}14 \times 10^{-12} \qquad 5.55$$

Substituting now with $C_A^{\infty} = 1 \times 10^{-3}$ mol cm^{-3} and $D_H = 7{\cdot}5 \times 10^{-5}$ cm^2 s^{-1}, (5.55) becomes

$$k_2 C_H^{\infty 2} = 8{\cdot}19 \times 10^{-5} \qquad 5.56$$

A value for C_H^{∞} may be obtained from the equilibrium equation, noting that the pK_a of acetic acid is 4·75 (in mol l^{-1}) [133] ; thus

$$K_a = \frac{C_A^{\infty} C_H^{\infty}}{C_{HA}^{\infty}} \cdot \frac{\gamma_A \gamma_H}{\gamma_{HA}} \qquad 5.57$$

$$= 1{\cdot}75 \times 10^{-8} \text{mol cm}^{-3}$$

where γ_i represents the activity coefficient of species i present in solution. The activity coefficients may be calculated from the Debye-Huckel expression, defined by [94]

$$\ln \gamma_i = \frac{0{\cdot}5115 \ |z| \sqrt{I}}{1 + 0{\cdot}329 \mathring{a} \sqrt{I}} \qquad 5.58$$

at 25°C, where I is the ionic strength of the solution; z the charge on species i and a the effective ionic radius, (for acetic acid $\mathring{a}_H = 9$, $\mathring{a}_A = 4{\cdot}5$ in the appropriate units for (5.58) [94]).

For a one molar solution of a 1:1 electrolyte (i.e. $I \simeq 1$), it is found by inserting the appropriate values into (5.58) that

$$\gamma_H = 0{\cdot}74 \qquad 5.59$$

$$\gamma_A = 0{\cdot}62 \qquad 5.60$$

Assuming furthermore, that for an uncharged species

$$\gamma_{HA} \simeq 1 \qquad 5.61$$

substitution of these parameters into (5.57) together with the appropriate values for C^{∞}_{HA} and C^{∞}_{A} gives

$$C^{\infty}_{H} = 1{\cdot}52 \times 10^{-9} \text{mol cm}^{-3} \qquad 5.62$$

which, when inserted into (5.56) yields finally

$$k_2 = 3{\cdot}54 \times 10^{10} \text{l mol}^{-1}\ \text{s}^{-1} \qquad 5.63$$

This value, as can be seen from TABLE 4 compares favourably with results obtained by other workers using generally more sophisticated techniques.

It will be noted that this analysis does not take into consideration such factors as surface roughness, or the effect of the electric field at the electrode surface on the measured rate of recombination of the acid (the so called second Wien effect).

With a reaction layer thickness, μ , of Angstrom dimensions, where μ is defined by

$$\mu = \left(\frac{D}{k_2 C^{\infty}_{A}}\right)^{\frac{1}{2}} \qquad 5.64$$

so that for the acetic acid reaction studied above $\mu \simeq 2 \times 10^{-7}$cm, the surface roughness might be expected to exert a considerable influence on the

TABLE 4

$$CH_3COOH \underset{k_2}{\overset{k_1}{\rightleftharpoons}} CH_3COO^- + H^+$$

EXPERIMENTAL TECHNIQUE	k_2 ($l\ mol^{-1}\ s^{-1}$)	REFERENCES
Rotating Disc	$2{\cdot}6 \times 10^{10}$	(134)
	$5{\cdot}1 \times 10^{10}$	(135),(136)
Chronopotentiometry	$2{\cdot}7 \times 10^{10}$	(137)
	$9{\cdot}0 \times 10^{10}$	(138)
Relaxation methods	$4{\cdot}5 \times 10^{10}$	(139),(140)
Faradaic Rectification	$5{\cdot}0 \times 10^{10}$	(141)
	$9{\cdot}0 \times 10^{10}$	(142) - (144)
Microelectrodes	$3{\cdot}54 \times 10^{10}$	

measured rate of reaction. Inclusion of a roughness factor, θ , into the mathematical derivation at the beginning of this Chapter leads to an expression equivalent to (5.40) of the form

$$\frac{1}{i_s} = \frac{(k_2 C_A^{\infty})^{\frac{1}{2}}}{nF\theta(D_H)^{\frac{1}{2}}k_1 C_{HA}^{\infty}} + \frac{r_o}{nF\theta D_{HA} C_{HA}^{\infty}} \qquad 5.65$$

The value of θ in (5.65) is essentially unknown, although in the previous section it was shown that the true electrode area was much larger than the geometric area. However, noting that (5.40) and (5.65) are equivalent for $\theta = 1$, it would seem from the value of C_{HA}^{∞} calculated from the experimentally determined slope of FIG. 81, using (5.43) that a value of $\theta = 1$, corresponding to a surface roughness much less than the reaction layer thickness, leads to a satisfactory value for the recombination rate constant k_2 in terms of other reported results shown in TABLE 4. For this reason and the fact that a definitive value for is unknown, it has been excluded from the analysis shown above.

Another consequence of a very thin reaction layer is that the reaction may proceed within the diffuse double layer region resulting in changes of the cation and anion concentrations by the electric field. This effect may be minimised through the use high ionic strength electrolyte solutions.

Furthermore, the application of Fick's Laws in these very thin layers may also be unsound. However, for this analysis, in common with other techniques, Fick's Laws, albeit in spherical form, have been assumed to operate even in these very thin layers.

To conclude, therefore, platinum microelectrodes have demonstrated the capability of measuring the rates of fast homogeneous chemical reactions preceding an electron transfer reaction under slow linear potential sweep conditions in a relatively simple experimental technique.

CHAPTER 6 EXPERIMENTAL

6:i Electronic Equipment

Conventional cyclic voltammetry experiments with wire working electrodes were performed potentiostatically using a Chemical Electronics valve potentiostat and a Chemical Electronics waveform generator, type RB1. The current output was recorded on a Bryans X - Y recorder, type 26000, connected directly to the potentiostat.

Slow linear potential sweep experiments with platinum and tungsten microelectrodes were conducted in a simple two electrode assembly in view of the low potential drop in the solution due to the spherical geometry and the low currents passed, resulting in negligible 'iR' drop. The potential of the working electrode in these experiments was controlled by a Chemical Electronics Linear Sweep Generator coupled to a laboratory built variable voltage source for very low sweep experiments and by a waveform generator, type RB1 for fast sweep voltammetry. The current was measured initially by a Levell D.C. Multimeter, type TM9B, and later with a Keithley Picoammeter, type 417, connected in series with the cell. Both meters produced an output which was recorded on either a Bryans X - Y recorder or a Hewlett Packard X - Y recorder, type 7015A. The circuit diagrams for conventional cyclic voltammetry and slow potential sweep voltammetry are shown in FIG. 82.

In addition, during fast potential sweep experiments the current transient was stored, digitally, by a Hi - Tek signal averager, type AA1, prior to plotting onto an X - Y recorder. At the same time, the electrode response was monitored on a Hewlett Packard Memory Oscilloscope, type 1201A.

Because of the very low currents encountered

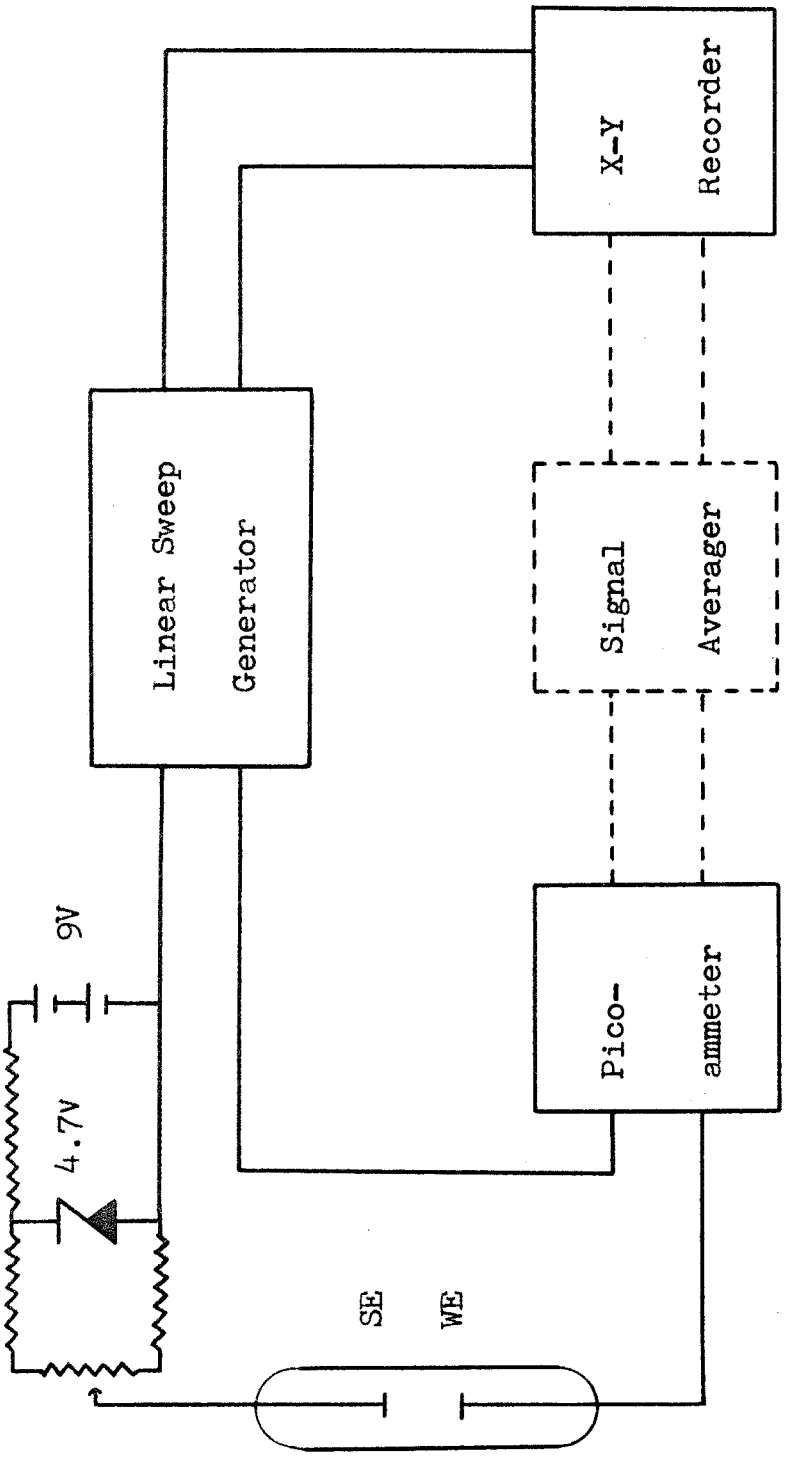

FIG 82 Circuit diagram for two electrode cell operation

in microelectrode experiments, it was found necessary to shield the cell electrically from its environment by placing it inside a specially designed aluminium box and using only very low noise coaxial cable, type RG 58U wherever possible. This reduced most mains 'pickup' to an extent which could be tolerated by the highly sensitive current measuring devices.

6:ii Reference Electrodes

A saturated calomel reference electrode (Radiometer, type K401) was used for all experiments conducted in aqueous media and also for some initial experiments in N,N Dimethylformamide performed in two compartment cells. For the majority of experiments in N,N Dimethylformamide however, a mercury pool reference was used in the presence of iodide ions from the supporting electrolyte. Silver/silver nitrate and silver/silver chloride reference electrodes were also used in Dimethylformamide solutions but rejected due to instability.

The silver/silver nitrate reference was freshly prepared before each experiment by immersing a silver wire into a solution of Dimethylformamide containing silver nitrate (0·01M) and the appropriate supporting electrolyte. The whole assembly was contained in a small glass tube fitted with a sinter at the base. Silver/silver chloride reference electrodes were formed in the standard manner [144] by anodising a silver wire in hydrochloric acid (5M) for approximately ten minutes. Normally, these electrodes were completely re-anodised before each experiment.

6:iii Cells

Cyclic voltammetry experiments with platinum and tungsten wire electrodes (area ~ $0{\cdot}2cm^2$) were carried out in a three electrode, two compartment cell of the type shown in FIG. 83. The cell contained an exchangeable working electrode and an adjustable Luggin capillary connecting the reference electrode compartment to the main working solution. A helical platinum wire acted as a secondary electrode.

Experiments with microelectrodes, as previously mentioned, were conducted in a two electrode cell. Several variations of cell design were required to accommodate the different reference electrodes used during the course of this work. Early experiments involving saturated calomel and silver/silver ion reference electrodes were performed in a two compartment cell as illustrated by FIG. 84, where the microelectrode and reference electrode were placed end to end along a vertical axis. A glass sinter was incorporated into the design in order to minimise contamination of the catholyte. Microelectrodes could not be exchanged however, except by draining the cell.

Later cell designs, with alternative reference systems were based on one compartment cells. FIGS. 85a and 85b illustrate the cells used with silver/silver chloride and mercury pool reference electrodes respectively. It can be seen that exchange of microelectrodes was now straightforward. As the development of microelectrodes progressed, minor modifications to the basic cell were made culminating in the cell shown in FIG. 86a for use with a 'standard' platinum microelectrode and mercury pool reference electrode.

Finally, in the study of homogeneous reactions in aqueous media, the cell shown in FIG. 86b was used. This cell incorporated a saturated calomel electrode placed parallel to the platinum microelectrode.

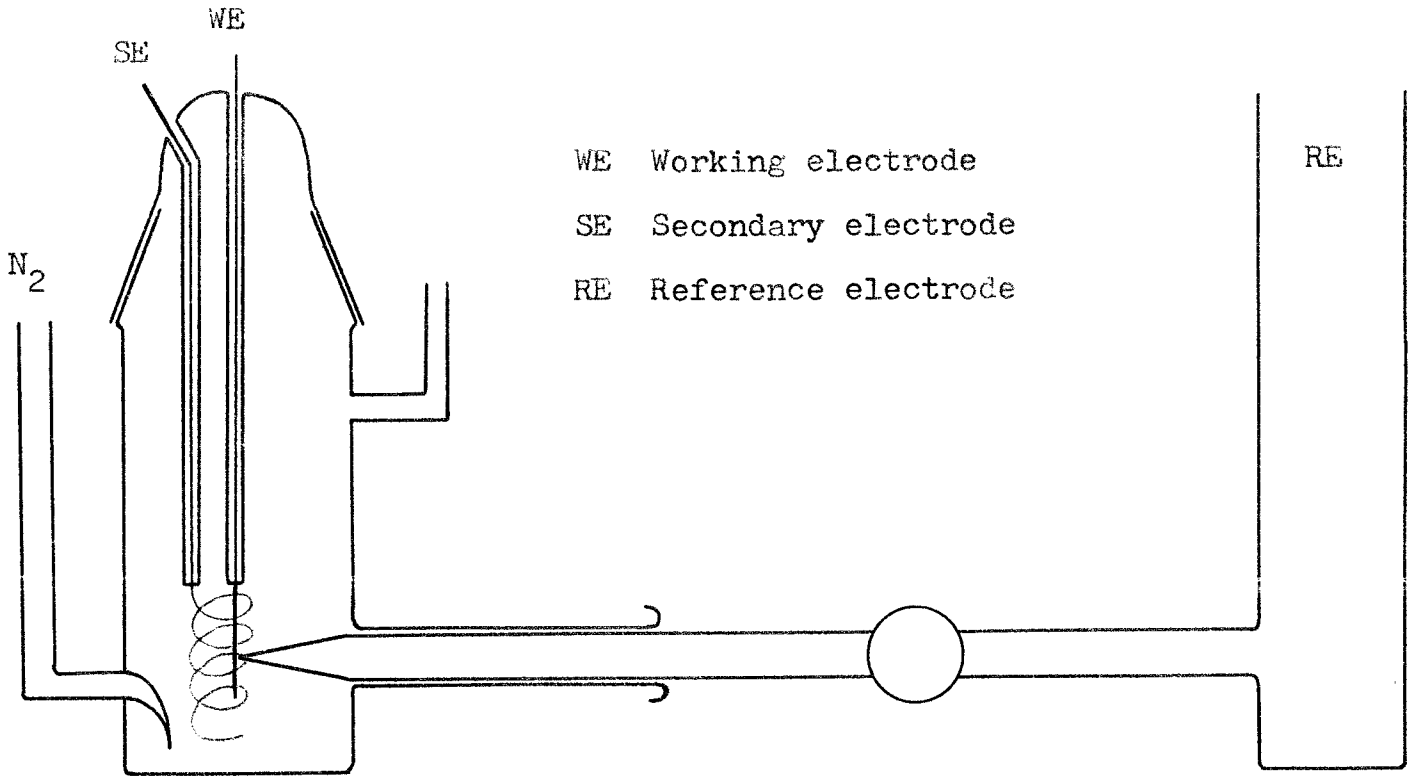

FIG 83 Three electrode cell assembly for use with platinum wire and tungsten rod working electrodes.

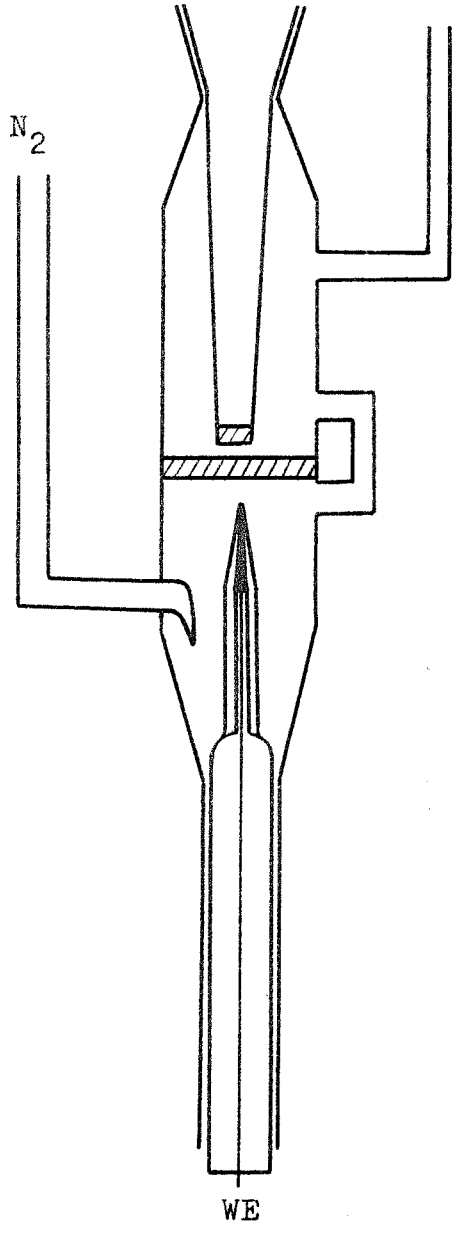

FIG 84 Two electrode cell assembly for lead/indium capillary microelectrodes with Ag/Ag^+ or saturated calomel reference electrode

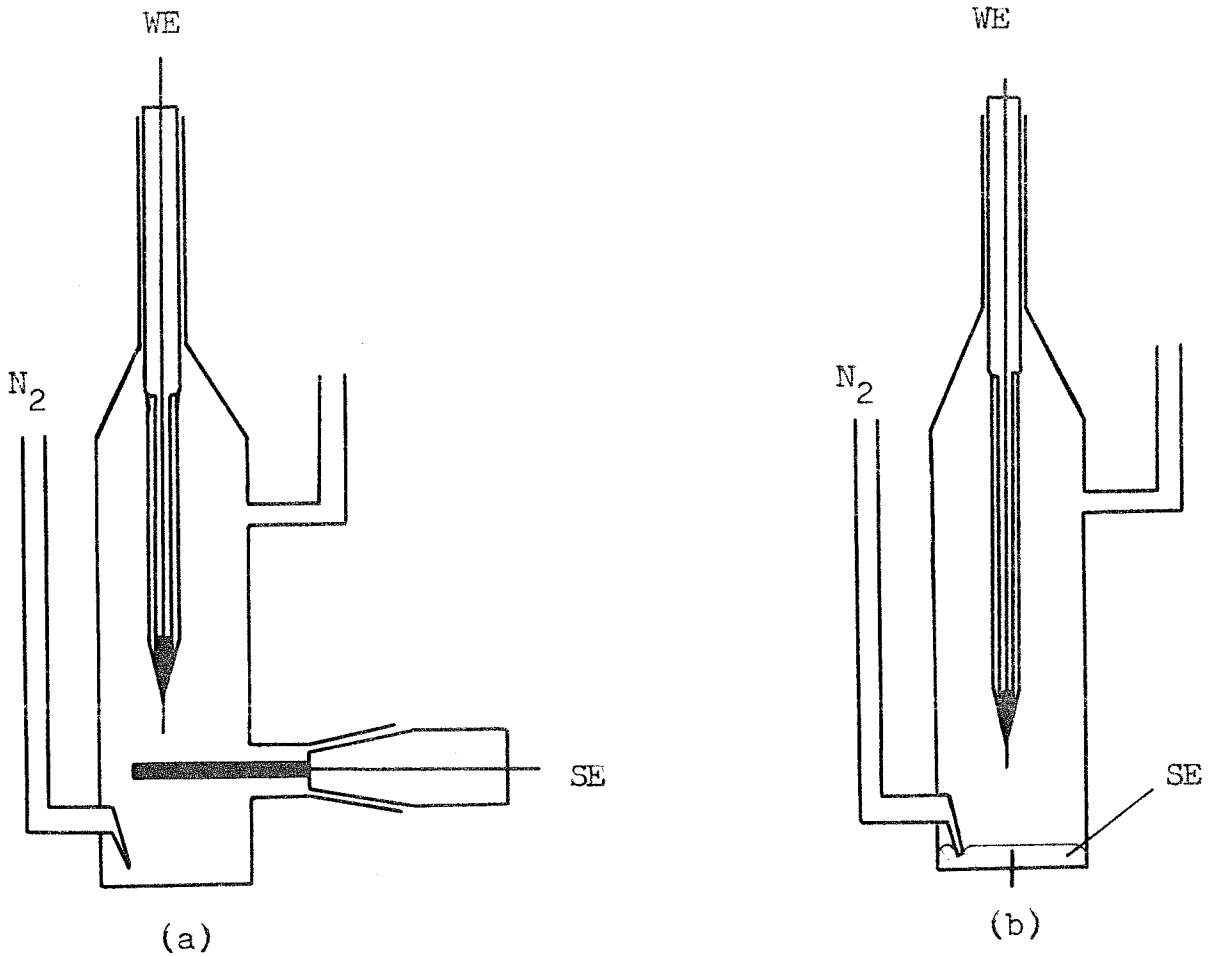

FIG 85 Two electrode cell assemblies for microelectrodes, for use with

(a) Ag/AgCl reference electrode

(b) Hg pool reference electrode

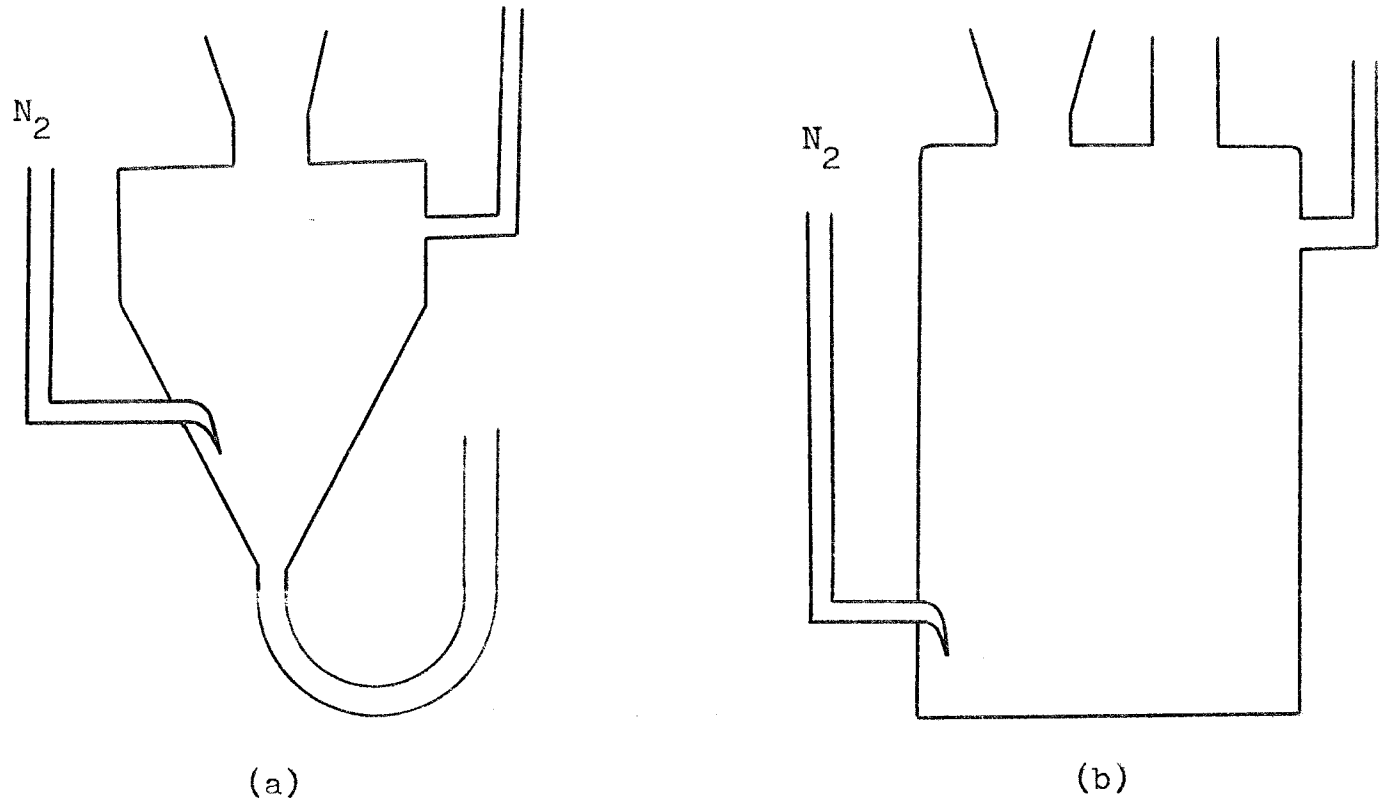

FIG 86 Two electrode cell assemblies for platinum microelectrodes for use with

(a) Hg pool reference electrode

(b) Saturated calomel reference electrode

The restriction of a uniform potential field at the working electrode was relaxed in this case to allow easy exchange of microelectrodes.

All cells were constructed in the laboratory from 'Pyrex' glass and had a gas inlet for deaeration of the working solution and an outlet to which could be attached a drying tube when working with non aqueous media, in order to maintain a dry working atmosphere within the cell.

6:iv Reagents

The solvent N,N Dimethylformamide (DMF), (B.D.H. Ltd., 'Analar' grade) was dried by distillation from phosphorus pentoxide (B.D.H. Ltd.) under an atmosphere of dry nitrogen, collecting the fraction which distilled in the range 149°C - 151°C and stored over either molecular sieve, type 4A, or alumina powder (Hopkin & Williams Ltd., 'Camag' grade), under an atmosphere of dry nitrogen [145]. Usually, distillation was performed on the day of use and in any event not more than three days in advance since deterioration of the solvent under these storage conditions was observed.

The supporting electrolyte tetrabutyl ammonium tetrafluoroborate (Bu_4NBF_4) was prepared by mixing hot aqueous solutions of tetrabutyl ammonium hydrogen sulphate (Labkemi AB, Stockholm) with an excess of sodium tetrafluoroborate (B.D.H. Ltd.). After cooling and filtering the precipitate was dissolved in the minimum quantity of hot methylene chloride which was then filtered again and any aqueous layer discarded. Ether was then added to the organic layer, with vigorous stirring, to precipitate the white crystals of tetrabutyl ammonium tetrafluoroborate, which were then filtered once more before drying at 100°C under vacuum.

Tetramethyl ammonium tetrafluoroborate (Me_4NBF_4) was prepared by the addition of an excess of tetrafluoroboric acid (40%, B.D.H. Ltd.) to a saturated aqueous solution of tetramethyl ammonium bromide (B.D.H. Ltd). After evaporating most of the water, the white crystals were filtered before recrystallising from triply distilled water, followed by drying at 100°C under vacuum.

Tetrabutyl ammonium iodide (Bu_4NI), (B.D.H. Ltd., 'Analar' grade) was recrystallised from a methylene chloride/ether mixture as described earlier and tetraethyl ammonium iodide (Et_4NI), (B.D.H. Ltd.,

'Analar' grade) was recrystallised from ethanol before use. In each case, the crystals were oven dried at 100°C under vacuum.

The aromatic hydrocarbons were all used as supplied without further purification.

Compound	Supplier	Grade
Perylene	Koch Light Ltd.	Puriss
9,10 Dimethylanthracene	Koch Light Ltd.	Puriss
9,10 Diphenylanthracene	Koch Light Ltd.	Puriss
9 Phenylanthracene	Koch Light Ltd.	Puriss
tert Nitrobutane	Cambrian Chemicals	Pure
Nitromesitylene	Koch Light Ltd.	Puriss
p Nitroaniline	Hopkin & Williams	Pure

Mercury, for use as the reference electrode was washed thoroughly with dilute nitric acid then distilled under vacuum before use.

'White spot' nitrogen (B.O.C. Ltd.) was used throughout for deaeration of the working solutions. When used with non aqueous media however, it was passed through a series of drying tubes containing $KOH/CaCl_2/P_2O_5$ and silica gel prior to use.

Aqueous solutions of hydrochloric acid, perchloric acid, sodium perchlorate, acetic acid, sodium acetate and sulphuric acid were all prepared using B.D.H. Ltd. 'Analar' grade reagents in triply distilled water (i.e. distilled water redistilled successively from solutions of potassium permanganate and orthophosphoric acid).

APPENDIX A

```
50 DIM X(50),Y(50),E(50),I(50)
100 PRINT "THIS PROGRAM EVALUATES THE STEADY STATE
    EXPRESSION"
150 PRINT:PRINT:PRINT
200 INPUT "NO. OF POINTS";N
300 F=96487: R=8•314: T=298
400 FOR K=1 TO N
500 PRINT "E(";K;")=";  :  INPUT E(K)
600 PRINT "I(";K;")=";  :  INPUT I(K)
700 NEXT K
800 PRINT "E          I"
900 PRINT E(K),I(K) FOR K=1 TO N
1000 PRINT "CORRECT ANY ERRORS NOW, EG TYPE: E(5)=-1•3
     TO CONTINUE TYPE: CONT"
1100 STOP
1200 INPUT "LIMITING CURRENT";I9
1300 INPUT "HALF WAVE POTENTIAL";E2
1400 FOR K=1 TO N
1500 X(K)=E(K) - E2
1600 Z=I(K)/(I9-I(K)*(1+EXP(F*X(K)/R*T))))
1700 IF Z=0 THEN PRINT "ZERO LOG ARGUMENT AT POINT
     NO.";K: GOTO 2200
1800 IF Z<0 THEN PRINT "NEGATIVE LOG ARGUMENT AT POINT
     NO.";K: GOTO 2200
1900 Y(K)=LOG(Z)
2000 NEXT K
2100 GOTO 2400
2200 X(K)=X(1):Y(K)=Y(1)
2300 GOTO 2000
2400 PRINT "LN( )          E - E1/2"
2500 PRINT Y(K),X(K) FOR K=1 TO N
2600 PRINT:PRINT:PRINT
2700 INPUT "MORE CALCULATIONS WITH THESE VALUES";Q1£
2800 IF Q1£="NO" GOTO 3000
2900 GOTO 1300
3000 END
```

APPENDIX B

```
10 DIM I(50),T(60),U(50),J(50)
20 PRINT "THIS PROGRAM EVALUATES THE CONVOLUTION
   INTEGRAL"
30 PRINT:PRINT:PRINT
40 INPUT "NO. OF POINTS";B
50 N=B
60 FOR K=1 TO N
70 PRINT "I(";K;")=";     :INPUT I(K)
80 PRINT "U(";K;")=";     :INPUT U(K)
90 NEXT K
100 PRINT
102 PRINT "I      U(N)"
104 PRINT
110 PRINT I(K),U(K) FOR K=1 TO N
120 PRINT:PRINT
130 PRINT "CORRECT ANY ERRORS NOW, EG TYPE: I(4)=3·4
    TO CONTINUE TYPE: CONT"
140 STOP
145 V=U(2)-U(1)
150 PRINT
160 INPUT "VALUE OF DIFFUSION COEFFICIENT";D
170 PRINT
180 PRINT "FOR PLANAR ANALYSIS TYPE: P"
185 PRINT
190 INPUT "FOR SPHERICAL ANALYSIS TYPE: S";Q1£
200 IF Q1£="P" GOTO 230
205 IF Q1£="S" GOTO 210
210 PRINT
220 INPUT "VALUE OF ELECTRODE RADIUS (CMS)";A
230 PRINT
240 PRINT " M IS THE VALUE OF THE CONVOLUTION INTEGRAL"
250 PRINT
260 PRINT " M        U(N)"
270 PRINT
280 T=U(N)
290 IF Q1£="P" GOTO 300
295 IF Q1£="S" GOTO 340
```

```
300 FOR K=1 TO N-1
310 J(K)=I(K)/(T-U(K))↑0·5
320 NEXT K
330 GOTO 370
340 FOR K=1 TO N-1
350 J(K)=((I(K)*(A↑3)*0·5)/(D*(T-U(K)))↑1·5)-((I(K)*
    (A↑5)*0·75)/(D*(T-U(K)))↑2·5)+((I(K)*(A↑7)*1·875)
    /(D*(T-U(K)))↑3·5)
360 NEXT K
370 F=0·5*J(1)+1·5*J(N-1)
380 FOR K=2 TO N-2
390 F=F+J(K)
400 NEXT K
410 M=V*F
420 PRINT M,U(N)
430 N=N-1
440 IF N=1 GOTO 460
450 GOTO 280
460 PRINT:PRINT:PRINT
470 INPUT "MORE CALCULATIONS WITH THESE VALUES";Q2£
480 IF Q2£="YES" GOTO 490 ELSE 510
490 N=B
500 GOTO 180
510 END
```

REFERENCES

1	Parsons R	Trans. Farad. Soc. 47 1332 (1951)
2	Delahay P	'Double Layer and Electrode Kinetics' Wiley & Sons Ltd. (1965)
3	Conway B E	'Theory and Principles of Electrode Processes' Ronald Press. (1965)
4	Bockris J O'M	'Modern Electrochemistry' Plenum Press. (1970)
5	Marcus R A	J. Chem. Phys. 24 966 (1956)
6	Marcus R A	Ann. Rev. Phys. Chem. 15 155 (1964)
7	Marcus R A	J. Chem. Phys. 43 679 (1965)
8	Levich V G	Adv. Electrochem. and Electrochem. Eng. 4 249 (1966)
9	Dogonadze R R Kuznetsov A M Chernenko A A	Russ. Chem. Rev. 34 759 (1965)
10a	Hush N S	J. Chem. Phys. 28 962 (1958)
10b	Hush N S	Trans. Farad. Soc. 57 557 (1961)

11	Hale J M	in 'Reactions of Molecules at Electrodes' Ed. Hush Wiley Interscience (1970)
12	Gerischer H	Z. Physik Chem. (Frank.) 26 223 (1960)
13	Christov S G	J. Electroanal. Chem. 100 513 (1979)
14	Horiuti J Polanyi M	Acta Physicochem. URSS 2 505
15	Parsons R	Adv. Electrochem. and Electrochem. Eng. 1 1 (1961)
16	Heyrovsky J Schikata M	Rev. Trav. Chim. 44 496 (1925)
17	Levich V G	'Physicochemical Hydrodynamics' Prentice Hall. (1962)
18	Bernstein Ch Heindrichs A Vielstich W	J. Electroanal. Chem. 87 81 (1978)
19	Murray R W	in 'Physical Methods - Part IIa - Electrochemical Methods' Interscience (1971)
20	Gerischer H Vielstich W	Z. Physik Chem. (Frank.) 3 16 (1955)
21	Anson F C	Anal. Chem. 38 54 (1966)
22	Adams R N	'Electrochemistry at Solid Electrodes' Marcel Dekker (1969)

23 Nicholson R S
Shain I
Anal. Chem.
36 706 (1964)

24 Nicholson R S
Anal. Chem.
37 1351 (1965)

25 Nadjo L
Saveant J M
J. Electroanal. Chem.
48 113 (1973)

26 Perone S P
Kretlow W J
Anal. Chem.
38 1760 (1966)

27 Delahay P
'New Instrumental Methods of Electrochemistry'
Interscience (1958)

28 Delahay P
Adv. Electrochem. and Electrochem. Eng.
1 233 (1961)

29 Delahay P
Berzins T
J. Am. Chem. Soc.
75 2486 (1953)

30 Berzins T
Delahay P
J. Am. Chem. Soc.
77 6448 (1955)

31 Berzins T
Delahay P
J. Chem. Phys.
23 972 (1955)

32 Kooijman D
Sluyters J H
J. Electroanal. Chem.
13 152 (1967)

33 Nagy Z
J. Electrochem. Soc.
125 1809 (1979)

34 Nagy Z
J. Electrochem. Soc.
126 1148 (1979)

35 Kogoma M
Rohka T
Aoyagui S
J. Electroanal. Chem.
38 45 (1972)

36 Mizota H
Matsuda H
Kanzaki Y
Aoyagui S
J. Electroanal. Chem.
45 385 (1973)

37 Matsuda H
Aoyagui S
J. Electroanal. Chem.
87 155 (1978)

38 Smith D E
in 'Electroanalytical Chemistry' Ed. Bard A J
Vol. I Marcel Dekker (1966)

39 Sluyters-Rehbach M
Sluyters J H
in 'Electroanalytical Chemistry' Ed. Bard A J
Vol. IV Marcel Dekker (1970)

40 Smith D E
CRC Crit. Rev. Anal. Chem.
2 247 (1971)

41 Breyer B
Bauer H
'A C Polarography and Tensammetry'
Interscience (1963)

42 Agarwal H P
in 'Electroanalytical Chemistry' Ed. Bard A J
Vol. VII Marcel Dekker (1974)

43 Van der Pol F
Sluyters-Rehbach M
Sluyters J H
J. Electroanal. Chem.
40 209 (1972)

44 Van der Pol F
Sluyters-Rehbach M
Sluyters J H
J. Electroanal. Chem.
45 377 (1973)

45	Van der Pol F Sluyters-Rehbach M Sluyters J H	J. Electroanal. Chem. 58 177 (1975)
46	Kakutani K Kinoshita H Senda M	Rev. Polarog. Japan 20 15 (1974)
47	Meites L	'Polarographic Techniques' Wiley & Sons Ltd. (1965)
48	Kolthoff I M Lingane J J	'Polarography' Interscience (1952)
49	Riddiford A C	Adv. Electrochem. and Electrochem. Eng. Vol. IV (1966)
50	Frumkin A N Tedoradse G	Z. Elektrochem. 62 251 (1958)
51	Budewski E Toschev S	Doklady Akad. Nauk. URSS 130 1047 (1960)
52	Jahn D Vielstich W	J. Electrochem. Soc. 109 849 (1962)
53	Bindra P Brown A P Fleischmann M F Pletcher D	J. Electroanal. Chem. 58 31 (1975)
54	Bindra P Brown A P Fleischmann M F Pletcher D	J. Electroanal. Chem. 58 39 (1975)

55 Koizumi N, Saji T, Aoyagui S — J. Electroanal. Chem 81 403 (1977)

56 Dayton M A, Brown J C, Stutts K J, Wightman R M — To be published

57 Ponchon J-L, Cespuglio R, Gonon F, Jouvet M, Pujol J-F — Anal. Chem. 51 1483 (1979)

58 Crank J — 'Mathematics of Diffusion' O.U.P. (1956)

59 Speigel M R — 'Theory and Problems of Laplace Transforms' M^{c}Graw Hill (1965)

60 Randles J E B — Trans. Farad. Soc. 44 327 (1948)

61 Sevcik A — Coll. Czech. Chem. Comm. 13 349 (1948)

62 Delahay P — J. Am. Chem. Soc. 75 1190 (1953)

63 Matsuda H, Ayabe Y — Z. Elektrochem. 59 494 (1955)

64 Nicholson M M — J. Am. Chem. Soc. 76 2539 (1954)

65 Frankenthal R P, Shain I — J. Am. Chem. Soc. 78 2969 (1956)

66 Rheinmuth W H — Anal. Chem. 33 185 (1961)

67 Rheinmuth W H — Anal. Chem. 33 1793 (1961)

68 Rheinmuth W H — J. Am. Chem. Soc. 79 6358 (1957)

69 De Mars R D, Shain I — J. Am. Chem. Soc. 81 2654 (1959)

70 Oldham K B, Spanier J — J. Electroanal. Chem. 26 331 (1970)

71 Imbeaux J C, Saveant J M — J. Electroanal. Chem. 44 169 (1973)

72 Ammar F, Saveant J M — J. Electroanal. Chem. 47 215 (1973)

73 Nadjo L, Saveant J M, Tessier D — J. Electroanal. Chem. 52 403 (1974)

74 Saveant J M, Tessier D — J. Electroanal. Chem. 65 57 (1975)

75 Saveant J M, Tessier D — J. Electroanal. Chem. 77 225 (1977)

76 Oldham K B — Anal. Chem. 44 196 (1972)

77 Grenness M, Oldham K B — Anal. Chem. 44 1121 (1972)

78 Oldham K B — J. Electroanal. Chem. 41 351 (1973)

79 Goto M
Oldham K B
Anal. Chem.
45 2043 (1973)

80 Goto M
Oldham K B
Anal. Chem.
48 1671 (1976)

81 Oldham K B
J. Electroanal. Chem.
72 371 (1976)

82 Goto M
Oldham K B
Anal. Chem.
46 1522 (1974)

83 Dalrymple-Alford P
Goto M
Oldham K B
J. Electroanal. Chem.
85 1 (1977)

84 Dalrymple-Alford P
Goto M
Oldham K B
Anal. Chem.
49 1390 (1977)

85 Miller W
Gordon A R
J. Phys. Chem.
35 2785 (1931)

86 Ferris C D
'Introduction to Bioelectrodes'
Plenum Press (1974)

87 Dowben R W
Rose J E
Science
118 22 (1953)

88 Gesteland R C
Howland B
Lettvin J Y
Pitts W H
Proc. IRE
47 1856 (1959)

89 Hubel D H
Science
125 550 (1957)

90 Wolbarscht M L, M^{c}Nichol E F Jr, Wagner H G — Science 132 1309 (1960)

91 Amatniek E — Trans. IRE 10 3 (1958)

92 Ilkovic D — Coll. Czech. Chem. Comm. 8 13 (1936)

93 Nemec L — J. Electroanal. Chem. 8 166 (1964)

94 Robinson R A, Stokes R H — 'Electrolytic Solutions' Butterworths (1955)

95 Given P H — J. Chem. Soc. 1602 (1959)

96 Tanaka N, Tamashui R — Electrochim. Acta 9 963 (1964)

97 Tamashui R — 'Kinetic Parameters of Electrode Reactions of Metallic Compounds' Butterworths (1975)

98 Mann C K, Barnes K K — 'Electrochemical Reactions in Nonaqueous Systems' Marcel Dekker (1970)

99 Dietz R, Peover M — Farad. Soc. Disc. 45 154 (1968)

100 Jensen B S, Parker V D — J. Am. Chem. Soc. 97 5619 (1975)

101 Butler J — Adv. Electrochem. and Electrochem. Eng. Vol. VII (1969)

102	Given P H Peover M Schoen J	J. Chem. Soc. 2674 (1958)
103	Hammerich O Parker V D	Electrochim. Acta 18 537 (1973)
104	Gesteland R C Howland B Lettvin J Y Pitts W H	Proc. IRE 47 1856 (1959)
105	Dogonadze R R	in 'Reactions of Molecules at Electrodes' Ed. Hush Wiley Interscience (1971)
106	Peover M Powell J S	J. Electroanal. Chem. 20 427 (1969)
107	Corrigan D A Evans D H	J. Electroanal. Chem. 106 287 (1980)
108	Lane R L Hubbard A T	J. Phys. Chem. 81 734 (1977)
109	Saveant J M Tessier D	J. Phys. Chem. 81 2192 (1977)
110	Loeb A L Overbeek J Th G Wiersema P H	'The Electrical Double Layer around a Spherical Colloidal Particle' M I T Press (1961)
111	Dickinson T Angell D H	J. Electroanal. Chem. 35 55 (1972)
112	Samec Z Weber J	J. Electroanal. Chem. 44 229 (1973)

113 Samec Z
Weber J
J. Electroanal. Chem.
77 163 (1977)

114 M^{c}Donald D D
'Transient Techniques in Electrochemistry'
Plenum (1978)

115 Gleitenberg Von D
Kutschker A
Stackelberg M V
Ber. Bunsenges
72 562 (1968)

116 Horiuti J
in 'Physical Chemistry'
Ed. Eyring, Henderson, Jost
Vol. IXb Academic (1970)

117a Breiter M W
J. Electroanal. Chem.
7 38 (1964)

117b Breiter M W
J. Electroanal. Chem.
8 449 (1964)

118 Will F G
J. Electrochem. Soc.
112 451 (1965)

119 Tuseeva E K
Skundin A M
Bagotskii V S
Elektrokhimaya
10 974 (1974)

120 Schuldiner S
Rosen M
J. Electrochem. Soc.
118 1138 (1971)

121 Ross P N
J. Electrochem. Soc.
126 67 (1979)

122 Ross P N
J. Electrochem. Soc.
126 79 (1979)

123 Hubbard A T
Ishikawa R M
Katekaru J
J. Electroanal. Chem.
86 271 (1978)

124 Yamamoto K
Kolb D M
Kotz R
Lehmpfuhl G
J. Electroanal. Chem.
96 233 (1979)

125 Stonehart P
Washington E
Lundquist J T
Bett J
Electrochim. Acta
18 343 (1973)

126 Lundquist J T
Stonehart P
Electrochim. Acta
18 349 (1973)

127 Stonehart P
Lundquist J T
Electrochim. Acta
18 907 (1973)

128 Kinoshita K
Ferrier D R
Stonehart P
Electrochim. Acta
23 45 (1978)

129 Somorjai G A
'Principles of Surface Chemistry'
Prentice Hall (1972)

130 May J W
Ind. Eng. Chem.
57 19 (1965)

131 Pendry J B
'Low Energy Diffraction'
Academic (1974)

132 Kinoshita K
Stonehart P
Electrochim. Acta
20 101 (1975)

133 CRC
'Handbook of Chemistry and Physics'

134 Vielstich W
Jahn D
Z. Elektrochem.
64 43 (1960)

135 Albery W
Bell R P
Proc. Chem. Soc.
169 (1963)

136 Albery W
'Electrode Kinetics'
Clarendon (1975)

137 Giner J
Vielstich W
Z. Elektrochem.
64 128 (1960)

138 Delahay P
Vielstich W
J. Am. Chem. Soc.
77 4955 (1955)

139 Eigen M
Schoen J
Z. Elektrochem.
59 483 (1955)

140 Eigen M
Z. Elektrochem.
64 115 (1960)

141 Barker G C
Nurnberg H W
Naturwiss.
51 191 (1964)

142 Nurnberg H W
Disc. Farad. Soc.
39 136 (1965)

143 Nurnberg H W
Duerbeck H W
Z. anal. Chem.
205 217 (1964)

144 Ives D G J
in 'Reference Electrodes'
Ed. Ives and Janz
Academic (1961)

145 Butler J
Adv. Electrochem. and
Electrochem. Eng.
7 77 (1969)

ACKNOWLEDGEMENTS

I am indebted to my supervisor, Prof. Martin Fleischmann, for his guidance, encouragement, never failing inventiveness and above all patience shown during the course of this work. His contributions to the mathematical development of reactions at microelectrodes presented in Chapters 2 and 5 are also gratefully acknowledged.

Special thanks are due to Clive Godden, without whose dexterity the formation of microelectrodes would have been severely curtailed.

Also, many thanks are due to all members of the Electrochemistry Group, Southampton University, for their many suggestions, however unwitting, for preparing microelectrodes.